This is to certify that the

dissertation entitled

QUANTIFICATION OF INDUCED ELECTROMAGNETIC FIELDS INSIDE MATERIAL SAMPLES PLACED INSIDE AN ENERGIZED MICROWAVE CAVITY BY FINITE-DIFFERENCE TIME-DOMAIN (FDTD) METHOD

presented by

Yao-Chiang Kan

has been accepted towards fulfillment
of the requirements for

Ph.D. degree in ECE

Major professor

Date Aug. 9, 2000

PLACE IN RETURN BOX to remove this checkout from your record.
TO AVOID FINES return on or before date due.
MAY BE RECALLED with earlier due date if requested.

DATE DUE	DATE DUE	DATE DUE

QUAN
INSID
MICRO

QUANTIFICATION OF INDUCED ELECTROMAGNETIC FIELDS INSIDE MATERIAL SAMPLES PLACED INSIDE AN ENERGIZED MICROWAVE CAVITY BY FINITE-DIFFERENCE TIME-DOMAIN (FDTD) METHOD

By

Yao-Chiang Kan

A DISSERTATION

Submitted to
Michigan State University
in partial fulfillment of the requirements
for the degree of

DOCTOR OF PHILOSOPHY

Department of Electrical and Computer Engineering

2000

QUANTIFIC
INSIDE MAT
MICROWAV

The investiga

requires the und

material sample

distribution of the

the cavity.

The goal of th

in the presence o

method, which h

study is based o

order FDTD sch

The numeric

first discussed a

fourth-order FD

rectangular cavi

frequency of a c

by Prony's meth

ABSTRACT

QUANTIFICATION OF INDUCED ELECTROMAGNETIC FIELDS INSIDE MATERIAL SAMPLES PLACED INSIDE AN ENERGIZED MICROWAVE CAVITY BY FINITE-DIFFERENCE TIME-DOMAIN (FDTD) METHOD

By

Yao-Chiang Kan

The investigation of the heating of a material sample in an energized microwave cavity requires the understanding of the interaction of the electromagnetic fields with the material sample in the cavity. The key factor for this understanding is to quantify the distribution of the induced electromagnetic field inside the material sample placed inside the cavity.

The goal of this research is to solve Maxwell's equations in an electromagnetic cavity in the presence of a material sample based on the finite-difference time-domain (FDTD) method, which has been successfully applied to several areas in electromagnetics. This study is based on Yee algorithm, a second-order FDTD scheme, and an improved fourth-order FDTD scheme.

The numerical dispersion equations of Yee and other fourth-order FDTD schemes are first discussed and the disadvantages of Yee scheme are discussed. An implicit staggered fourth-order FDTD method is then employed to calculate the filed distribution in a rectangular cavity with lossless or lossy samples. The quality factor and the resonant frequency of a cavity are obtained by a derived time-domain Poynting's theorem and also by Prony's method. The quality factors calculated by these two different methods are very

consistent.

In applying the

of cylindrical coor

FDTD method is ap

with samples with

forward. Moreover,

computationally effic

the general 3D cylin

3D cylindrical FDTD

implementation and

FDTD method is p

cylindrical FDTD m

consistent.

In applying the FDTD method to cylindrical coordinates, the singularities at the center of cylindrical coordinates become the major problem. The body of revolution (BOR) FDTD method is applied to solve the filed distributions in the cylindrical cavities loaded with samples with symmetries. The treatment in BOR FDTD method is quite straight forward. Moreover, the BOR FDTD method is a 2.5D FDTD method which is much more computationally efficient than a 3D FDTD method. For a sample with any arbitrary shape, the general 3D cylindrical FDTD method is needed to do the calculation. The traditional 3D cylindrical FDTD method encounters the difficulties of the mode-dependent source implementation and the treatment of singularities. In this study, a general fourth-order FDTD method is proposed to overcome the problems encountered in a traditional 3D cylindrical FDTD method.

To my parents and family

First and forem

M. Chen, for introd

Without his guidanc

not have been possi

a researcher and an

I would like to

Edward Rothwell, a

My special thanks

discussions. Speci

my simulation prog

I would also li

Computing Servic

special thanks to D

job for the past ye

Ph.D. at Michigan

My very speci

children and me w

Finally, I wou

complete this stud

work.

ACKNOWLEDGMENTS

First and foremost, I would like to express my deep gratitude to my advisor, Dr. Kun-Mu Chen, for introducing me to Electromagnetics, and his invaluable help and patience. Without his guidance and expert knowledge in Electromagnetics, this dissertation would not have been possible. I am grateful for the opportunity to learn from his example as both a researcher and an engineer.

I would like to thank the other members of my committee, Dr. Dennis Nyquist, Dr. Edward Rothwell, and Dr. Byron Drachman for many helpful comments on this research. My special thanks to Dr. Rothwell for giving constructive criticism in many fruitful discussions. Special thanks go to Dr. Leo Kempel for providing me a workstation to run my simulation program.

I would also like to thank Ms. Jackie Carlson, director of Division of Engineering Computing Services, for appointing me as a graduate assistant from 1994 to 1998. My special thanks to Dr. Guilin Cui, owner of Vertex Computer in Lansing, for providing me a job for the past year. Without those financial supports, I would not be able to study my Ph.D. at Michigan State University.

My very special thanks to my wife, Ya-Ling Peng, who have been taking care of our children and me well so I am able to focus on my research and work.

Finally, I would like to thank my parents for providing me with the opportunity to complete this study. Their love and support accompanied me through the years of this work.

TABLE OF CONTENTS

LIST OF TABLES

LIST OF FIGURES

CHAPTER 1

INTRODUCTION

The research reported in this dissertation was motivated by the investigation of microwave heating of material samples. Microwave heating techniques have been widely utilized in industrial process. Since the microwave heating of material samples is usually conducted within an energized electromagnetic cavity, to understand the heating mechanism it is essential to study the interaction of the microwave field with a material sample in an electromagnetic cavity. The key factor in understanding this interaction is to quantify the induced electromagnetic field inside the material sample by the cavity field. The finite-difference time-domain (FDTD) method is employed in this dissertation to quantify the electromagnetic field inside an EM cavity loaded with material samples.

The finite-difference time-domain (FDTD) method has been used in computational fluid dynamics (CFD) [1] for a long time and yields very accurate results for CFD problems. In 1966, Kane Yee originated a set of finite-difference equations for the time-dependent Maxwell's curl equations system for the lossless materials case [2]. The FDTD method was not popular in (Electromagnetic) EM research area until late 1980 and becomes a very popular method in EM area between 1993 and 1997. Regarding to the FDTD method applied to eigenvalue problems in EM research, Choi and Hoefer [4] published the first FDTD simulation of waveguide/cavity structures in 1986. There are

several papers.
distributions in
detailed analys
heat transfer eq
since the consti
method is a star
using FDTD sc
algorithm used i
However, the diss
will be discussed

Most papers in
approximations w
accuracy and perfo
[15]. Among these
implicit staggered
second order finite
[17]. Combining w
essential FDTD tec
area.

In this disserta
coordinates are stu
revolution (BOR) sc
BOR FDTD method

several papers, [5]-[10], that utilized the FDTD method to investigate the fields and power distributions in a loaded EM cavity. The paper by Torres and Jecko [9] provides a very detailed analysis of microwave heating by combining the Maxwell's equations and the heat transfer equations. The FDTD method used in this paper is called $(FD)^2TD$ method since the constitutive parameters are assumed to be frequency-dependent. This $(FD)^2TD$ method is a standard method to investigate EM interaction with a lossy material sample using FDTD scheme. Moreover, the combined electromagnetic and thermal FDTD algorithm used in this paper provides a basic framework for the FDTD calculation. However, the dissipated power model in this paper is not clear and the improved model will be discussed in this dissertation.

Most papers in the FDTD literature are based on second order spatial and temporal approximations which are originated from Yee algorithm. Due to the requirement of accuracy and performance, several higher order FDTD methods have been proposed [11]-[15]. Among these higher order FDTD methods, Ty(2,4) FDTD method, which uses the implicit staggered fourth order finite difference approximation in space and the explicit second order finite difference approximation in time, provides the most promising features [17]. Combining with the $(FD)^2TD$ method, the Ty(2,4) $(FD)^2TD$ method becomes the essential FDTD technique in the investigation for the eigenvalue problems in EM research area.

In this dissertation, the Ty(2,4) $(FD)^2TD$ method in rectangular and cylindrical coordinates are studied. For a cylindrical cavity with azimuthal symmetry, the body of revolution (BOR) scheme is employed to facilitate the FDTD calculation. In this case, the BOR FDTD method can give very accuracy results with excellent performance; hence, the

Ty2.4) FDTD

In chapter 2

introduced. Als

representation is

and numerical d

and the dispersi

in details. A time

FDTD calculatio

factors (Q) of ca

electrical conducti

and PEC walls, an

end of this chapter

estimation.

In chapter 3, th

is derived. Mode

presented. The trea

In this chapter, the

PEC wall is replac

FDTD formulation

domain approxima

cylindrical cavity w

are presented at the

FDTD method for c

Ty(2,4) FDTD method is not used.

In chapter 2, a set of general finite difference equations for Maxwell equations is introduced. Also, the loaded material is modeled by Debye equations and its FDTD representation is presented. Then a brief introduction of Yee algorithm, stability condition and numerical dispersion is presented. The fourth order spatial derivatives are presented and the dispersion analysis is studied. After that, the Ty(2,4) $(FD)^2TD$ method is presented in details. A time-domain power analysis based on Poynting's theorem is derived. In this FDTD calculation for cavities, the Prony's method is employed to estimate the quality factors (Q) of cavities. The numerical results of a single empty cavity with perfect electrical conductive(PEC) walls, a cavity loaded cavity with a lossless material sample and PEC walls, and a lossy dielectric loaded cavity with PEC walls are presented at the end of this chapter. The numerical results are shown to be consistent with the theoretical estimation.

In chapter 3, the body of revolution (BOR) FDTD formulation of Maxwell's equations is derived. Mode selection and source implementation in BOR FDTD algorithm are presented. The treatment for the singularity in BOR FDTD formulation is also presented. In this chapter, the cavities with finite electrical conductive (FEC) walls is studied and the FEC wall is replaced by a planar surface impedance boundary condition (PSIBC). The FDTD formulation of PSIBC is achieved by three different approachs and the frequency domain approximation is chosen due to its simplicity. Numerical results of an empty cylindrical cavity with PEC and FEC walls and a loaded cylindrical cavity with PEC walls are presented at the end of this chapter. Consistent results are obtained by using this BOR FDTD method for cavities with azimuthal symmetry.

In chapter 4

studied. The d

coordinates are

singularity in

generalized. By

treatment for th

Lorent model's

cylindrical coord

Some derivati

In chapter 4, a general 3D FDTD method in cylindrical coordinates is considered and studied. The disadvantages of conventional second order FDTD method in cylindrical coordinates are presented and its improvements are also proposed. The treatment for the singularity in conventional cylindrical FDTD is mode-dependent and difficult to be generalized. By the introduction of Ty(2,4) FDTD in cylindrical coordinates, a general treatment for the singularity in cylindrical FDTD can be obtained. With the Debye or Lorent models for loaded material samples, a general Ty(2,4) $(FD)^2TD$ method in cylindrical coordinates is obtained.

Some derivations that are useful in this dissertation are provided in Appendices.

SOLVIN

IN

In this chapte

formulation in th

cavities. The finite

second-order acc

implicit staggered

this chapter. Ano

implicit fourth-ord

(1) In multis

or more s

memory r

(2) The accu

appropria

Ty(4,4) ma

(3) The Ty(2,4

In FDTD calculatio

CHAPTER 2

SOLVING MAXWELL'S EQUATIONS BY FDTD IN RECTANGULAR COORDINATE

In this chapter we considers the frequency-dependent implicit, fourth-order FDTD formulation in the rectangular coordinate system and its application to rectangular cavities. The finite difference approximation to time-stepping in those formulations is of second-order accuracy. The second-order accuracy in time-stepping combined with implicit staggered fourth-order accuracy in space, denoted by Ty(2,4)[17], is the focus of this chapter. Another scheme, Ty(4,4), that uses fourth-order in time-stepping with implicit fourth-order in space-stepping is not discussed because of the following reasons:

(1) In multistage time discretization schemes (e.g., Runge-Kutta schemes with three or more stages), boundary conditions must be applied at intermediate levels, then memory requirement and computer running time are increased.

(2) The accuracies of Ty(2,4) and Ty(4,4) are made comparable by choosing an appropriate time step[14][17] although the stability of the FDTD formulation of Ty(4,4) may be improved[15].

(3) The Ty(2,4) is nondissipative, while Ty(4,4) introduces a slight dissipation.

In FDTD calculations for cavities, a many time steps are usually required if the quality factor. Q. of th

coarser meshes

Ty(4.4) is not a

The freque

stepping of Ma

equation is used

The original

section 2.2. The s

in Yee's algorithm

In section 2.3

higher-oder spati

the same dispers

require a smaller

mesh reduction.

schemes are dis

schemes requirin

discussed in sect

boundary treatme

is also discussed.

The excitatio

boundary and loa

cavities are infini

The source used f

loaded cavities wi

factor, Q, of the cavity is high. The Ty(2,4) is used to speed up the computation time since coarser meshes are chosen than that in the original Yee scheme. A dissipation scheme like Ty(4,4) is not a good choice for a long time integration.

The frequency-dependent FDTD formulation with second-order leapfrog time-stepping of Maxwell's equations is discussed in section 2.1. The one-relaxation Debye equation is used to account for the frequency-dependent properties.

The original Yee's algorithm is derived from this general scheme for validation in section 2.2. The stability condition of Yee's algorithm is also presented and the dispersion in Yee's algorithm is then explained.

In section 2.3, the Ty(2,4) $(FD)^2TD$ scheme is obtained from this general scheme. The higher-oder spatial schemes requires much fewer mesh points than Yee's scheme does for the same dispersion error. Although the former usually complicates the FDTD scheme and require a smaller time step for stability, the computer running time is complemented by the mesh reduction. The numerical dispersions of explicit fourth-order and Ty(2,4) $(FD)^2TD$ schemes are discussed in section 2.3.2 and section 2.3.3. The compact finite difference schemes requiring special treatments at the boundary and those numerical treatments are discussed in section 2.3.4 and section 2.3.5. The stability of introducting the numerical boundary treatment is discussed. The treatment of the finitely conducting (FEC) boundary is also discussed.

The excitation source is discussed in section 2.4. For the empty cavities with PEC boundary and loaded cavities with lossless dielectric material samples, the Q values of the cavities are infinite so only transient-state solution are obtained to validate the program. The source used for this case is a Blackman-Harris type that has very low sidelobes. For loaded cavities with lossy dielectric material sample, a single frequency sinusoidal source is used. For cavities, the Q factor and the resonant frequency are most desired quantities that need to be calculated. The Prony method in section 2.5 provides a method to estimates those two values without running a lenghty FDTD computation. The numerical results and discussion are presented in section 2.6, section 2.7 and section 2.8.

2.1 Frequency-Dependent FDTD Formulations with Second-Order Leapfrog Time-Stepping of Maxwell's Equations

2.1.1 The Scalar Equations of Maxwell's Equations

In differential form, Maxwell's equations in a dielectric dispersive medium can be written as

$$\begin{aligned} \nabla\times\vec{E} &= -[\mu]\frac{\partial\vec{H}}{\partial t} \\ \nabla\times\vec{H} &= \frac{\partial\vec{D}}{\partial t} + [\sigma]\vec{E} + \vec{J}_s \end{aligned} \tag{2.1}$$

where $[\sigma]$ and $[\mu]$, are electric conductivity, magnetic permeability which are non-dispersive in tensor form, respectively. $\vec{J}_s$ is the known impressed current source. The above constitutive parameters are further assumed to have the biaxial tensor form in the rectangular coordinate system given by

$$[\alpha] = \begin{bmatrix} \alpha_x & 0 & 0 \\ 0 & \alpha_y & 0 \\ 0 & 0 & \alpha_z \end{bmatrix} \tag{2.2}$$

where α represents the magnetic permeability or the electric conductivity.

For frequency-dependent dielectric material, the one-relaxation Debye equation is where the subsc

imaginary parts

related to the or

where ε'_{rs} and ε'

very large freque

values when τ_{ε} is

between $\vec{D}$ and

where ε_{rx}, ε_{ry},

Debye equation. (

The scalar eq

$$\varepsilon_r(\omega) = \varepsilon'_r(\omega) - j\varepsilon''_r(\omega) = \varepsilon'_{r\infty} + \frac{\varepsilon'_{rs} - \varepsilon'_{r\infty}}{1 + j\omega\tau_e} \tag{2.3}$$

where the subscript, r, denotes the word "relative". Moreover, ε'_r and ε''_r are the real and imaginary parts of the relative permittivity. The τ_e is a new *relaxation time constant* related to *the original relaxation time constant* τ by [19]

$$\tau_e = \tau\frac{\varepsilon'_{rs} + 2}{\varepsilon'_{r\infty} + 2} \tag{2.4}$$

where ε'_{rs} and $\varepsilon'_{r\infty}$ are the real part of the complex permittivity at zero frequency and at a very large frequency, respectively. Note that $\varepsilon_r(\omega)$ is equal to $\varepsilon'_r(\omega)$ and $\varepsilon'_{r\infty}$ can be any values when τ_e is equal to zero, the frequency-independent case. The constitutive relation between $\vec{D}$ and $\vec{E}$ is

$$\vec{D}(\omega) = \varepsilon_0\begin{bmatrix} \varepsilon_{rx} & 0 & 0 \\ 0 & \varepsilon_{ry} & 0 \\ 0 & 0 & \varepsilon_{rz} \end{bmatrix}\vec{E}(\omega) \tag{2.5}$$

where ε_{rx}, ε_{ry}, and ε_{rz} are the relative permittivities in different directions and satisfy Debye equation, (2.3).

The scalar equations of (2.1) in time domain can be written as

$$\begin{aligned} \mu_x\frac{\partial H_x}{\partial t} &= \frac{\partial E_y}{\partial z} - \frac{\partial E_z}{\partial y} \\ \mu_y\frac{\partial H_y}{\partial t} &= \frac{\partial E_z}{\partial x} - \frac{\partial E_x}{\partial z} \\ \mu_z\frac{\partial H_z}{\partial t} &= \frac{\partial E_x}{\partial y} - \frac{\partial E_y}{\partial x} \end{aligned} \tag{2.6}$$

The equation (2.

then the inverse

follow

2.1.2 The Fi

For the time

(2.7), and (2.9).

but $\vec{H}$ and the t

the time step n.

For the spatial

used. The finite

$$
\begin{aligned}
\frac{\partial D_x}{\partial t} &= \frac{\partial H_z}{\partial y} - \frac{\partial H_y}{\partial z} - \sigma_x E_x - J_{sx} \\
\frac{\partial D_y}{\partial t} &= \frac{\partial H_x}{\partial z} - \frac{\partial H_z}{\partial x} - \sigma_y E_y - J_{sy} . \\
\frac{\partial D_z}{\partial t} &= \frac{\partial H_y}{\partial x} - \frac{\partial H_x}{\partial y} - \sigma_z E_z - J_{sz}
\end{aligned}
\tag{2.7}
$$

The equation (2.5) can be written as

$$
\begin{aligned}
(1 + j\omega\tau_{ex})D_x &= \varepsilon_0 \varepsilon'_{rxs} E_x + \varepsilon_0 \varepsilon'_{rx\infty} \tau_{ex} j\omega E_x \\
(1 + j\omega\tau_{ey})D_y &= \varepsilon_0 \varepsilon'_{rys} E_y + \varepsilon_0 \varepsilon'_{ry\infty} \tau_{ey} j\omega E_y , \\
(1 + j\omega\tau_{ez})D_z &= \varepsilon_0 \varepsilon'_{rzs} E_z + \varepsilon_0 \varepsilon'_{rz\infty} \tau_{ez} j\omega E_z
\end{aligned}
\tag{2.8}
$$

then the inverse Fourier transform is applied; hence, the scalar equations are obtained as follow

$$
\begin{aligned}
D_x + \tau_{ex} \frac{\partial D_x}{\partial t} &= \varepsilon_0 \varepsilon'_{rxs} E_x + \varepsilon_0 \varepsilon'_{rx\infty} \tau_{ex} \frac{\partial E_x}{\partial t} \\
D_y + \tau_{ey} \frac{\partial D_y}{\partial t} &= \varepsilon_0 \varepsilon'_{rys} E_y + \varepsilon_0 \varepsilon'_{ry\infty} \tau_{ey} \frac{\partial E_y}{\partial t} . \\
D_z + \tau_{ez} \frac{\partial D_z}{\partial t} &= \varepsilon_0 \varepsilon'_{rzs} E_z + \varepsilon_0 \varepsilon'_{rz\infty} \tau_{ez} \frac{\partial E_z}{\partial t}
\end{aligned}
\tag{2.9}
$$

2.1.2 The Finite Difference Equations

For the time-stepping scheme, the leapfrog second-order scheme is applied to (2.6), (2.7), and (2.9). $\vec{D}$, $\vec{E}$, and the temporal derivative of $\vec{H}$ are evaluated at integer time step but $\vec{H}$ and the temporal derivative of $\vec{D}$ and $\vec{E}$ are evaluated at half integer time step. For the time step *n*, the $\vec{E}\big|^n$, $\vec{D}\big|^n$, and $\vec{H}\big|^{n+1/2}$ are considered to be the field distributions. For the spatial discretion, the second-order Yee scheme or higher-order scheme can be used. The finite difference approximation to the first derivative of those quantities is denoted by δ_t

one of H, E, D

locates at the s...

at half integer s...

ates; so are the

evaluated at inte...

space step along

of $\vec{E}$ are evalua...

locations as $\vec{E}$ ...

$$\delta_t H_x\Big|^{n}_{i,j+\ldots}$$

$$\delta_t H_y\Big|^{n}_{i+1\ldots}$$

$$\delta_t H_z\Big|^{n}_{i+1\ldots}$$

$$\delta_t D_x\Big|^{n+1/2}_{i+1/2,j,k}$$

$$\delta_t D_y\Big|^{n+1/2}_{i,j+1/2,k}$$

$$\delta_t D_z\Big|^{n+1/2}_{i,j,k+1/2}$$

$$D_x\Big|^{n+1/2}_{i+1/2,j,k} + \tau$$

$$D_y\Big|^{n+1/2}_{i,j+1/2,k} + \tau$$

$$D_z\Big|^{n+1/2}_{i,j,k+1/2} + \tau$$

denoted by $\delta_\alpha A_\beta$ where α and β represent one of x, y, z, and t parameters and A denotes one of H, E, D fields. The spatial locations of $\vec{E}$ and $\vec{H}$ are plotted in Figure 2.1 and $\vec{D}$, locates at the same location as $\vec{E}$ does. Note that E_x, $\partial E_x/\partial t$, and $\partial D_x/\partial t$ are evaluated at half integer spatial step along the x axis, but at integer spatial step along the other two axes; so are the E_y, E_z, and their corresponding time derivatives. The H_x, H_y, H_z are evaluated at integer spatial step along the x, y, and z axes, respectively, but at half integer space step along the other two axes; so is the time derivatives of $\vec{H}$. The spatial derivatives of $\vec{E}$ are evaluated at the same locations as $\vec{H}$ and that of $\vec{H}$ are evaluated at the same locations as $\vec{E}$. Hence, (2.6), (2.7), and (2.9) can be rewritten as

$$
\begin{aligned}
\delta_t H_x\Big|^n_{i,\,j+1/2,\,k+1/2} &= \frac{1}{\mu_x}\left(\delta_z E_y\Big|^n_{i,\,j+1/2,\,k+1/2} - \delta_y E_z\Big|^n_{i,\,j+1/2,\,k+1/2}\right)\\
\delta_t H_y\Big|^n_{i+1/2,\,j,\,k+1/2} &= \frac{1}{\mu_y}\left(\delta_x E_z\Big|^n_{i+1/2,\,j,\,k+1/2} - \delta_z E_x\Big|^n_{i+1/2,\,j,\,k+1/2}\right)\\
\delta_t H_z\Big|^n_{i+1/2,\,j+1/2,\,k} &= \frac{1}{\mu_z}\left(\delta_y E_x\Big|^n_{i+1/2,\,j+1/2,\,k} - \delta_x E_y\Big|^n_{i+1/2,\,j+1/2,\,k}\right)
\end{aligned}
\tag{2.10}
$$

$$
\begin{aligned}
\delta_t D_x\Big|^{n+1/2}_{i+1/2,\,j,\,k} &= \left(\delta_y H_z\Big|^{n+1/2}_{i+1/2,\,j,\,k} - \delta_z H_y\Big|^{n+1/2}_{i+1/2,\,j,\,k}\right) - \sigma_x E_x\Big|^{n+1/2}_{i+1/2,\,j,\,k} - J_x\Big|^{n+1/2}_{i+1/2,\,j,\,k}\\
\delta_t D_y\Big|^{n+1/2}_{i,\,j+1/2,\,k} &= \left(\delta_z H_x\Big|^{n+1/2}_{i,\,j+1/2,\,k} - \delta_x H_z\Big|^{n+1/2}_{i,\,j+1/2,\,k}\right) - \sigma_y E_y\Big|^{n+1/2}_{i,\,j+1/2,\,k} - J_y\Big|^{n+1/2}_{i,\,j+1/2,\,k}\\
\delta_t D_z\Big|^{n+1/2}_{i,\,j,\,k+1/2} &= \left(\delta_x H_y\Big|^{n+1/2}_{i,\,j,\,k+1/2} - \delta_y H_x\Big|^{n+1/2}_{i,\,j,\,k+1/2}\right) - \sigma_z E_z\Big|^{n+1/2}_{i,\,j,\,k+1/2} - J_z\Big|^{n+1/2}_{i,\,j,\,k+1/2}
\end{aligned}
\tag{2.11}
$$

$$
\begin{aligned}
D_x\Big|^{n+1/2}_{i+1/2,\,j,\,k} + \tau_{ex}\delta_t D_x\Big|^{n+1/2}_{i+1/2,\,j,\,k} &= \varepsilon_0\varepsilon'_{rxs}E_x\Big|^{n+1/2}_{i+1/2,\,j,\,k} + \varepsilon_0\varepsilon'_{rx\infty}\tau_{ex}\delta_t E_x\Big|^{n+1/2}_{i+1/2,\,j,\,k}\\
D_y\Big|^{n+1/2}_{i,\,j+1/2,\,k} + \tau_{ey}\delta_t D_y\Big|^{n+1/2}_{i,\,j+1/2,\,k} &= \varepsilon_0\varepsilon'_{rys}E_y\Big|^{n+1/2}_{i,\,j+1/2,\,k} + \varepsilon_0\varepsilon'_{ry\infty}\tau_{ey}\delta_t E_y\Big|^{n+1/2}_{i,\,j+1/2,\,k}\\
D_z\Big|^{n+1/2}_{i,\,j,\,k+1/2} + \tau_{ez}\delta_t D_z\Big|^{n+1/2}_{i,\,j,\,k+1/2} &= \varepsilon_0\varepsilon'_{rzs}E_z\Big|^{n+1/2}_{i,\,j,\,k+1/2} + \varepsilon_0\varepsilon'_{rz\infty}\tau_{ez}\delta_t E_z\Big|^{n+1/2}_{i,\,j,\,k+1/2}
\end{aligned}
\tag{2.12}
$$

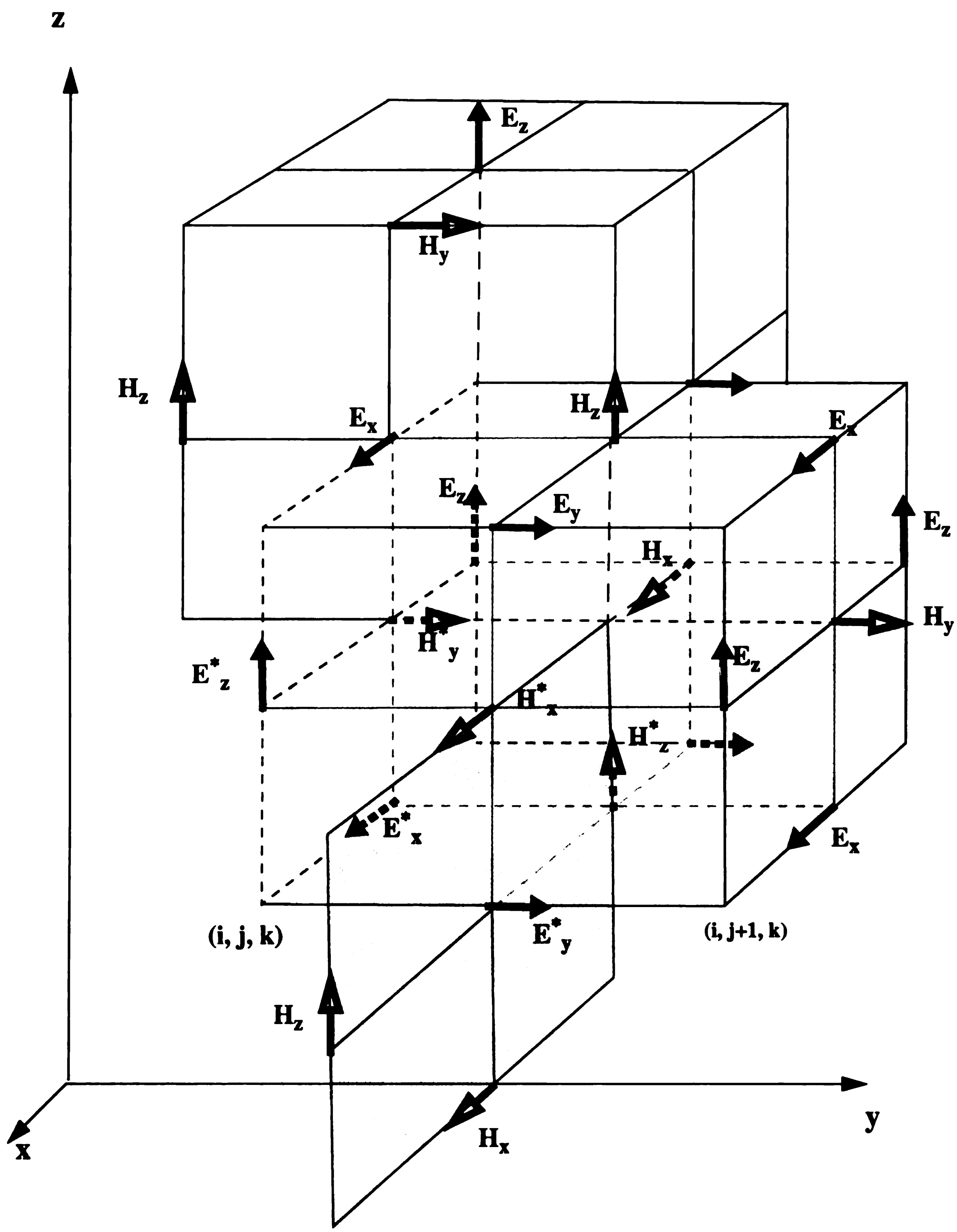

Figure 2.1 FDTD space lattice

Apply the

approximate th

rewritten as fo

$H_x|^{n+1/2}_{i,j+1/2}$

$H_y|^{n+1/2}_{i+1/2}$

$H_z|^{n+1/2}_{i+1/2}$

$D_x|^{n+}_{i+}$

$D_y|^{n+}_{i,j}$

Apply the second-order leapfrog scheme to time stepping and use the average value to approximate the D, E, J at $n + 1/2$ time steps, equations (2.10), (2.11), and (2.12) can be rewritten as follow.

$$\begin{aligned} H_x\Big|_{i,\,j+1/2,\,k+1/2}^{n+1/2} &= H_x\Big|_{i,\,j+1/2,\,k+1/2}^{n-1/2} \\ &\quad + \frac{\Delta t}{\mu_x}\left(\delta_z E_y\Big|_{i,\,j+1/2,\,k+1/2}^{n} - \delta_y E_z\Big|_{i,\,j+1/2,\,k+1/2}^{n}\right) \end{aligned} \tag{2.13}$$

$$\begin{aligned} H_y\Big|_{i+1/2,\,j,\,k+1/2}^{n+1/2} &= H_y\Big|_{i+1/2,\,j,\,k+1/2}^{n-1/2} \\ &\quad + \frac{\Delta t}{\mu_y}\left(\delta_x E_z\Big|_{i+1/2,\,j,\,k+1/2}^{n} - \delta_z E_x\Big|_{i+1/2,\,j,\,k+1/2}^{n}\right) \end{aligned} \tag{2.14}$$

$$\begin{aligned} H_z\Big|_{i+1/2,\,j+1/2,\,k}^{n+1/2} &= H_z\Big|_{i+1/2,\,j+1/2,\,k}^{n-1/2} \\ &\quad + \frac{\Delta t}{\mu_z}\left(\delta_y E_x\Big|_{i+1/2,\,j+1/2,\,k}^{n} - \delta_x E_y\Big|_{i+1/2,\,j+1/2,\,k}^{n}\right) \end{aligned} \tag{2.15}$$

$$\begin{aligned} D_x\Big|_{i+1/2,\,j,\,k}^{n+1} + \frac{\sigma_x \Delta t}{2} E_x\Big|_{i+1/2,\,j,\,k}^{n+1} &= D_x\Big|_{i+1/2,\,j,\,k}^{n} \\ -\frac{\sigma_x \Delta t}{2} E_x\Big|_{i+1/2,\,j,\,k}^{n} &+ \Delta t\left(\delta_y H_z\Big|_{i+1/2,\,j,\,k}^{n+1/2} - \delta_z H_y\Big|_{i+1/2,\,j,\,k}^{n+1/2}\right) \\ -\frac{\Delta t}{2}\left(J_x\Big|_{i+1/2,\,j,\,k}^{n+1} + J_x\Big|_{i+1/2,\,j,\,k}^{n}\right) & \end{aligned} \tag{2.16}$$

$$\begin{aligned} D_y\Big|_{i,\,j+1/2,\,k}^{n+1} + \frac{\sigma_y \Delta t}{2} E_y\Big|_{i,\,j+1/2,\,k}^{n+1} &= D_y\Big|_{i,\,j+1/2,\,k}^{n} \\ -\frac{\sigma_y \Delta t}{2} E_y\Big|_{i,\,j+1/2,\,k}^{n} &+ \Delta t\left(\delta_z H_x\Big|_{i,\,j+1/2,\,k}^{n+1/2} - \delta_x H_z\Big|_{i,\,j+1/2,\,k}^{n+1/2}\right) \\ -\frac{\Delta t}{2}\left(J_y\Big|_{i,\,j+1/2,\,k}^{n+1} + J_y\Big|_{i,\,j+1/2,\,k}^{n}\right) & \end{aligned} \tag{2.17}$$

D.

$1 +$

$= -$

$1 +$

$= -$

$1 +$

$= -$

If we solve

obtain the finite

$$
\begin{aligned}
D_z\Big|_{i,j,k+1/2}^{n+1} + \frac{\sigma_z \Delta t}{2} E_z\Big|_{i,j,k+1/2}^{n+1} &= D_z\Big|_{i,j,k+1/2}^{n} \\
&- \frac{\sigma_z \Delta t}{2} E_z\Big|_{i,j,k+1/2}^{n} + \Delta t\left(\delta_x H_y\Big|_{i,j,k+1/2}^{n+1/2} - \delta_y H_x\Big|_{i,j,k+1/2}^{n+1/2}\right) \\
&- \frac{\Delta t}{2}\left(J_z\Big|_{i,j,k+1/2}^{n+1} + J_z\Big|_{i,j,k+1/2}^{n}\right)
\end{aligned} \tag{2.18}
$$

$$
\begin{aligned}
&\left(1 + \frac{2\tau_{ex}}{\Delta t}\right) D_x\Big|_{i+1/2,j,k}^{n+1} - \varepsilon_0\left(\varepsilon'_{rxs} + \varepsilon'_{rx\infty}\frac{2\tau_{ex}}{\Delta t}\right) E_x\Big|_{i+1/2,j,k}^{n+1} \\
&= -\left(1 - \frac{2\tau_{ex}}{\Delta t}\right) D_x\Big|_{i+1/2,j,k}^{n} + \varepsilon_0\left(\varepsilon'_{rxs} - \varepsilon'_{rx\infty}\frac{2\tau_{ex}}{\Delta t}\right) E_x\Big|_{i+1/2,j,k}^{n}
\end{aligned} \tag{2.19}
$$

$$
\begin{aligned}
&\left(1 + \frac{2\tau_{ey}}{\Delta t}\right) D_y\Big|_{i,j+1/2,k}^{n+1} - \varepsilon_0\left(\varepsilon'_{rys} + \varepsilon'_{ry\infty}\frac{2\tau_{ey}}{\Delta t}\right) E_y\Big|_{i,j+1/2,k}^{n+1} \\
&= -\left(1 - \frac{2\tau_{ey}}{\Delta t}\right) D_y\Big|_{i,j+1/2,k}^{n} + \varepsilon_0\left(\varepsilon'_{rys} - \varepsilon'_{ry\infty}\frac{2\tau_{ey}}{\Delta t}\right) E_y\Big|_{i,j+1/2,k}^{n}
\end{aligned} \tag{2.20}
$$

$$
\begin{aligned}
&\left(1 + \frac{2\tau_{ez}}{\Delta t}\right) D_z\Big|_{i,j,k+1/2}^{n+1} - \varepsilon_0\left(\varepsilon'_{rzs} + \varepsilon'_{rz\infty}\frac{2\tau_{ez}}{\Delta t}\right) E_z\Big|_{i,j,k+1/2}^{n+1} \\
&= -\left(1 - \frac{2\tau_{ez}}{\Delta t}\right) D_z\Big|_{i,j,k+1/2}^{n} + \varepsilon_0\left(\varepsilon'_{rzs} - \varepsilon'_{rz\infty}\frac{2\tau_{ez}}{\Delta t}\right) E_z\Big|_{i,j,k+1/2}^{n}
\end{aligned} \tag{2.21}
$$

If we solve the equations (2.16) to (2.18) and (2.19) to (2.21) simultaneously, we will obtain the finite difference expression for $\vec{D}$ and $\vec{E}$ as follow

$$
\begin{aligned}
D_x\Big|_{i+1/2,j,k}^{n+1} &= \beta_{1x} D_x\Big|_{i+1/2,j,k}^{n} - \beta_{2x} E_x\Big|_{i+1/2,j,k}^{n} \\
&+ \beta_{3x}\left(\delta_y H_z\Big|_{i+1/2,j,k}^{n+1/2} - \delta_z H_y\Big|_{i+1/2,j,k}^{n+1/2}\right) \\
&- \frac{\beta_{3x}}{2}\left(J_x\Big|_{i+1/2,j,k}^{n+1} + J_x\Big|_{i+1/2,j,k}^{n}\right)
\end{aligned} \tag{2.22}
$$

D

E

E

E =

here

$$
\begin{aligned}
D_y\Big|_{i,\,j+1/2,\,k}^{n+1} = {} & \beta_{1y} D_y\Big|_{i,\,j+1/2,\,k}^{n} - \beta_{2y} E_y\Big|_{i,\,j+1/2,\,k}^{n} \\
& + \beta_{3y}\left(\delta_z H_x\Big|_{i,\,j+1/2,\,k}^{n+1/2} - \delta_x H_z\Big|_{i,\,j+1/2,\,k}^{n+1/2}\right) \\
& - \frac{\beta_{3y}}{2}\left(J_y\Big|_{i,\,j+1/2,\,k}^{n+1} + J_y\Big|_{i,\,j+1/2,\,k}^{n}\right)
\end{aligned} \tag{2.23}
$$

$$
\begin{aligned}
D_z\Big|_{i,\,j,\,k+1/2}^{n+1} = {} & \beta_{1z} D_z\Big|_{i,\,j,\,k+1/2}^{n} - \beta_{2z} E_z\Big|_{i,\,j,\,k+1/2}^{n} \\
& + \beta_{3z}\left(\delta_x H_y\Big|_{i,\,j,\,k+1/2}^{n+1/2} - \delta_y H_x\Big|_{i,\,j,\,k+1/2}^{n+1/2}\right) \\
& - \frac{\beta_{3z}}{2}\left(J_z\Big|_{i,\,j,\,k+1/2}^{n+1} + J_z\Big|_{i,\,j,\,k+1/2}^{n}\right)
\end{aligned} \tag{2.24}
$$

$$
\begin{aligned}
E_x\Big|_{i+1/2,\,j,\,k}^{n+1} = {} & \gamma_{1x} D_x\Big|_{i+1/2,\,j,\,k}^{n} - \gamma_{2x} E_x\Big|_{i+1/2,\,j,\,k}^{n} \\
& + \gamma_{3x}\left(\delta_y H_z\Big|_{i+1/2,\,j,\,k}^{n+1/2} - \delta_z H_y\Big|_{i+1/2,\,j,\,k}^{n+1/2}\right) \\
& - \frac{\gamma_{3x}}{2}\left(J_x\Big|_{i+1/2,\,j,\,k}^{n+1} + J_x\Big|_{i+1/2,\,j,\,k}^{n}\right)
\end{aligned} \tag{2.25}
$$

$$
\begin{aligned}
E_y\Big|_{i,\,j+1/2,\,k}^{n+1} = {} & \gamma_{1y} D_y\Big|_{i,\,j+1/2,\,k}^{n} - \gamma_{2y} E_y\Big|_{i,\,j+1/2,\,k}^{n} \\
& + \gamma_{3y}\left(\delta_z H_x\Big|_{i,\,j+1/2,\,k}^{n+1/2} - \delta_x H_z\Big|_{i,\,j+1/2,\,k}^{n+1/2}\right) \\
& - \frac{\gamma_{3y}}{2}\left(J_y\Big|_{i,\,j+1/2,\,k}^{n+1} + J_y\Big|_{i,\,j+1/2,\,k}^{n}\right)
\end{aligned} \tag{2.26}
$$

$$
\begin{aligned}
E_z\Big|_{i,\,j,\,k+1/2}^{n+1} = {} & \gamma_{1z} D_z\Big|_{i,\,j,\,k+1/2}^{n} - \gamma_{2z} E_z\Big|_{i,\,j,\,k+1/2}^{n} \\
& + \gamma_{3z}\left(\delta_x H_y\Big|_{i,\,j,\,k+1/2}^{n+1/2} - \delta_y H_x\Big|_{i,\,j,\,k+1/2}^{n+1/2}\right) \\
& - \frac{\gamma_{3z}}{2}\left(J_z\Big|_{i,\,j,\,k+1/2}^{n+1} + J_z\Big|_{i,\,j,\,k+1/2}^{n}\right)
\end{aligned} \tag{2.27}
$$

where

and $\alpha = x, y, or$

Equations (2.

are used to calc

independent case.

$$\beta_{1\alpha} = \frac{\sigma_\alpha\left(\tau_{e\alpha} - \frac{\Delta t}{2}\right) + \varepsilon_0\left(\varepsilon'_{r\alpha s} + \varepsilon'_{r\alpha\infty}\frac{2\tau_{e\alpha}}{\Delta t}\right)}{\sigma_\alpha\left(\tau_{e\alpha} + \frac{\Delta t}{2}\right) + \varepsilon_0\left(\varepsilon'_{r\alpha s} + \varepsilon'_{r\alpha\infty}\frac{2\tau_{e\alpha}}{\Delta t}\right)} \tag{2.28}$$

$$\beta_{2\alpha} = \frac{2\sigma_\alpha\tau_{e\alpha}\varepsilon_0\varepsilon'_{r\alpha\infty}}{\sigma_\alpha\left(\frac{\Delta t}{2} + \tau_{e\alpha}\right) + \varepsilon_0\left(\varepsilon'_{r\alpha s} + \varepsilon'_{r\alpha\infty}\frac{2\tau_{e\alpha}}{\Delta t}\right)} \tag{2.29}$$

$$\beta_{3\alpha} = \frac{\varepsilon_0\left(\varepsilon'_{r\alpha s} + \varepsilon'_{r\alpha\infty}\frac{2\tau_{e\alpha}}{\Delta t}\right)\Delta t}{\sigma_\alpha\left(\frac{\Delta t}{2} + \tau_{e\alpha}\right) + \varepsilon_0\left(\varepsilon'_{r\alpha s} + \varepsilon'_{r\alpha\infty}\frac{2\tau_{e\alpha}}{\Delta t}\right)} \tag{2.30}$$

$$\gamma_{1\alpha} = \frac{2}{\sigma_\alpha\left(\frac{\Delta t}{2} + \tau_{e\alpha}\right) + \varepsilon_0\left(\varepsilon'_{r\alpha s} + \varepsilon'_{r\alpha\infty}\frac{2\tau_{e\alpha}}{\Delta t}\right)} \tag{2.31}$$

$$\gamma_{2\alpha} = \frac{\sigma_\alpha\left(\frac{\Delta t}{2} + \tau_{e\alpha}\right) + \varepsilon_0\left(\varepsilon'_{r\alpha s} - \varepsilon'_{r\alpha\infty}\frac{2\tau_{e\alpha}}{\Delta t}\right)}{\sigma_\alpha\left(\frac{\Delta t}{2} + \tau_{e\alpha}\right) + \varepsilon_0\left(\varepsilon'_{r\alpha s} + \varepsilon'_{r\alpha\infty}\frac{2\tau_{e\alpha}}{\Delta t}\right)} \tag{2.32}$$

$$\gamma_{3\alpha} = \frac{\Delta t + 2\tau_{e\alpha}}{\sigma_\alpha\left(\frac{\Delta t}{2} + \tau_{e\alpha}\right) + \varepsilon_0\left(\varepsilon'_{r\alpha s} + \varepsilon'_{r\alpha\infty}\frac{2\tau_{e\alpha}}{\Delta t}\right)} \tag{2.33}$$

and $\alpha = x, y, or\ z$.

Equations (2.13) to (2.15) and (2.22) to (2.27) are the finite difference equations that are used to calculate the field strength. When $\tau_{e\alpha}$ is equal to zero, the frequency-independent case, equations (2.28) to (2.33) become

$$\beta_{1\alpha} = \frac{\varepsilon_0 \varepsilon'_{r\alpha s} - \sigma_\alpha \frac{\Delta t}{2}}{\varepsilon_0 \varepsilon'_{r\alpha s} + \sigma_\alpha \frac{\Delta t}{2}}, \tag{2.34}$$

$$\beta_{2\alpha} = 0, \tag{2.35}$$

$$\beta_{3\alpha} = \frac{\varepsilon_0 \varepsilon'_{r\alpha s} \Delta t}{\varepsilon_0 \varepsilon'_{r\alpha s} + \sigma_\alpha \frac{\Delta t}{2}}, \tag{2.36}$$

$$\gamma_{1\alpha} = \frac{2}{\varepsilon_0 \varepsilon'_{r\alpha s} + \sigma_\alpha \frac{\Delta t}{2}}, \tag{2.37}$$

$$\gamma_{2\alpha} = 1, \tag{2.38}$$

and

$$\gamma_{3\alpha} = \frac{\Delta t}{\varepsilon_0 \varepsilon'_{r\alpha s} + \sigma_\alpha \frac{\Delta t}{2}}. \tag{2.39}$$

Hence, the equations (2.24) and (2.27) become the same equation as follows:

$$\begin{aligned} E_x\Big|_{i+1/2,\,j,\,k}^{n+1} &= \frac{1 - \dfrac{\sigma_x \Delta t}{2\varepsilon_0 \varepsilon'_{rxs}}}{1 + \dfrac{\sigma_x \Delta t}{2\varepsilon_0 \varepsilon'_{rxs}}} E_x\Big|_{i+1/2,\,j,\,k}^{n} - \frac{1}{2}\frac{\dfrac{\Delta t}{\varepsilon_0 \varepsilon'_{rxs}}}{1 + \dfrac{\sigma_x \Delta t}{2\varepsilon_0 \varepsilon'_{rxs}}}\left(J_x\Big|_{i+1/2,\,j,\,k}^{n+1} + J_x\Big|_{i+1/2,\,j,\,k}^{n}\right) \\ &\quad + \frac{\dfrac{\Delta t}{\varepsilon_0 \varepsilon'_{rxs}}}{1 + \dfrac{\sigma_x \Delta t}{2\varepsilon_0 \varepsilon'_{rxs}}}\left(\delta_y H_z\Big|_{i+1/2,\,j,\,k}^{n+1/2} - \delta_z H_y\Big|_{i+1/2,\,j,\,k}^{n+1/2}\right) \end{aligned} \tag{2.40}$$

$E_x\Big|_{i,j+1/2,k}^{n+1} =$

$E_z\Big|_{i,j,k+1/2}^{n+1} =$

and the original

and equations (

2.2 The Yee

Using the s

and (2.42) an

representation o

$H_x\Big|_{i,j+1/2}^{n+1/2}$

$+\frac{\Delta t}{\mu_x}\Big(E$

$$E_y\Big|_{i,j+1/2,k}^{n+1} = \frac{1-\dfrac{\sigma_y\Delta t}{2\varepsilon_0\varepsilon'_{rys}}}{1+\dfrac{\sigma_y\Delta t}{2\varepsilon_0\varepsilon'_{rys}}}E_y\Big|_{i,j+1/2,k}^{n} - \frac{1}{2}\frac{\dfrac{\Delta t}{\varepsilon_0\varepsilon'_{rys}}}{1+\dfrac{\sigma_y\Delta t}{2\varepsilon_0\varepsilon'_{rys}}}\left(J_y\Big|_{i,j+1/2,k}^{n+1} + J_y\Big|_{i,j+1/2,k}^{n}\right)$$

$$+\frac{\dfrac{\Delta t}{\varepsilon_0\varepsilon'_{rys}}}{1+\dfrac{\sigma_y\Delta t}{2\varepsilon_0\varepsilon'_{rys}}}\left(\delta_z H_x\Big|_{i,j+1/2,k}^{n+1/2} - \delta_x H_z\Big|_{i,j+1/2,k}^{n+1/2}\right) \tag{2.41}$$

$$E_z\Big|_{i,j,k+1/2}^{n+1} = \frac{1-\dfrac{\sigma_z\Delta t}{2\varepsilon_0\varepsilon'_{rzs}}}{1+\dfrac{\sigma_z\Delta t}{2\varepsilon_0\varepsilon'_{rzs}}}E_z\Big|_{i,j,k+1/2}^{n} - \frac{1}{2}\frac{\dfrac{\Delta t}{\varepsilon_0\varepsilon'_{rzs}}}{1+\dfrac{\sigma_z\Delta t}{2\varepsilon_0\varepsilon'_{rzs}}}\left(J_z\Big|_{i,j,k+1/2}^{n+1} + J_z\Big|_{i,j,k+1/2}^{n}\right)$$

$$+\frac{\dfrac{\Delta t}{\varepsilon_0\varepsilon'_{rzs}}}{1+\dfrac{\sigma_z\Delta t}{2\varepsilon_0\varepsilon'_{rzs}}}\left(\delta_x H_y\Big|_{i,j,k+1/2}^{n+1/2} - \delta_y H_x\Big|_{i,j,k+1/2}^{n+1/2}\right) \tag{2.42}$$

and the original Yee's finite difference expression can be derived from the above equations and equations (2.13) to (2.15).

2.2 The Yee's Algorithm

Using the second-order central difference approximation to space derivative in (2.15) and (2.42) and no current source inside the computational space then the Yee's representation of Maxwell's equations are

$$H_x\Big|_{i,j+1/2,k+1/2}^{n+1/2} = H_x\Big|_{i,j+1/2,k+1/2}^{n-1/2}$$

$$+\frac{\Delta t}{\mu_x}\left(\frac{E_y\Big|_{i,j+1/2,k+1/2}^{n} - E_y\Big|_{i,j+1/2,k}^{n}}{\Delta z} - \frac{E_z\Big|_{i,j+1,k+1/2}^{n} - E_z\Big|_{i,j,k+1/2}^{n}}{\Delta y}\right) \tag{2.43}$$

$H|^{n+1}_{i+1}$

$+\frac{\Delta t}{\mu}$

$H_z|^{n+1/2}_{i+1/2}$

$+\frac{\Delta t}{\mu_z}\frac{E_x}{}$

$E_x|^{n+1}_{i+1/2,j,k} =$

$H_z|^{n+1/2}_{i+1/2}$

$E_y|^{n+1}_{i,j+1/2,k} =$

$H_x|^{n+1/2}_{i,j+1/2}$

$E_z|^{n+1}_{i,j,k+1/2} =$

$H_y|^{n+1/2}_{i+1/2,j}$

$$H_y\Big|_{i+1/2,\,j,\,k+1/2}^{n+1/2} = H_y\Big|_{i+1/2,\,j,\,k+1/2}^{n-1/2} + \frac{\Delta t}{\mu_y}\left(\frac{E_z\Big|_{i+1,\,j,\,k+1/2}^{n} - E_z\Big|_{i,\,j,\,k+1/2}^{n}}{\Delta x} - \frac{E_x\Big|_{i+1/2,\,j,\,k+1}^{n} - E_x\Big|_{i+1/2,\,j,\,k}^{n}}{\Delta z}\right) \tag{2.44}$$

$$H_z\Big|_{i+1/2,\,j+1/2,\,k}^{n+1/2} = H_z\Big|_{i+1/2,\,j+1/2,\,k}^{n-1/2} + \frac{\Delta t}{\mu_z}\left(\frac{E_x\Big|_{i+1/2,\,j+1,\,k}^{n} - E_x\Big|_{i+1/2,\,j,\,k}^{n}}{\Delta y} - \frac{E_y\Big|_{i+1,\,j+1/2,\,k}^{n} - E_y\Big|_{i+1,\,j+1/2,\,k}^{n}}{\Delta x}\right) \tag{2.45}$$

$$E_x\Big|_{i+1/2,\,j,\,k}^{n+1} = \frac{1 - \dfrac{\sigma_x \Delta t}{2\varepsilon_0 \varepsilon'_{rxs}}}{1 + \dfrac{\sigma_x \Delta t}{2\varepsilon_0 \varepsilon'_{rxs}}} E_x\Big|_{i+1/2,\,j,\,k}^{n} + \frac{\dfrac{\Delta t}{\varepsilon_0 \varepsilon'_{rxs}}}{1 + \dfrac{\sigma_x \Delta t}{2\varepsilon_0 \varepsilon'_{rxs}}} \cdot \left(\frac{H_z\Big|_{i+1/2,\,j+1/2,\,k}^{n+1/2} - H_z\Big|_{i+1/2,\,j-1/2,\,k}^{n+1/2}}{\Delta y} - \frac{H_z\Big|_{i+1/2,\,j,\,k+1/2}^{n+1/2} - H_z\Big|_{i+1/2,\,j,\,k-1/2}^{n+1/2}}{\Delta z}\right) \tag{2.46}$$

$$E_y\Big|_{i,\,j+1/2,\,k}^{n+1} = \frac{1 - \dfrac{\sigma_y \Delta t}{2\varepsilon_0 \varepsilon'_{rys}}}{1 + \dfrac{\sigma_y \Delta t}{2\varepsilon_0 \varepsilon'_{rys}}} E_y\Big|_{i,\,j+1/2,\,k}^{n} + \frac{\dfrac{\Delta t}{\varepsilon_0 \varepsilon'_{rys}}}{1 + \dfrac{\sigma_y \Delta t}{2\varepsilon_0 \varepsilon'_{rys}}} \cdot \left(\frac{H_x\Big|_{i,\,j+1/2,\,k+1/2}^{n+1/2} - H_x\Big|_{i,\,j+1/2,\,k-1/2}^{n+1/2}}{\Delta z} - \frac{H_z\Big|_{i+1/2,\,j+1/2,\,k}^{n+1/2} - H_z\Big|_{i-1/2,\,j+1/2,\,k}^{n+1/2}}{\Delta x}\right) \tag{2.47}$$

$$E_z\Big|_{i,\,j,\,k+1/2}^{n+1} = \frac{1 - \dfrac{\sigma_z \Delta t}{2\varepsilon_0 \varepsilon'_{rzs}}}{1 + \dfrac{\sigma_z \Delta t}{2\varepsilon_0 \varepsilon'_{rzs}}} E_z\Big|_{i,\,j,\,k+1/2}^{n} + \frac{\dfrac{\Delta t}{\varepsilon_0 \varepsilon'_{rzs}}}{1 + \dfrac{\sigma_z \Delta t}{2\varepsilon_0 \varepsilon'_{rzs}}} \cdot \left(\frac{H_y\Big|_{i+1/2,\,j,\,k+1/2}^{n+1/2} - H_y\Big|_{i-1/2,\,j,\,k+1/2}^{n+1/2}}{\Delta x} - \frac{H_x\Big|_{i,\,j+1/2,\,k+1/2}^{n+1/2} - H_x\Big|_{i,\,j-1/2,\,k+1/2}^{n+1/2}}{\Delta y}\right) \tag{2.48}$$

2.2.1 Stabil

The stabi

approximation

presented by T

where Δt is th

directions, res

condition. Not

region. Genera

which is less t

An exact

depends on

material prop

stability can b

time step. In

diverges then

2.2.2 Nume

The phase

vacuum spee

2.2.1 Stability Condition

The stability condition is required to avoid numerical instability in finite difference approximation schemes. The stability condition of Yee algorithm is first correctly presented by Taflove[3] and is

$$\Delta t \leq \frac{1}{c\sqrt{\frac{1}{(\Delta x)^2}+\frac{1}{(\Delta y)^2}+\frac{1}{(\Delta z)^2}}} \tag{2.49}$$

where Δt is the time step and Δx, Δy, and Δz are mesh sizes along the x, y, and z directions, respectively. The (2.49) is also called the Courant-Friedrichs-Lewy (CFL) condition. Note that the CFL condition is derived by assuming a homogenous spatial region. Generally, the CFL value is defined as follow:

$$CFL = c\Delta t\sqrt{\frac{1}{(\Delta x)^2}+\frac{1}{(\Delta y)^2}+\frac{1}{(\Delta z)^2}} \tag{2.50}$$

which is less than or equal to *1*.

An exact stability condition for general case is usually difficult to derived since it depends on numerical boundary conditions, variable and unstructured meshing, and material properties. However, substantial modeling experience has shown that numerical stability can be maintained for many thousands of iterations with the proper choice of the time step. In the practical modeling, (2.49) is usually used. If the numerical computation diverges then a smaller time step is used, and so on.

2.2.2 Numerical Dispersion

The phase velocity of numerical wave modes in the FDTD grid can differ from the vacuum speed of light, in fact varying with the modal wavelength, the direction of propagation n

The dispe

where c is the

along the x, y, z

The numeric

the plane mon

implementation

dimension Yee a

$$\left[\frac{1}{c\Delta t}\sin\left(\frac{\omega}{2}\right.\right.$$

where $\tilde{k}_x$, $\tilde{k}_y$, a

Assume Δx =

number of grid

$$\frac{3}{a^2}\left[\sin\left(\frac{a}{\sqrt{}}\right.\right.$$

where $\tilde{k} = \lambda\tilde{k}/$

computational s

angles in the sp

Several con

follow.

propagation in the grid, and the grid discretization.

The dispersion relation for a plane wave in a continuous lossless medium is simply

$$\frac{\omega^2}{c^2} = k_x^2 + k_y^2 + k_z^2 \tag{2.51}$$

where c is the speed of light, ω is the radian frequency, and k_x, k_y, k_z are wavenumbers along the x, y, z axes in this medium.

The numerical dispersion equation for FDTD scheme can be obtained by substituting the plane monochromatic traveling-wave trial solutions into the finite-difference implementation of Maxwell's equations. The dispersion equation[16] of full three-dimension Yee algorithm is

$$\left[\frac{1}{c\Delta t}\sin\left(\frac{\omega\Delta t}{2}\right)\right]^2 = \left[\frac{1}{\Delta x}\sin\left(\frac{\tilde{k}_x\Delta x}{2}\right)\right]^2 + \left[\frac{1}{\Delta y}\sin\left(\frac{\tilde{k}_y\Delta y}{2}\right)\right]^2 + \left[\frac{1}{\Delta z}\sin\left(\frac{\tilde{k}_z\Delta z}{2}\right)\right]^2 \tag{2.52}$$

where $\tilde{k}_x$, $\tilde{k}_y$, and $\tilde{k}_z$ are wavenumbers along the x, y, z axes in the computational space. Assume $\Delta x = \Delta y = \Delta z = \Delta$, choose $CFL = a$, and define $R = \lambda/\Delta$ which is the number of grid cells in one wavelength, then (2.52) can be rewritten as

$$\frac{3}{a^2}\left[\sin\left(\frac{a\pi}{\sqrt{3}R}\right)\right]^2 = \sin\left(\frac{\bar{k}\sin\theta\cos\phi}{R}\right)^2 + \sin\left(\frac{\bar{k}\sin\theta\sin\phi}{R}\right)^2 + \sin\left(\frac{\bar{k}\cos\theta}{R}\right)^2 \tag{2.53}$$

where $\bar{k} = \lambda\tilde{k}/2$ which is equivalent to $\bar{v}_p/c = \pi/\bar{k}$ where $\bar{v}_p$ is speed of wave in computational space and $\tilde{k}^2 = \tilde{k}_x^{\ 2} + \tilde{k}_y^{\ 2} + \tilde{k}_z^{\ 2}$. The θ and ϕ are polar and azimuthal angles in the spherical coordinate system.

Several conclusions can be observed from (2.52) and (2.53) and are summarized as follow.

(1) The Y
tiona
cal in
(2) The s
(3) The la
ing the
CFL va
(4) There is
schemes
(5) The num
ical pha
FDTD g
(6) The num
nents of
nents. Th
pass cha
(7) The num
cal mode

(1) The Yee's FDTD scheme gives a phase error. The speed of wave in the computational space is less than that in free space. However, (2.52) and (2.53) are indentical in the limit as Δt, Δx, Δy, and Δz all go to zero.

(2) The smaller the CFL values, the larger the phase error from Figure 2.2.

(3) The larger the R, the smaller the phase error from Figure 2.3. The effect on reducing the phase error due to change of R is about 100 time that due to change of CFL values.

(4) There is a numerical phase velocity anisotropy in Yee algorithm or other FDTD schemes from Figure 2.3 and Figure 2.4.

(5) The number of grids in one wavelength has a lower bound that makes the numerical phase velocity goes to zero and the wave can no longer propagate in the FDTD grid from Figure 2.5.

(6) The numerical dispersion occurs because the higher-spatial-frequency components of wave propagate more slowly than the lower-spatial-frequency components. This numerical dispersion causes pulse broadening due to the spatial low-pass characters in FDTD schemes.

(7) The numerical dispersion can lead to spurious refraction of propagation numerical modes if the grid cell size is a function of position in the grid.

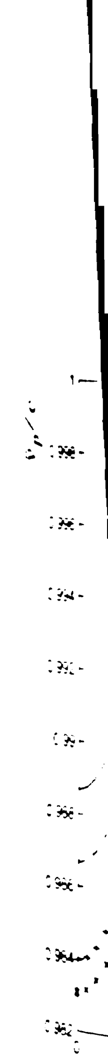

Fig
CH

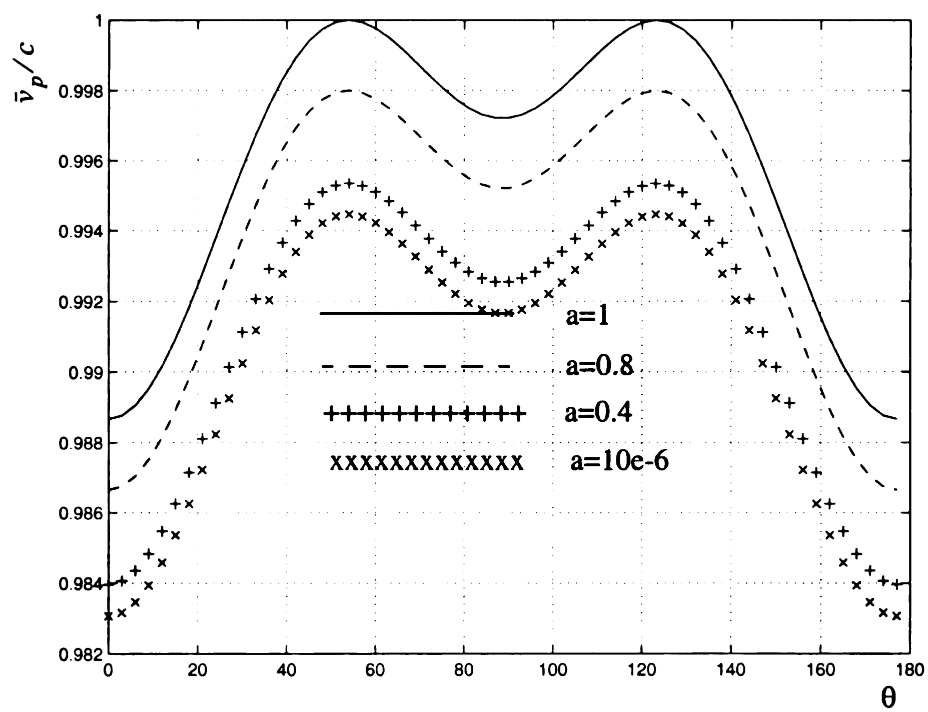

Figure 2.2 Variation of the numerical phase velocity with CFL values at $R = 10$ and $\phi = \pi/4$.

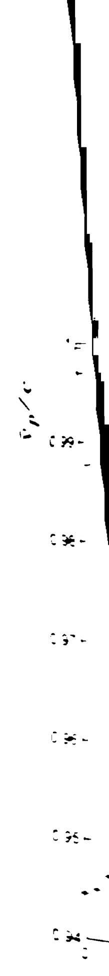

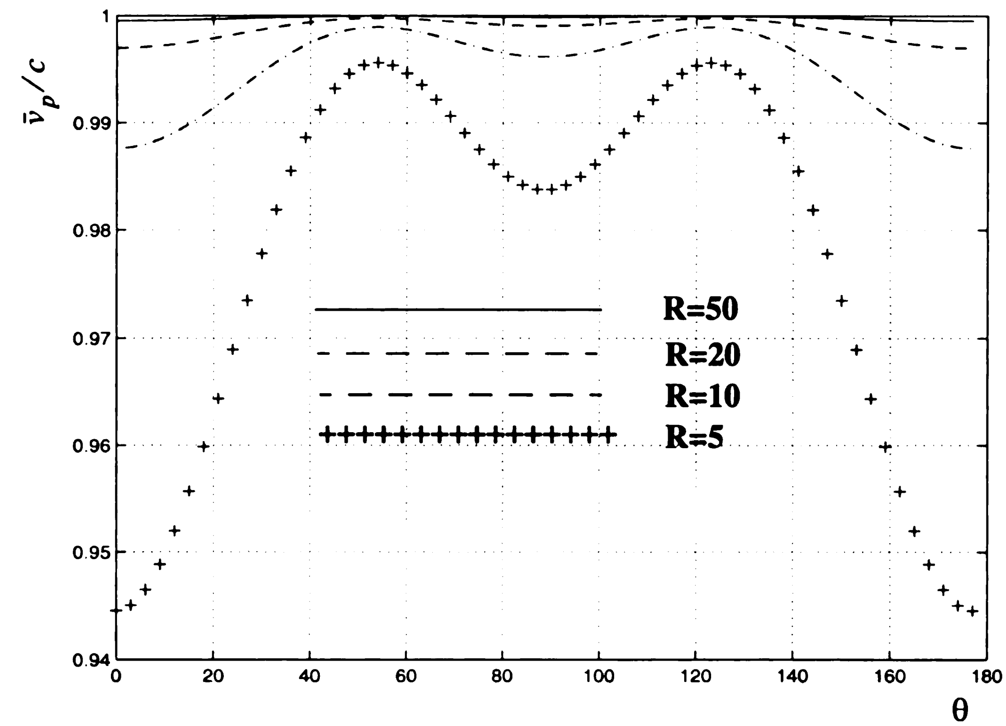

Figure 2.3 Variation of the numerical phase velocity with R at a = 0.9 and $\phi = \pi/4$.

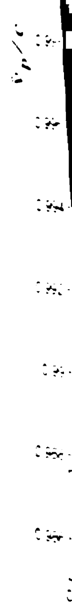

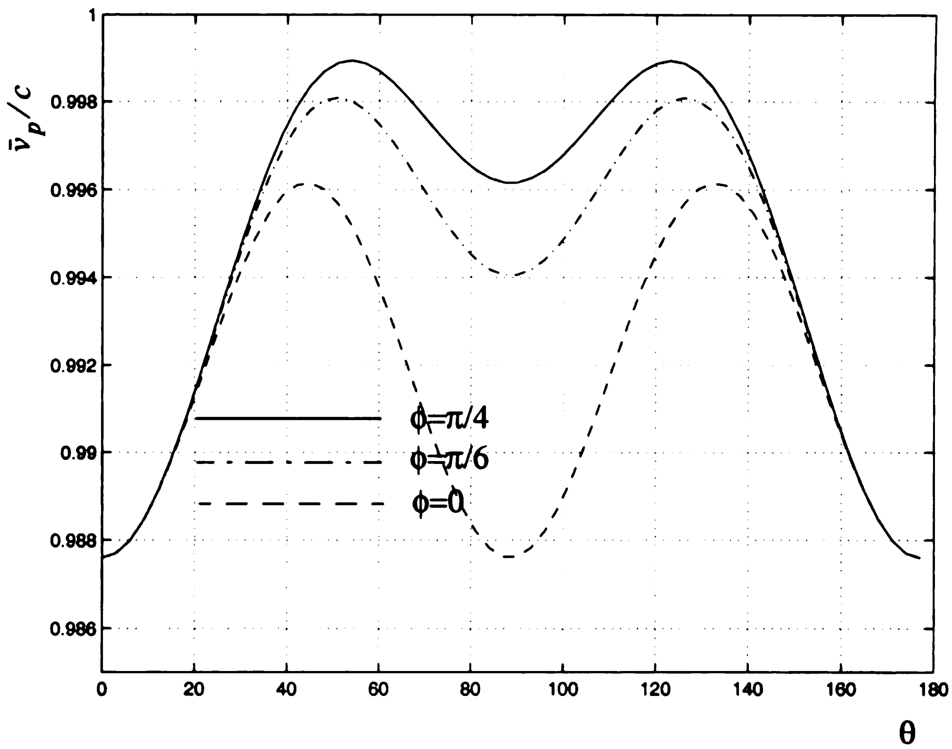

Figure 2.4 Variation of the numerical phase velocity with φ at *a=0.9* and *R=10*.

Fi
wi

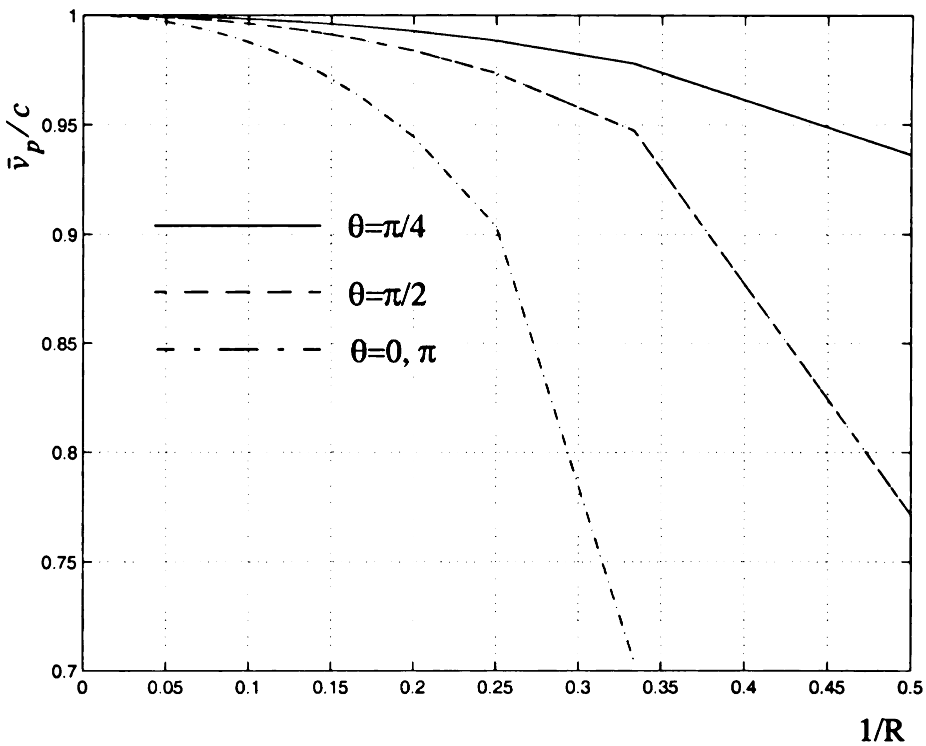

Figure 2.5 Variation of the numerical phase velocity with *1/R* at *a=0.9* and φ=π/4.

2.3 The T

From the

from the calc

more accura

boundary pr

approximation

spatial derivati

spatial scheme.

main disadvanta

time step is usu

troublesome w

spatial finite di

field points and

2.3.1 The Fo

The fourth-

and implicit sch

Explicit col

Explicit sta

2.3 The Ty(2,4) $(FD)^2TD$ Algorithm

From the analysis in section 2.2.2, the phase error in Yee algorithm keeps this scheme from the calculation EM fields of an electrical larger object or from applications that need more accuracy, such as the phase cancellation technique. In the cavities with FEC boundary problem, the phase error and the error from surface impedance boundary approximation are two main errors in the FDTD formulation. Hence, the fourth-order spatial derivatives is employed to reduce the cumulative phase error. For fourth-order spatial scheme, special boundary treatment and degraded stability condition are the two main disadvantage. The degraded stability condition is not very significant since a smaller time step is usually used in FDTD schemes. The larger stencil on the FDTD mesh is very troublesome when dealing with material discontinuities. However, the implicit staggered spatial finite difference schemes used in this chapter simplifies this problem by using two field points and three field derivative points.

2.3.1 The Fourth-Order Space Derivatives

The fourth-order finite difference expression can be categorized as explicit schemes and implicit schemes as follow:

Explicit collocated scheme

$$\left(\frac{\partial u}{\partial x}\right)_i \cong \frac{8(u_{i+1}-u_{i-1})-(u_{i+2}-u_{i-2})}{12\Delta x} \tag{2.54}$$

Explicit staggered scheme

$$\left(\frac{\partial u}{\partial x}\right)_i \cong \frac{27(u_{i+1/2}-u_{i-1/2})-(u_{i+3/2}-u_{i-3/2})}{24\Delta x} \tag{2.55}$$

Implicit

Implicit s

All above equa

The compact fi

of (2.57).

2.3.2 Disper

For simplic

$\varepsilon = 1,\ \sigma = 0$

where $\vec{V} = \vec{H}$

difference to th

then the followi

Implicit collocated scheme

$$\frac{\left(\frac{\partial u}{\partial x}\right)_{i+1}+\left(\frac{\partial u}{\partial x}\right)_{i-1}}{6}+\frac{2}{3}\left(\frac{\partial u}{\partial x}\right)_i \cong \frac{u_{i+1}-u_{i-1}}{2\Delta x} \tag{2.56}$$

Implicit staggered scheme

$$\frac{\left(\frac{\partial u}{\partial x}\right)_{i+1}+\left(\frac{\partial u}{\partial x}\right)_{i-1}}{24}+\frac{11}{12}\left(\frac{\partial u}{\partial x}\right)_i \cong \frac{u_{i+1/2}-u_{i-1/2}}{\Delta x}. \tag{2.57}$$

All above equations can be derived by Taylor expansion and the details are in Appendix A. The compact finite difference scheme used in this thesis is the implicit staggered schemes of (2.57).

2.3.2 Dispersion Analysis for Explicit Staggered Scheme

For simplicity, Maxwell's equations in a normalized region of free space with $\mu = 1$, $\varepsilon = 1$, $\sigma = 0$, and $c = 1$ are considered and can be obtained as

$$j\nabla\times\vec{V} = \frac{\partial\vec{V}}{\partial t} \tag{2.58}$$

where $\vec{V} = \vec{H}+j\vec{E}$. Apply (2.55) to the left hand side of (2.58) and the central difference to the right hand side of (2.58) and let

$$\vec{V}\Big|_{I,J,K}^{n} = \vec{V}_0 e^{j(\tilde{k}_x I\Delta x+\tilde{k}_y J\Delta y+\tilde{k}_z K\Delta z-\omega n\Delta t)}, \tag{2.59}$$

then the following equations are obtained sin

$j\frac{27}{}$

$j\frac{27\sin(k}{}$

For non-trivial

numerical disp

$\left[\frac{\sin(\omega\Delta t}{c\Delta t}\right.$ 2

$+\left[\frac{27\sin(}{}\right.$

The numerical

$\frac{1728}{a^2}$

If $\Delta = \Delta x = \Delta$

From Figure

scheme. The ph

$$\frac{\sin(\omega\Delta t/2)}{\Delta t}V_x\Big|_{I,J,K} - j\frac{27\sin(\tilde{k}_z\Delta z/2) - \sin(3\tilde{k}_z\Delta z/2)}{24\Delta y}V_y\Big|_{I,J,K}$$
$$+ j\frac{27\sin(\tilde{k}_y\Delta y/2) - \sin(3\tilde{k}_y\Delta y/2)}{24\Delta y}V_z\Big|_{I,J,K} = 0 \tag{2.60}$$

$$j\frac{27\sin(\tilde{k}_z\Delta z/2) - \sin(3\tilde{k}_z\Delta z/2)}{24\Delta z}V_x\Big|_{I,J,K} + \frac{\sin(\omega\Delta t/2)}{\Delta t}V_y\Big|_{I,J,K}$$
$$-j\frac{27\sin(\tilde{k}_x\Delta x/2) - \sin(3\tilde{k}_x\Delta x/2)}{24\Delta x}V_z\Big|_{I,J,K} = 0 \tag{2.61}$$

$$-j\frac{27\sin(\tilde{k}_y\Delta y/2) - \sin(3\tilde{k}_y\Delta y/2)}{24\Delta y}V_x\Big|_{I,J,K} +$$
$$j\frac{27\sin(\tilde{k}_x\Delta x/2) - \sin(3\tilde{k}_x\Delta x/2)}{24\Delta x}V_y\Big|_{I,J,K} + \frac{\sin(\omega\Delta t/2)}{\Delta t}V_z\Big|_{I,J,K} = 0 \tag{2.62}$$

For non-trivial solution, the determinant of the above equations is set to zero and the numerical dispersion relation is

$$\left[\frac{\sin(\omega\Delta t/2)}{c\Delta t}\right]^2 = \left[\frac{27\sin(\tilde{k}_x\Delta x/2) - \sin(3\tilde{k}_x\Delta x/2)}{24\Delta x}\right]^2$$
$$+\left[\frac{27\sin(\tilde{k}_y\Delta y/2) - \sin(3\tilde{k}_y\Delta y/2)}{24\Delta y}\right]^2 + \left[\frac{27\sin(\tilde{k}_z\Delta z/2) - \sin(3\tilde{k}_z\Delta z/2)}{24\Delta z}\right]^2 . \tag{2.63}$$

The numerical dispersion relation can be further reduced to

$$\frac{1728}{a^2}\left[\sin\left(\frac{a\pi}{\sqrt{3}R}\right)\right]^2 = \left[27\sin\left(\frac{\bar{k}\sin\theta\cos\phi}{R}\right) - \sin\left(\frac{3\bar{k}\sin\theta\cos\phi}{R}\right)\right]^2$$
$$+\left[27\sin\left(\frac{\bar{k}\sin\theta\sin\phi}{R}\right) - \sin\left(\frac{3\bar{k}\sin\theta\sin\phi}{R}\right)\right]^2 \tag{2.64}$$
$$+\left[27\sin\left(\frac{\bar{k}\cos\theta}{R}\right) - \sin\left(\frac{3\bar{k}\cos\theta}{R}\right)\right]^2$$

if $\Delta = \Delta x = \Delta y = \Delta z$.

From Figure 2.6, the phase error of fourth-order scheme is much less than that of Yee scheme. The phase error of fourth-order scheme at R=5 falls between that of Yee scheme at R=13 and

fourth-order

2.3.3 Dispe

For implic

scalar equatio

equation is

where A is a N

$X = \left[\frac{\partial V}{\partial y} \right.$

and $B = \frac{M\hat{B}}{\Delta y}$

$\hat{B} = \left[V \right.$

The elements o

boundary appro

where $\overline{M} = A^{-}$

Apply (2.59

at R=13 and R=40 as shown in Figure 2.7. Hence, a coarser mesh can be chosen for fourth-order scheme if the same phase error is required.

2.3.3 Dispersion Analysis for Implicit Staggered Scheme

For implicit staggered scheme given in (2.57) with numerical boundary condition, the scalar equations of $\nabla \times \vec{V}$ can be rewritten in a matrix form. For $\partial V_z / \partial y$, the matrix equation is

$$AX = B \tag{2.65}$$

where A is a (N+1) by (N+1) matrix, N is the number of partition along the y axis,

$$X = \left[\left.\frac{\partial V_z}{\partial y}\right|_{j=0} \left.\frac{\partial V_z}{\partial y}\right|_{j=1} \left.\frac{\partial V_z}{\partial y}\right|_{j=2} \cdots \left.\frac{\partial V_z}{\partial y}\right|_{j=N-2} \left.\frac{\partial V_z}{\partial y}\right|_{j=N-1} \left.\frac{\partial V_z}{\partial y}\right|_{j=N} \right]^T, \tag{2.66}$$

and $B = \frac{M\hat{B}}{\Delta y}$ where M is a (N+1) by N matrix and

$$\hat{B} = \left[V_z\big|_{j=\frac{1}{2}} V_z\big|_{j=\frac{3}{2}} V_z\big|_{j=\frac{5}{2}} \cdots V_z\big|_{j=\frac{2N-5}{2}} V_z\big|_{j=\frac{2N-3}{2}} V_z\big|_{j=\frac{2N-1}{2}} \right]. \tag{2.67}$$

The elements of matrices A and M depend on the coefficients in (2.57) and numerical boundary approximation. The (2.65) can be rewritten as

$$X = \frac{\overline{M}\hat{B}}{\Delta y} \tag{2.68}$$

where $\overline{M} = A^{-1}M$ and A^{-1} is the inverse of matrix A.

Apply (2.59) to (2.68) and after some calculation, the j component of X becomes where $\bar{m}_{jn}$

similarly and

of above eq

obtained as

The (2.70) dep

equation is very

the explicit stag

be further reduc

which make $\bar{k}$

researched base

$$\left.\frac{\partial V_z}{\partial y}\right|_j = \frac{V_z|_j}{\Delta y}\sum_{n=0}^{N-1}\bar{m}_{jn}e^{-j\bar{k}_y\left(j-\frac{2n+1}{2}\right)\Delta y} \tag{2.69}$$

where $\bar{m}_{jn}$ is the (j,n) element of matrix $\bar{M}$. Other derivatives of $\vec{V}$ can be obtained similarly and a system of equations for V_x, V_y, and V_z are setup. Setting the determinant of above equations to be zero and $\Delta = \Delta x = \Delta y = \Delta z$, the dispersion relation is obtained as

$$\begin{aligned}\frac{12}{a^2}\left[\sin\left(\frac{a\pi}{\sqrt{3}R}\right)\right]^2 &= \left[\sum_{n=0}^{N-1}\bar{m}_{In}e^{-\frac{j\bar{k}\sin\theta\cos\phi(2I-(2n+1))}{R}}\right]^2 \\ &+ \left[\sum_{n=0}^{N-1}\bar{m}_{Jn}e^{-\frac{j\bar{k}\sin\theta\sin\phi(2J-(2n+1))}{R}}\right]^2 \\ &+ \left[\sum_{n=0}^{N-1}\bar{m}_{Kn}e^{-\frac{j\bar{k}\cos\theta(2K-(2n+1))}{R}}\right]^2\end{aligned} \quad . \tag{2.70}$$

The (2.70) depends on locations of points and matrix $\bar{M}$; hence, the analysis of this equation is very complex. The phase error in implicit staggered scheme is close to that in the explicit staggered scheme. Moreover, the phase error in implicit staggered scheme can be further reduced if the suitable optimization method is used. The optimization methods, which make $\bar{k}$ close to π or v_p/c close to one while maintaining smaller R, can be researched based on (2.70).

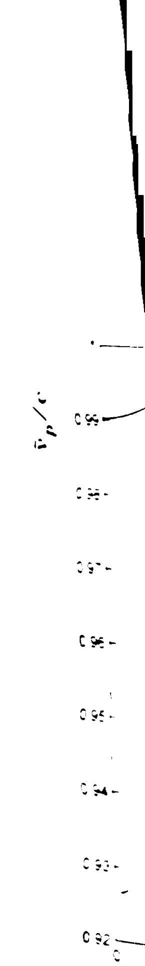

Fi
be
***R*=**

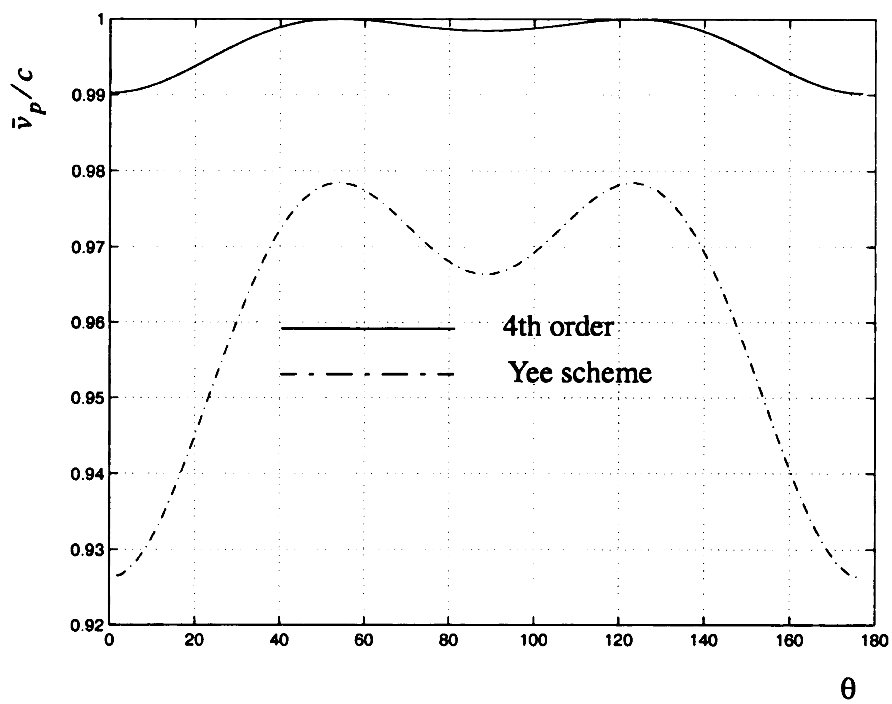

Figure 2.6 Comparison of numerical phase velocity between explicit 4th-order scheme and Yee scheme at *R=5*, *a=0.24*, and $\phi=\pi/4$.

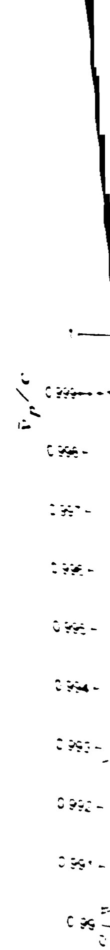

F
b
a

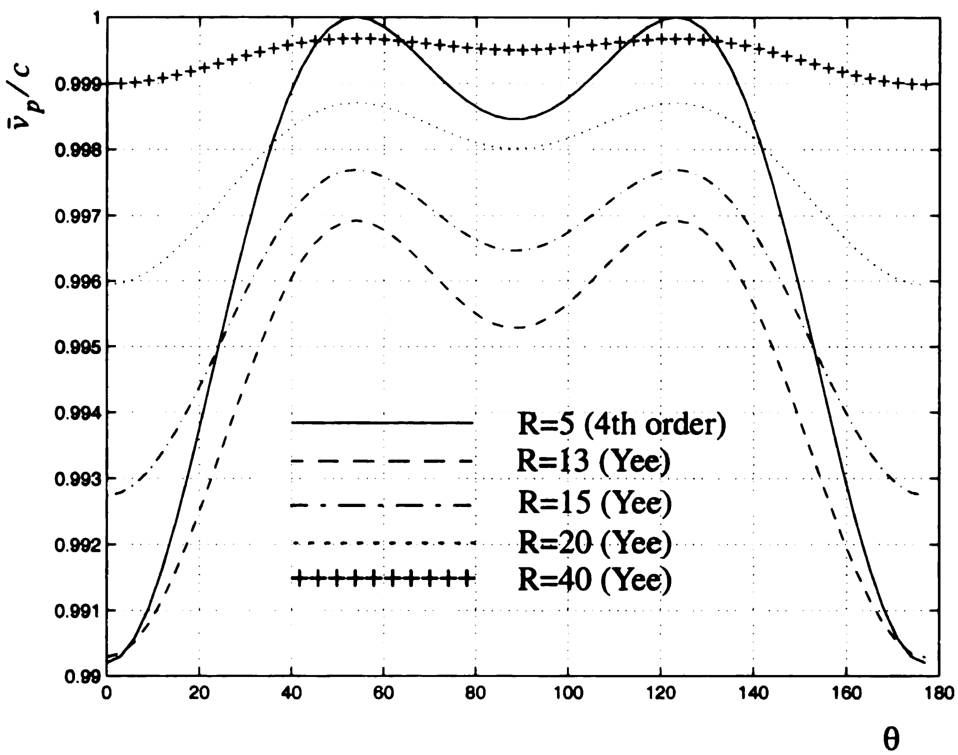

Figure 2.7 Comparison of numerical phase velocity between explicit 4th-order scheme and Yee scheme at *a=0.24*, and $\phi=\pi/4$.

2.3.4 Calculatio

The derivatives

considered here as

which is close t

$\partial E_y\, \partial z|_{k=3/2}$, E_y

outside the physical b

so is the value of ∂E

mesh points other th

derivatives of $\vec{E}$.

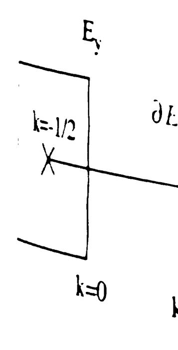

Figure 2.

x and y.

The following t

derivatives of $\vec{E}$ on th

2.3.4 Calculation of Derivative of $\vec{E}$ in Ty(2,4)

The derivatives of $\vec{E}$ along x, y, and z are first considered. The term $\partial E_y/\partial z$ case is considered here as an example. From the Figure 2.8, the evaluation of $\partial E_y/\partial z|_{k=1/2}$ which is close to the boundary by $\Delta z/2$ needs values of $\partial E_y/\partial z|_{k=-1/2}$, $\partial E_y/\partial z|_{k=3/2}$, $E_y|_{k=0}$, and $E_y|_{k=1}$ if (2.57) is used. However, $\partial E_y/\partial z|_{k=-1/2}$ is outside the physical boundary, hence, the value of $\partial E_y/\partial z|_{k=1/2}$ has to be approximated, so is the value of $\partial E_y/\partial z|_{k=N_z-1/2}$ where N_z is the number of partition along z axis. For mesh points other than $k = 1/2$ and $k = N_z - 1/2$, the (2.57) is applied to yield the derivatives of $\vec{E}$.

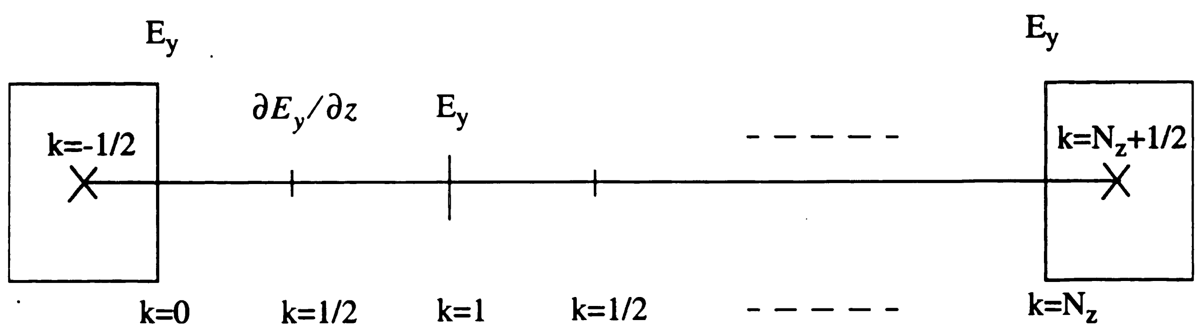

Figure 2.8 The lattices of *Ey* and $\partial E_y/\partial z$ along the z axis at fix x and y.

The following two fourth-order approximations are used to approximate the derivatives of $\vec{E}$ on those two special points:

$$-\frac{1}{24}\frac{\partial E_x}{\partial z}\bigg|_{k=\frac{-}{2}} +$$

$$\frac{13}{12}\frac{\partial E_x}{\partial z}\bigg|_{k=}$$

A system of equa

where

$$X = \bigg[\frac{\partial}{\partial}$$

$$-\frac{1}{24}\frac{\partial E_y}{\partial z}\bigg|_{k=\frac{7}{2}}+\frac{1}{12}\frac{\partial E_y}{\partial z}\bigg|_{k=\frac{5}{2}}-\frac{5}{24}\frac{\partial E_y}{\partial z}\bigg|_{k=\frac{3}{2}}+\frac{13}{12}\frac{\partial E_y}{\partial z}\bigg|_{k=\frac{1}{2}}=\frac{E_y|_{k=1}-E_y|_{k=0}}{\Delta z}, \quad (2.71)$$

$$\frac{13}{12}\frac{\partial E_y}{\partial z}\bigg|_{k=N_z-\frac{1}{2}}-\frac{5}{24}\frac{\partial E_y}{\partial z}\bigg|_{k=N_z-\frac{3}{2}}+\frac{1}{12}\frac{\partial E_y}{\partial z}\bigg|_{k=N_z-\frac{5}{2}}-\frac{1}{24}\frac{\partial E_y}{\partial z}\bigg|_{k=N_z-\frac{7}{2}} = \frac{E_y|_{k=N_z}-E_y|_{k=N_z-1}}{\Delta z} \quad (2.72)$$

A system of equations are derived and written in matrix form,

$$AX = B \quad (2.73)$$

where

$$A = \begin{bmatrix} 26 & -5 & 4 & -1 & \cdot & \cdot & 0 \\ 1 & 22 & 1 & 0 & \cdot & \cdot & 0 \\ 0 & 1 & 22 & 1 & 0 & \cdot & 0 \\ \cdot & \cdot & \cdot & \cdot & \cdot & \cdot & \cdot \\ 0 & \cdot & 0 & 1 & 22 & 1 & 0 \\ 0 & \cdot & 0 & 0 & 1 & 22 & 1 \\ 0 & \cdot & 0 & -1 & 4 & -5 & 26 \end{bmatrix}, \quad (2.74)$$

$$X = \left[\frac{\partial E_y}{\partial z}\bigg|_{k=\frac{1}{2}} \quad \frac{\partial E_y}{\partial z}\bigg|_{k=\frac{3}{2}} \quad \cdot \quad \cdot \quad \cdot \quad \frac{\partial E_y}{\partial z}\bigg|_{k=N_z-\frac{3}{2}} \quad \frac{\partial E_y}{\partial z}\bigg|_{k=N_z-\frac{1}{2}}\right]^T, \quad (2.75)$$

$$B = \frac{24}{\Delta z}\begin{bmatrix} E_y|_{k=1}-E_y|_{k=0} \\ E_y|_{k=2}-E_y|_{k=1} \\ \cdot \\ \cdot \\ E_y|_{k=N_z-1}-E_y|_{k=N_z-2} \\ E_y|_{k=N_z}-E_y|_{k=N_z-1} \end{bmatrix}, \quad (2.76)$$

and T denotes the t

$\vec{E}$ at every points o

2.3.5 Calculatio

The calculation

configuration along

$\partial H_z \ \partial y$

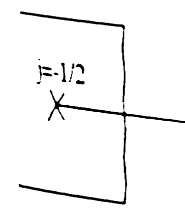

j=0

Figure

x and

If the boundar

the derivatives of

becomes

and T denotes the transpose of a matrix. By using the LU decomposition, the derivatives of $\vec{E}$ at every points can be determined.

2.3.5 Calculation of Derivative of $\vec{H}$ in Ty(2,4)

The calculation of $\partial H_z/\partial y$ is shown as an example. Figure 2.9 shows the grid configuration along y direction.

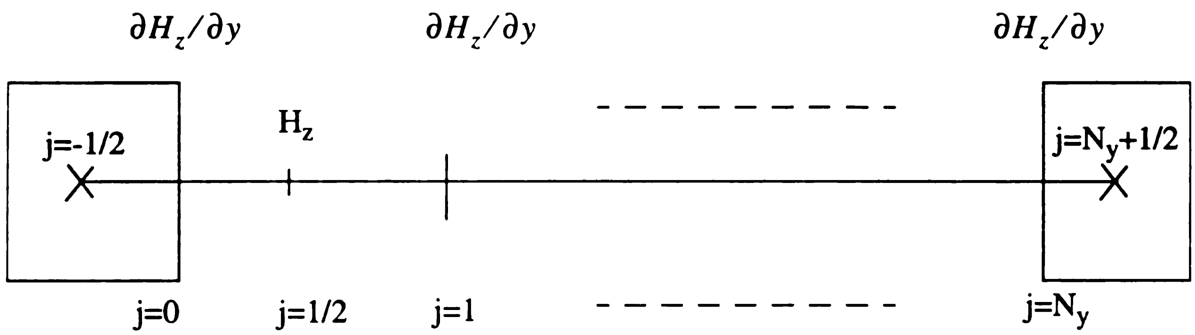

Figure 2.9 The lattices of H_z and $\partial H_z/\partial y$ along the y axis at fix x and z.

If the boundary is PEC, then E_x, E_z, and H_y are zero according to Figure 2.1. Hence, the derivatives of H_z on the boundary are zero, also. The matrix equations, $AX = B$ becomes

$$A = \begin{bmatrix} 22 & 1 & 0 & \cdot & 0 \\ 1 & 22 & 1 & \cdot & 0 \\ \cdot & \cdot & \cdot & \cdot & 0 \\ 0 & \cdot & 1 & 22 & 1 \\ 0 & \cdot & 0 & 1 & 22 \end{bmatrix}, \tag{2.77}$$

$$X = \left[\frac{\partial H}{\partial y} \right.$$

and

If the bound

approximated. T

used:

$$\left. \frac{\partial H_z}{\partial y} \right|_{j = 0} =$$

and

$$\left. \frac{\partial H_z}{\partial y} \right|_{j =}$$

The components

$$X = \left[\frac{\partial H_z}{\partial y}\bigg|_{j=1} \; \frac{\partial H_z}{\partial y}\bigg|_{j=2} \; \cdot \; \cdot \; \cdot \frac{\partial H_z}{\partial y}\bigg|_{j=N_y-2} \; \frac{\partial H_z}{\partial y}\bigg|_{j=N_y-1} \right]^T, \tag{2.78}$$

$$B = \frac{24}{\Delta y} \begin{bmatrix} H_z|_{j=3/2} - H_z|_{j=1/2} \\ H_z|_{j=5/2} - H_z|_{j=3/2} \\ \cdot \\ \cdot \\ H_z|_{j=N_y-3/2} - H_z|_{j=N_y-5/2} \\ H_z|_{j=N_y-1/2} - H_z|_{j=N_y-3/2} \end{bmatrix}, \tag{2.79}$$

and

$$\frac{\partial H_z}{\partial y}\bigg|_{j=0} = 0, \frac{\partial H_z}{\partial y}\bigg|_{j=N_y} = 0. \tag{2.80}$$

If the boundary is not PEC then $\partial H_z/\partial y|_{j=0}$ and $\partial H_z/\partial y|_{j=N_y}$ need to be approximated. The following fourth-order one-way finite difference approximations are used:

$$\frac{\partial H_z}{\partial y}\bigg|_{j=0} = \frac{-\frac{31}{8}H_z\big|_{j=\frac{1}{2}} + \frac{229}{24}H_z\big|_{j=\frac{3}{2}} - \frac{75}{8}H_z\big|_{j=\frac{5}{2}} + \frac{37}{8}H_z\big|_{j=\frac{7}{2}} - \frac{11}{12}H_z\big|_{j=\frac{9}{2}}}{\Delta y} \tag{2.81}$$

and

$$\begin{aligned} \frac{\partial H_z}{\partial y}\bigg|_{j=N_y} = \bigg(& -\frac{31}{8}H_z\big|_{j=N_y-\frac{1}{2}} + \frac{229}{24}H_z\big|_{j=N_y-\frac{3}{2}} - \frac{75}{8}H_z\big|_{j=N_y-\frac{5}{2}} \\ & + \frac{37}{8}H_z\big|_{j=N_y-\frac{7}{2}} - \frac{11}{12}H_z\big|_{j=N_y-\frac{9}{2}} \bigg) \Big/ \Delta y \end{aligned}. \tag{2.82}$$

The components of the corresponding matrix equation are

$$X = \left[\frac{\partial H_z}{\partial y} \right|_{y = 0}$$

and

$$B = \frac{24}{\Delta y} \left[-\frac{31}{8} H \right.$$

where

$$f =$$

$$A = \begin{bmatrix} 24 & 0 & 0 & \cdot & 0 \\ 1 & 22 & 1 & \cdot & 0 \\ \cdot & \cdot & \cdot & \cdot & 0 \\ 0 & \cdot & 1 & 22 & 1 \\ 0 & \cdot & 0 & 0 & 24 \end{bmatrix}, \tag{2.83}$$

$$X = \left[\left.\frac{\partial H_z}{\partial y}\right|_{j=0} \quad \left.\frac{\partial H_z}{\partial y}\right|_{j=1} \quad \cdot \quad \cdot \quad \cdot \left.\frac{\partial H_z}{\partial y}\right|_{j=N_y-2} \quad \left.\frac{\partial H_z}{\partial y}\right|_{j=N_y-1} \quad \left.\frac{\partial H_z}{\partial y}\right|_{j=N_y} \right]^T, \tag{2.84}$$

and

$$B = \frac{24}{\Delta y} \begin{bmatrix} -\frac{31}{8} H_z\big|_{j=\frac{1}{2}} + \frac{229}{24} H_z\big|_{j=\frac{3}{2}} - \frac{75}{8} H_z\big|_{j=\frac{5}{2}} + \frac{37}{8} H_z\big|_{j=\frac{7}{2}} - \frac{11}{12} H_z\big|_{j=\frac{9}{2}} \\ H_z\big|_{j=3/2} - H_z\big|_{j=1/2} \\ H_z\big|_{j=5/2} - H_z\big|_{j=3/2} \\ \cdot \\ \\ H_z\big|_{j=N_y-3/2} - H_z\big|_{j=N_y-5/2} \\ H_z\big|_{j=N_y-1/2} - H_z\big|_{j=N_y-3/2} \\ f \end{bmatrix} \tag{2.85}$$

where

$$f = \left(-\frac{31}{8} H_z\big|_{j=N_y-\frac{1}{2}} + \frac{229}{24} H_z\big|_{j=N_y-\frac{3}{2}} - \frac{75}{8} H_z\big|_{j=N_y-\frac{5}{2}} \right. \\ \left. + \frac{37}{8} H_z\big|_{j=N_y-\frac{7}{2}} - \frac{11}{12} H_z\big|_{j=N_y-\frac{9}{2}} \right) / \Delta y \quad . \tag{2.86}$$

2.4 Excitation

2.4.1 Excitatio

An excitation :

density of the probe

$\vec{J} = (I(x)\delta(y - y_0$

where

$w(t)$ is the time de

For empty PEC

contain a finite ene

time. The sidelobe

dB and provides

follow.

$h(t_n) = \{ 0.3$

where $w(t) = h(t$

N_{half} is the design

2.4 Excitation Source and Power Analysis

2.4.1 Excitation Source

An excitation probe is placed parallelly to one of the rectangular axes. The current density of the probe is modeled by induced EMF method and represented as

$$\vec{J} = (I(x)\delta(y-y_0)\delta(z-z_0),\ \delta(x-x_0)I(y)\delta(z-z_0),\ \delta(x-x_0)\delta(y-y_0)I(z))w(t) \quad (2.87)$$

where

$$I(\alpha) = I_0\frac{\sin k(h_\alpha - \alpha)}{\sin kh_\alpha} \qquad \alpha = x, y, z, \quad (2.88)$$

$w(t)$ is the time dependence of $\vec{J}$ and h_α is the length of probe along the α direction.

For empty PEC rectangular cavities, the source frequency is 2.45 GHz. In order to contain a finite energy in the cavity, the signal source needs to be turned off at some given time. The sidelobe level of the Blackman-Harris (BH) window[20] is approximately -92 dB and provides a smooth transition of excitation. The BH function is discretized as follow,

$$h(t_n) = \begin{cases} 0.35875 + 0.48829\cos\left(\dfrac{\pi(t_n - t_c)}{N_{half}}\right) & \\ \quad + 0.14128\cos\left(\dfrac{2\pi(t_n - t_c)}{N_{half}}\right) & t_n \in [t_c - N_{half}, t_c + N_{half}] \\ \quad + 0.01168\cos\left(\dfrac{3\pi(t_n - t_c)}{N_{half}}\right) & \\ 0 & otherwise \end{cases} \quad (2.89)$$

where $w(t) = h(t)\cos\omega t$, t_n is the time step, t_c is the center of the BH window, and N_{half} is the designed half width of the BH window function.

For a loaded

frequency sinuso

the finite value of

The excited m

where the Green's f

and $\sum_n$ denotes the

modes, the probe mu

2.4.2 Power Anal

The integral form

$$-\int_V \vec{E} \cdot \vec{J}_s dV =$$

where $\vec{J}_s$ is the sourc

source turned off is

The FDTD approxima

For a loaded PEC rectangular or an aperture-coupled cascaded cavity, a single frequency sinusoidal source is used. The loss of material sample in the cavity accounts for the finite value of Q.

The excited modes are determined by the location of the probe according to

$$\vec{E}(\vec{r}) = \int \vec{J}(\vec{r})\bar{G}(\vec{r}, \vec{r}_0)dv_0 \tag{2.90}$$

where the Green's function is

$$\bar{G}(\vec{r}, \vec{r}_0) = -j\omega\mu\sum_n \frac{\vec{E}_n(\vec{r}_0)\vec{E}_n(\vec{r})}{k_n^2 - k^2} \tag{2.91}$$

and $\sum_n$ denotes the sum of all the TE_{nml} and TM_{nml} modes. For example, to excite TM modes, the probe must have J_z component only.

2.4.2 Power Analysis

The integral form of the Poynting's theorem is

$$-\int_V \vec{E} \cdot \vec{J}_s dV = \int_V \vec{E} \cdot \vec{J} dV + \int_V \left(\vec{E} \cdot \frac{\partial \vec{D}}{\partial t} + \vec{H} \cdot \frac{\partial \vec{B}}{\partial t}\right) dV + \oint_S (\vec{E} \times \vec{H}) \cdot \hat{n} dS \tag{2.92}$$

where $\vec{J}_s$ is the source current. For lossless case, the power stored inside a cavity after the source turned off is

$$P_s = \int_V \left(\vec{E} \cdot \frac{\partial \vec{D}}{\partial t} + \vec{H} \cdot \frac{\partial \vec{B}}{\partial t}\right) dV . \tag{2.93}$$

The FDTD approximation of the first integrand, evaluated at time step n, in (2.93) is

$P^n_{sE} =$

and that of the seco

$P^n_{sH} = \frac{\mu_0}{2\Delta}$

where the nonmag

time step n is

where $\Delta v = \Delta x \Delta y$

For material w

hand side of (2.92

formulation is eas

material is contain

dissipated power d

summation of the

material sample. F

needed for power a

also presented belo

$$P_{sE}^{n} = \frac{1}{2\Delta t}\left\{E_x\Big|^n\left(D_x\Big|^{n+1} - D_x\Big|^{n-1}\right) + E_y\Big|^n\left(D_y\Big|^{n+1} - D_y\Big|^{n-1}\right)\right.$$
$$\left. + E_z\Big|^n\left(D_z\Big|^{n+1} - D_z\Big|^{n-1}\right)\right\} \tag{2.94}$$

and that of the second integrand, evaluated at time step n, is

$$P_{sH}^{n} = \frac{\mu_0}{2\Delta t}\left\{\left[\left(H_x\Big|^{n+\frac{1}{2}}\right)^2 - \left(H_x\Big|^{n-\frac{1}{2}}\right)^2\right] + \left[\left(H_y\Big|^{n+\frac{1}{2}}\right)^2 - \left(H_y\Big|^{n-\frac{1}{2}}\right)^2\right]\right.$$
$$\left. + \left[\left(H_z\Big|^{n+\frac{1}{2}}\right)^2 - \left(H_z\Big|^{n-\frac{1}{2}}\right)^2\right]\right\} \tag{2.95}$$

where the nonmagnetic material is assumed. Hence, the power stored inside the cavity at time step n is

$$P_s^n \approx \sum (P_{sE}^n + P_{sH}^n)\Delta v \tag{2.96}$$

where $\Delta v = \Delta x \Delta y \Delta z$ for uniform partitions.

For material with conductive loss, the dissipated power is the first term on the right-hand side of (2.92). The conductive dissipated power density is σE^2 and its time domain formulation is easy to determined. However, the dissipated power for a lossy dielectric material is contained in the second term on the right-hand side of (2.92) and the dielectric dissipated power density in the time domain has to be extracted. For this case, (2.93) is the summation of the stored power of the whole cavity and dissipated power due to the lossy material sample. Hence, only the calculation of the (2.93) and the dissipated power are needed for power analysis. However, the stored power inside the loaded material region is also presented below to form a general Poynting theorem.

Assume the o

in $\vec{E}\cdot\frac{\partial \vec{D}}{\partial t}$ is

$$\frac{1}{2\pi}(E_{x}$$

where $\varepsilon'(\omega)$ and ε

sign, $\otimes$, stands for t

to E_x and the secon

relation of the perm

rewritten as stored a

$$\frac{1}{2\pi}\{E_x(\omega)\,\varepsilon$$

and

$$\frac{1}{2\pi}\frac{(\varepsilon_{x}}{}$$

The corresponding

and

where $g_x(t)$ is th

Assume the one-relaxation Debye medium, the Fourier transform of the x component in $\vec{E} \cdot \frac{\partial \vec{D}}{\partial t}$ is

$$\frac{1}{2\pi}(E_x(\omega) \otimes [j\omega\varepsilon'(\omega)E_x(\omega)] + E_x(\omega) \otimes [\omega\varepsilon''(\omega)E_x(\omega)]) \tag{2.97}$$

where $\varepsilon'(\omega)$ and $\varepsilon''(\omega)$ are the real and imaginary parts of electric permittivity and the sign, $\otimes$, stands for the convolution. The first term in (2.97) is the stored power density due to E_x and the second term is the dissipated power per volume due to E_x. Substituting the relation of the permittivity with static and infinity frequency permittivities, (2.97) can be rewritten as stored and dissipated powers as

$$\frac{1}{2\pi}\left\{E_x(\omega) \otimes [j\omega\varepsilon'_{x\infty}E_x(\omega)] + E_x(\omega) \otimes \left[(\varepsilon'_{xs} - \varepsilon'_{x\infty})j\omega\frac{E_x(\omega)}{1 + (\omega\tau_{ex})^2}\right]\right\} \tag{2.98}$$

and

$$\frac{1}{2\pi}\frac{(\varepsilon_{xs}' - \varepsilon_{x\infty}')}{\tau_e}\left(E_x(\omega) \otimes E_x(\omega) - E_x(\omega) \otimes \left[\frac{E_x(\omega)}{1 + (\omega\tau_{ex})^2}\right]\right). \tag{2.99}$$

The corresponding time domain equations for above equations are

$$\varepsilon'_{x\infty}E_x(t)\frac{dE_x(t)}{dt} + E_x(t)\left[(\varepsilon'_{xs} - \varepsilon'_{x\infty})\frac{dg_x(t)}{dt}\right] \tag{2.100}$$

and

$$\frac{(\varepsilon'_{xs} - \varepsilon'_{x\infty})}{\tau_{ex}}(E_x(t)E_x(t) - E_x(t)g_x(t)) \tag{2.101}$$

where $g_x(t)$ is the inverse Fourier transform of $E_x(\omega)/[1 + (\omega\tau_{ex})^2]$. Hence, the

Poynting theorem

$$\int_V \vec{E}^s \cdot \vec{J}$$

$$+\int_V [\vec{E}$$

where

and

where the V_s is the

term in (2.102) can b

Poynting theorem for nonmagnetic material can be rewritten as

$$\int_V \vec{E}^s \cdot \vec{J}\,dV = \int_V [\sigma]\vec{E}\cdot\vec{E}\,dV + \int_{V_s} ([\xi_3]\vec{E}\cdot\vec{E} - [\xi_3]\vec{E}\cdot\vec{g})\,dV$$
$$+ \int_V \left([\xi_1]\vec{E}\cdot\frac{\partial\vec{E}}{\partial t} + [\xi_2]\vec{E}\cdot\frac{\partial\vec{g}}{\partial t} + \vec{H}\cdot\frac{\partial\vec{B}}{\partial t}\right)dV + \oint_S (\vec{E}\times\vec{H})\cdot\hat{n}\,dS \tag{2.102}$$

where

$$[\xi_1] = \begin{bmatrix} \varepsilon'_{x\infty} & 0 & 0 \\ 0 & \varepsilon'_{y\infty} & 0 \\ 0 & 0 & \varepsilon'_{z\infty} \end{bmatrix}, \tag{2.103}$$

$$[\xi_2] = \begin{bmatrix} \varepsilon'_{xs} - \varepsilon'_{x\infty} & 0 & 0 \\ 0 & \varepsilon'_{ys} - \varepsilon'_{y\infty} & 0 \\ 0 & 0 & \varepsilon'_{zs} - \varepsilon'_{z\infty} \end{bmatrix}, \tag{2.104}$$

$$[\sigma] = \begin{bmatrix} \sigma_x & 0 & 0 \\ 0 & \sigma_y & 0 \\ 0 & 0 & \sigma_z \end{bmatrix}, \tag{2.105}$$

and

$$[\xi_3] = \begin{bmatrix} \dfrac{\varepsilon'_{xs} - \varepsilon'_{x\infty}}{\tau_{ex}} & 0 & 0 \\ 0 & \dfrac{\varepsilon'_{ys} - \varepsilon'_{y\infty}}{\tau_{ey}} & 0 \\ 0 & 0 & \dfrac{\varepsilon'_{zs} - \varepsilon'_{z\infty}}{\tau_{ez}} \end{bmatrix}. \tag{2.106}$$

where the V_s is the volume of the material sample. Note that the summation of the third term in (2.102) can be obtained by subtracting the second term in (2.102) from (2.93).

Evaluating the

$1/[1+(\omega\tau_e)^2]$.

impractical in th

approximated by

recursive equation

pair, $e^{-a\,t}$ and $2a$.

$$g_x(n\Delta t) = \frac{\Delta t}{4\tau_{ex}} E$$

Hence, the stored p

version of (2.100)

(2.101) and (2.107).

The other meth

section 2.1.1. Let

then its time domain

By using the secon

(2.108) becomes

$$g_x((n+1)\Delta t) =$$

The (2.107) is obvio

However, the homog

Evaluating the $g_x(t)$ involves the convolution of $E_x(t)$ and the time domain version of $1/[1+(\omega\tau_e)^2]$. To get the convolution, a history of $E_x(t)$ is required and this is impractical in the program implementation. Hence, the convolution need to be approximated by a recursive equation. The first method is to discrete $g_x(t)$ into a recursive equation by discreting the convolution directly. By using the Fourier transform pair, $e^{-a|t|}$ and $2a/(a^2+\omega^2)$, the discrete version of $g_x(t)$ is

$$g_x(n\Delta t) = \frac{\Delta t}{4\tau_{ex}}E_x(n\Delta t) + \frac{\Delta t}{4\tau_{ex}}e^{-\Delta t/\tau_{ex}}E_x((n-1)\Delta t) + e^{-\Delta t/\tau_{ex}}g_x((n-1)\Delta t). \quad (2.107)$$

Hence, the stored power density due to E_x at time step n is calculated from the discrete version of (2.100) and (2.107) and that of dissipated power from discrete version of (2.101) and (2.107).

The other method uses a procedure similar to what we did to Debye equation in section 2.1.1. Let $g_x(\omega) = E_x(\omega)/[1+(\omega\tau_{ex})^2]$ or $[1+(\omega\tau_{ex})^2]g_x(\omega) = E_x(\omega)$, then its time domain expression is

$$g_x(t) - \tau_{ex}^2\frac{d^2g_x(t)}{dt^2} = E_x(t). \quad (2.108)$$

By using the second order central difference approximation of the second derivative, (2.108) becomes

$$g_x((n+1)\Delta t) = \left[2+\left(\frac{\Delta t}{\tau_{ex}}\right)^2\right]g_x(n\Delta t) - g_x((n-1)\Delta t) - \left(\frac{\Delta t}{\tau_{ex}}\right)^2E_x(n\Delta t). \quad (2.109)$$

The (2.107) is obvious first order accurate but (2.109) is second order accurate in time. However, the homogenous solution of (2.108) contains a divergent term, $e^{t/\tau_{ex}}$, and its

FDTD for

general De

2.5 Pro

Results

response a

algorithm.

limitation i

observation

of iterations

the time-do

of viewing

$T = N\Delta t$.

the true spe

The Pro

of complex

and Q of a

characterized

2.5.1 The

The Pron

form

FDTD formulation cannot be used. More general FDTD formulation of power for a general Debye medium will be discussed in the next chapter.

2.5 Prony's Method

Results in the frequency domain are usually obtained by recording the time-domain response at the selected observation points of the FDTD mesh and applying the FFT algorithm. There are, however, several limitations in the FFT approach. The main limitation is that of the frequency resolution Δf, which is roughly the reciprocal of observation time, i.e., $\Delta f = 1/(N\Delta t)$ where Δt is the time step and N the total number of iterations used in the FDTD method. A second limitation arises from the windowing of the time-domain data because the FDTD response is truncated in time. This has the effect of viewing the true time-domain response through a rectangular windows of duration $T = N\Delta t$. In the frequency domain this windowing is translated into the convolution of the true spectrum with the function $\sin f/f$.

The Prony's method is a technique for modeling sampled data as a linear combination of complex exponentials and is particularly suitable for calculating the resonant frequency and Q of a resonating structure, since the impulse response of such a structure is characterized by a superposition of decaying exponentials[21].

2.5.1 Theory

The Prony's method fits an exponential approximation with unknown exponents of the form

$f(m$

to a function $f(t)$

of variables has

$m = 0, 1, 2, \ldots n -$

equation can be wr

or in the matrix for

where $f_i = f(i)$ ar

equation

$\mu^p + \alpha_1 \mu^p$

then we can get the fo

$$f(m) = C_1 e^{A_1 m} + C_2 e^{A_2 m} + \cdots + C_Q e^{A_Q m} = \sum_{k=1}^{p} C_k \mu_k^m \tag{2.110}$$

to a function $f(t)$ by sampling at n equally spaced points and $\mu_k = e^{A_k}$. A linear change of variables has been introduced in advance such that the data points are $m = 0, 1, 2, \ldots n-1$. The coefficients C_k and μ_k can be complex numbers. The above equation can be written as follow,

$$\begin{aligned} C_1 + C_2 + \ldots + C_p &= f_0 \\ C_1\mu_1 + C_2\mu_2 + \ldots + C_p\mu_p &= f_1 \\ C_1\mu_1^2 + C_2\mu_2^2 + \ldots + C_p\mu_p^2 &= f_2 \\ &\cdots \\ C_1\mu_1^{n-1} + C_2\mu_2^{n-1} + \ldots + C_p\mu_p^{n-1} &= f_{n-1} \end{aligned} \tag{2.111}$$

or in the matrix form

$$\begin{bmatrix} 1 & 1 & 1 & \cdots & 1 \\ \mu_1 & \mu_2 & \mu_3 & \cdots & \mu_p \\ \mu_1^2 & \mu_2^2 & \mu_3^2 & \cdots & \mu_p^2 \\ \vdots & \vdots & \vdots & & \vdots \\ \mu_1^{n-1} & \mu_2^{n-1} & \mu_3^{n-1} & \cdots & \mu_p^{n-1} \end{bmatrix} \begin{bmatrix} C_1 \\ C_2 \\ C_3 \\ \vdots \\ C_p \end{bmatrix} = \begin{bmatrix} f_0 \\ f_1 \\ f_2 \\ \vdots \\ f_{n-1} \end{bmatrix} \tag{2.112}$$

where $f_i = f(i)$ and $i = 0, 1, 2, \ldots, n-1$. Let $\mu_1, \ldots, \mu_p$ be the roots of the following equation

$$\mu^p + \alpha_1\mu^{p-1} + \alpha_2\mu^{p-2} + \ldots + \alpha_{p-1}\mu + \alpha_p = \sum_{k=1}^{p} \alpha_k\mu^k = 0 \tag{2.113}$$

then we can get the following equations from (2.111) and (2.113)

$f.$

or the followin

equal sign

f

f

which is linear in α.

The Prony's met

(2.114), a linear equ

(2.111) where $i = 1$.

The original Pron

perfectly well when

the data. However, w

largely due to the extr

in (2.113). The least

become overdetermin

(SVD) is used to solv

Determining p is

$$
\begin{aligned}
f_p + f_{p-1}\alpha_1 + f_{p-2}\alpha_2 + \cdots + f_0\alpha_p &= 0 \\
f_{p+1} + f_p\alpha_1 + f_{p-1}\alpha_2 + \cdots + f_1\alpha_p &= 0 \\
\cdots \\
f_{n-1} + f_{n-2}\alpha_1 + f_{n-3}\alpha_2 + \cdots + f_{n-p-1}\alpha_p &= 0
\end{aligned}
\tag{2.114}
$$

or the following one by shifting the first terms on the left hand side to right side of equal sign

$$
\begin{bmatrix}
f_{p-1} & f_{p-2} & \cdots & f_0 \\
f_p & f_{p-1} & \cdots & f_1 \\
f_{p+1} & f_p & \cdots & f_2 \\
\vdots & \vdots & & \vdots \\
f_{n-2} & f_{n-3} & & f_{n-p-1}
\end{bmatrix}
\begin{bmatrix} \alpha_1 \\ \alpha_2 \\ \vdots \\ \alpha_p \end{bmatrix}
= (-1)
\begin{bmatrix} f_p \\ f_{p+1} \\ f_{p+2} \\ \vdots \\ f_{n-1} \end{bmatrix}
\tag{2.115}
$$

which is linear in α.

The Prony's method solves the (2.110), a nonlinear equation in μ, by solving α_i in (2.114), a linear equation in α, finding the roots, μ_i, in (2.113), and obtaining C_i in (2.111) where $i = 1, 2, 3, \ldots, p$.

The original Prony method chooses $n = 2p + 1$. The original Prony method works perfectly well when no noise (truncation error or measurement imprecision) is present in the data. However, when a noise is introduced, then this method performs very poorly, largely due to the extreme sensitivity of root locations to the coefficients of the polynomial in (2.113). The least squares Prony method uses $n > 2p + 1$, then (2.112) and (2.115) become overdetermined linear equations systems and the singular value decomposition (SVD) is used to solve those equations.

Determining p is an important issue of applying Prony method to frequency domain analysis or pred

less than the nu

poor[21]. Howev

modes introduce

method with the

2.5.2 Estimati
Method

From the defi

the FDTD time-d

superposition of th

$E_{\ldots}$

with $\alpha_k = \omega_k/(2Q$

be obtained if $E_x(m$

and

where μ_k is the calc

analysis or prediction since every μ_i represents a frequency component. If the value of p is less than the number of actual modes excited in the structure, the spectral resolution is poor[21]. However, if p is selected to be too high, nonphysical modes appear. Nonphysical modes introduced by Prony estimation can be suppressed by the application of Prony's method with the time sequence of the sample points in reverse order[22].

2.5.2 Estimation of Resonant Frequency and Quality Factor by Prony Method

From the definition of quality factor,

$$Q = \omega_0 \frac{\text{Stored } Energy}{\text{Power loss}} \tag{2.116}$$

the FDTD time-domain response, say E_x, of a cavity can be expressed in terms of a superposition of the resonant modes[24]

$$E_x(m\Delta t) = \sum_{k=1}^{p} C_k e^{-(\alpha_k + j2\pi f_k)m\Delta t} = \sum_{k=1}^{p} C_k \mu_k^m \tag{2.117}$$

with $\alpha_k = \omega_k/(2Q)$ where $m = (0, \ldots,)N-1$. By Prony method, the C_k and μ_k can be obtained if $E_x(m\Delta t)$ are known. Hence, the resonant frequency and damping factor are

$$f_k = -\frac{\text{imag}(\ln(\mu_k))}{2\pi\Delta t} \tag{2.118}$$

and

$$\alpha_k = -\frac{\text{real}(\ln(\mu_k))}{\Delta t} \tag{2.119}$$

where μ_k is the calculated mode corresponding to f_k, $\text{imag}(\ln(\mu_k))$ is the imaginary part of $\ln(\mu_k)$, ar

Once the dam

factor can be easil

Note that (2.120) is

Prony method pro

distribution at trans

2.6 A Single E

An empty recta

of this cavity is int

the results presente

2.6.1 Configur

The configurat

excitation probe is

assumed to be ver

2.6.2 Numerica

For TE_{011} moc

J_x at 2.45GHz is

time steps, spanni

and $b3$ all equal

part of $\ln(\mu_k)$, and $\mathrm{real}(\ln(\mu_k))$ is the real part of $\ln(\mu_k)$.

Once the damping factor and the resonant frequency have been determined, the quality factor can be easily obtained as

$$Q_k = \left|\frac{\pi f_k}{\alpha_k}\right|. \tag{2.120}$$

Note that (2.120) is obtained when the cavity mode is at a steady state[23]. However, the Prony method provides a way to estimate quality factor of cavities from the field distribution at transient state.

2.6 A Single Empty Cavity with PEC Walls

An empty rectangular cavity with PEC boundary is studied in this section. The Q value of this cavity is infinite so the time to achieve the steady state is almost infinite. Hence, all the results presented here are obtained in the transient state.

2.6.1 Configuration

The configuration of the empty cavity with PEC walls is shown in Figure 2.10. The excitation probe is located at one of the six faces of the rectangular cavity and its length is assumed to be very small. The dimensions of the cavity are: *b1*x*b2*x*b3*.

2.6.2 Numerical Results of Field Distributions

For TE_{011} mode, the excitation probe is located at the center of the y-z plane and only J_x at 2.45GHz is provided. The BH source is used and automatically turned off at 18,875 time steps, spanning over 0.2516μs, with $\Delta t = 13.3299\ ps$. The cubic cavity with *b1*, *b2*, and *b3* all equal to *0.08658* meter is assumed. For this dimension and frequency, the

TE

be

pa

mo

and

y or

res

amp

sum

resp

is p

men

disp

from

zero

T

its fr

mod

TE

freq

TE_{101}, TE_{011}, and TM_{110} modes can be excited; however, only TE_{011} can be excited because only J_x is provided on the probe and E_xs of other modes are zero. The numbers of partitions along the x, y, and z are all *10*.

The x, y, and z dependences of E_x are shown in Figure 2.11 to Figure 2.15. For TE_{011} mode, E_x is constant along x at fixed z and the numerical results are shown in Figure 2.11 and Figure 2.12. The E_x is proportional to $\sin(\pi\alpha/0.08658)$ along the α axis where α is y or z and are shown in Figure 2.13, Figure 2.14 and Figure 2.15. Note that the numerical results at those grid points are exactly equal to $D\sin(\pi\alpha/0.08658)$ where D is a amplitude factor if α is from 0 to *0.08658* with increasing *0.008658* for every step. The summations of E_y, E_z, and H_x over all grid points are 3.7386e-06, 1.9023e-06, and 0 respectively and it shows that no E_y, E_z, and H_x exist.

For TM_{111} mode, the probe is located at the center on the bottom x-y plane and only J_z is provided since E_z of TE_{111} modes is zero. The length of the cubic cavity is 0.10604 meter and the BH source is off at 0.25131μs, with $\Delta t = 16.3265$ *ps*. The electric field distributions are plotted from Figure 2.17 to Figure 2.21, and they are consistent to those from theory[19]. The summation of H_z over all grid points is -5.7932e-31 which is almost zero, thus confirms the excited dominant mode being a TM mode.

The time dependence of E_x for TE_{011} mode at given point is plotted in Figure 2.23 and its frequency response in Figure 2.24. From Figure 2.24, the resonant frequency of TE_{011} mode is observed to be close to 2.5 GHz. However, the estimated resonant frequency of TE_{011} mode by Prony's method is 2.4528 GHz which is much closer to the source frequency. The estimated resonant frequency of TM_{111} is 2.4548 GHz by Prony method.

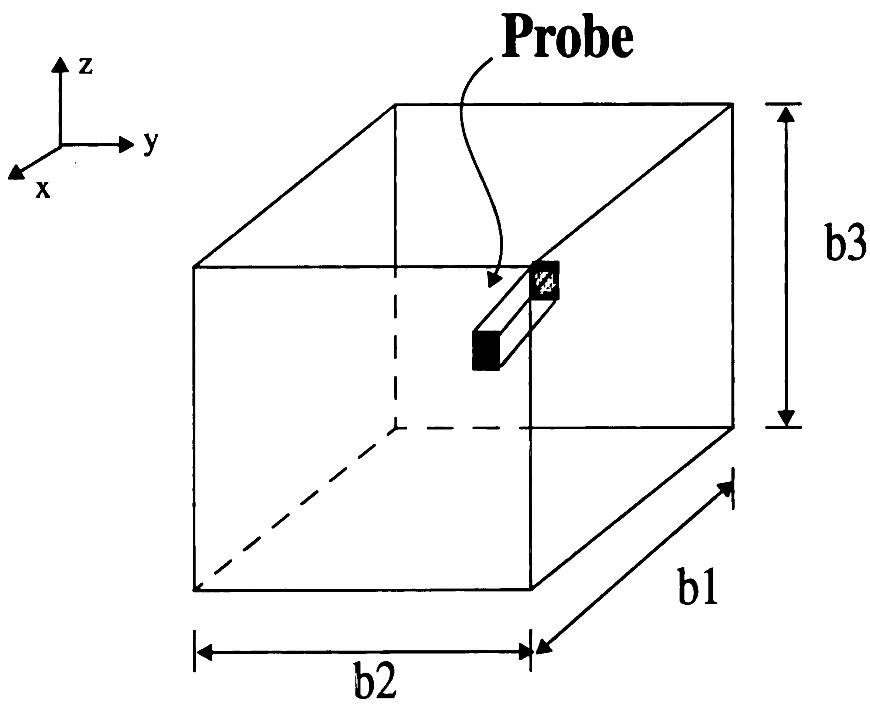

Figure 2.10 The configuration of the empty rectangular cavity with PEC boundary. The excitation probe is located on one of the six faces.

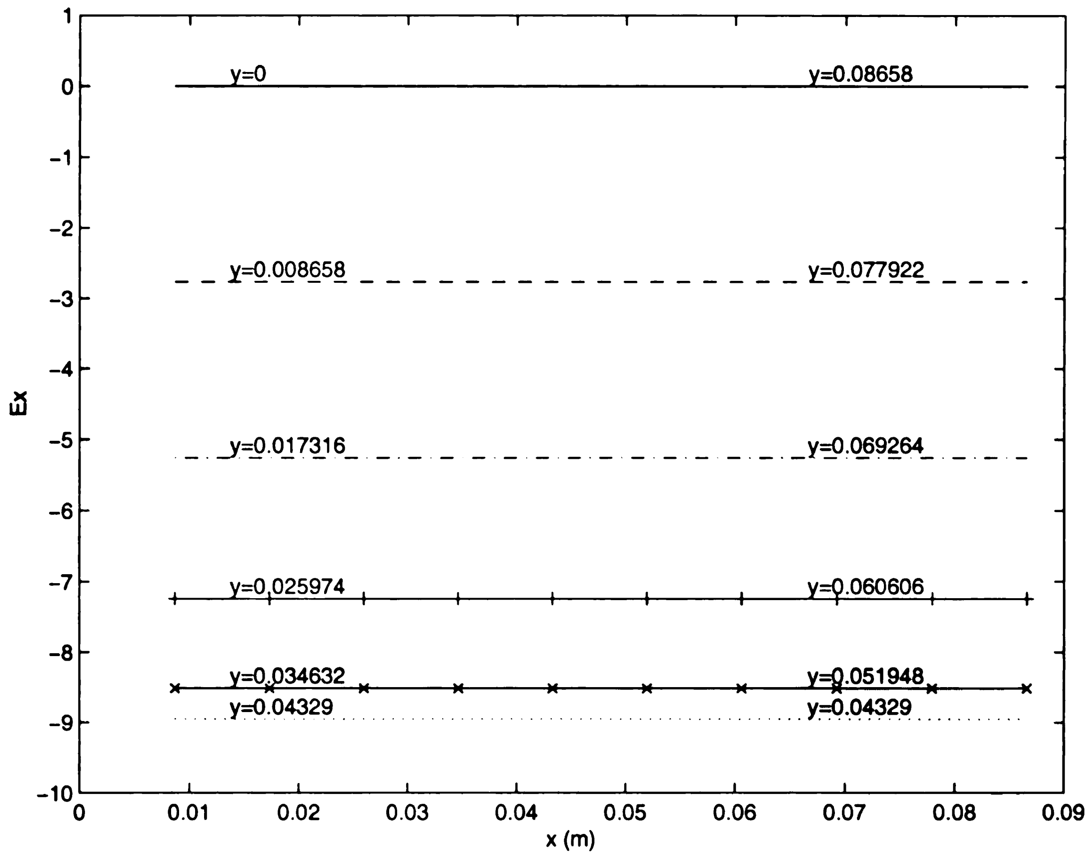

Figure 2.11 The *x* dependence of E_x at *z= 0.025974* and *t= 0.26658* μs for TE_{011} mode.

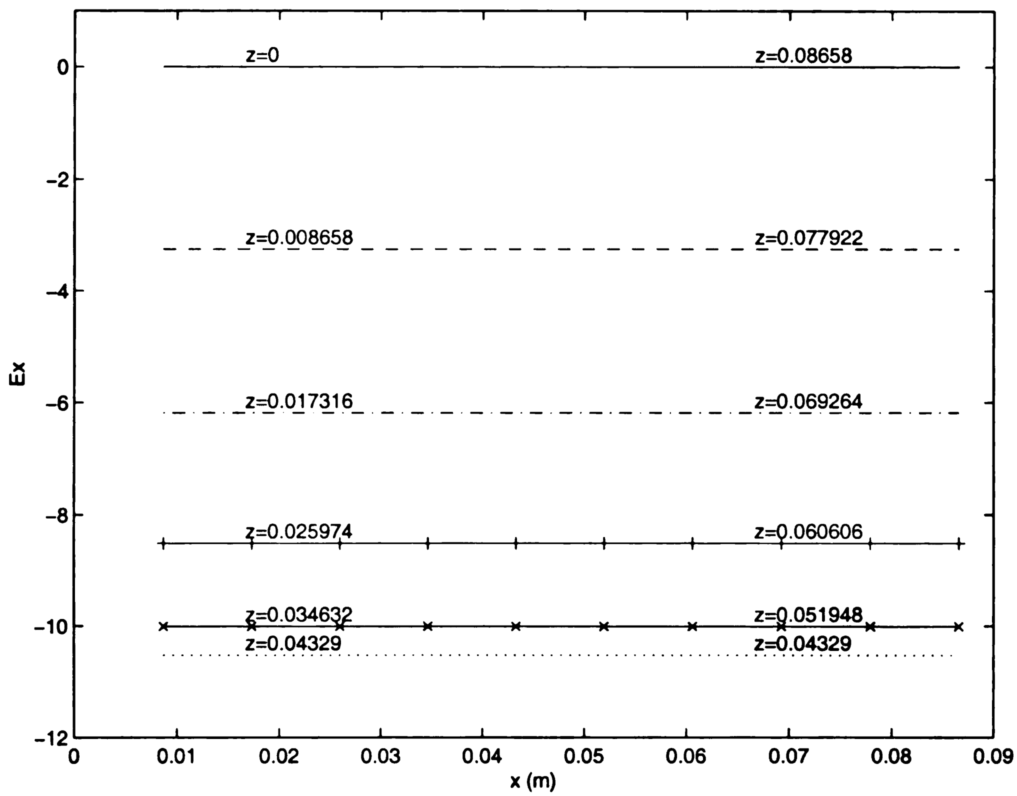

Figure 2.12 The x dependence of E_x at y= *0.034632* and t= *0.26658* μs for TE_{011} mode.

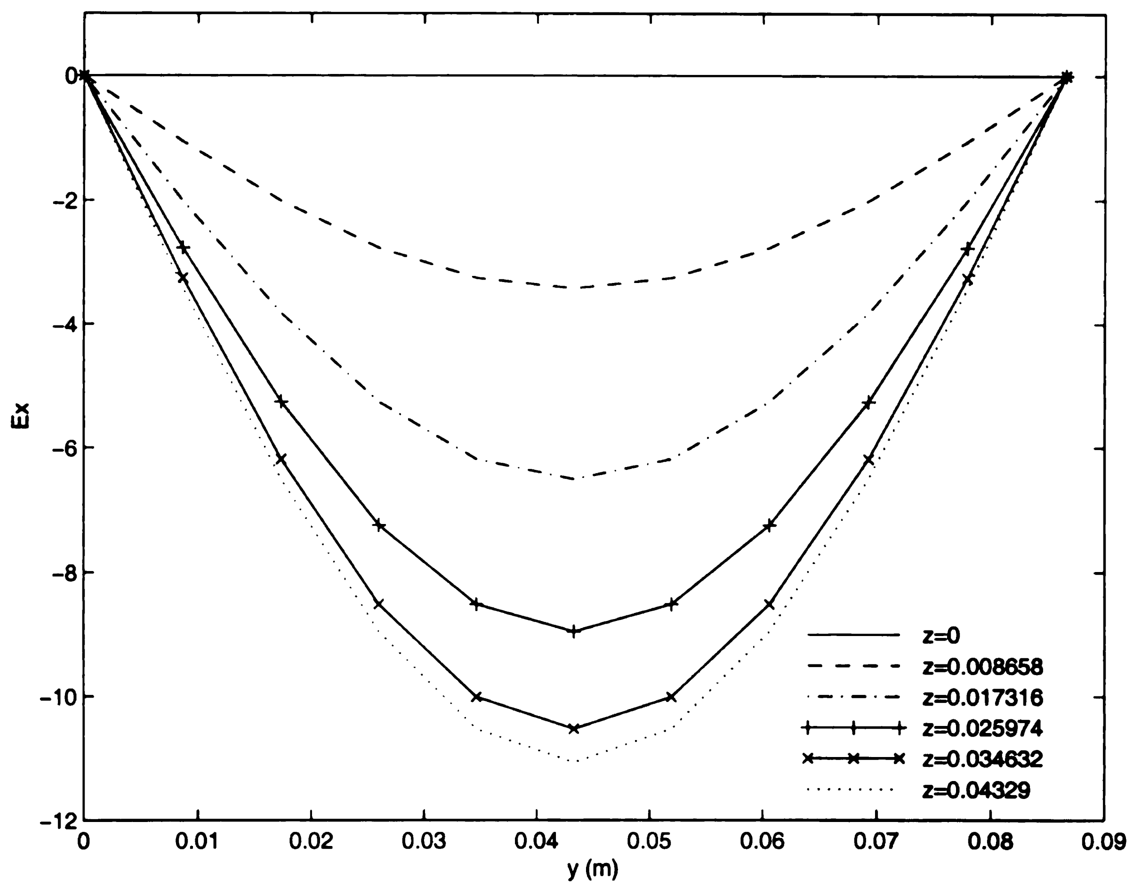

Figure 2.13 The *y* dependence of E_x at *x= 0.025974* and *t= 0.26658* μs for TE_{011} mode.

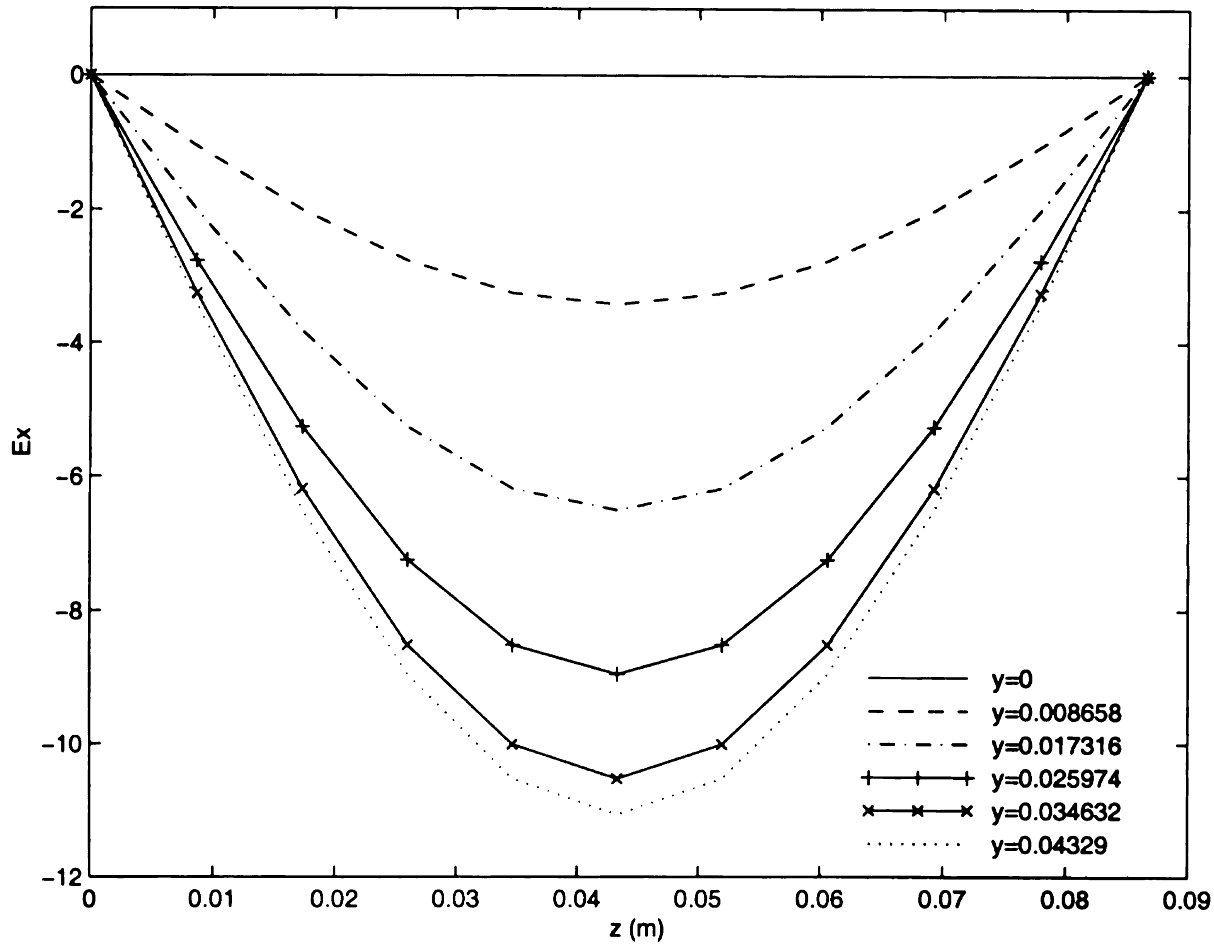

Figure 2.14 The z dependence of E_x at x= *0.034632* and t= *0.26658* μs for TE_{011} mode.

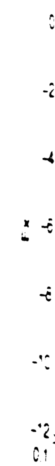

Figu
0.26(

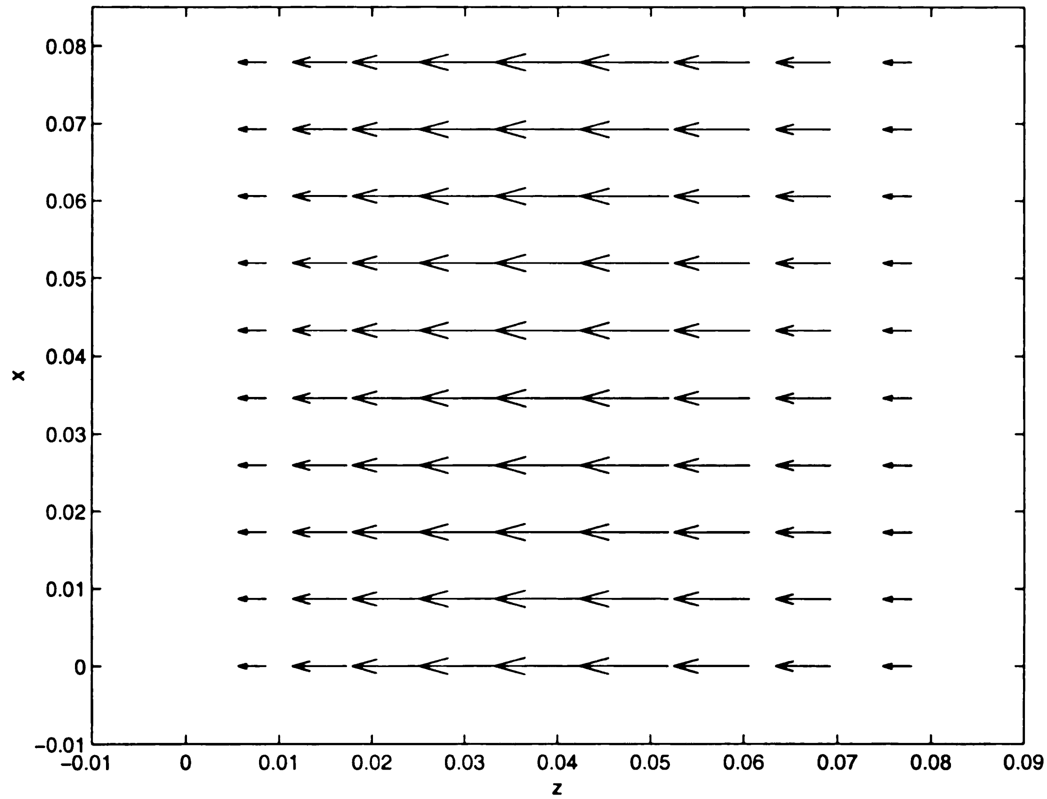

Figure 2.16 The E field on the *xz* plane at *y= 0.034632* and *t= 0.26658* μs for TE_{011} mode.

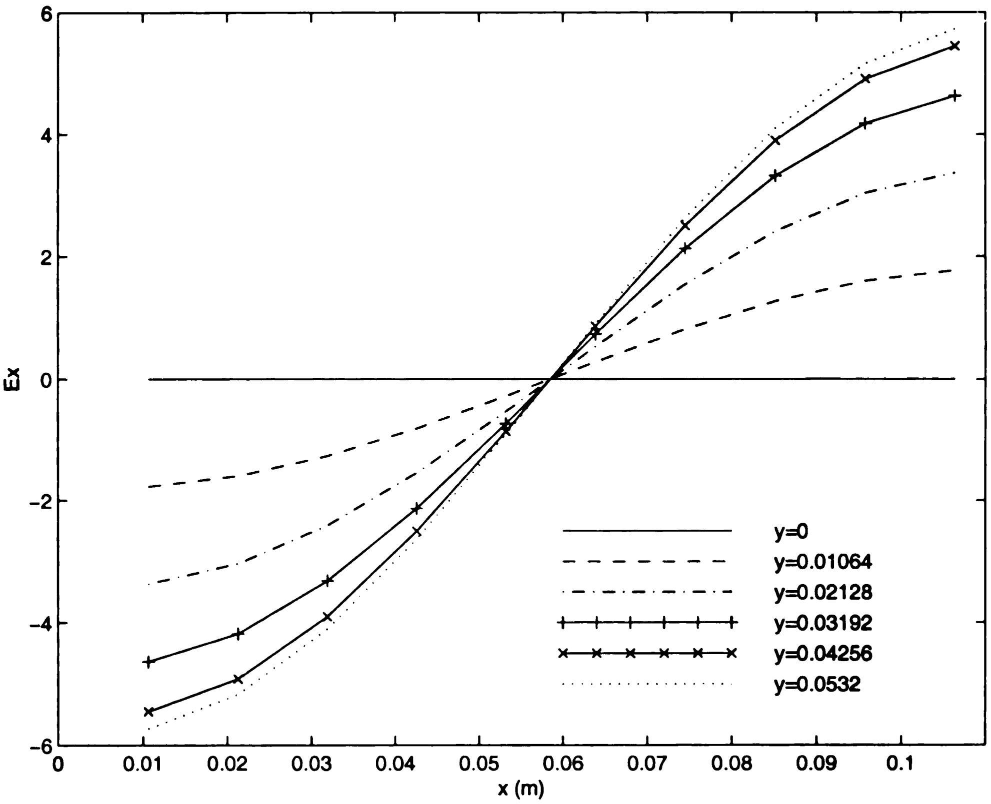

Figure 2.17 The *x* dependence of E_x at *z= 0.03192* and *t= 0.31019* μs for TM_{111} mode.

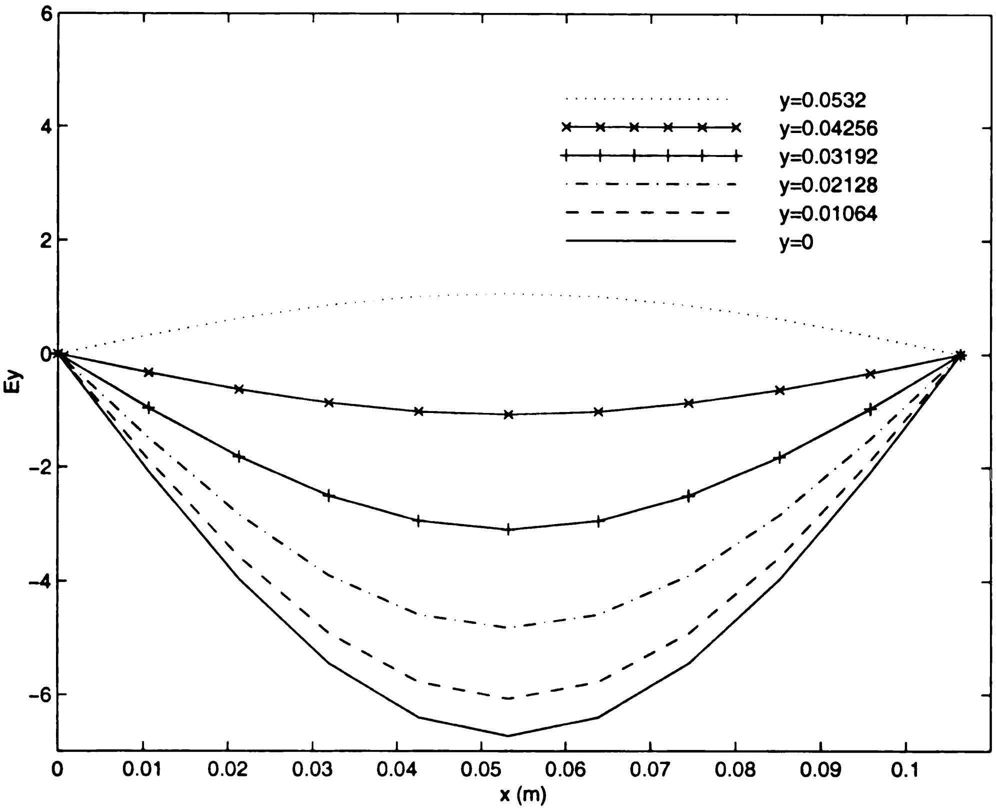

Figure 2.18 The *x* dependence of E_y at *z= 0.04256* and *t= 0.31019* μs for TM_{111} mode.

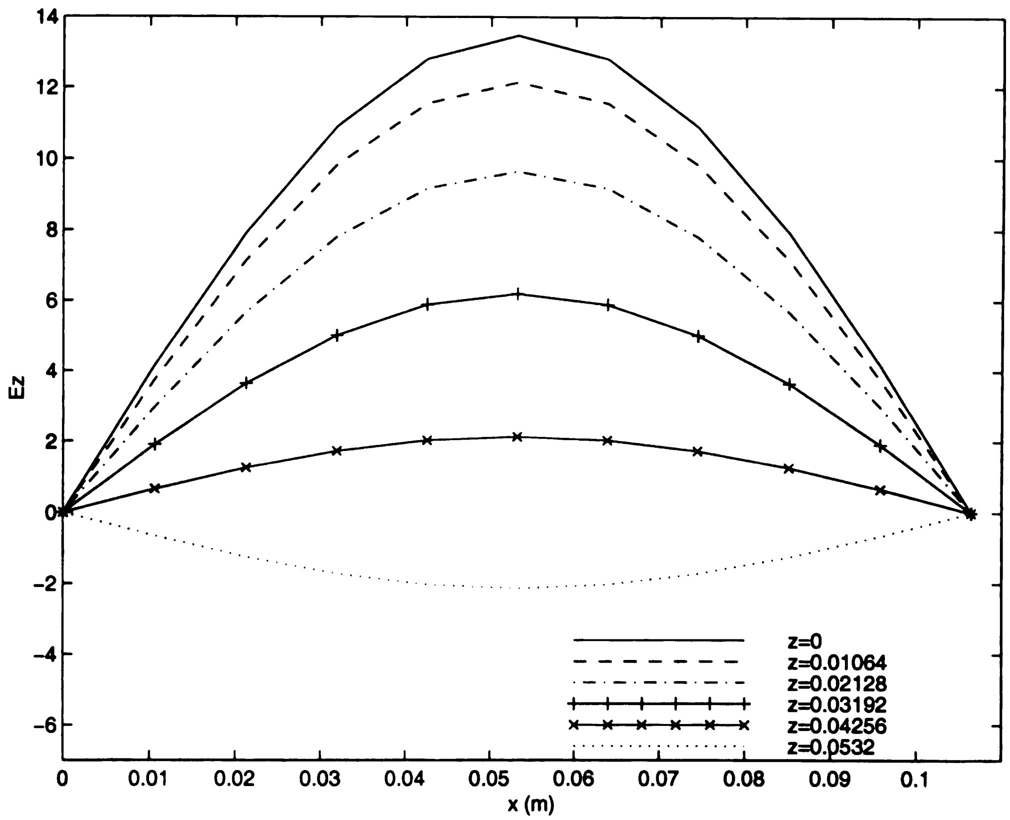

Figure 2.19 The *x* dependence of E_z at *y= 0.04256* and *t= 0.31019* μs for TM_{111} mode.

Fi
fo

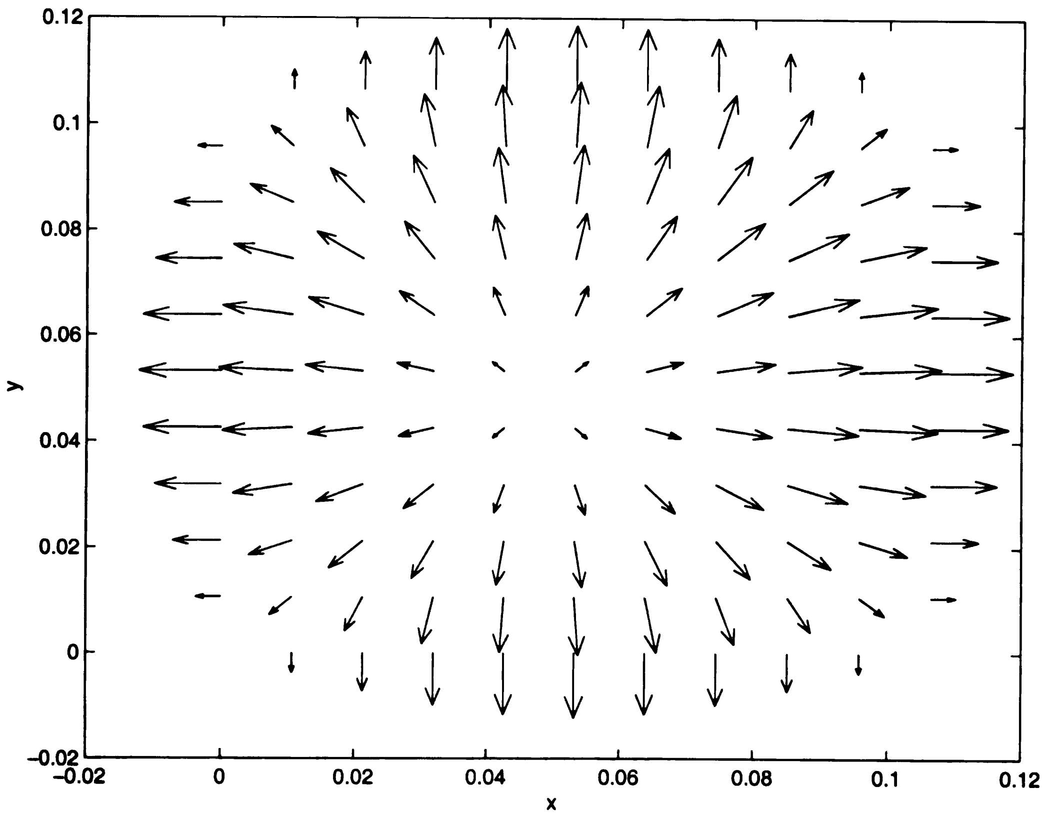

Figure 2.20 The E field on the *xy* plane at *z= 0.04265* and *t= 0.31019* μs for TM_{111} mode.

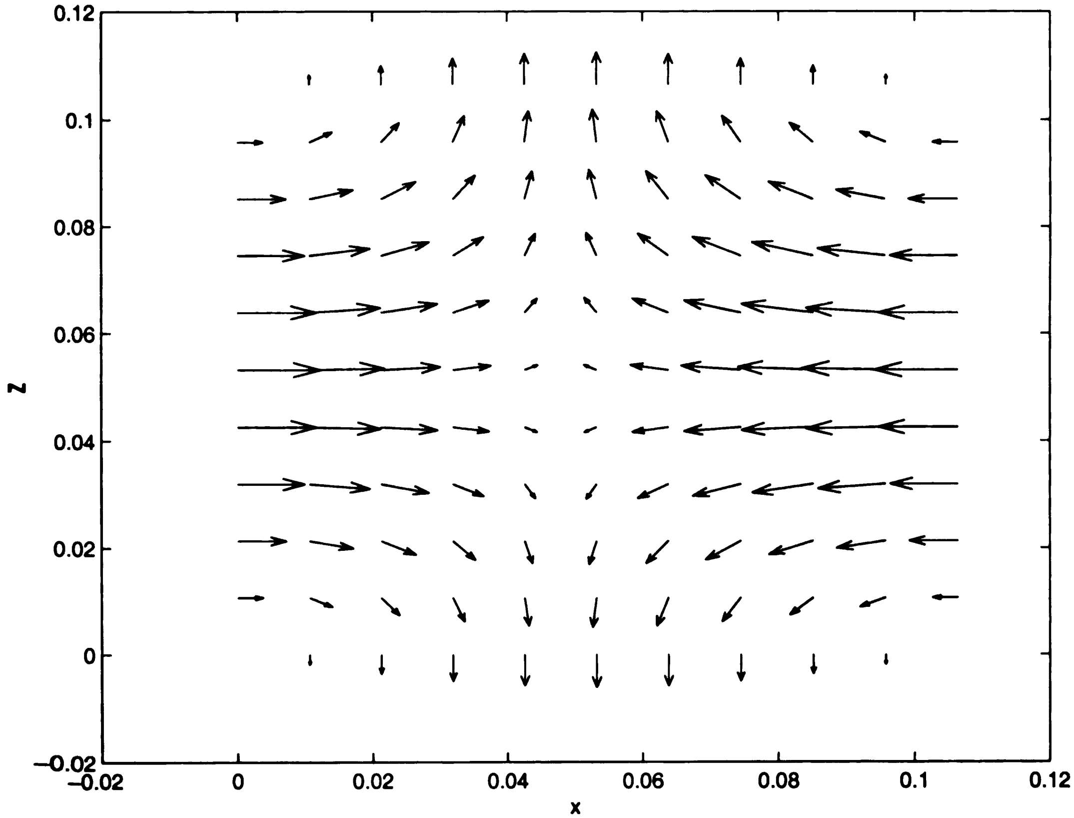

Figure 2.21 The E field on the *xz* plane at *y= 0.04265* and *t= 0.31019* μs for TM_{111} mode.

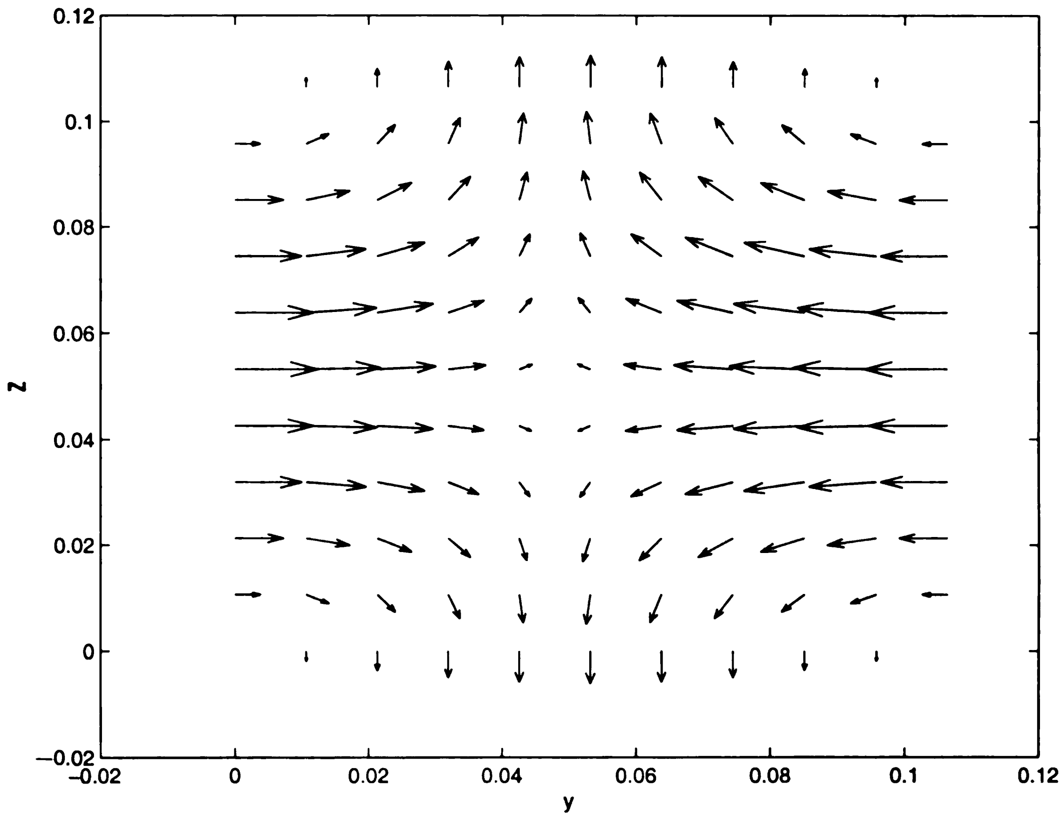

Figure 2.22 The E field on the *yz* plane at *x= 0.04265* and *t= 0.31019* μs for TM_{111} mode.

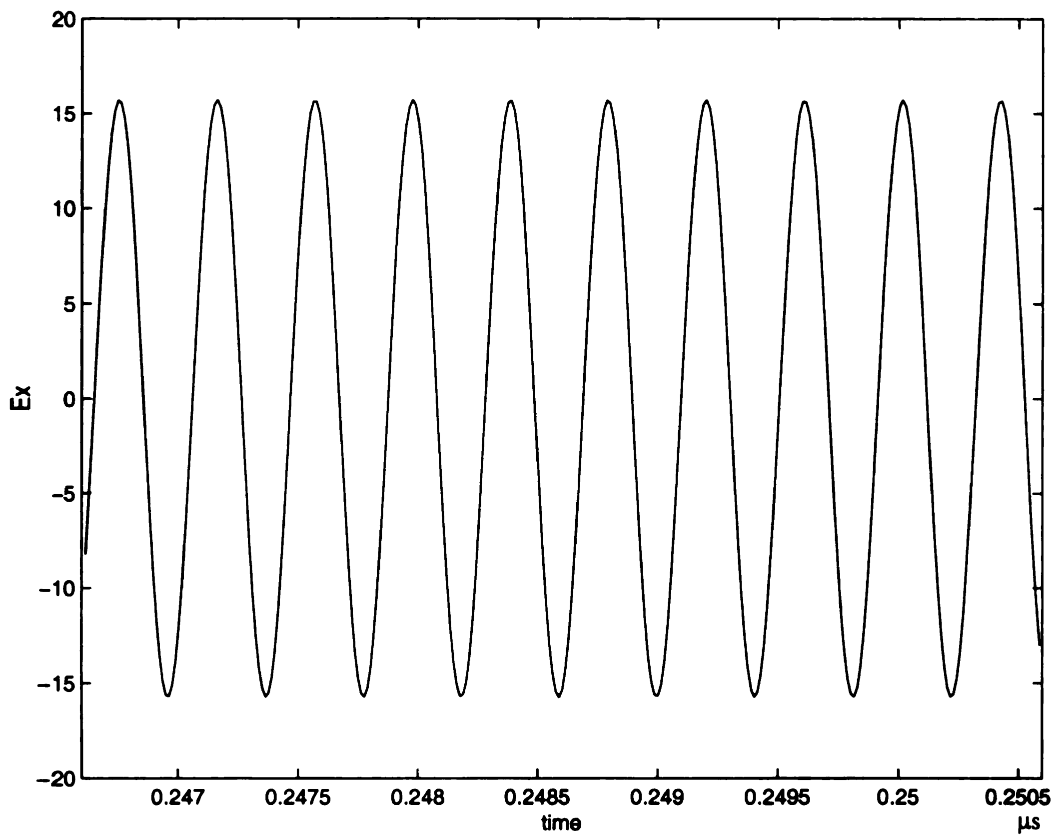

Figure 2.23 The time variation of Ex at x=0.04329, y=0.04329, and z=0.034632 for TE_{011} mode.

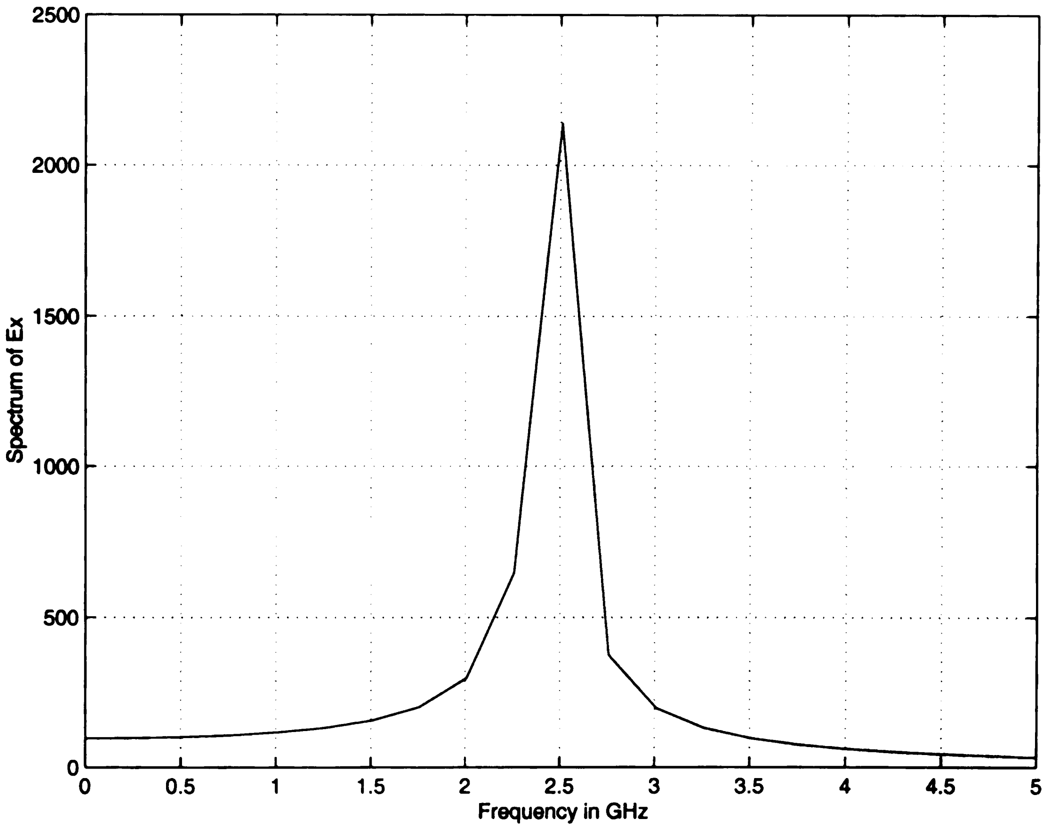

Figure 2.24 The frequency response of Figure 2.23.

2.

ar

re

Th

the

2.4

pre

sel

au

2.7

cen

x_0=

have

alon

loca

of n

Δx =

W

induc

induc

2.7 A Lossless Loaded Cavity with PEC Walls

In this section, the numerical computations of lossless loaded cavity with PEC walls are considered. A lossless rectangular material sample is placed in the center of the rectangular cavity and the dimensions of the rectangular cavity are shown in Figure 2.25. The excitation probe is located at the center of the *xz* plane and is very short comparing to the dimension of the cavity. The excited field is TE_{101} mode and the operation frequency is *2.45GHz* with the wavelength λ equal to *0.12245m* when there is no material sample present. In order to compare with theoretical estimations, three material samples with selected shape and dimensions have been studied. The excitation source is off automatically and all the numerical results are based on transient state solution.

2.7.1 Quasi-cubic Case

A quasi-cubic material sample which has almost equal dimensions is placed in the center of the rectangular cavity. The dimensions of the material sample are set to be $x_0=0.00343m$, $y_0=0.0034m$, and $z_0=0.00352m$. This sample is assumed to be lossless and have the relative permittivity of $\varepsilon_r = 2.5$. In this computation, the number of partitions along the *x*, *y*, and *z* directions are 21, 20, and 33 respectively. The material sample is located at node 10, node 9, and node 16 along the x, y, and z directions where the number of nodes starts from 0. The excitation source spans over about 67,412 time steps with $\Delta t = 3.72822ps$ and the computation stops at 68000 time steps.

With this electrically very small sample, $x_0/\lambda = 0.028$, the static electric field induced inside of a dielectric sphere, $E_{ws} = (3/(2+\varepsilon_r))E_{ns}$, is used to estimate the induced electric field in the sample where E_{ws} is the electric field inside the dielectric

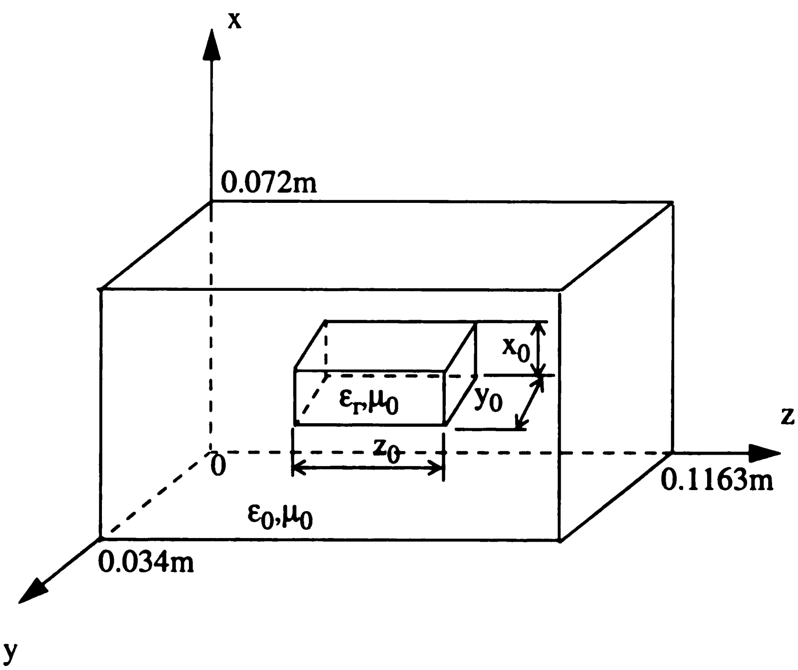

Figure 2.25 Dimensions of the rectangular cavity and the loaded material sample. The center of the material sample is consistent with the center of the cavity.

sphere and E_{ns} is that in the region of sphere before the dielectric sphere is placed. For TE_{101} mode, only E_y exists since E_x and E_z are zeros for this mode.

The variation of E_y along y axis at $x=0.034286m$, $z=0.056388m$ and at t=0.25352μs is plotted in Figure 2.26 and the calculated ratios of E_{ws}/E_{ns} inside the sample are 0.6550 and 0.6352 at node 9 and node 10, respectively, and the electrostatic estimated ratio is 0.6667. E_{ns} is approximated by the electric field at first node because E_y is constant along y axis in TE_{101} mode when there is no sample present. The closeness of the numerical results and the electrostatic estimation gives confidence to the numerical accuracy. The ratios of E_{ws}/E_{ns} along the y axis at several different times are shown in Table 2.1 and those ratios are almost independent with time for the lossless case.

Table 2.1 E_{ws}/E_{ns} ratio at different times

Time Step	E_{ws}/E_{ns} at node 9	E_{ws}/E_{ns} at node 10
67999	0.6550	0.6352
67979	0.6550	0.6352
67959	0.6550	0.6352
67951	0.6550	0.6352

Due to the induced charge on the material sample surface and the induced current in the material sample, the other components of the electric field are induced to satisfy the boundary conditions. The E_x, E_y, and E_z along the y axis are shown in Figure 2.26 and shows that the excited cavity mode is not a pure TE_{101} mode anymore since there are E_x and E_z inside the material sample. However, the TE_{101} mode still dominates inside the material sample judging from the amplitudes of E_y versus E_x and E_z in Figure 2.26.

The estimated resonant frequency of TE_{101} mode for PEC empty cavity with the dimensions shown in Figure 2.25 is 2.4532 GHz while that for PEC loaded cavity with a quasi-square cubic sample is 2.4478 GHz. The resonant frequency decreases about 0.22% after the material sample is placed inside the cavity.

2.7.2 Thin Square Plate Case

The material sample with a shape of a thin square plate, having its height much smaller than its width, is placed in the center of the cavity. The numbers of partition in this FDTD calculation are 15x17x10 and the dimensions of the material sample are *0.024m*, *0.002m*, and *0.02326m* along the *x*, *y*, and *z* directions. This sample is also assumed to be lossless with the relative permittivity of $\varepsilon_r = 2.5$.

The x dependence of E_y is plotted in Figure 2.27 and then a *sine* function is used to fit that curve. By this way, the E_{ns} is obtained since the E_y versus y plot is not a constant anymore. The induced electric field inside the material sample is estimated by the boundary condition of $E_{ws} = (1/\varepsilon_r)E_{ns}$. The ratios of E_{ws}/E_{ns} along the *x* direction for different locations of *z* are plotted in Figure 2.28. Those ratios inside the material sample varies from 0.39 to 0.45 which are close to the electrostatic estimation of 0.4. The ratios of E_{ws}/E_{ns} varies slightly at different times for this case.

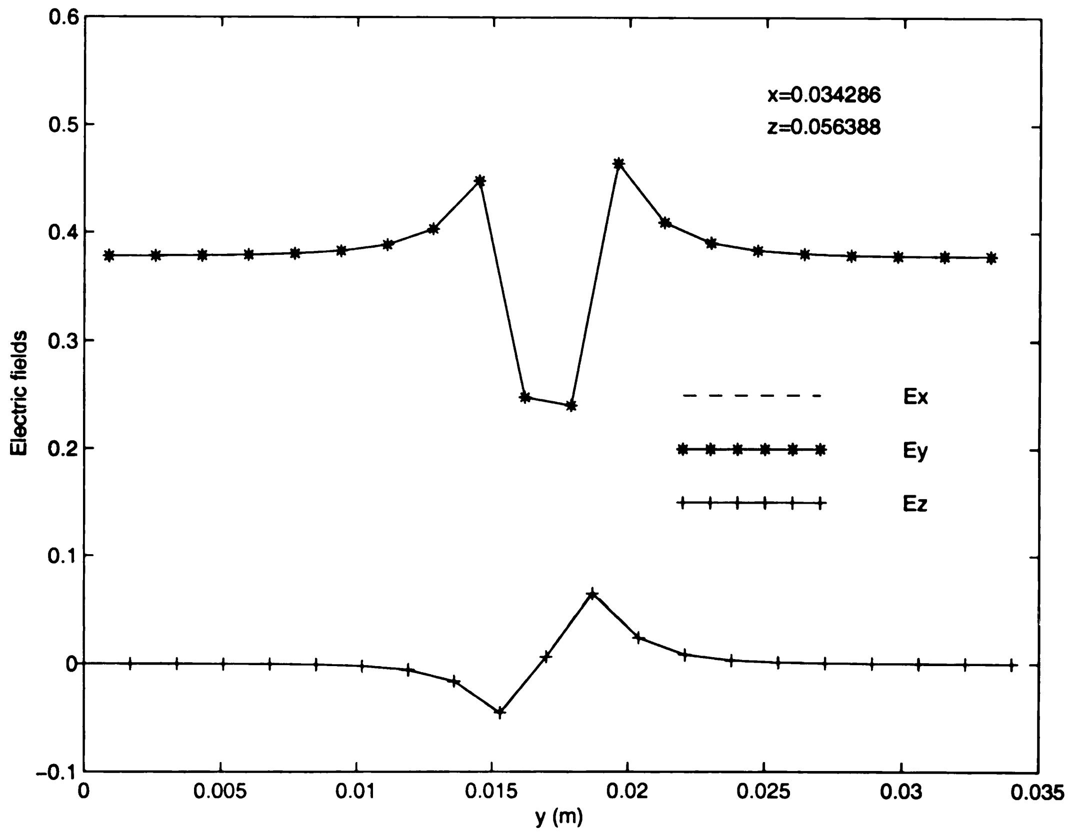

Figure 2.26 The variation of electric fields in the y direction at $t = 0.2535\mu s$.

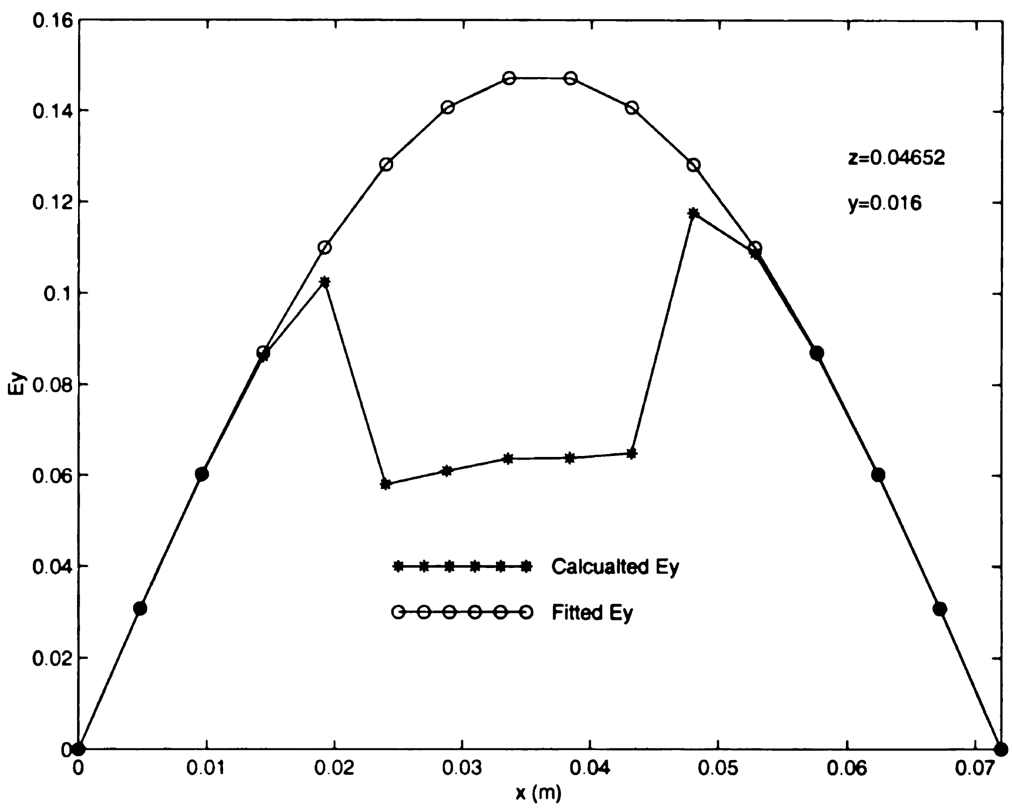

Figure 2.27 The variation of E_y in the x direction at $t = 0.24289\mu s$. The line with star symbol is the calculated values and the line with circle symbol is the fitted values for the empty cavity.

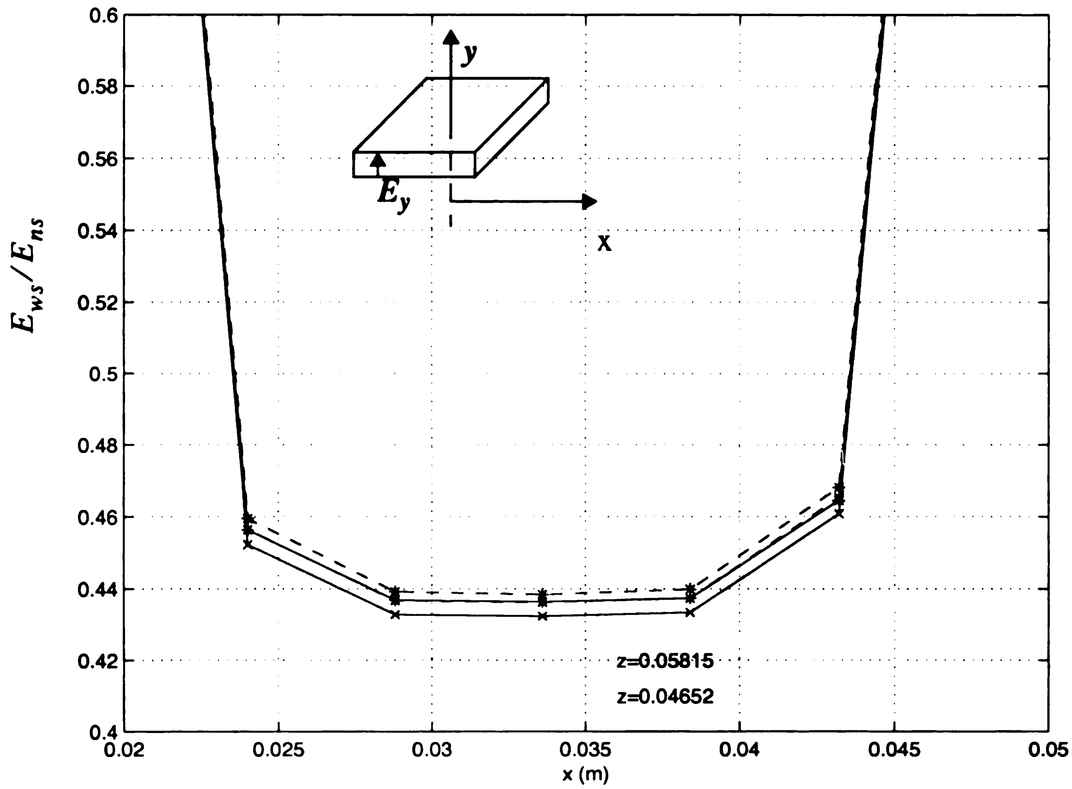

Figure 2.28 Variations of E_{ws}/E_{ns} in the x-directions. Each curve represents this ratio as a function of x for different locations of z. The relative permittivity of the thin square plate material sample is $\varepsilon_r = 2.5$. The solid line with symbols is the ratios at $t = 0.24289\mu s$ and the dash line with symbols is those at $t = 0.24301\mu s$.

The excitation source is off at 0.239μs which covers 49,049 time steps with $\Delta t = 4.862ps$ and the computation stops at 50,000 time steps. The calculated resonant frequency is 2.4382 GHz and the frequency shift is 0.61% comparing to 2.4532 GHz which is the resonant frequency in empty cavity. The maximum of E_x and E_z inside the material sample is in the order of 10^{-4} which is very small comparing to the E_y. This is because the material sample is very thin in the *y* direction so that there is no significant induced field E_x and E_z.

2.7.3 Narrow Strip Case

The dimensions of this narrow strip sample are *0.002322m*, *0.02125m*, and *0.002115m* along the *x*, *y*, and *z* directions. This sample is also assumed to be lossless and have the relative permittivity of $\varepsilon_r = 2.5$. The number of partitions of this FDTD calculation is 31x16x55.

Theoretical estimation of the induced electric field in the material sample may be close to the electric field when the cavity is empty because the initial electric field is tangential to the major part of the material sample surface, and the continuity of the tangential component of the electric field at the material sample surface requires this estimation. The variation of electric field along y is plotted in Figure 2.29 and the ratios of E_{ws}/E_{ns} are shown in Figure 2.30. The induced E_x and E_z fields inside the material sample are almost zero and E_y is the dominant field. The ratios of E_{ws}/E_{ns} inside the material sample range from 0.94 to 0.99 which are close to the theoretical estimation of 1.

The excitation source is off at 74,835 time steps which spans over *0.25133μs* with

$\Delta t = 3.35841\,ps$, and the computation stops at 75,000 time steps. The calculated resonant frequency for this narrow strip case is 2.4464 GHz and the frequency shift is 0.28% from the resonant frequency of the empty cavity of 2.4532 GHz.

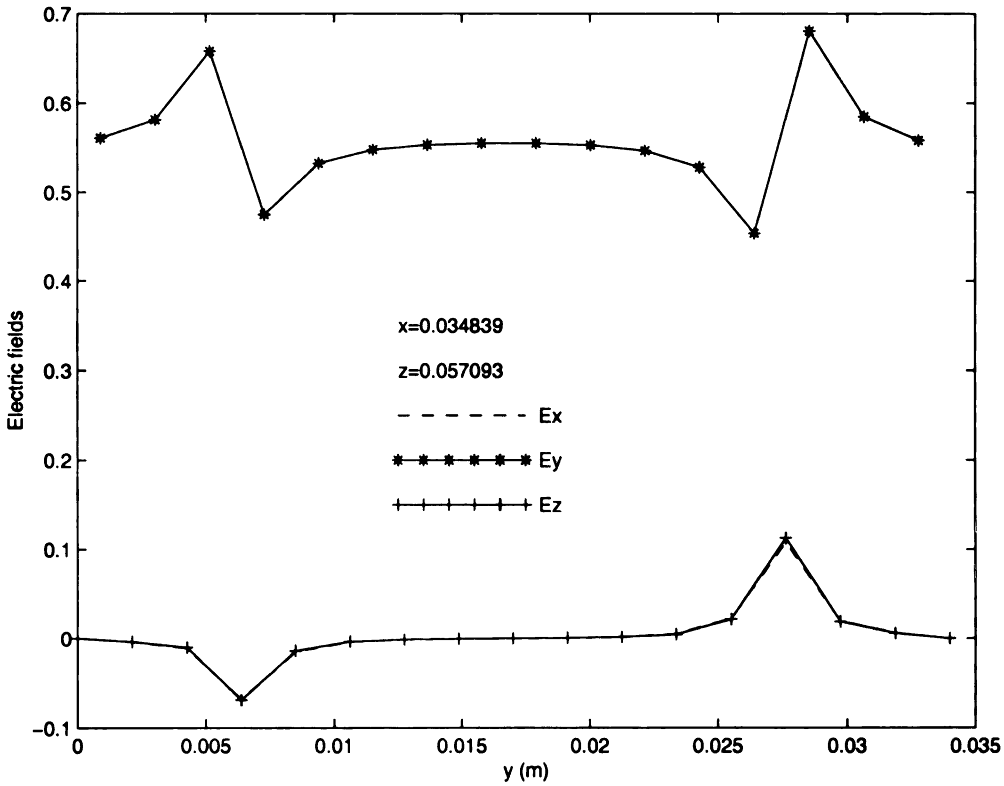

Figure 2.29 The variation of electric fields in the y directions at x=0.34839m, z=0.057093m, and t=0.252μs.

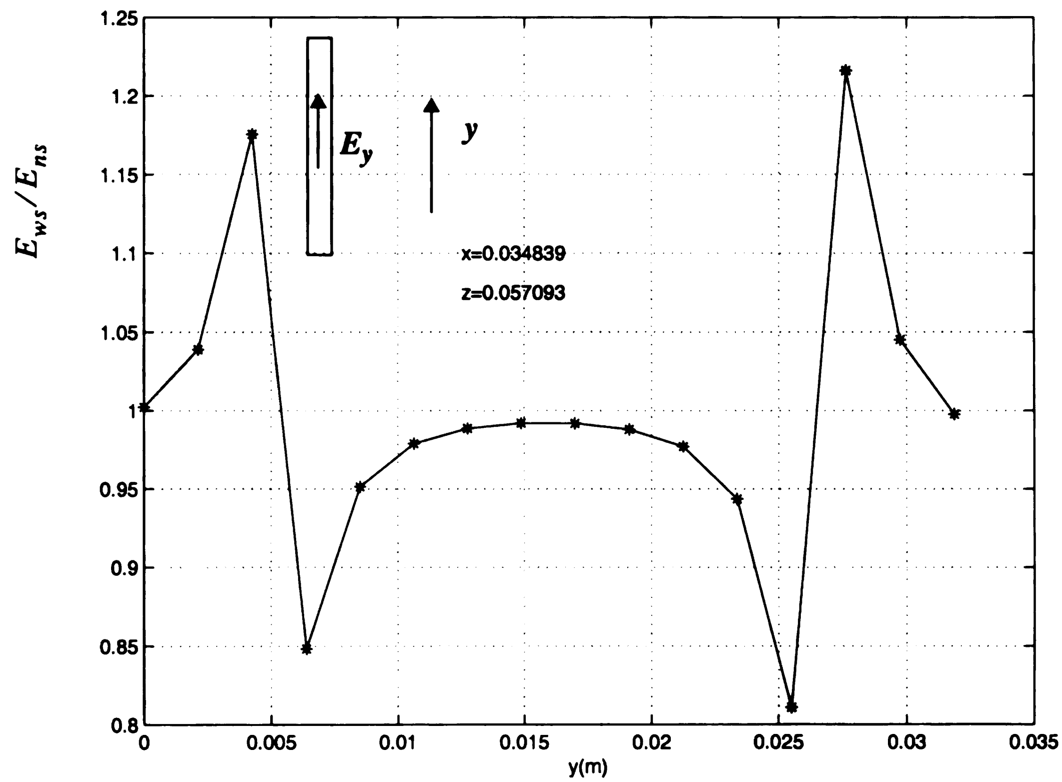

Figure 2.30 The ratios of E_{ws}/E_{ns} in y directions.

2.8 A Lossy Dielectric Loaded Cavity with PEC Walls

The field distributions of a cavity loaded with a lossy dielectric material sample with PEC wall is discussed in this section. The excitation source for this lossy case is a single frequency sinusoidal source turned on all the time. The size of material sample is chosen large enough to cause a relatively low quality factor of the cavity. The relation of cavity quality factor and number of the time steps which is needed to reach the steady state is also studied in this section. In order to identify the time steps to reach the steady state, the FDTD formulation of power analysis is used.

2.8.1 Configurations

The physical configuration of this case is the same as that in Figure 2.25 but with a larger material sample. The numbers of partition along x, y, and z are *15*, *17*, and *10* and the dimensions of the material sample are: *0.0336*x*0.014*x*0.0698 m*.

The real and imaginary parts of the relative permittivity in (2.3) can be obtained as

$$\varepsilon'_r(\omega) = \varepsilon'_{r\infty} + \frac{\varepsilon'_{rs} - \varepsilon'_{r\infty}}{1 + (\omega\tau_e)^2} \tag{2.121}$$

$$\varepsilon''_r(\omega) = \frac{(\varepsilon'_{rs} - \varepsilon'_{r\infty})\omega\tau_e}{1 + (\omega\tau_e)^2} \tag{2.122}$$

and the ε'_r and ε''_r can be expressed as follow:

$$\varepsilon'_{rs} = \varepsilon'_r(\omega) + \omega\tau_e\varepsilon''_r \tag{2.123}$$

$$\varepsilon'_{r\infty} = \varepsilon'_r(\omega) - \frac{\varepsilon''_r}{\omega\tau_e}. \tag{2.124}$$

For the lossy material sample, the relaxation time, τ_e, is not zero and it depends on the properties of the material. In this FDTD computation, τ_e is assumed to be 10^{-9} seconds and the ε'_r is set to 2.5 with four different ε''_r as listed in Table 2.2.

Table 2.2 Permittivities mapping at $\tau_e = 1ns$, $\omega = 2\pi(2.45e9)$

$\varepsilon'_r(\omega)$	$\varepsilon''_r(\omega)$	ε'_{rs}	$\varepsilon'_{r\infty}$
2.5	0.1	4.0394	2.4935
2.5	0.5	10.1969	2.4675
2.5	2.5	40.9845	2.3376
2.5	5	79.469	2.1752

According to the analysis in section 2.3.3, the stability of the Ty(2,4) $(FD)^2TD$ scheme depends on the material properties. Hence, for the first two permittivities in Table 2.2 we choose $\Delta t = 4.25442ps$ and the last two at $\Delta t = 4.8622ps$. Note that a smaller Δt needs to be used if a small $\varepsilon''_r(\omega)$ is chosen.

2.8.2 Numerical Results and Discussions

The approximate time steps to reach the steady state needs to be identified first in the lossy case calculation. When the average input power is equal to the average dissipated power, the system reaches the steady state. The dissipated powers for the first case with $\varepsilon'_r(\omega) = 2.5$ and $\varepsilon''_r(\omega) = 0.1$ are plotted in Figure 2.33 and the corresponding stored energy is shown in Figure 2.32. Note that the input power is calculated from (2.93) since the induced EMF method used is not accurate to calculate the input power at the probe location. The stored energy is calculated from the integral of the difference of input power and dissipated power. In order to determine the average power, a *sine* function is used to fit the calculated data between *33,900* and *34,000* time steps in those two figures as shown in Figure 2.34 and Figure 2.35. When the difference of this fitting data and the dissipated power data in the period of zero to 35,000 is plotted, we obtain Figure 2.36. From Figure 2.36, it is observed that the approximate time step to reach the steady state is about *25,000* for this case. By using the same approach, the time steps for other cases are obtained. The average loss power and the time-average stored energy are listed in Table 2.3.

Table 2.3 The loss power and stored energy

$\varepsilon''_r(\omega)$	The average loss power	The time-average stored energy
0.1	2.45e-10	8.905e-18
0.5	1.1258e-9	8.8e-18
2.5	3.035e-9	7.55e-18
5	3.205e-9	7.45e-18

In Table 2.4, the major resonant frequency and the Q factor in the fifth column are calculated by using Prony's method. In order to obtain the Q factor by Prony's method, a windowed sinusoidal source is used. The fourth column is the Q factor calculated from the definition. The number of time steps to reach the steady state is roughly equal to the Q

Table 2.4 Properties of four different lossy cases

$\varepsilon''_r(\omega)$	Major Resonant Frequency (GHz)	Frequency Shift (%)	$Q = \omega_0 \frac{\text{Stored energy}}{\text{Power loss}}$	Q Prony's Method	Approximated Time Steps
0.1	2.4503	0.12	559.5	523.6	25,000
0.5	2.45	0.13	120.3	125	5,000
2.5	2.45	0.13	38.3	37.1	1,400
5	2.45	0.13	35.7	34.2	1,300

factor divided by twice the resonant frequency times the period of one time step. Hence, a very long time integration is needed if a high Q cavity is dealt with. The field distribution calculation scheme for the high Q cavity is shown in Figure 2.31. This algorithm is easy to corporate with other temperature related equations to calculate the temperature change in a cavity.

The field distribution of E_y in the steady state and the fitting *sine* function are plotted in Figure 2.37. The ratios of the calculated and fitted E_y are plotted in Figure 2.38. The ratios are no longer close to *0.4* as that in Figure 2.28; however, the ratios at those points which are near to the middle point of the material sample is still around *0.4*. In this case, the material sample is much larger than that in section 2.7, so the field distribution is no longer easy to be fitted by a pure sinusoidal function which is shown in Figure 2.37.

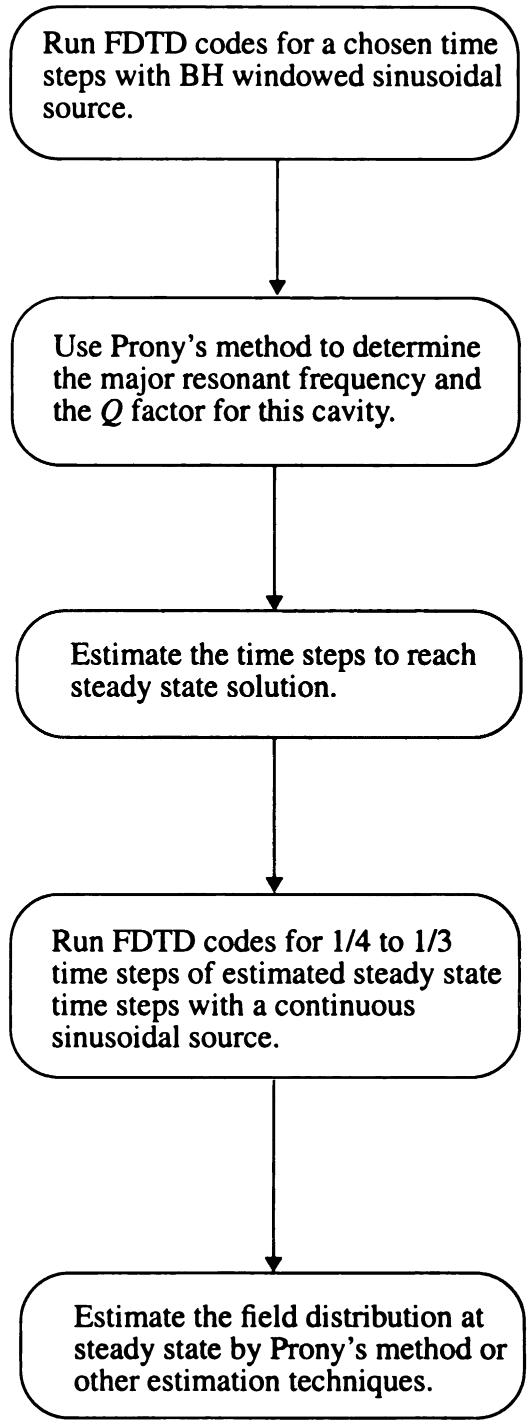

Figure 2.31 The flow chart of calculating the field distribution at steady state for high Q cavities.

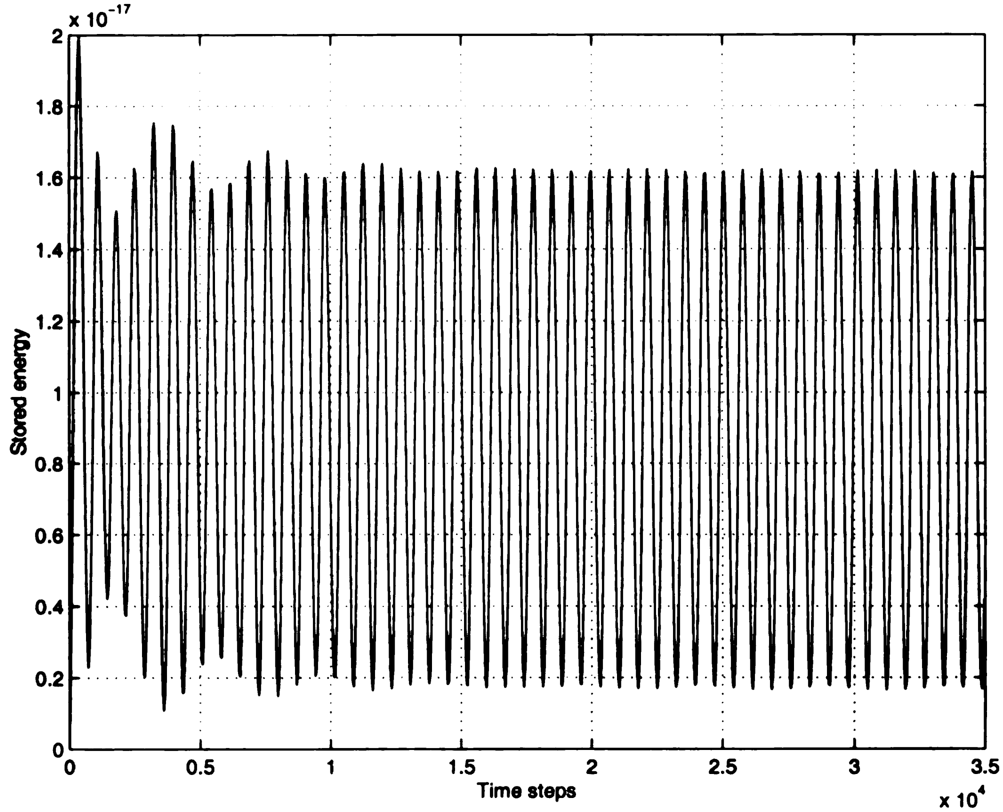

Figure 2.32 Stored energy for the cavity with material sample of $\varepsilon'_r(\omega) = 2.5$ and $\varepsilon''_r(\omega) = 0.1$. Note that one time step is equal to *4.25442 ps* and this is a downsampling plot.

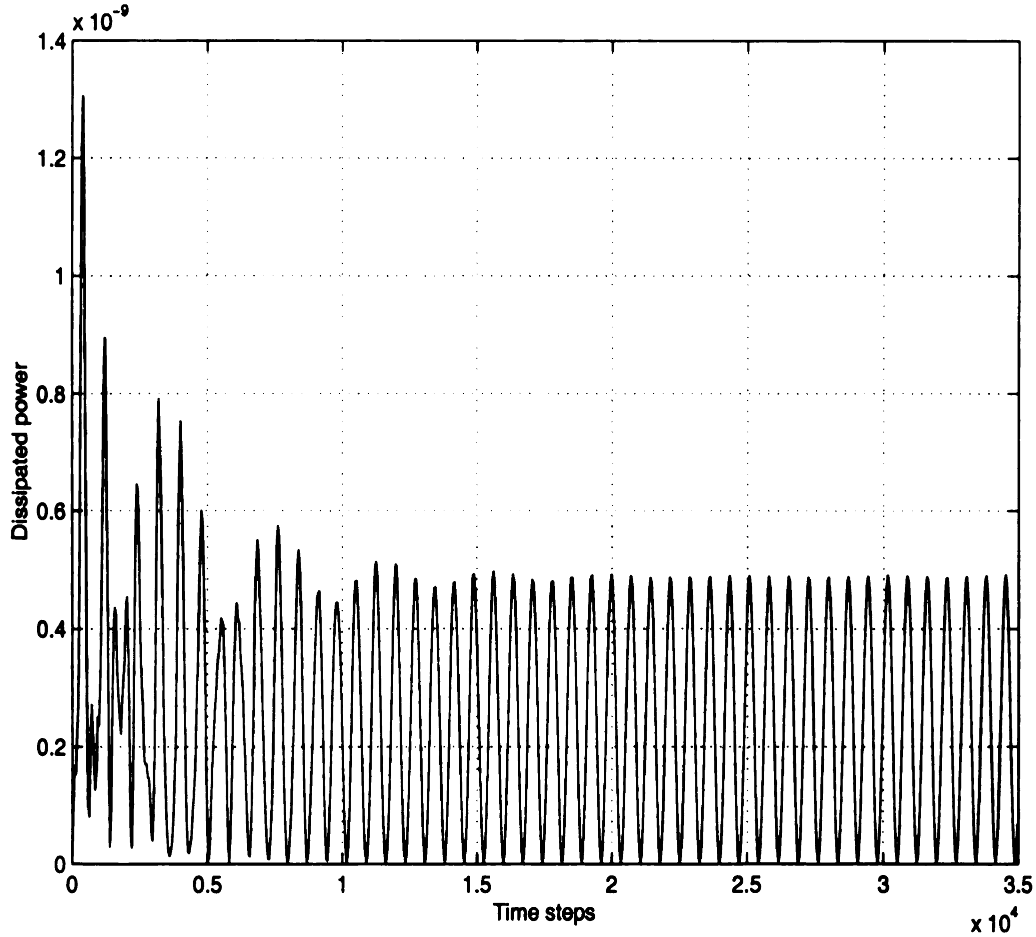

Figure 2.33 Instantaneous dissipated power for the cavity with material sample of $\varepsilon'_r(\omega) = 2.5$ and $\varepsilon''_r(\omega) = 0.1$. Note that one time step is equal to *4.25442 ps* and this is a downsampling plot.

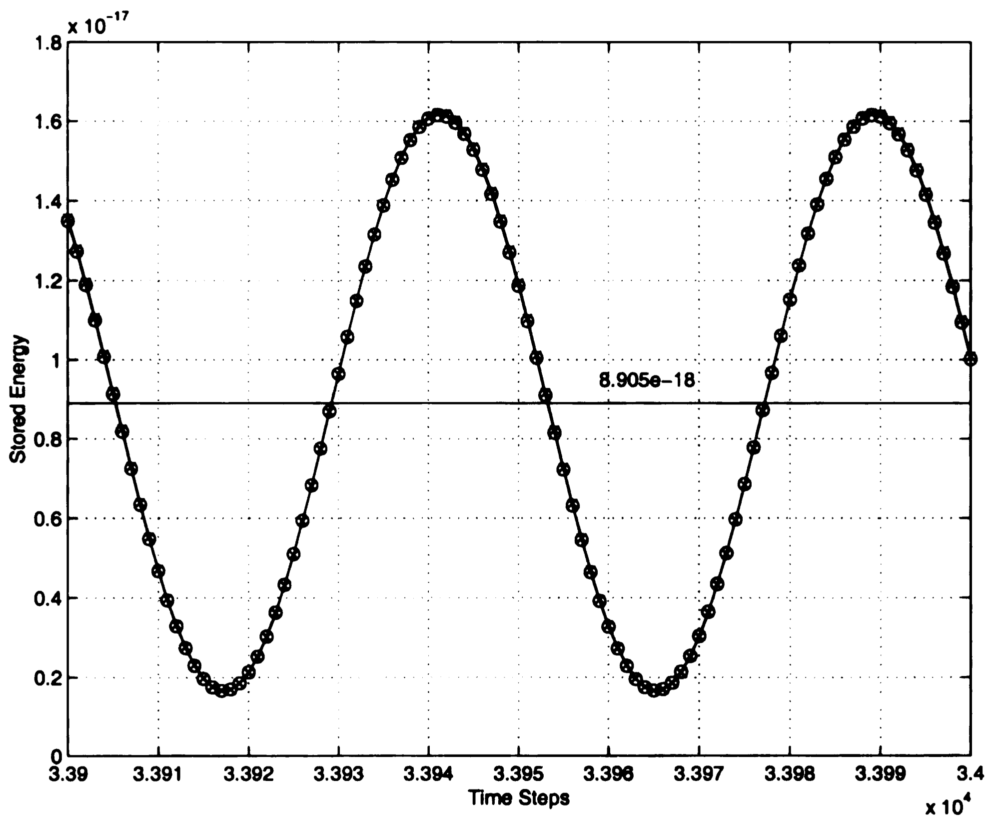

Figure 2.34 The plot of the fitting and calculated data for stored energy for the first case. The line with circle is the fitting data and that with cross is the calculated power data. The average input power is *$2.45x10^{-10}$* and the time average stored energy is *$8.905e^{-18}$*.

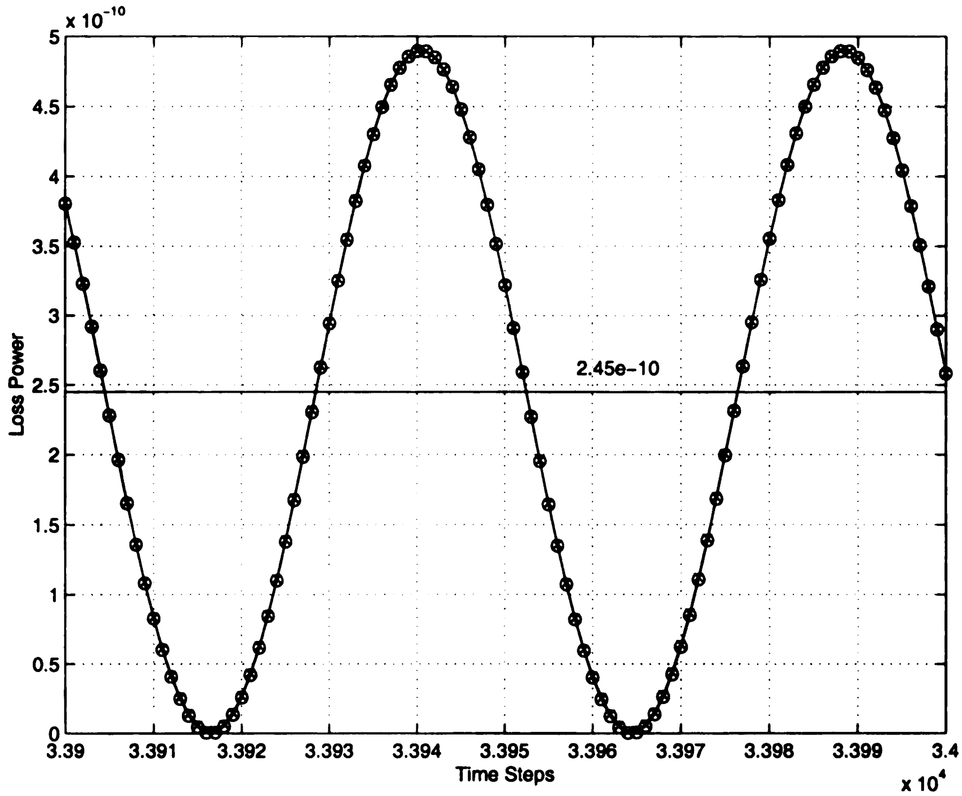

Figure 2.35 The plot of the fitting and calculated data for dissipated power for the first case. The line with circle is the fitting data and that with cross is the calculated power data. The average input power is ***$2.45x10^{-10}$*****.**

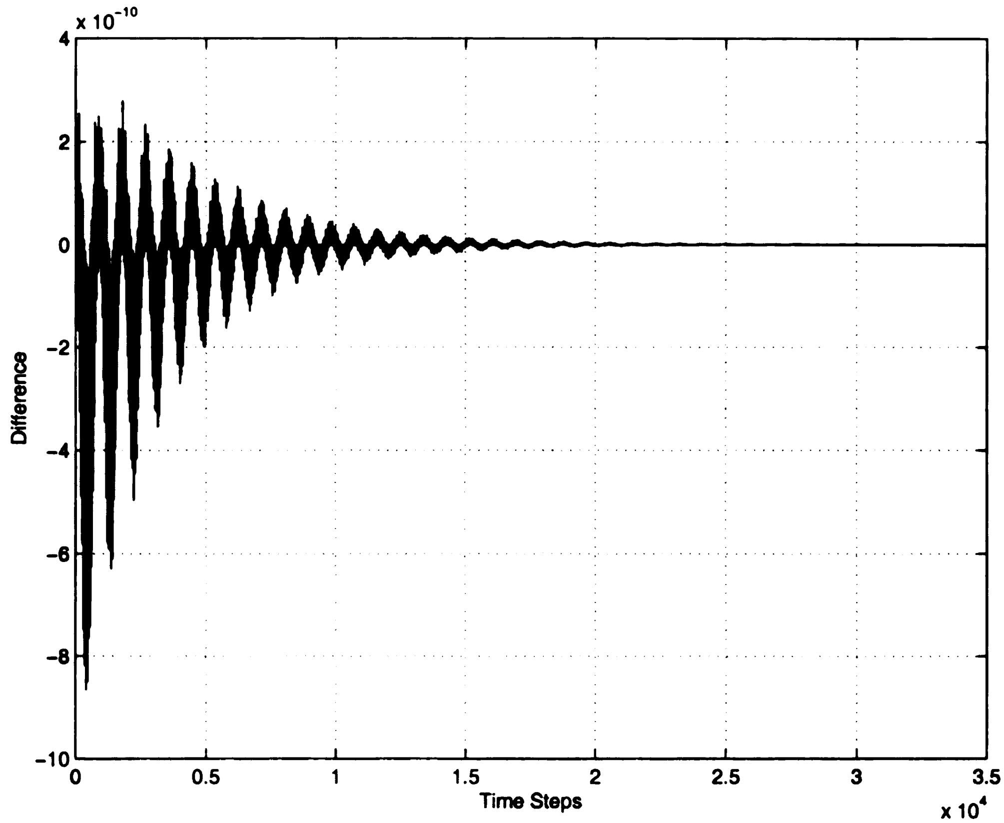

Figure 2.36 The plot of the difference between fitting and dissipated power data. The one time step is equal to *4.25442 ps*.

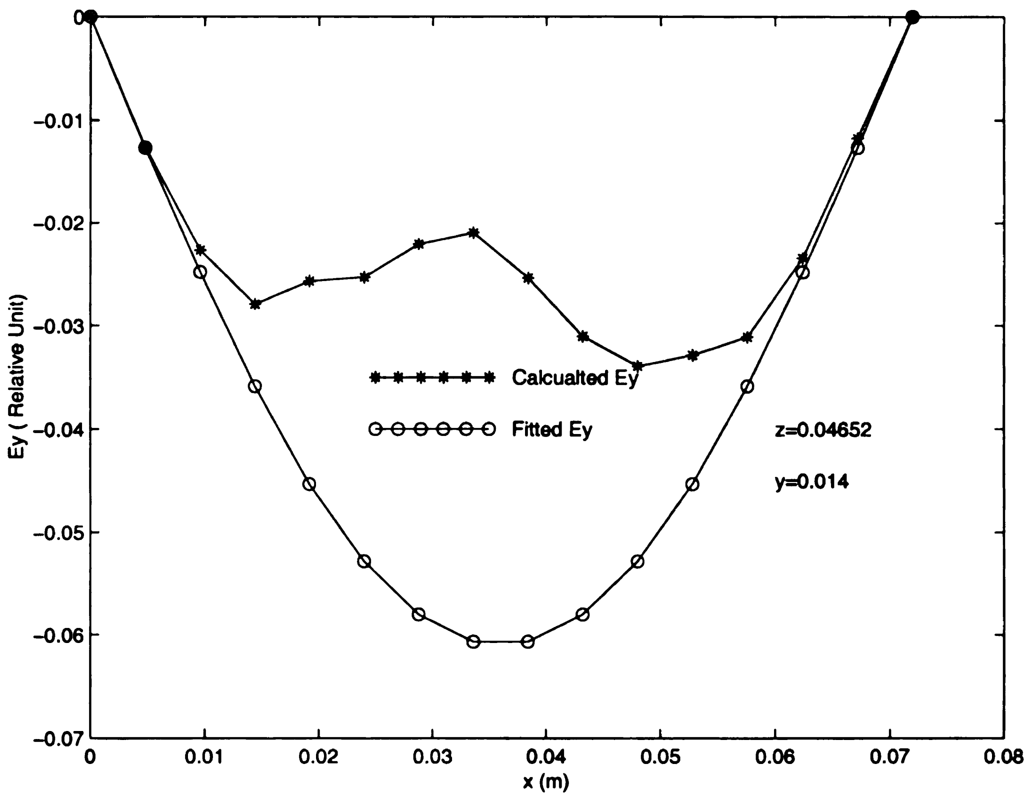

Figure 2.37 Field distributions of E_y along x axis at 0.14868 μs. $\varepsilon'_r(\omega)$ is equal to *2.5* and $\varepsilon''_r(\omega)$ is *0.1*.

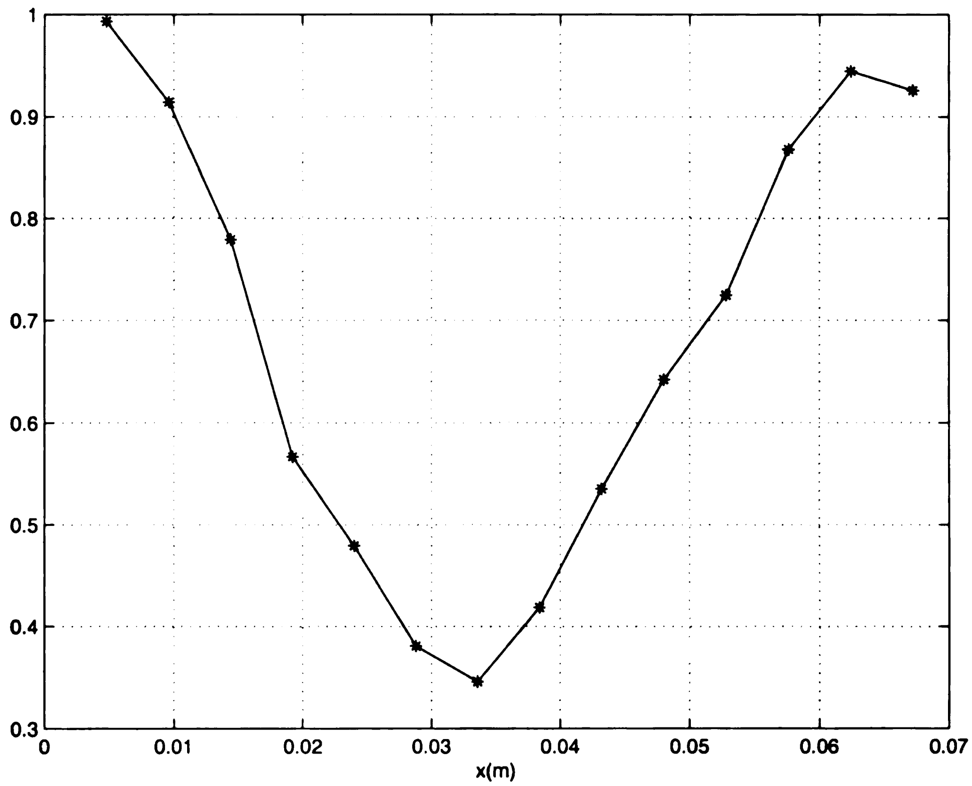

Figure 2.38 The ratio of calculated and fitting E_y along x axis at 0.14868 μs.

CHAPTER 3

SOLVING MAXWELL'S EQUATIONS BY BODY OF REVOLUTION FDTD

In the study of the interaction of microwave radiation with non-ionic materials, a material sample is placed in a cylindrical EM cavity which is excited with a fundamental cavity mode. Most of the time, objects that are symmetric about an axis are encountered; hence the body of revolution (BOR) FDTD is examined and used to solve the problems involving cylindrical cavity loaded with symmetric material sample.

The cylindrical cavities with perfectly electrically conducting (PEC) boundaries are first studied in this chapter. The BOR FDTD formulation of Maxwell's equations in cylindrical coordinates is first constructed in section 3.1. Two sets of equations are derived for the FDTD formulation. The selection of which set of equations to be used for field calculation in cavity problem is determined by the characteristic of cavity modes. Then the singularity problems at $\rho = 0$ is discussed. The Blackman-Harris (BH) function is used to construct the excitation source in the cylindrical PEC cavity calculation since the sidelobe of BH function is approximately -92 dB. The excitation probe is assumed to be located at a point on the cylindrical wall. In section 3.2, the surface impedance boundary condition (SIBC) is used to simulate the finitely electrically conducting (FEC) boundary. Three methods of the FDTD formulation for SIBC is presented and the frequency domain approximation is used in the actual calculation since it gives stable numerical solutions. For the cavity with lossy wall, a continuous source is used and the time step to reach the steady state is studied. TM_{012} and TE_{111} modes of the empty cylindrical PEC and FEC cavities are calculated and the results of the former case is compared to the analytical solution in section 3.3. The field distributions of TM_{012} and TE_{111} modes with a cylindrical PEC cavity loaded by a small cylindrical material centered in $\rho = 0$ are then calculated. The results of the former case are compared with corresponding theoretical estimation. The field distributions of the cavities with a thin rod or a thin disk material are also calculated and compared to theoretical estimations.

After the induced electric field inside the material sample is accurately quantified, the dissipated power density inside the material sample can be calculated. This dissipated power density acts as the heating source to raise the temperature of the material sample.

3.1 The BOR Formulation of Maxwell's Equations[28]

Consider Maxwell's curl equations in non-dispersive medium written in cylindrical coordinates in a linear material,

$$\nabla\times\vec{H} = [\varepsilon]\frac{\partial\vec{E}}{\partial t} + [\sigma]\vec{E} + \vec{J}_s \tag{3.1}$$

$$\nabla\times\vec{E} = -[\mu]\frac{\partial\vec{H}}{\partial t} + [\sigma^*]\vec{H} \tag{3.2}$$

where $[\varepsilon]$, $[\sigma]$, $[\mu]$, and $[\sigma^*]$ are electric permittivity, electric conductivity, permeability, and magnetic conductivity in tensor form, respectively. $\vec{J}_s$ is the known impressed current source. These constitutive parameters can be expressed in tensor form in cylindrical coordinates as

$$[\alpha] = \begin{bmatrix} \alpha_{\rho\rho} & \alpha_{\rho\phi} & \alpha_{\rho z} \\ \alpha_{\phi\rho} & \alpha_{\phi\phi} & \alpha_{\phi z} \\ \alpha_{z\rho} & \alpha_{z\phi} & \alpha_{zz} \end{bmatrix} \tag{3.3}$$

where α represents the relative permittivity, relative permeability, the electric conductivity, or magnetic conductivity. It is noted that if the medium is dispersive the approach used in chapter 2 can be applied.

The azimuthal dependence of field is expressed as a Fourier series,

$$\vec{E} = \sum_{m=0}^{\infty} (\vec{e}_u \cos m\phi + \vec{e}_v \sin m\phi) \tag{3.4}$$

$$\vec{H} = \sum_{m=0}^{\infty} (\vec{h}_u \cos m\phi + \vec{h}_v \sin m\phi) \tag{3.5}$$

$$\vec{J}_s = \sum_{m=0}^{\infty} (\vec{j}_u \cos m\phi + \vec{j}_v \sin m\phi) \tag{3.6}$$

where m is the mode number and is an integer because of single valueness of azimuthal dependence of the field. Fourier coefficients $\vec{e}_u$, $\vec{e}_v$, $\vec{h}_u$, $\vec{h}_v$, $\vec{j}_u$, and $\vec{j}_v$ are dependent on r, z, t, and m where u and v stand for the even and odd azimuthal dependence, respectively. The fields, $\vec{E}$ and $\vec{H}$, in (3.4) and (3.5) describe the fields at any point in the entire space of interest because the objects considered are symmetric about the z-axis. If the objects considered are not symmetric about the z-axis, then different pairs of model expansion are needed for different regions, followed by matching boundary conditions between those different regions. It is not suitable to use BOR scheme for this non-symmetrical problem. Note that if the loaded material is lossy, then Maxwell's equations with $\vec{B}$ and $\vec{D}$ pair are needed to perform the Fourier series expansion. Other relations for the lossy case are described by the Debye equation as we did in chapter 2.

Substituting (3.4), (3.5), and (3.6) into (3.1) and (3.2), we have the following pair of equations:

$$\pm\frac{m}{\rho}\hat{\phi}\times\vec{h}_{v,u}+\nabla\times\vec{h}_{u,v} = [\varepsilon]\frac{\partial\vec{e}_{u,v}}{\partial t}+[\sigma]\vec{e}_{u,v}+j_{u,v} \tag{3.7}$$

$$\pm\frac{m}{\rho}\hat{\phi}\times\vec{e}_{v,u}+\nabla\times\vec{e}_{u,v} = -[\mu]\frac{\partial\vec{h}_{u,v}}{\partial t}+[\sigma^*]\vec{h}_{u,v}. \tag{3.8}$$

The above two vector equations can be separated into two independent groups of six scalar equations. These groups represent modes that are azimuthally perpendicular to each other. The first group is as follow:

$$[\varepsilon]\frac{\partial e_{\rho,v}}{\partial t}+[\sigma]e_{\rho,v} = -\frac{\partial h_{\phi,v}}{\partial z}-\frac{m}{\rho}h_{z,u}-j_{\rho,v} \tag{3.9}$$

$$[\varepsilon]\frac{\partial e_{\phi,u}}{\partial t}+[\sigma]e_{\phi,u} = \frac{\partial h_{\rho,u}}{\partial z}-\frac{\partial h_{z,u}}{\partial\rho}-j_{\phi,u} \tag{3.10}$$

$$[\varepsilon]\frac{\partial e_{z,v}}{\partial t}+[\sigma]e_{z,v} = \frac{1}{\rho}\frac{\partial(\rho h_{\phi,v})}{\partial\rho}+\frac{m}{\rho}h_{r,u}-j_{z,v} \tag{3.11}$$

$$[\mu]\frac{\partial h_{\rho,u}}{\partial t}+[\sigma^*]h_{\rho,u} = \frac{\partial e_{\phi,u}}{\partial z}-\frac{m}{\rho}e_{z,v} \tag{3.12}$$

$$[\mu]\frac{\partial h_{\phi,v}}{\partial t}+[\sigma^*]h_{\phi,v} = -\frac{\partial e_{r,v}}{\partial z}+\frac{\partial e_{z,v}}{\partial\rho} \tag{3.13}$$

$$[\mu]\frac{\partial h_{z,u}}{\partial t} + [\sigma^*]h_{z,u} = -\frac{1}{\rho}\frac{\partial(\rho e_{\phi,u})}{\partial \rho} + \frac{m}{\rho}e_{\rho,v}. \tag{3.14}$$

The second group can be obtained by a similar procedure. Note that the signs of terms that contain $\frac{m}{\rho}$ in the second group are different from those in the first group. The summary of fields that depend on r, z, and t for those two groups are listed in Table 3.1.

Table 3.1 BOR representation of Maxwell's equations

Fields of first group	Fields of second group
$e_{\rho,v}$	$e_{\rho,u}$
$e_{\phi,u}$	$e_{\phi,v}$
$e_{z,v}$	$e_{z,u}$
$h_{\rho,u}$	$h_{\rho,v}$
$h_{\phi,v}$	$h_{\phi,u}$
$h_{z,u}$	$h_{z,v}$

Assume that those constitutive parameters have the biaxial tensor form in cylindrical coordinates given by

$$[\alpha] = \begin{bmatrix} \alpha_\rho & 0 & 0 \\ 0 & \alpha_\phi & 0 \\ 0 & 0 & \alpha_z \end{bmatrix}. \tag{3.15}$$

Then these two groups of equations can be represented in matrix form[27] as

$$\begin{bmatrix} 0 & -\partial_z & \pm\frac{m}{\rho} \\ \partial_z & 0 & -\partial_\rho \\ \mp\frac{m}{\rho} & \frac{1}{\rho}\frac{\partial}{\partial\rho}\rho & 0 \end{bmatrix} \begin{bmatrix} e_\rho \\ e_\phi \\ e_z \end{bmatrix} = -\begin{bmatrix} (\mu_0\mu_\rho\partial_t + \sigma^*{}_\rho)h_\rho \\ (\mu_0\mu_\phi\partial_t + \sigma^*{}_\phi)h_\phi \\ (\mu_0\mu_z\partial_t + \sigma^*{}_z)h_z \end{bmatrix} \tag{3.16}$$

$$\begin{bmatrix} 0 & -\partial_z & \mp\frac{m}{\rho} \\ \partial_z & 0 & -\partial_\rho \\ \pm\frac{m}{\rho} & \frac{1}{\rho}\frac{\partial}{\partial\rho}\rho & 0 \end{bmatrix} \begin{bmatrix} h_\rho \\ h_\phi \\ h_z \end{bmatrix} = \begin{bmatrix} (\varepsilon_0\varepsilon_\rho\partial_t + \sigma_\rho)e_\rho + j_\rho \\ (\varepsilon_0\varepsilon_\phi\partial_t + \sigma_\phi)e_\phi + j_\phi \\ (\varepsilon_0\varepsilon_z\partial_t + \sigma_z)e_z + j_z \end{bmatrix} \tag{3.17}$$

where ∂_α denotes $\frac{\partial}{\partial\alpha}$ and $\alpha = \rho, z, t$.

3.1.1 Mode Selection in BOR Algorithm

There are two important issues that need to be determined in applying BOR algorithm. The first one is which group of equations should be used and the second one is how many modes should be included to solve the problem. These two issues are determined by the incident wave or the impressed current source.

For scattering problem, the field distribution of the incident wave determines the number of modes and the group of equations to be used. Consider the incident filed[25],

$$\vec{E}^i = f(\rho)E\left(t - \frac{z}{c}\right)[\hat{\rho}\cos\phi - \hat{\phi}\sin\phi] = \hat{\rho}E^i{}_\rho + \hat{\phi}E^i{}_\phi \tag{3.18}$$

where c is the speed of light and ρ, ϕ, and z are the cylindrical coordinates. The $E^i{}_\rho$ is even functions with respect to ϕ so is $H^i{}_\phi$ by Maxwell's equations. Similarly, $E^i{}_\phi$, $H^i{}_\rho$, and H^i_z are odd functions w.r.t ϕ. The total fields denoted by a superscript t will preserve this angular dependence[19] because of the symmetry about the z-axis of the object. Therefore, these total fields components can be expanded in terms of a Fourier cosine or sine series. The E^t_ρ, H^t_ϕ, and E^t_z, are even functions and H^t_ρ, E^t_ϕ, and H^t_z are odd functions w.r.t ϕ; hence the second group of equations is selected to solve this problem. From (3.18), only $\cos\phi$ and $\sin\phi$ are involved, so only mode m=1 is needed to solve this problem.

In the cavity problem we considered, the source is assumed to be a line current source located at a point (ϕ_0, z_0). The source can be expressed as

$$\vec{J} = -\hat{\rho} f(\rho)\delta(z-z_0)\frac{\delta(\phi-\phi_0)}{\rho}g(t) \tag{3.19}$$

where $f(\rho)$ and g(t) are variation of $\vec{J}$ along ρ and t, respectively. Symbol δ is Dirac delta function. If we let ϕ_0 to be zero then the delta function $\delta(\phi)$ can be expanded by Fourier cosine series as:

$$\delta(\phi) = \sum_{m=0}^{\infty} \frac{\varepsilon_{0m}}{\pi}\cos m\phi \tag{3.20}$$

where

$$\varepsilon_{0m} = \begin{cases} 1 & m = 0 \\ 2 & m \neq 0 \end{cases}. \tag{3.21}$$

Form theory, the lowest TE mode is TE_{011} and its ρ component, E_ρ, is equal to zero. Hence, the ϕ dependence of E_ϕ is $\cos m\phi$ in order to keep E_ϕ from becoming zero for

TE_{011} mode[26]. Therefore, the first group of equations need to be used in this FDTD calculation for cavity problems and (3.19) becomes

$$\vec{J} = \hat{\rho} \sum_{m=0}^{\infty} j_m \cos m\phi \tag{3.22}$$

where

$$j_m = -\frac{\varepsilon_{0m}}{\pi}\frac{f(\rho)}{\rho}\delta(z - z_0)g(t). \tag{3.23}$$

3.1.2 The BOR-FDTD Formulation[28]

In this section, the BOR-FDTD formulation will be derived by using the leapfrog scheme with $\sigma^* = 0$. Consider the first equation in (3.17),

$$\varepsilon_\rho \frac{\partial e_\rho}{\partial t} = -\sigma_\rho e_\rho - j_\rho - \frac{\partial h_\phi}{\partial z} \mp \frac{m}{\rho} h_z \tag{3.24}$$

where the right hand size will be evaluated at $t = \left(n + \frac{1}{2}\right)\Delta t$ since h field is evaluated at $t = \left(n + \frac{1}{2}\right)\Delta t$. The standard FDTD notation will be used in this derivation, $\rho = i\Delta\rho$ and $z = j\Delta z$. Using field locations in Figure 3.1, (3.24) becomes

$$\begin{aligned} \frac{\varepsilon_\rho}{\Delta t}[e_\rho^{n+1}(i, j) - e_\rho^n(i, j)] &= -\sigma_\rho e_\rho^{n+1/2}(i, j) - j_\rho^{n+1/2}(i, j) \\ &- \frac{h_\phi^{n+1/2}(i, j) - h_\phi^{n+1/2}(i, j-1)}{\Delta z} \mp \frac{m}{\rho_{i+1/2}} h_z^{n+1/2}(i, j) \end{aligned} \tag{3.25}$$

The components, $e_\rho^{n+1/2}(i, j)$ and $j_\rho^{n+1/2}(i, j)$, have to be approximated by those values adjacent to them since they are sampled at integer time step n. The second-order approximation used here is

$$f_\rho^{n+1/2}(i,j) = \frac{3f_\rho^{n+1}(i,j) + 6f_\rho^{n}(i,j) - f_\rho^{n-1}(i,j)}{8} \tag{3.26}$$

where f is e or j. The FDTD representation of equation (3.24) is then

$$\begin{aligned} e_\rho^{n+1}(i,j) &= A_\rho \cdot e_\rho^{n}(i,j) + B_\rho \cdot e_\rho^{n-1}(i,j) \\ &\quad -C_\rho \cdot \left[j_\rho^{n+\frac{1}{2}}(i,j) + \frac{h_\phi^{n+1/2}(i,j) - h_\phi^{n+1/2}(i,j-1)}{\Delta z} \pm \frac{m}{\rho_{i+1/2}} h_z^{n+1/2}(i,j) \right] \end{aligned} \tag{3.27}$$

where

$$A_x = \frac{1 - \frac{3}{4}\frac{\sigma_x}{\varepsilon_0\varepsilon_x}\Delta t}{1 + \frac{3}{8}\frac{\sigma_x}{\varepsilon_0\varepsilon_x}\Delta t} \tag{3.28}$$

$$B_x = \frac{\frac{1}{8}\frac{\sigma_x}{\varepsilon_0\varepsilon_x}\Delta t}{1 + \frac{3}{8}\frac{\sigma_x}{\varepsilon_0\varepsilon_x}\Delta t} \tag{3.29}$$

$$C_x = \frac{\frac{1}{\varepsilon_0\varepsilon_x}\Delta t}{1 + \frac{3}{8}\frac{\sigma_x}{\varepsilon_0\varepsilon_x}\Delta t} \tag{3.30}$$

and $x = \rho, \phi, or\ z$. Note that $j_\rho^{n+1/2}$ is not replaced by the approximation of (3.26) in (3.27).

The other five FDTD equations can be derived by using the similar procedure and are listed below:

$$e_\phi^{n+1}(i,j) = A_\phi \cdot e_\phi^n(i,j) + B_\phi \cdot e_\phi^{n-1}(i,j) - C_\phi \cdot \left[j_\phi^{n+\frac{1}{2}}(i,j) + \frac{h_z^{n+1/2}(i,j) - h_z^{n+1/2}(i-1,j)}{\Delta\rho} - \frac{h_\rho^{n+1/2}(i,j) - h_\rho^{n+1/2}(i,j-1)}{\Delta z} \right] \tag{3.31}$$

$$e_z^{n+1}(i,j) = A_z \cdot e_z^n(i,j) + B_z \cdot e_z^{n-1}(i,j) - C_z \cdot \left[j_z^{n+\frac{1}{2}}(i,j) \mp \frac{m}{\rho_i} h_\rho^{n+1/2}(i,j) - \frac{\rho_{i+1/2} h_\phi^{n+1/2}(i,j) - \rho_{i-1/2} h_\phi^{n+1/2}(i-1,j)}{\rho_i \Delta\rho} \right] \tag{3.32}$$

$$h_\rho^{n+1/2}(i,j) = h_\rho^{n-1/2}(i,j) \mp G_\rho \frac{m}{\rho_i} e_z^n(i,j) + G_\rho \left[\frac{e_\phi^n(i,j+1) - e_\phi^n(i,j)}{\Delta z} \right] \tag{3.33}$$

$$h_\phi^{n+1/2}(i,j) = h_\phi^{n-1/2}(i,j) - G_\phi \left[\frac{e_\rho^n(i,j+1) - e_\rho^n(i,j)}{\Delta z} - \frac{e_z^n(i+1,j) - e_z^n(i,j)}{\Delta\rho} \right] \tag{3.34}$$

$$h_z^{n+1/2}(i,j) = h_z^{n-1/2}(i,j) \pm G_z \frac{m}{\rho_{i+1/2}} e_\rho^n(i,j) - G_z \left[\frac{\rho_{i+1} e_\phi^n(i+1,j) - \rho_i e_\phi^n(i,j)}{\rho_{i+1/2} \Delta\rho} \right] \tag{3.35}$$

where $G_x = \Delta t/(\mu_0 \mu_x)$, $x = \rho, \phi, or\ z$ and $\rho_i = (i-1/2)\Delta\rho$ and $\rho_{1/2} = \rho_0 = 0$, and the fields associated with the coordinate (i, j) are shown in Figure 3.1. In Chen's paper [28], those BOR FDTD equations are obtained by using a first-order approximation,

$$f_\rho^{n+1/2}(i,j) = \frac{f_\rho^{n+1}(i,j) + f_\rho^n(i,j)}{2}, \tag{3.36}$$

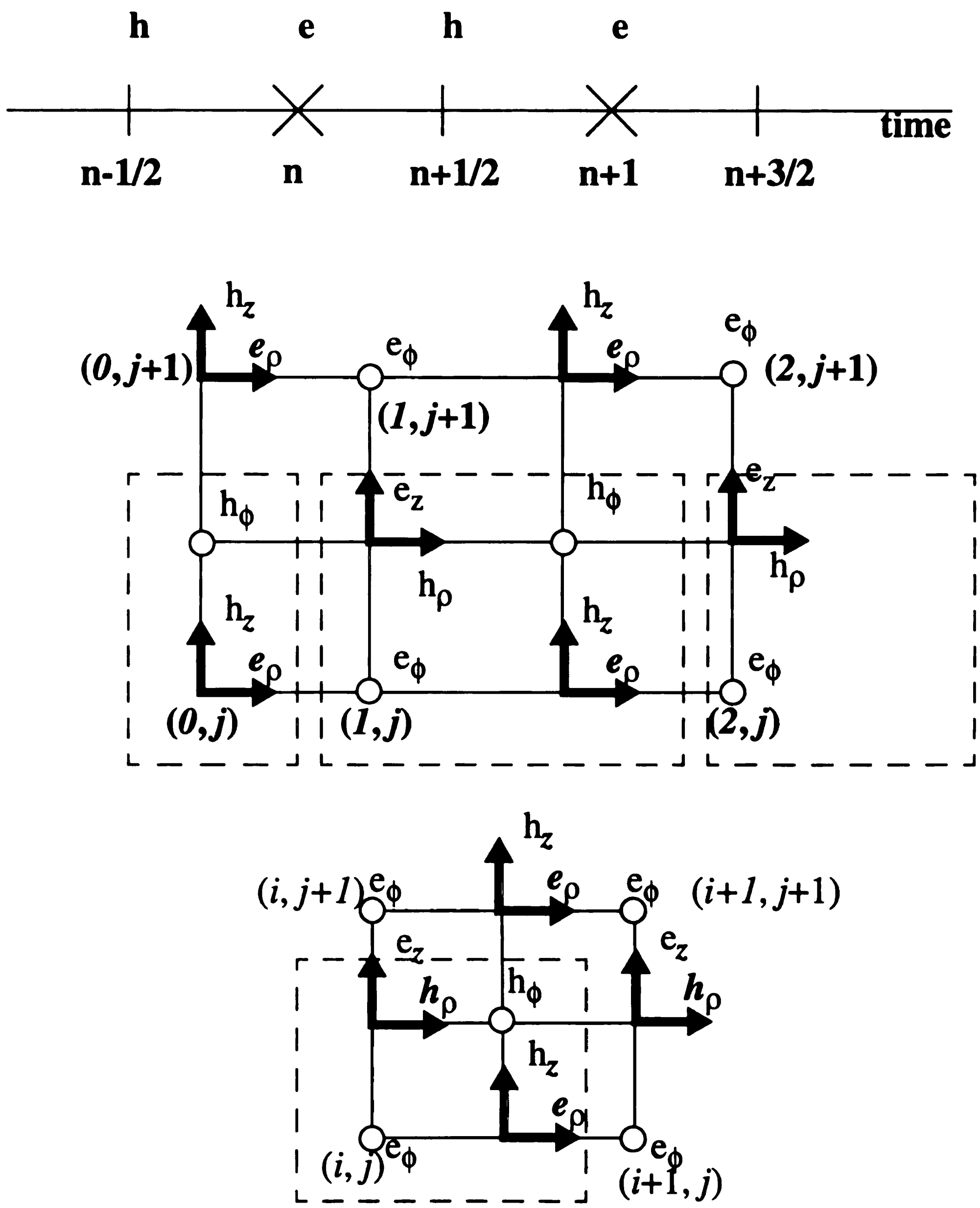

FIGURE 3.1 The field locations for BOR FDTD in time and space.

for fields at the half time step. Smaller time steps or spacial steps are required in Chen's paper than that in this chapter. This problem becomes more serious in calculating the cavity modes with $n \neq 0$.

3.1.3 Singularity in BOR-FDTD Formulation at $\rho = 0$

As observed from (3.27), there is a $\rho_{1/2}$ factor, which is equal to zero, in the denominator of the fourth term when calculating the $e_\rho(0, j)$. Hence, $e_\rho(0, j)$ is infinite at $\rho = 0$ and this makes $h_\phi(0, j)$ in (3.34) infinity, also. The filed, $h_z(0, j)$, is infinite by the same reason in (3.35). Other fields, e_ρ, h_ϕ, and h_z at the $\rho = 0$ also exhibit singularities; however, the actual fields must be finite in both the time and frequency domains. Hence, the these singularities must be removed before above FDTD equations can be used for time stepping.

As observed from (3.31) and (3.32), only the components $h_\phi(0, j)$ and $h_z(0, j)$ are needed to update the adjacent $e_z(1, j)$ and $e_\phi(1, j)$ fields internal to the mesh. The $e_\rho(0, j)$ and $e_\rho(0, j+1)$ are needed to evaluate $h_\phi(0, j)$. The field, $h_\phi(0, j)$, is not needed actually to calculate the $e_z(1, j)$ since

$$\begin{aligned} e_z^{n+1}(1, j) = {} & A_z \cdot e_z^n(1, j) + B_z \cdot e_z^{n-1}(1, j) \\ & -C_z \cdot \left[j_z^{n+\frac{1}{2}}(1, j) \mp \frac{m}{\rho_i} h_\rho^{n+1/2}(1, j) \right. \\ & \left. -\frac{\rho_{3/2} h_\phi^{n+1/2}(1, j) - \rho_{1/2} h_\phi^{n+1/2}(0, j)}{\rho_1 \Delta\rho} \right] \end{aligned} \tag{3.37}$$

with $\rho_{1/2} = 0$; hence, $e_\rho(0, j)$ is not needed, neither. In actual calculation, $h_\phi(0, j)$ and

$e_\rho(0, j)$ are set to zeros to avoid cumulation error.

Now, only $h_z(0, j)$ is needed to update the fields point in the FDTD lattice. Note that h_z is zero at $\rho = 0$ for $m \neq 0$ by (3.17); hence, we only need to evaluate $h_z(0, j)$ for $m = 0$. From the integral form of Maxwell's equation in the time domain, we can obtain the following time update equation for $h_z(0, j)$ when $m = 0$

$$h_z^{n+1/2}(0, j) = h_z^{n-1/2}(0, j) - \frac{4\Delta t}{\mu_0 \mu_z \Delta\rho} e_\phi^n(1, j) \,. \tag{3.38}$$

Once $h_z(0, j)$ is known the rest of the field components can be evaluated using (3.27) and (3.31) to (3.34).

3.2 Surface Impedance Boundary Condition

When the boundary of a cavity has a finite electrical conductivity (FEC), there are two FDTD approaches to calculate the field distributions in the EM cavity. For a cavity with good conductor wall which is considered in this chapter, the skin depth and the local wavelength are very small compared to the radius of curvature of the cavity wall. Hence, the planar surface impedance boundary condition (PSIBC) is used to approximate the lossy conductor wall. For more accurate simulation, an absorption boundary condition (ABC) has to be used outside the cavity and as shown in Figure 3.2. In this chapter, only the PSIBC case is considered.

3.2.1 Planar Surface Impedance Boundary Condition

The surface impedance is inherently a frequency-domain concept. Consider a time-harmonic plane wave incident at angle θ_i on the lossy dielectric half-space as shown in

Figure 3.3.

The surface impedance for a planar interface at $z = 0$ can be defined through the following relation:

$$\vec{E}_t(\omega) = Z(\omega)[\hat{n} \times \vec{H}_t(\omega)] \tag{3.39}$$

where $Z(\omega)$ is the surface impedance. The surface impedances of interface for TE and TM plane wave[30], respectively, are

$$Z_{TE}(\omega) = \frac{Z_2}{\cos\theta_2} \tag{3.40}$$

$$Z_{TM}(\omega) = Z_2 \cos\theta_2 \tag{3.41}$$

where

$$Z_k = \left(\frac{j\omega\mu_k}{j\omega\varepsilon_k + \sigma_k}\right)^{1/2} \tag{3.42}$$

$$\cos\theta_2 = \left[1 - \frac{\sin^2\theta_i}{\mu_r\varepsilon_r\left(1 - \frac{j\sigma}{\omega\varepsilon_0\varepsilon_r}\right)}\right]^{1/2} = (1 - \sin^2\theta_2)^{1/2}. \tag{3.43}$$

When $|\sin^2\theta_2| \ll 1$, then the surface impedance can be rewritten as

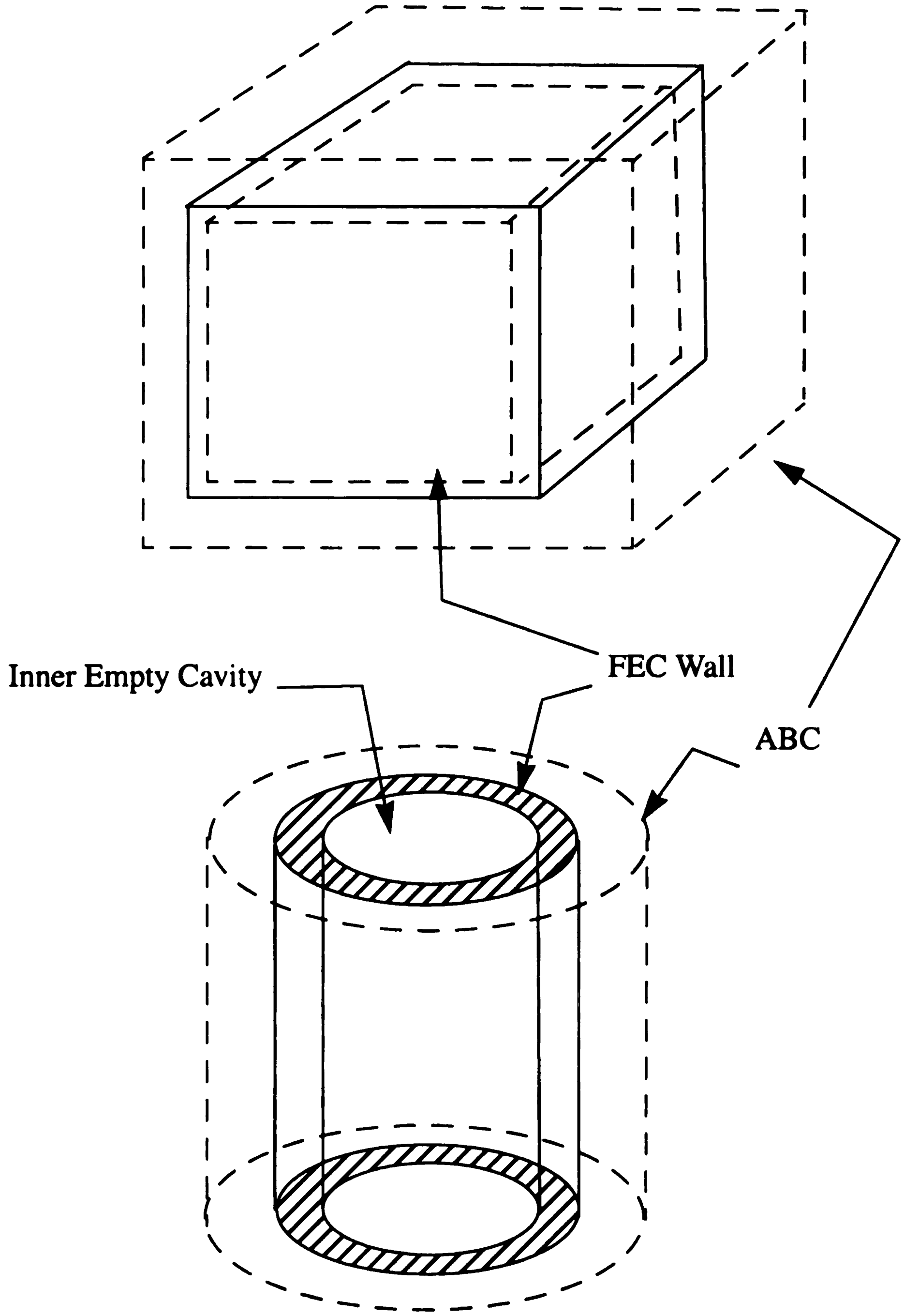

Figure 3.2 FDTD configuration for cavities with FEC wall

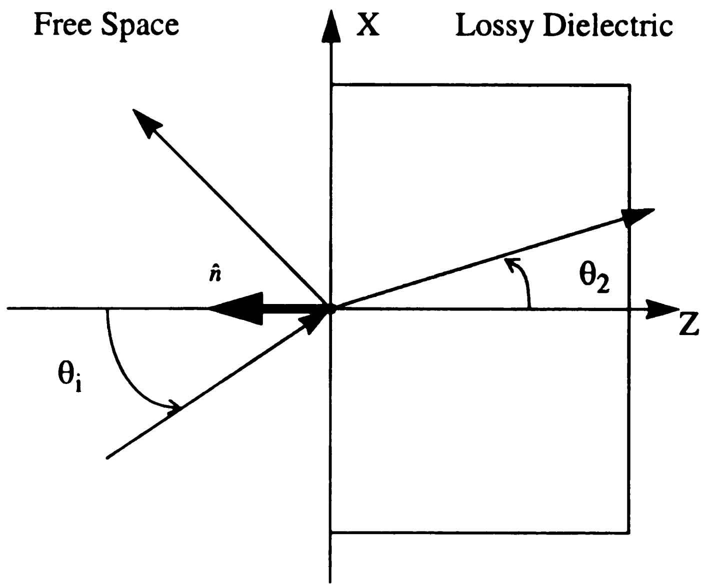

Figure 3.3 Coordinates for the incident and reflected plane waves upon a lossy surface

$$
\begin{aligned}
Z(\omega) = Z_{TE}(\omega) = Z_{TM}(\omega) &= \left(\frac{j\omega\mu_2}{j\omega\varepsilon_2 + \sigma_2}\right)^{1/2} \\
&= \eta_0\left(\frac{\mu_{2r}}{\varepsilon_{2r}}\right)^{1/2}\sqrt{\frac{s}{s + \sigma_2/\varepsilon_2}}
\end{aligned}
\tag{3.44}
$$

where $\eta_0 = \sqrt{\mu_0/\varepsilon_0}$ and $s = j\omega$. Equation (3.44) is the planar surface impedance used through this chapter.

3.2.2 FDTD Implementation of Planar Surface Impedance

In order to do FDTD calculations, the time domain expression of (3.39) needs to be obtained. The convolution in time domain is involved since there is a multiplication in frequency domain. The convolution in time domain needs to be approximated by some recursive expression in order to run on a computer. Three approximations are discussed in this section. The time domain approximation[29] is first considered; however, this approximation encounters some divergence problems when evaluating an integral and is not used to the FDTD implementation. The frequency-domain[31] and Z-transform approximation[32][33] are easier and more efficient to calculate than the time domain approximation.

3.2.2.1 Time-Domain Approximation by Prony's Method

The time-domain surface impedance is

$$z(t) = \eta_0\left(\frac{\mu_{2r}}{\varepsilon_{2r}}\right)^{1/2}\{\delta(t) + ae^{at}[I_1(at) + I_0(at)]U(t)\} \tag{3.45}$$

where $U(t)$ is the unit-step function, $a \equiv -\sigma_2/(2\varepsilon_2)$ and I_0 and I_1 are the modified Bessel functions of the first kind of zero and one order, respectively. Hence, the time domain expression of (3.39) is

$$\vec{E}_t(t) = \eta_0\left(\frac{\mu_{2r}}{\varepsilon_{2r}}\right)^{1/2}\left\{[\hat{n} \times \vec{H}_t(t)] + \int_0^t ae^{a\tau}[I_1(a\tau) + I_0(a\tau)][\hat{n} \times \vec{H}_t(t-\tau)]d\tau\right\} \tag{3.46}$$

and the discretization version of (3.46) is

$$\vec{E}_t(m) = \eta_0\left(\frac{\mu_{2r}}{\varepsilon_{2r}}\right)^{1/2}\left\{[\hat{n} \times \vec{H}_t(m)] + \sum_{q=0}^{m-1} F_0(q)[\hat{n} \times \vec{H}_t(m-q)]\right\} \tag{3.47}$$

where

$$F_0(q) = \int_{\phi}^{(q+1)}[1 - |\gamma - q|](a\Delta t)e^{(a\Delta t)r}[I_1(a\Delta t\gamma) + I_0(a\Delta t\gamma)]d\gamma \tag{3.48}$$

and

$$\phi = \begin{cases} 0 & q = 0 \\ q-1 & q > 0 \end{cases} . \tag{3.49}$$

The Prony's method is used to approximate the $F_0(q)$ and (3.47) is then

$$\vec{E}_t\Big|^n = \eta_2\left[\vec{H}_t\Big|^n + \sum_{k=1}^{Q} \vec{G}_k(n)\right] \tag{3.50}$$

where $\vec{G}_k(n) = C_k\vec{H}_t\Big|^n + \mu_k\vec{G}_k(n-1)$ and $k = 1, 2, 3, \ldots Q$.

3.2.2.2 Frequency Domain Approximation

The surface impedance, (3.44), is rewritten as

$$Z(s) = \eta_2\sqrt{\frac{s}{s+a}} \tag{3.51}$$

where $s = j\omega$, $\eta_2 = \eta_0\sqrt{\frac{\mu_{2r}}{\varepsilon_{2r}}}$, and $a = \sigma_2/\varepsilon_2$. Equation (3.51) can be approximated by a rational polynomials in frequency domain and is rewritten as

$$Z(s') = \sqrt{\frac{s'}{1+s'}} \approx 1 - \sum_{i=1}^{L} \frac{C_i}{\omega_i + s'} \tag{3.52}$$

where $s' = s/a$, the L is number of terms needed in that approximation and ω_i are known poles. The L and ω_i are determined using a rational Chebyshev approximation and is listed in Table 3.2[31]. This approximation is over the real axis interval $s' = [0, 3]$ which will accommodate most material up to several tens of Gigahertz. The (3.39) in s-plane is then

$$\vec{E}_t(s) \approx \eta_2\left[1 - \sum_{i=1}^{L} \frac{aC_i}{a\omega_i + s}\right][\hat{n} \times \vec{H}_t(s)]. \tag{3.53}$$

Assuming the waves are piecewise linear in time, (3.39) in discrete-time domain is given by

$$\vec{E}_t\Big|^n = \eta_2\left[\hat{n} \times \vec{H}_t\Big|^n\right] - \sum_{i=1}^{L} \vec{A}_i\Big|^n \tag{3.54}$$

where

$$\vec{A}_i\Big|^n = p_{i1}\left[\hat{n} \times \vec{H}_t\Big|^n\right] + p_{i2}\left[\hat{n} \times \vec{H}_t\Big|^{n-1}\right] + p_{i3}\vec{A}_t\Big|^{n-1} \tag{3.55}$$

and

$$p_{i1} = \eta_2\frac{C_i}{\omega_i}[1 + (e^{-a\omega_i\Delta t} - 1)/(\Delta t a\omega_i)] \tag{3.56}$$

$$p_{i2} = \eta_2\frac{C_i}{\omega_i}[1/(\Delta t a\omega_i) - e^{-a\omega_i\Delta t}(1 + 1/(\Delta t a\omega_i))] \tag{3.57}$$

$$p_{i3} = e^{-a\omega_i\Delta t}. \tag{3.58}$$

3.2.2.3 Z Transform and Digital Filters Approach

The term, $C_i/(\omega_i + s')$, in (3.52) is a analog lowpass filter with a single pole. The digital version of this term is a digital IIR filter. Hence, this become an IIR digital filter design from the analog filter in digital signal processing terminology.

A popular IIR filter design is the bilinear transformation which is appropriate for lowpass, bandpass, and highpass filters. The bilinear transformation is a mapping from the

Table 3.2 Rational Approximation Results

Number of Terms	C_i	ω_i
8	2.60266906380e-10	2.43632801126e-7
	3.31195847511e-8	1.06720343642e-5
	1.58725612150e-6	1.59612026325e-4
	4.35701245008e-5	1.59383673429e-3
	8.08657638450e-4	1.20627876345e-2
	1.07197254652e-2	7.22902130819e-2
	9.48589314718e-2	0.3267172939002
	0.3933263026213	0.8680755110248

s-plane to z-plane and can be linked to the trapezoidal formula for numerical integration[34]. The substitution of variable for bilinear transformation is

$$s = \frac{2}{T}\left(\frac{1 - z^{-1}}{1 + z^{-1}}\right) \tag{3.59}$$

where T is the period of one time step or the sampling factor. Applying the bilinear transformation, (3.59), to (3.53), then the time discrete version of (3.39) becomes

$$\vec{E}_t\Big|^n = \eta_2\left[\hat{n} \times \vec{H}_t\Big|^n\right] - \sum_{i=1}^{L} \vec{f}_i\Big|^n \tag{3.60}$$

where

$$\vec{f}_i\Big|^n = \left(\frac{2 - a\omega_i T}{2 + a\omega_i T}\right)\vec{f}_i\Big|^{n-1} + \left(\frac{aC_i\eta_2 T}{2 + a\omega_i T}\right)\left[\hat{n} \times \vec{H}_t\Big|^n + \hat{n} \times \vec{H}_t\Big|^{n-1}\right]. \tag{3.61}$$

The bilinear transformation maps the entire left half of the complex plane inside the unit circle in z-plane and the imaginary axis in the complex plane becomes the unit circle in z-plane. As a result, frequency compression or frequency warping will take place when transferring from the analog system to the digital system. The bilinear transformation is most useful when this distortion can be tolerated or compensated.

3.2.3 Fields Calculation on the Cavity Wall

From Figure 3.1, there are two tangential electric fields and one normal magnetic field on the physical cavity walls. By (3.50), (3.54), and (3.60) the tangential electric fields are evaluated from the tangential magnetic fields on the cavity walls at the same time step. However, the tangential magnetic field is evaluated at half-time step before the current time step and half cell in front of the cavities wall according to Yee's FDTD lattice in Figure 3.1. In the practical FDTD calculation, these tangential magnetic fields are used in (3.50), (3.54), and (3.60) to obtain the tangential electric fields on the cavity walls. Equations (3.54) and (3.60) can be rewritten as

$$\vec{E}_t\Big|^n = \eta_2\left[\hat{n}\times\vec{H}_t\Big|_h^{n-1/2}\right] - \sum_{i=1}^{L}\vec{A}_i\Big|^n \tag{3.62}$$

where

$$\vec{A}_i\Big|^n = p_{i1}\left[\hat{n}\times\vec{H}_t\Big|_h^{n-1/2}\right] + p_{i2}\left[\hat{n}\times\vec{H}_t\Big|_h^{n-3/2}\right] + p_{i3}\vec{A}_t\Big|^{n-1} \tag{3.63}$$

and

$$\vec{E}_t\Big|^n = \eta_2\left[\hat{n}\times\vec{H}_t\Big|_h^{n-1/2}\right] - \sum_{i=1}^{L}\vec{f}_i\Big|^n \tag{3.64}$$

where

$$\vec{f}_i\Big|^n = \left(\frac{2-a\omega_iT}{2+a\omega_iT}\right)\vec{f}_i\Big|^{n-1} + \left(\frac{aC_i\eta_2T}{2+a\omega_iT}\right)\left[\hat{n}\times\vec{H}_t\Big|_h^{n-1/2} + \hat{n}\times\vec{H}_t\Big|_h^{n-3/2}\right]. \tag{3.65}$$

Note that the subscript, h, stands for a half space step before the walls. The normal magnetic fields on the cavity walls are obtained by using the normal FDTD implementation of Maxwell's equations.

3.3 An Empty Cylindrical Cavity

The physical configuration of the cylindrical cavity is shown in Figure 3.4. The radius and height of the cavity are a and h and that of loaded material are b and l. The wall of the cylindrical cavity is assumed to be perfectly electrically conductive (PEC) or finitely electrically conductive (FEC) and the excitation probe is located on the side of the cylindrical cavity.

The TM_{012} mode of an empty cylindrical cavity with PEC boundary is first calculated to verify the program. The $g(t)$ in (3.19) is a Blackman-Harris (BH) windows function with the central frequency of 2.4571GHz and 0.1GHz bandwidth. The BH function makes the source turn off automatically and the 0.1GHz bandwidth is chosen because only TM_{012} is desired. The dimensions of the cavity are $a = 0.0762m$ and $l = 0.15458m$ and the dimensions of grids are $\Delta\rho = 0.0006m$ and $\Delta z = 0.00118$ which are lees than $\lambda/20$ where λ is the wavelength. The numbers of partition along ρ and z are 127 and 131, respectively, and the one time step is *1.69363* ps. The field distributions of E_ρ and E_z are plotted in Figure 3.5 to Figure 3.6 and the total time step is 15382. Form these figures, we conclude that the result of $m = 0$ mode is the dominant mode which is much larger than that of $m = 1$ mode and higher modes. The field distribution of E on the $\rho - z$ plane is plotted in Figure 3.7. Hence, only $m = 0$ mode is considered in the calculation of

TM_{012} mode for the FEC and the loaded cavity. For TE_{111} mode, the numbers of partition are *127* and *67* along ρ and z directions and the one time step is *1.29676 p*s. The field distributions of E_ρ, E_ϕ and E on the $\rho - z$ plane for TE_{111} mode are plotted in Figure 3.8 to Figure 3.10. For TE_{111} mode, the $m = 1$ mode is dominant mode as can be seen from these figures.

For the empty cylindrical cavity with FEC boundary, the FEC boundary is replaced by PSIBC. The continuous sine function is used for $g(t)$ in source equation (3.19) since there is a loss on the boundary. As observed in Figure 3.11 with $\Delta t = 1.2967608 ps$, the E field achieves a steady state about 23,135 time steps for $\sigma = 10^2\ S/m$ and 120,000 time steps for $\sigma = 10^4\ S/m$. It will need more than 600,000 time steps to evaluate the field distribution of TE_{111} mode for cavity with $\sigma = 10^6\ S/m$ which is usually encountered in regular cavities.

The field distributions of E_z and E on the ρ-z plane are shown in Figure 3.12 and Figure 3.13. There is some E_z near the boundary wall form Figure 3.12; however, the value of E_z is much smaller than that of E_ρ. The E field on the ρ-z plane is nearly identical in Figure 3.13 compared to that in Figure 3.10. Therefore, it is reasonable to use PEC wall assumption to do the FDTD calculation for field distributions in cavities since most cavity wall is made of metal with conductivity larger than $\sigma = 10^6\ S/m$. Moreover, this PEC assumption requires much less time steps in FDTD simulation.

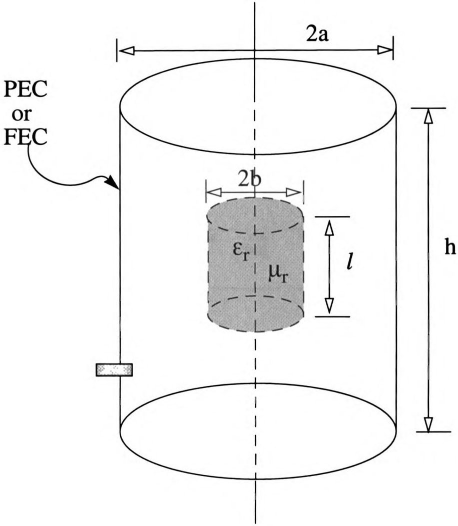

Figure 3.4 The physical configuration of a cylindrical cavity loaded with a material sample.

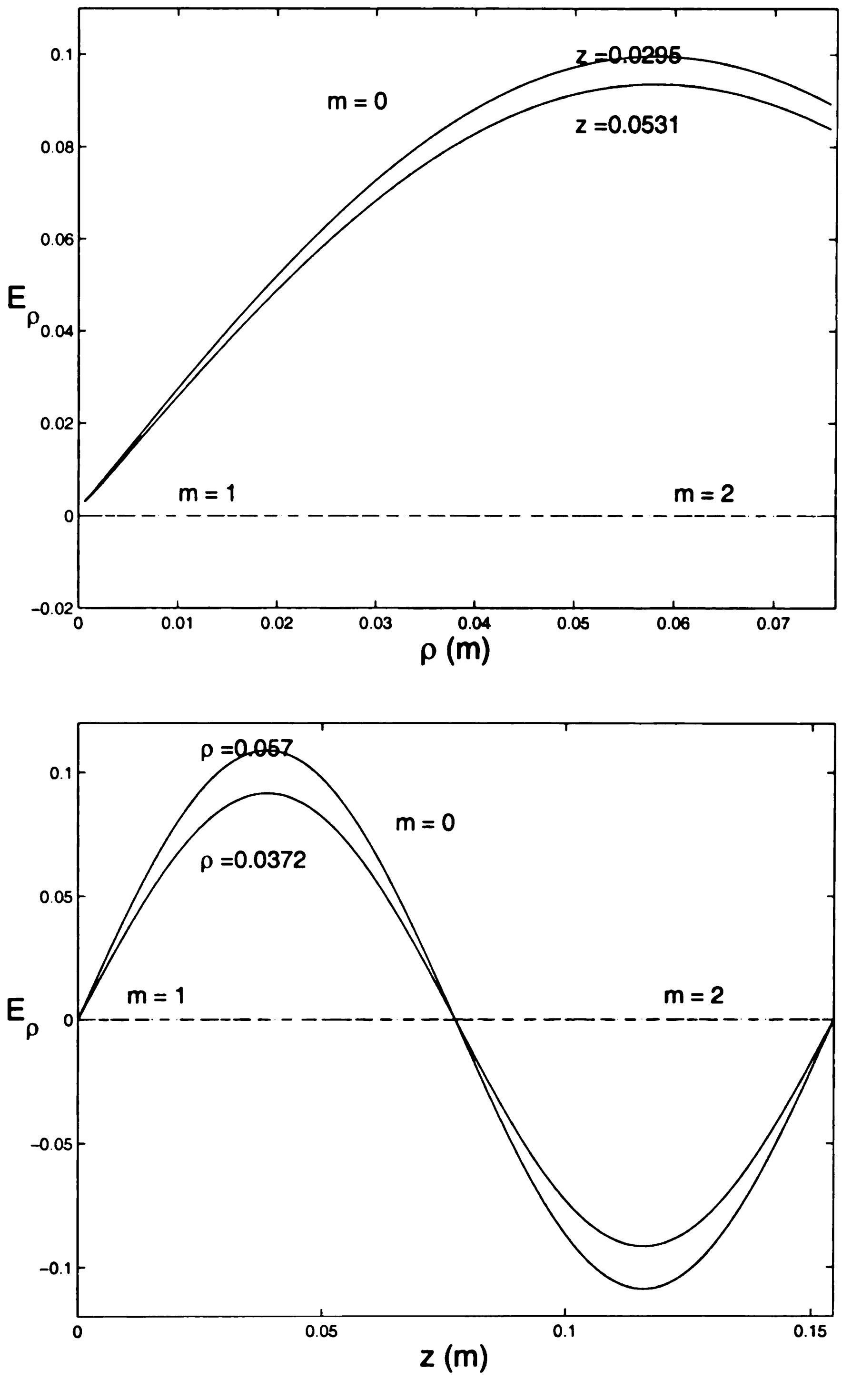

Figure 3.5 The variation of E_ρ of TM_{012} along the ρ and z directions in a PEC empty cylindrical cavity.

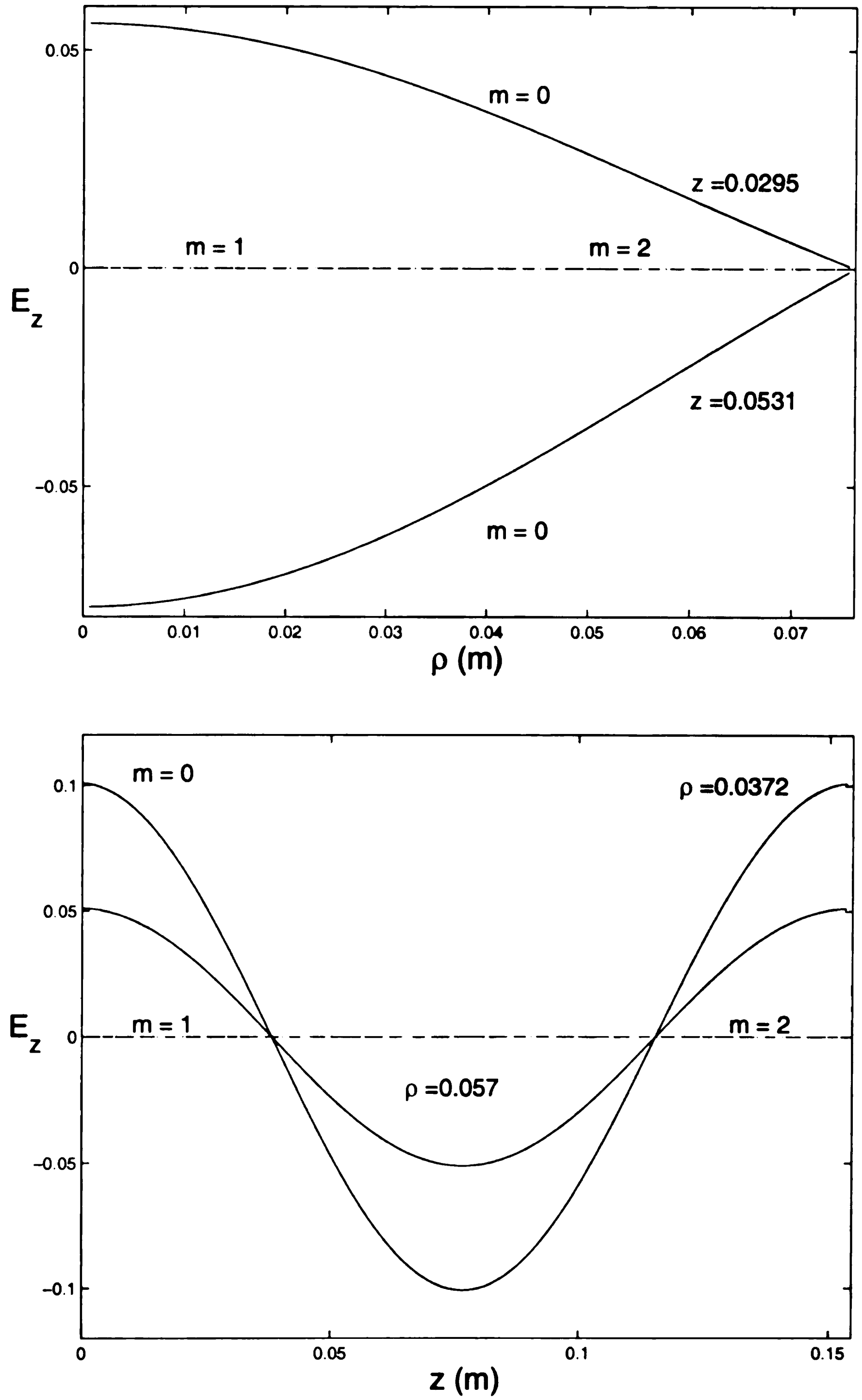

Figure 3.6 The variation of E_z of TM_{012} mode along the ρ and z directions in a PEC empty cylindrical cavity.

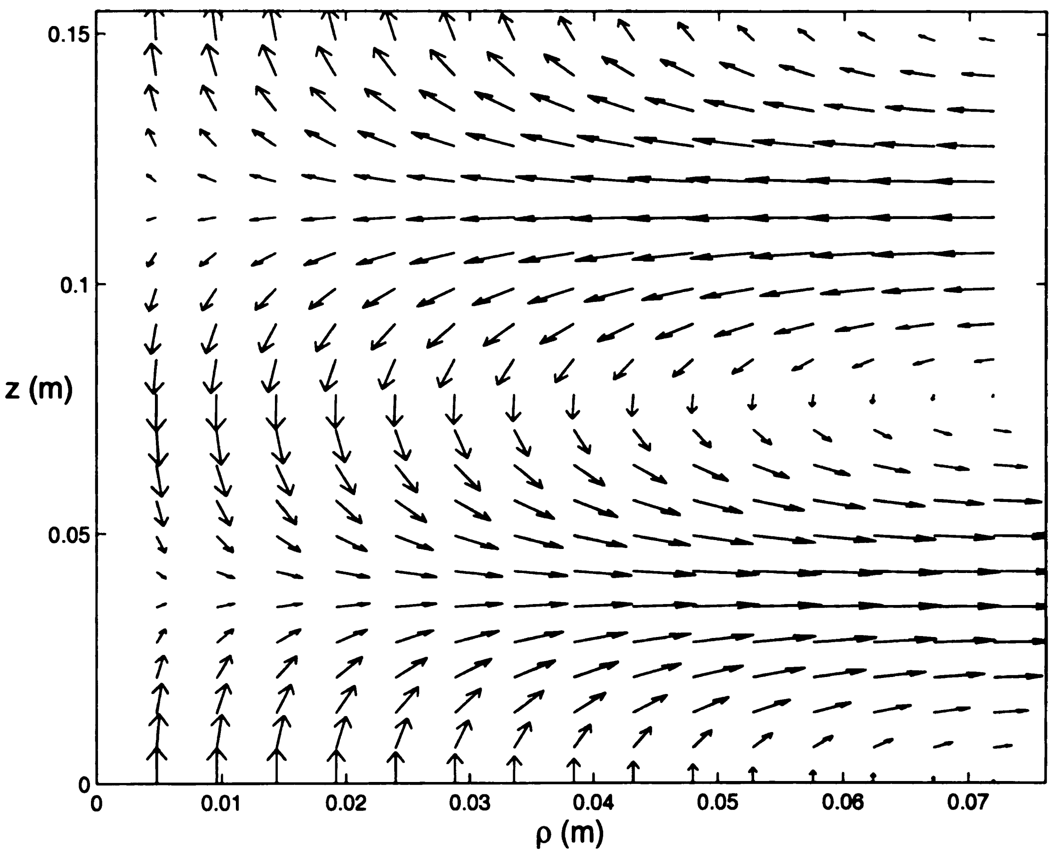

Figure 3.7 Plot of E field of TM_{012} mode on the ρ-z plane in an empty PEC cavity.

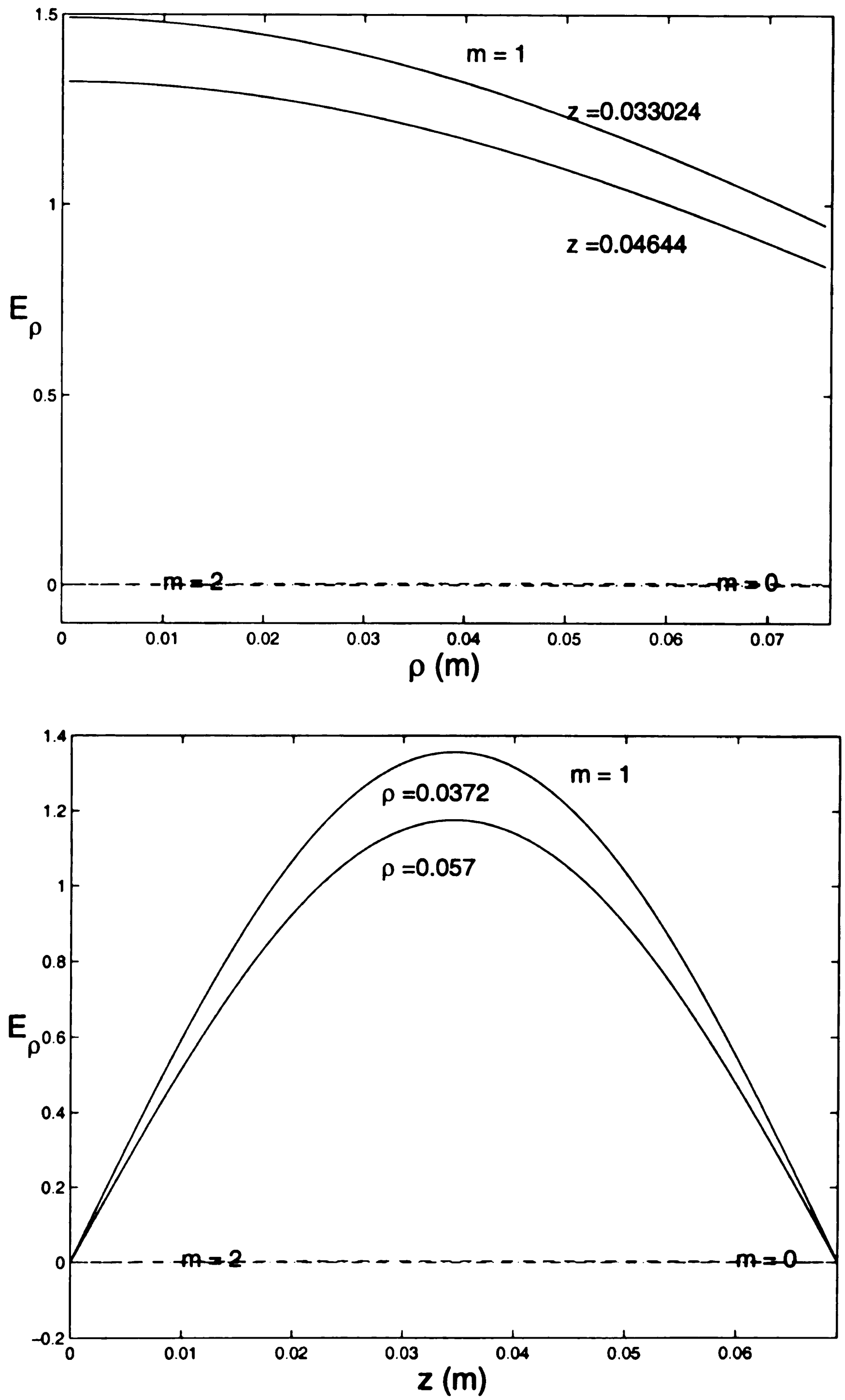

Figure 3.8 The variation of E_ρ of TE_{111} mode along the ρ and z directions in a PEC empty cylindrical cavity.

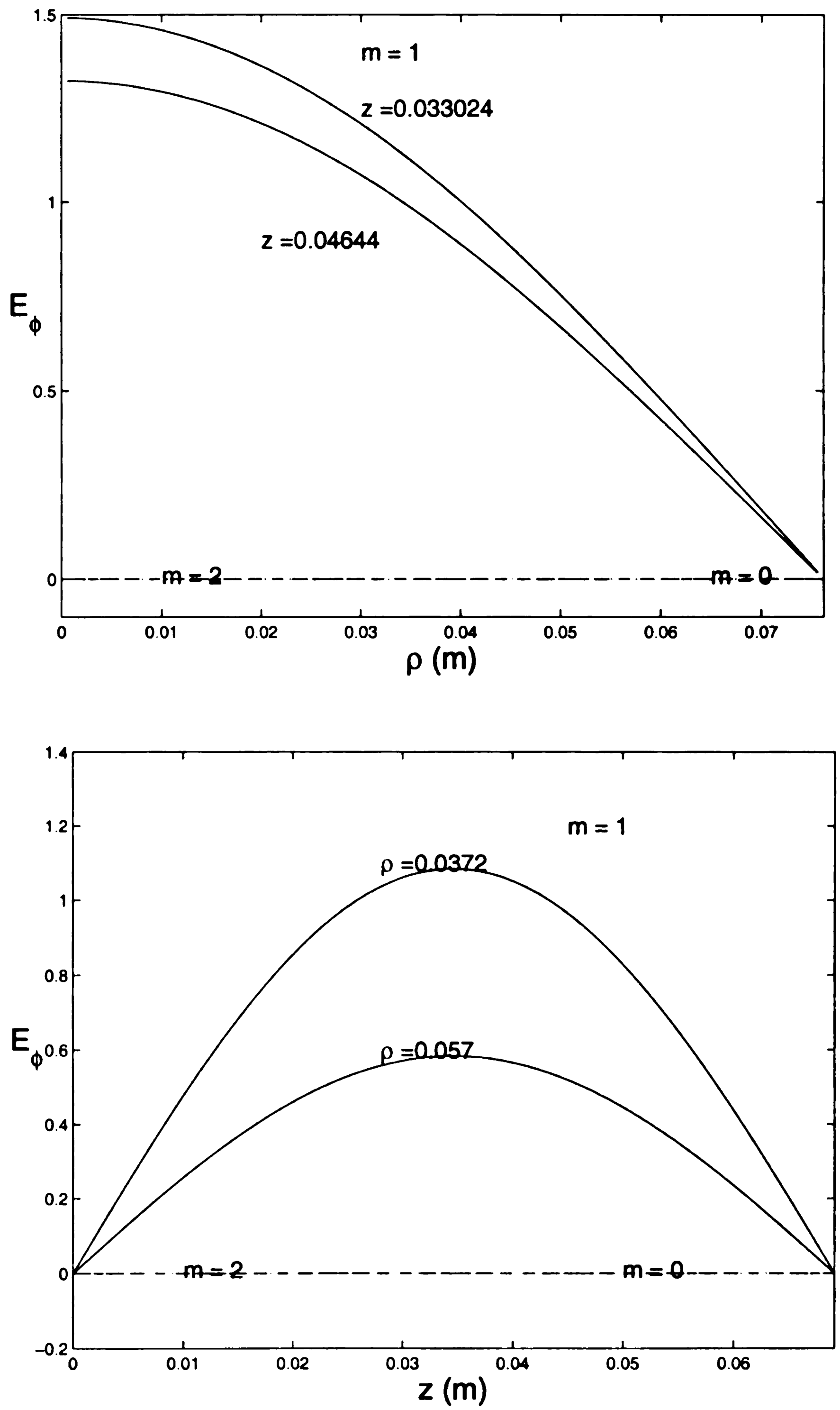

Figure 3.9 The variation of E_ϕ of TE_{111} mode along the ρ and z directions in a PEC empty cylindrical cavity.

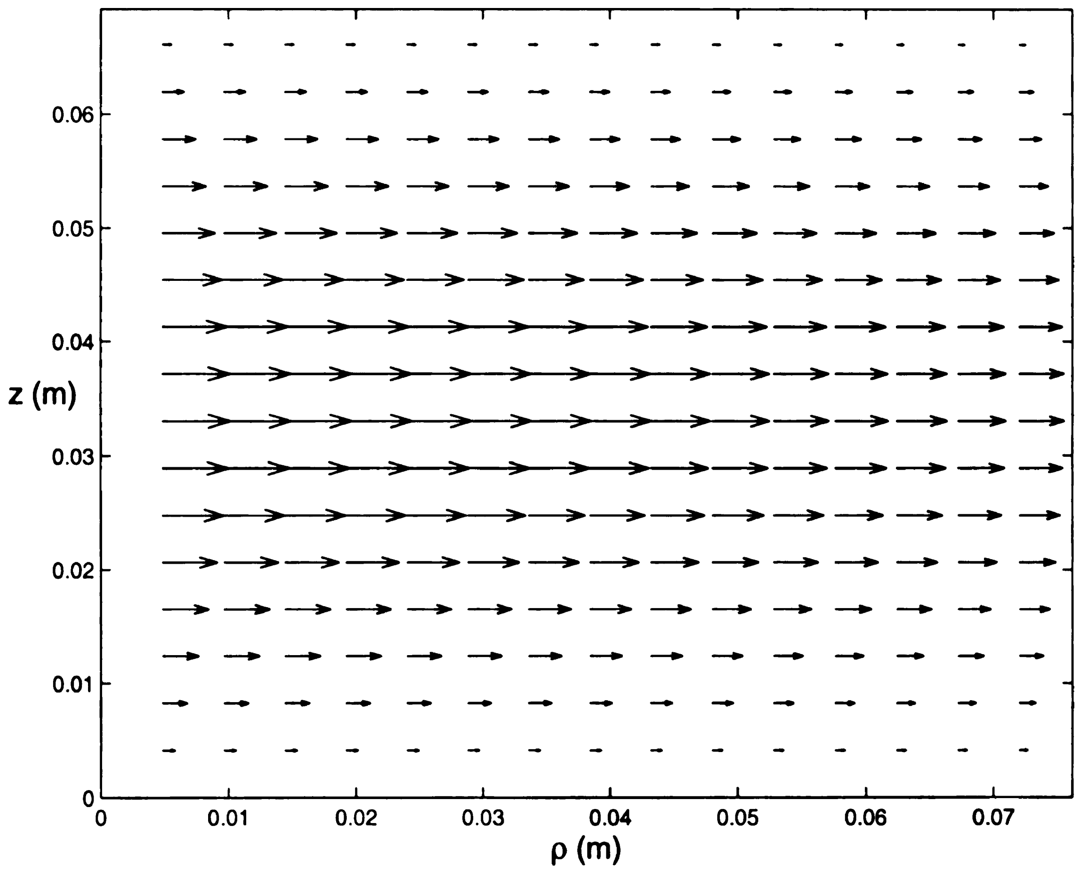

Figure 3.10 Plot of E field of TE_{111} mode on the ρ-z plane in an empty PEC cavity.

3.4 A Loaded Cylindrical Cavity

For a loaded cavity with PEC boundary, three cases for TM_{012} mode and one case for TE_{111} mode are calculated. The first one is a cavity loaded with a small cylindrical material, with $l \approx 2b$, centered at $\rho = 0$. The second one is a cavity loaded with a thin rod material with $l \gg 2b$ and a cavity loaded with a thin disk material with $l \ll 2b$ is the last case. For TE_{111} mode, only the case of a cavity loaded with a small cylinder material is studied.

3.4.1 Small cylindrical sample for TM_{012} mode

A material sample, having the diameter equal to the height, is placed in the center of the cylindrical cavity. The diameter is 0.006 meter and the height is 0.0059

meter; that is $l \approx 2b$. The induced electric field inside the material sample can be estimated by the electrostatic field induced inside of a dielectric sphere as $E_z = (3/(2+\varepsilon_r))E_z^i$.

The numbers of partition used along the ρ and z directions in this FDTD calculation are *127* and *131*, respectively, and the period of one time step is 1.29676 *p*s. Observing the electric field distribution in Figure 3.7, only E_z component of the electric is significant near the center of the empty cavity. Due to the small dimensions of the material sample, E_z is still the dominant component near the center of the loaded cavity if other components are compared with E_z in Figure 3.14 and Figure 3.15.

The ratio of E_z component of the induced field inside the material sample to that of the induced field in an empty cavity is plotted in Figure 3.16. The ratio is between 0.6 to 0.75

and it depends on the position of ρ and the fitting sine function. The electrostatic estimation of that ratio is 0.667 with $\varepsilon_r = 2.5$. The numerical results and the theoretical estimation are in satisfactory agreement.

3.4.2 Thin rod case for TM_{012} mode

A material sample with the shape of a thin rod, having its height much larger than its diameter, is placed in the center of the cylindrical cavity. The dimensions of the material sample are $l = 0.13098$ meter and $b = 0.0018$ meter. The ratio of the diameter to the wavelength is about 0.03. The numbers of the partition along the ρ and z directions and one period of time step are the same as those considered in section 3.4.1. The dominant component near the center of the cavity is still E_z if

E_ρ and E_z components are compared in Figure 3.17 and Figure 3.18. The field distribution of E_z along the ρ axis seems to be not affected at all in Figure 3.18. In fact, E_z is not affected by the placing of sample or the effect is too small to be noticeable. From Figure 3.19, we observe that the ratio of the z-component of the induced electric field to that of the electric field in an empty cavity is very close to 1 or slightly less than 1. The electrostatic estimation of that ratio is 1 based on the continuity of the tangential component of the electric field on the sample surface. This electrostatic estimation agrees with our numerical results.

3.4.3 Thin disk case for TM_{012} mode

A material sample with the shape of a thin disk, having its height much smaller than its diameter, is placed in the center of the cylindrical cavity. The dimensions of the material

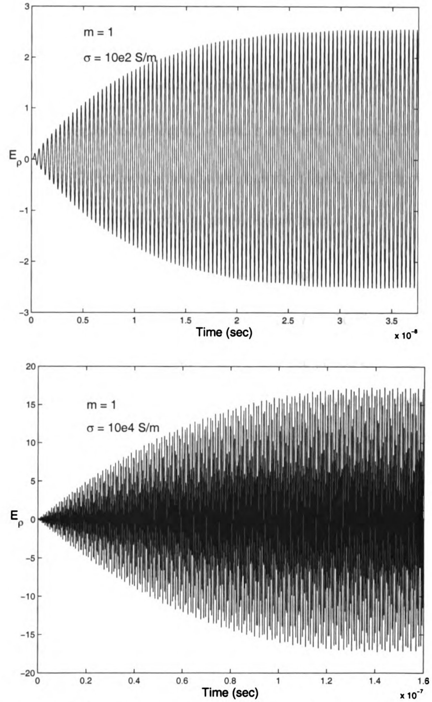

Figure 3.11 Plot of E_ρ of TE_{111} mode versus time in an empty FEC cavity with σ= 10^2 S/m and σ= 10^2 S/m with $m = 1$.

sample are $l = 0.00118$ meter and $b = 0.006$ meter and the ratio of diameter to wavelength is 0.1. The z component of the induced electric field inside the sample is still the dominant component. The induced electric field of this thin disk geometry can be estimated theoretically by the boundary condition of $E_z = (1/\varepsilon_r)E_z^i$.

The numbers of partition along the ρ and z axes are 131 and 262 and the one time step is *1.05171 ps*. The numerical results are shown in Figure 3.22. The ratio of E_z/E_z^i is about 0.42 which is consistent with the theoretic estimation.

3.4.4 Small cylindrical sample for TE_{111} mode

The dimensions of a small cylindrical material are $l = 0.00516$ *m* and $2b = 0.0048$ *m*. The numbers of partition along the ρ and z and one period time step are the same as those used in calculating the TE111 mode in an empty cavity. The numerical results of field distributions are shown form Figure 3.23 to Figure 3.25. There are some E_z near the center of the cylindrical cavity due to the placing of material sample as observed in Figure 3.25; however, the magnitude of E_z is much smaller than E_ρ or E_ϕ. When $\phi = \pi/2$, E_ϕ is zero since the first group of equations in Table 3.1 is used. Hence, the E_ρ is the dominant filed distribution near the center of the cavity. From Figure 3.23, we observe that the ratio of induced field E_ρ to E_ρ in an empty cavity is about 0.7 which is close to the theoretic estimation. Same results can be observed from Figure 3.24 for E_ϕ at $\phi = 0$.

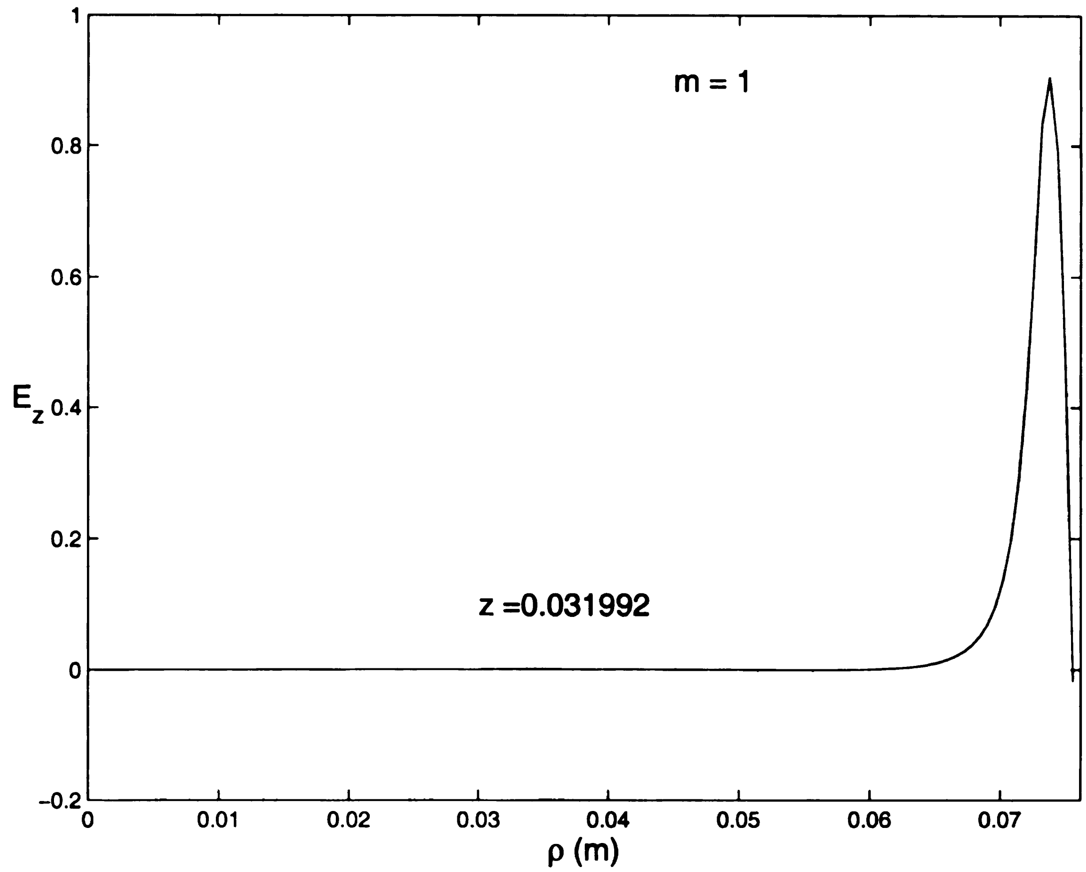

Figure 3.12 Plot of E_z of TE_{111} along ρ direction in an empty FEC cavity with conductivity 10^4 (S/m).

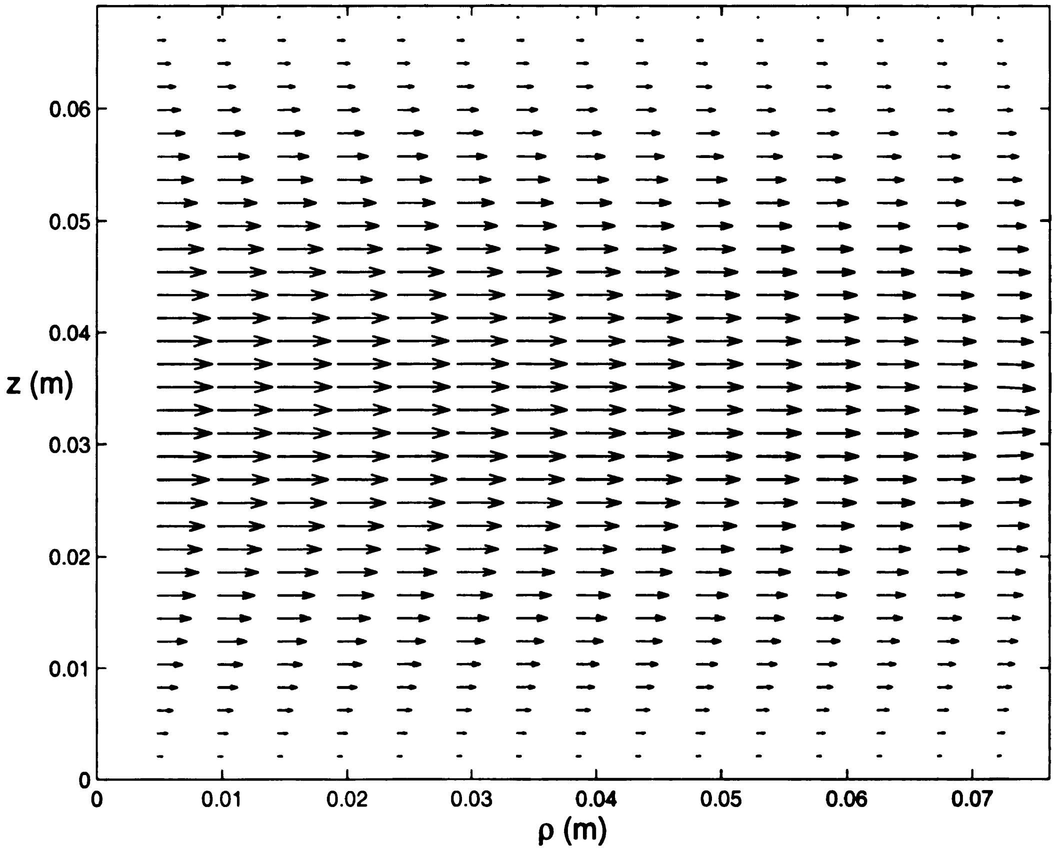

Figure 3.13 Plot of E field of TE_{111} mode on the ρ-z plane in an empty FEC cavity with conductivity 10^4 (S/m).

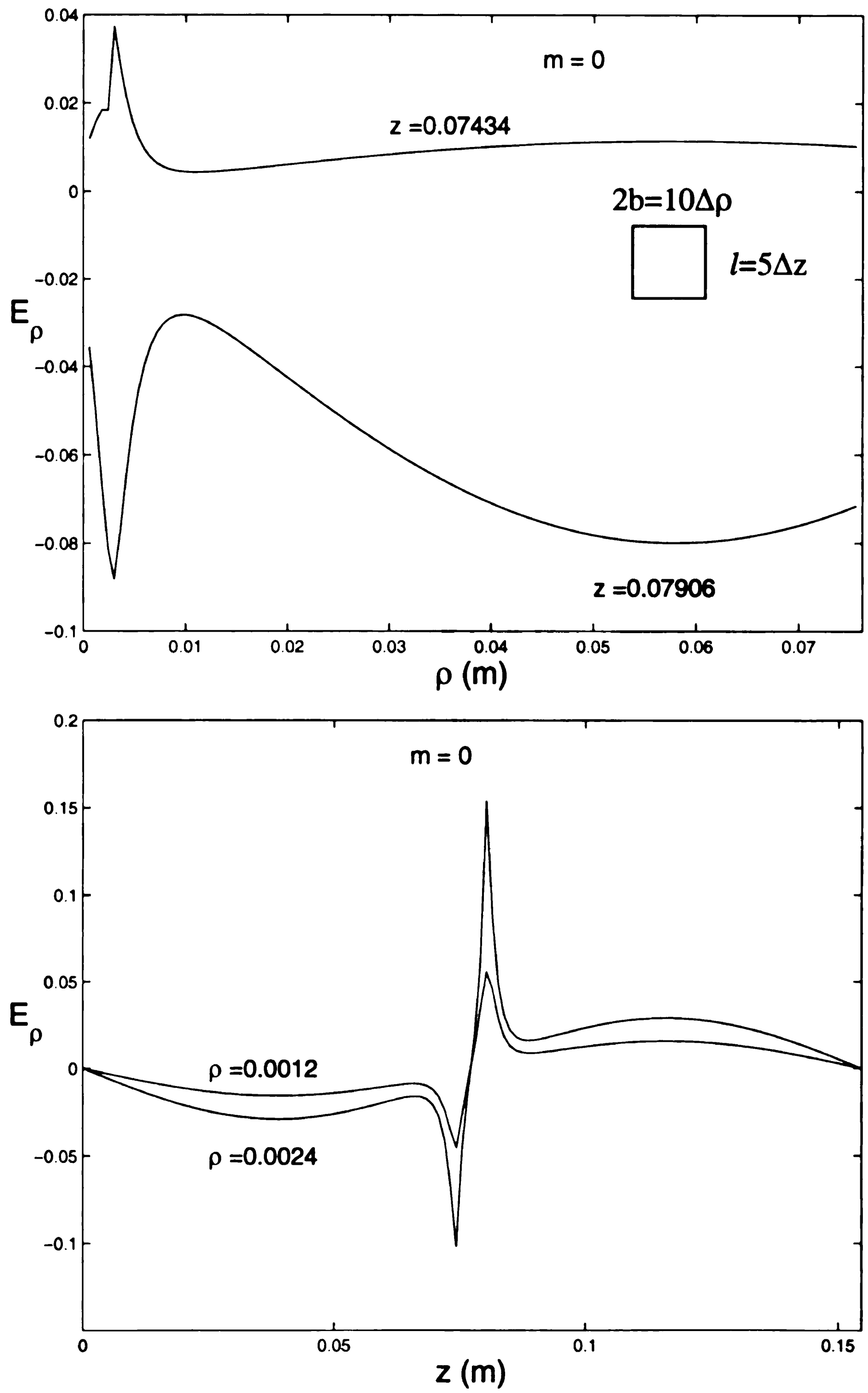

Figure 3.14 Plot of Eρ of TM_{012} mode in a PEC cavity loaded with a small cylindrical material sample.

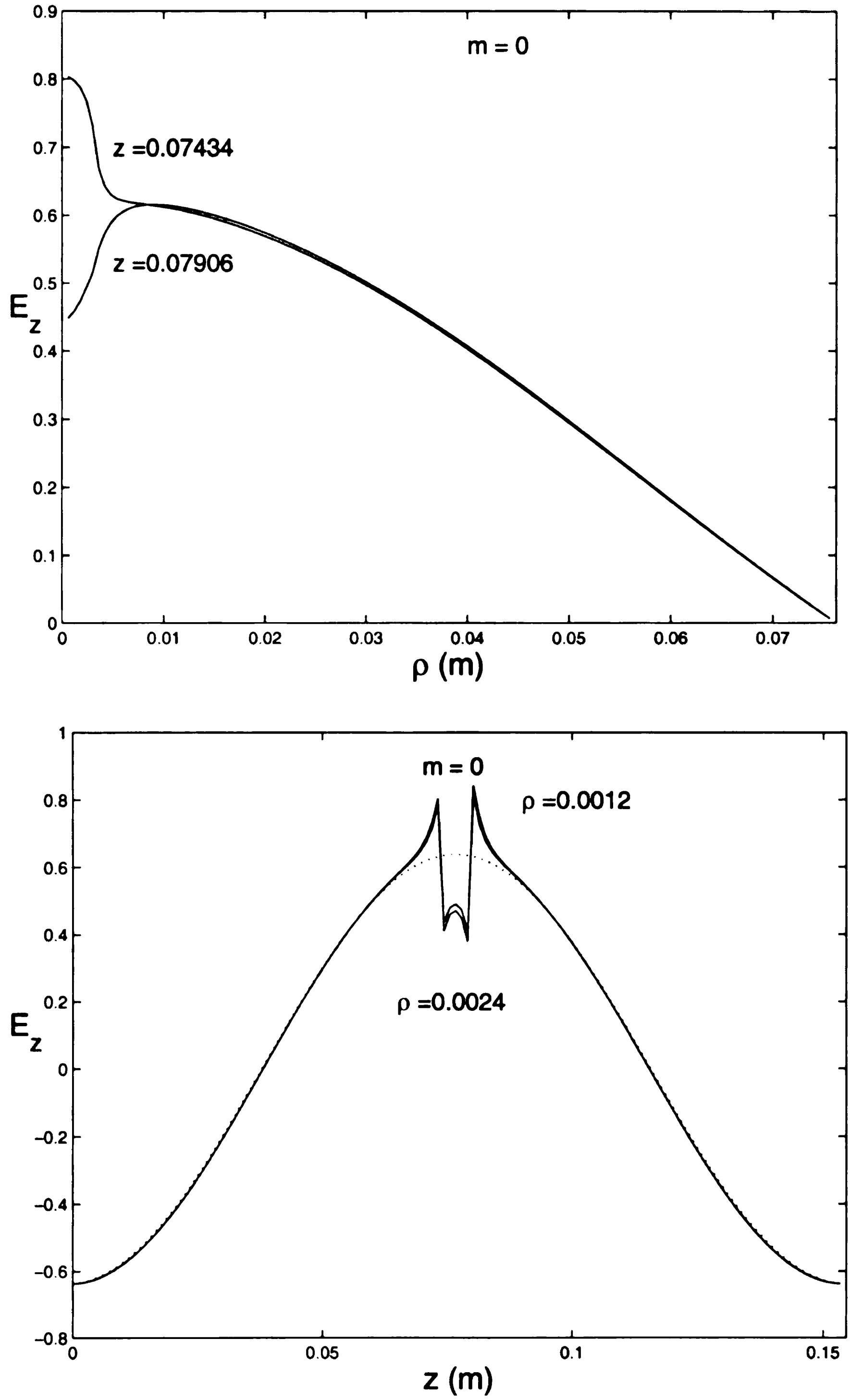

Figure 3.15 Plot of E_z of TM_{012} mode in a PEC cavity loaded with a small cylindrical material sample.

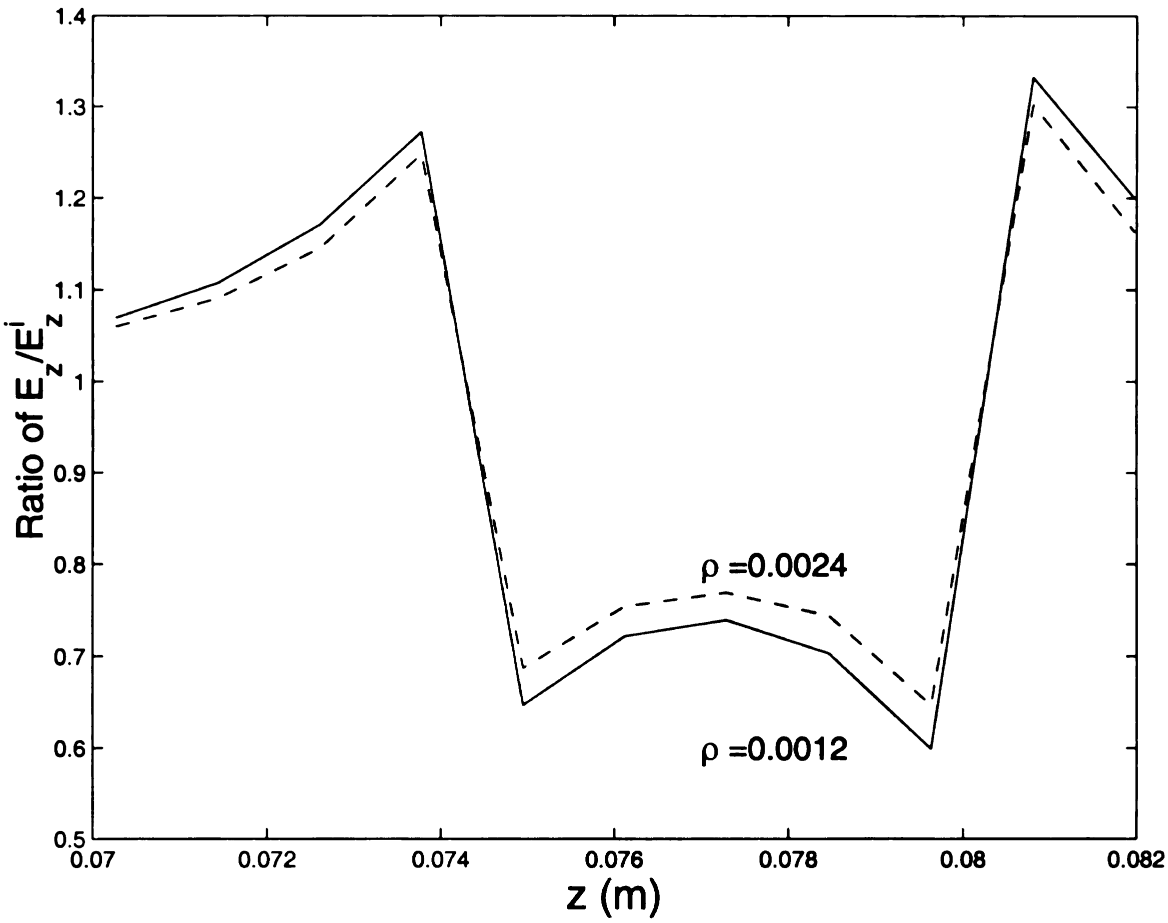

Figure 3.16 Plot of the ratio of E_z/E_z^i of TM_{012} mode along the z direction in the PEC cavity loaded with a small cylindrical material sample.

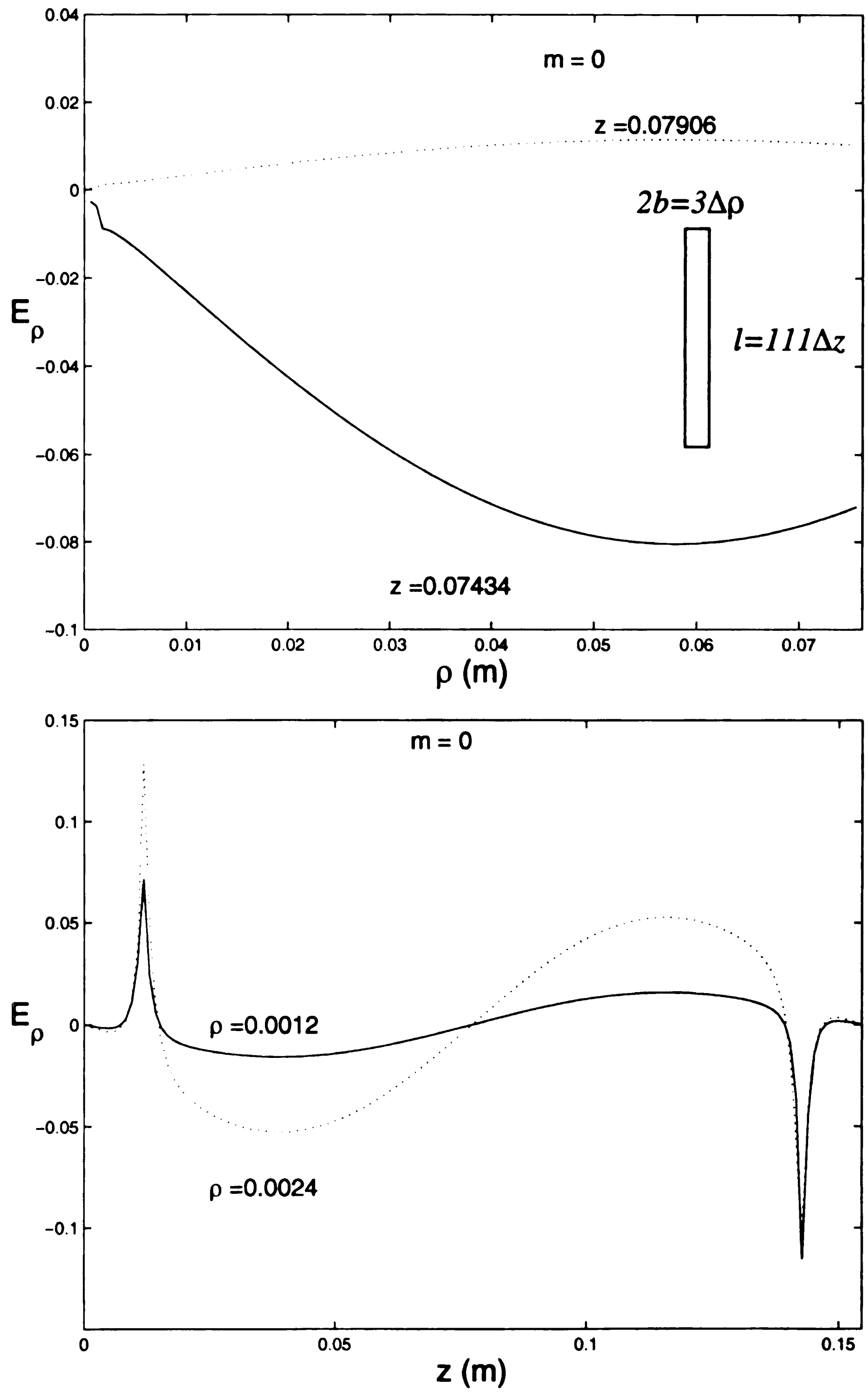

Figure 3.17 Plot of E_ρ of TM_{012} mode in a PEC cavity loaded with a thin rod material sample.

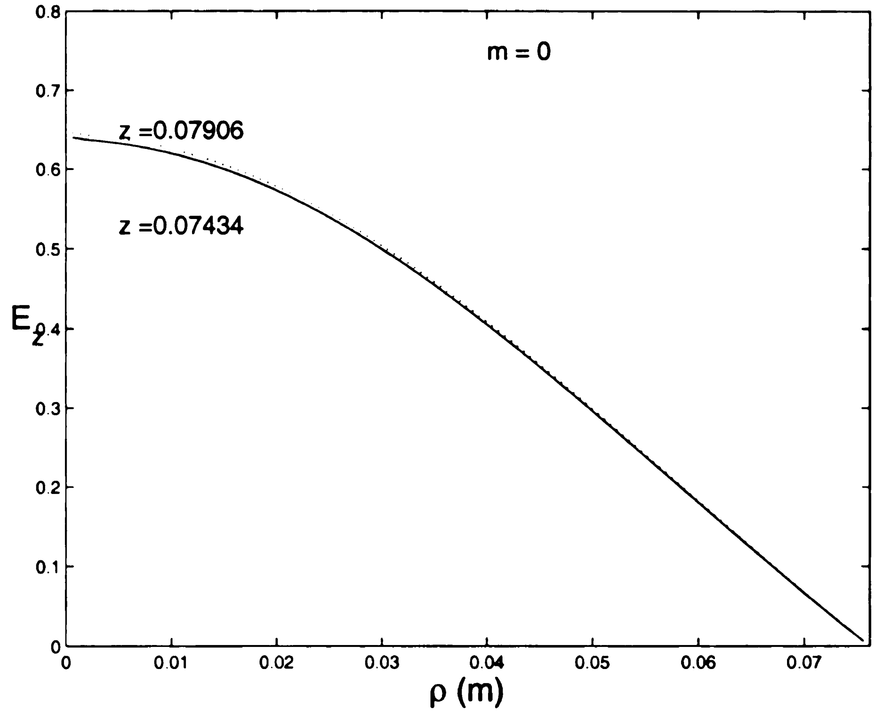

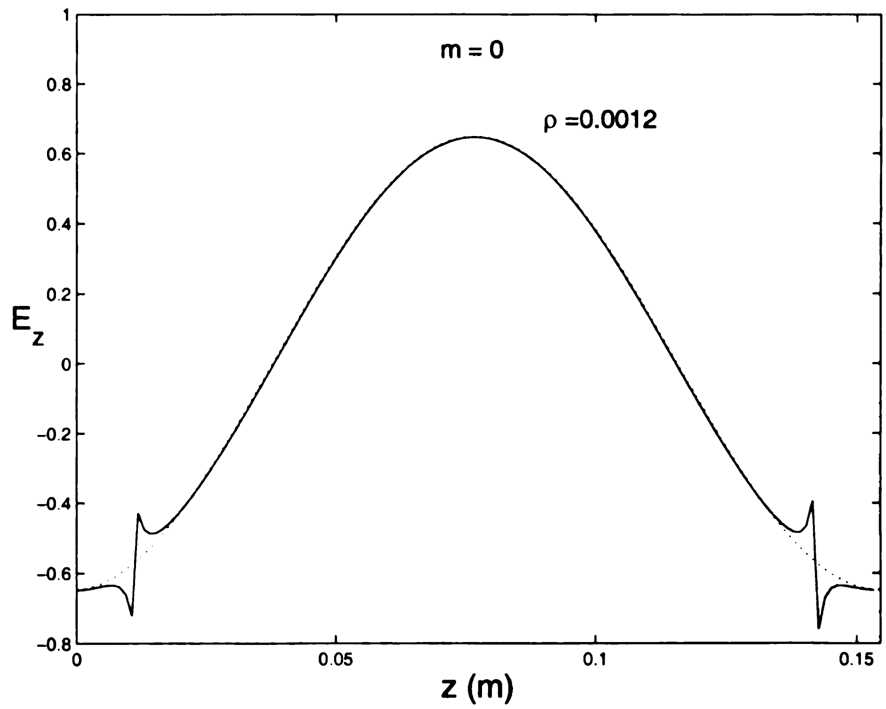

Figure 3.18 Plot of E_z of TM_{012} mode in a PEC cavity loaded with a thin rod material sample.

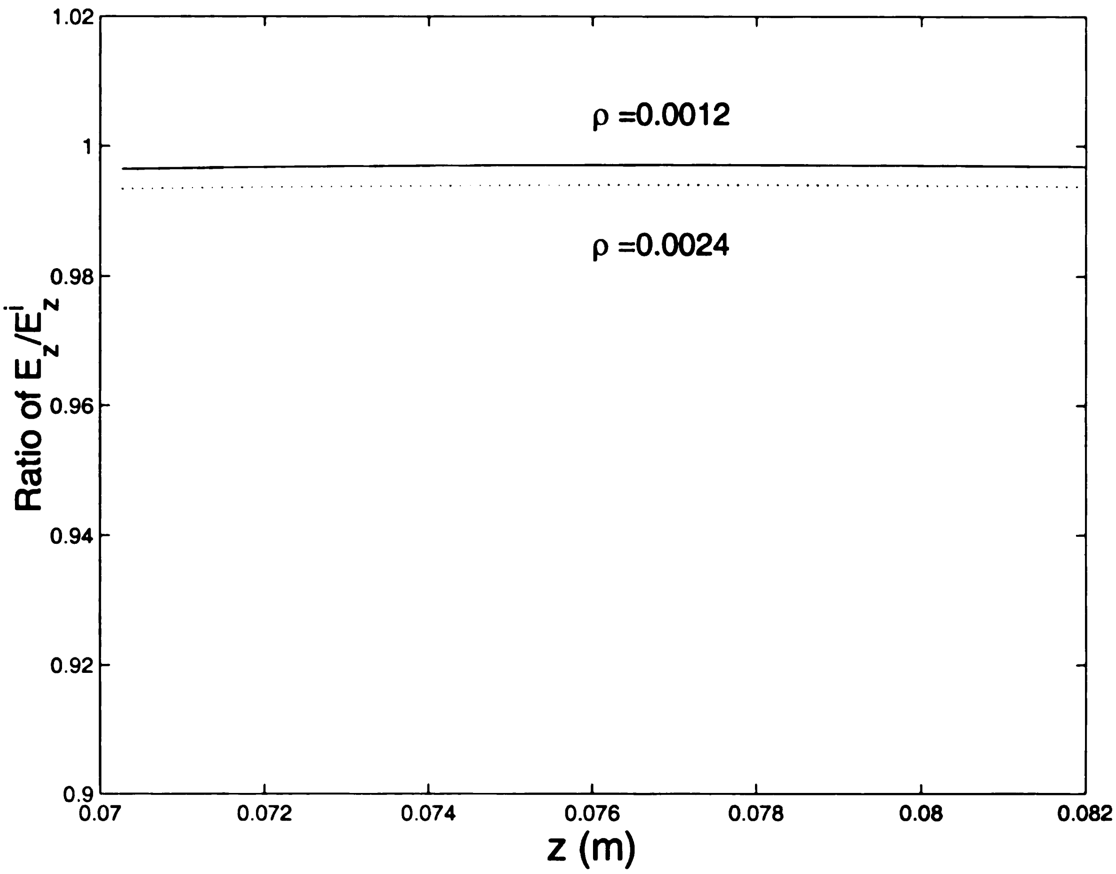

Figure 3.19 The ratio of E_z/E_z^i of TM_{012} mode in a PEC cavity loaded with a thin rod material sample.

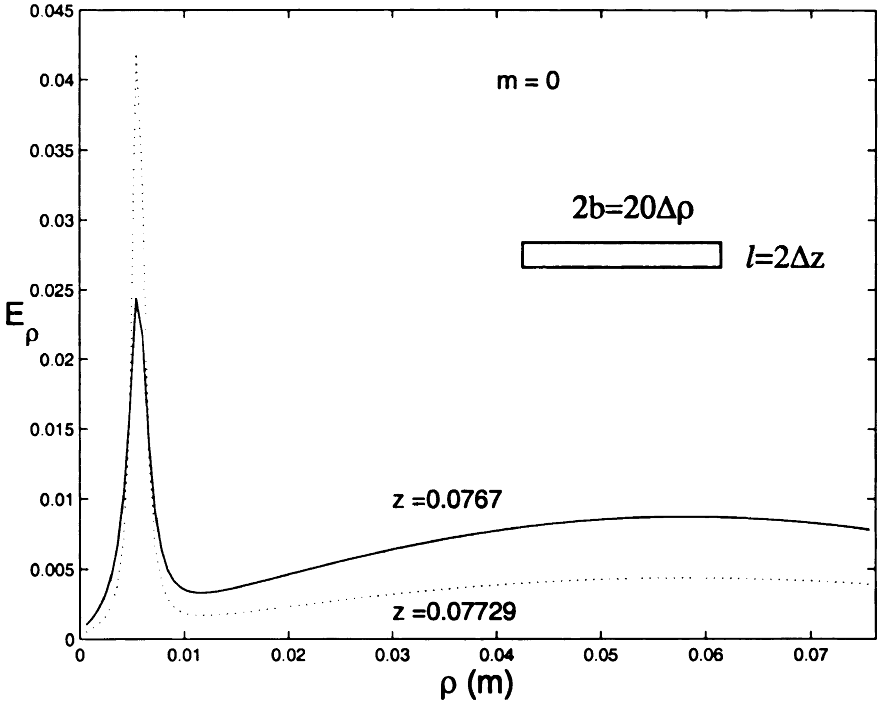

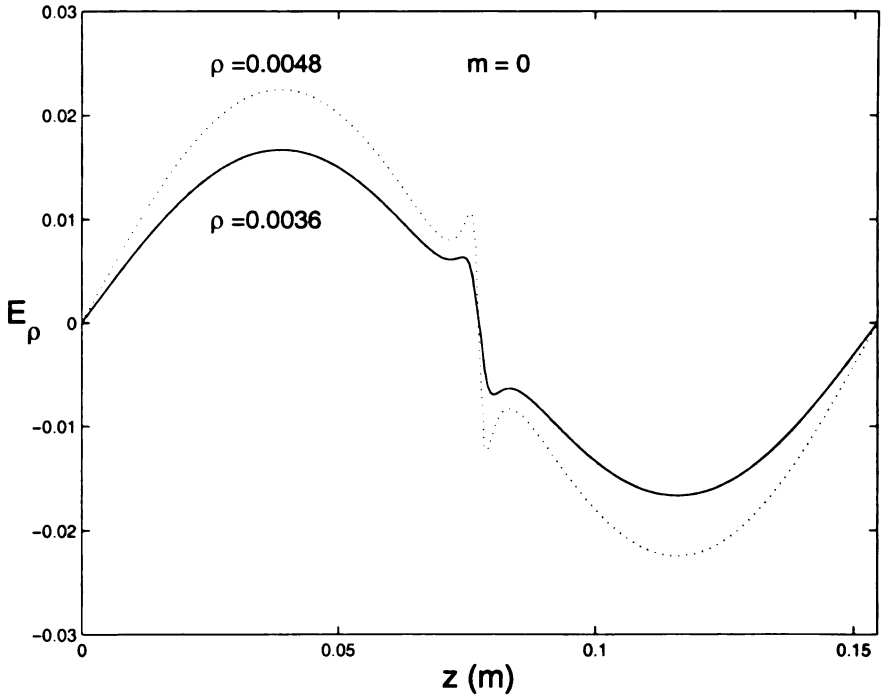

Figure 3.20 Plot of E_ρ of TM_{012} mode in a PEC cavity loaded with a thin disk material sample.

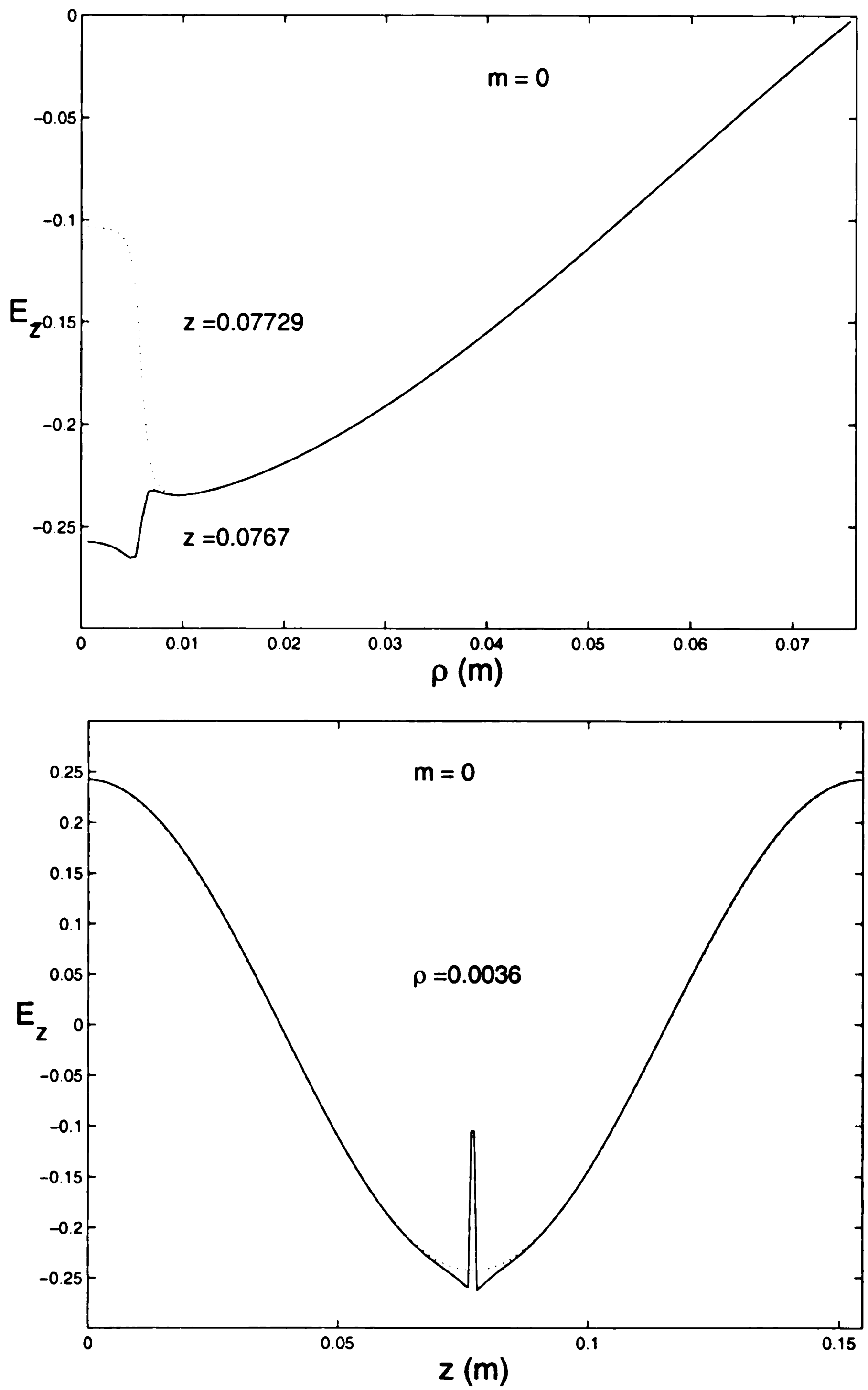

Figure 3.21 Plot of E_z of TM_{012} mode in a PEC cavity loaded with a thin disk material sample.

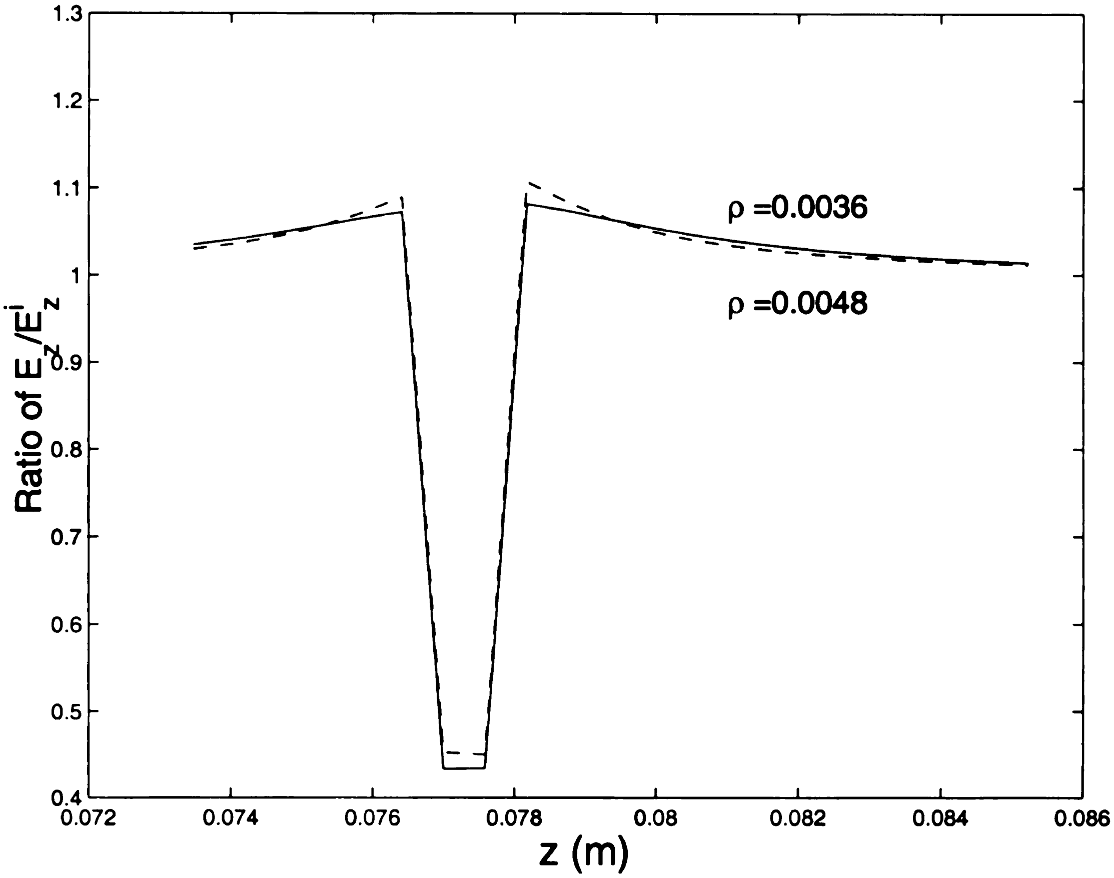

Figure 3.22 The ratio of E_z/E_z^i of TM_{012} mode in a PEC cavity loaded with a thin disk material sample.

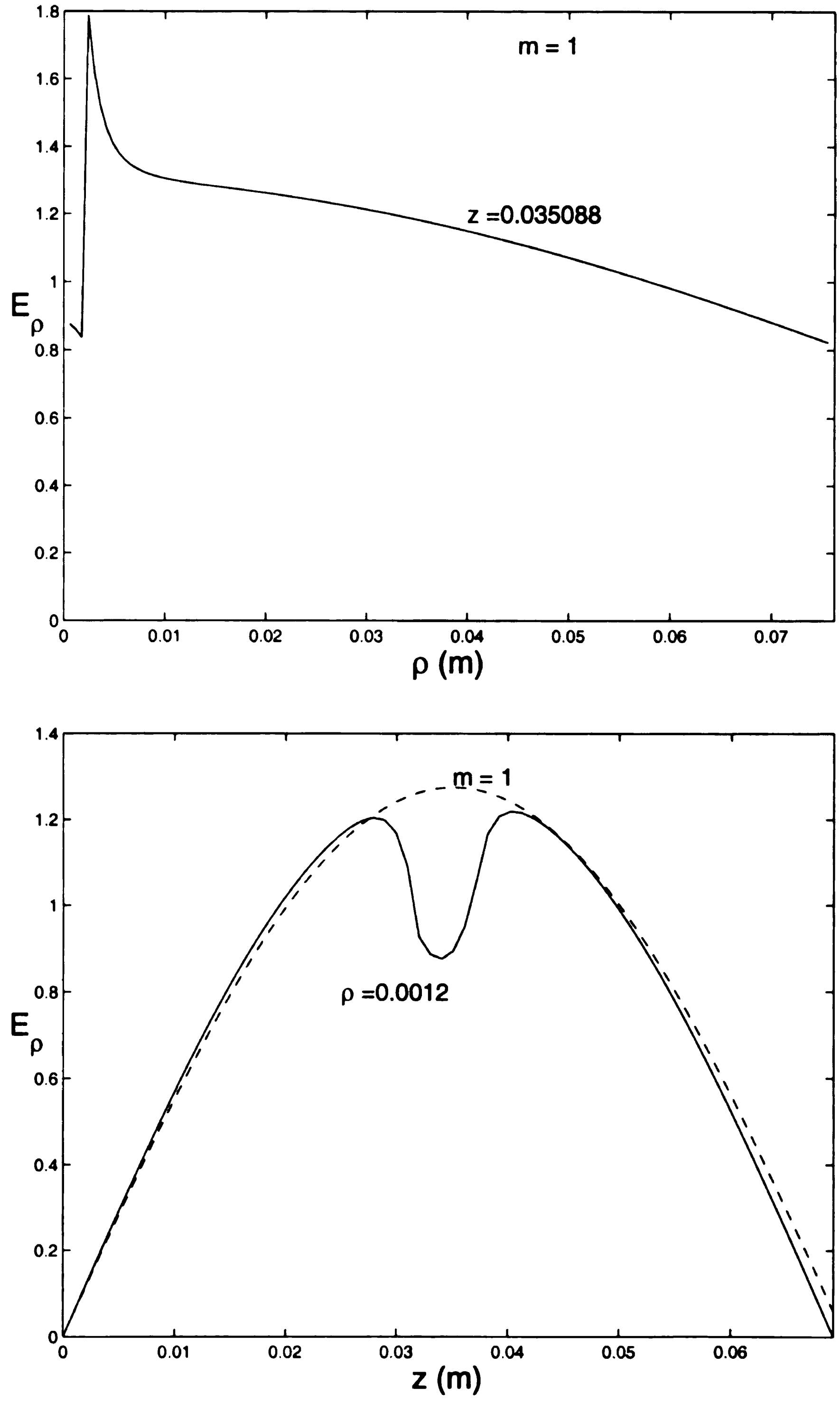

Figure 3.23 Plot of E_ρ of TE_{111} mode in a PEC cavity loaded with a small cylindrical material sample.

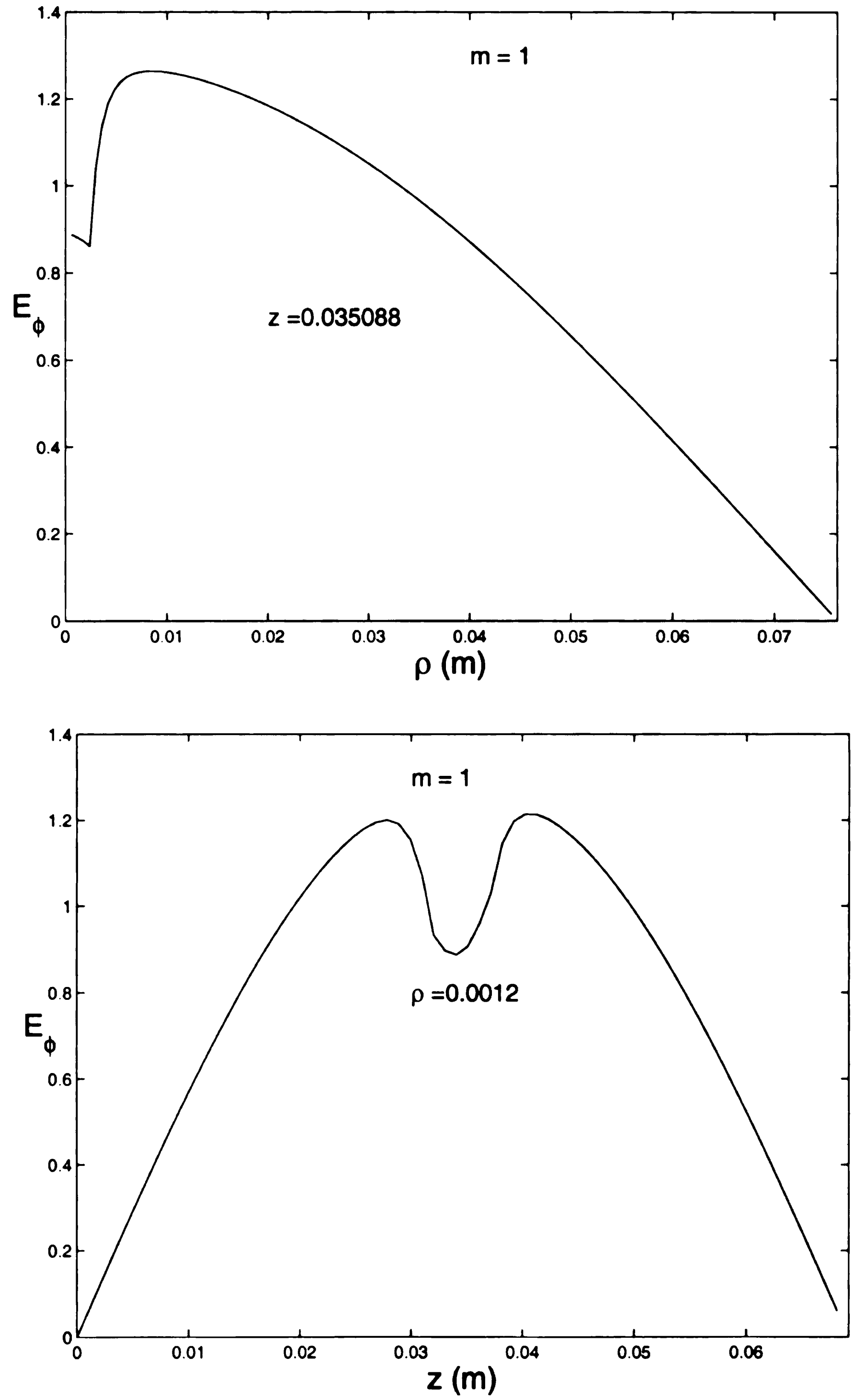

Figure 3.24 Plot of E_ϕ of TE_{111} mode in a PEC cavity loaded with a small cylindrical material sample.

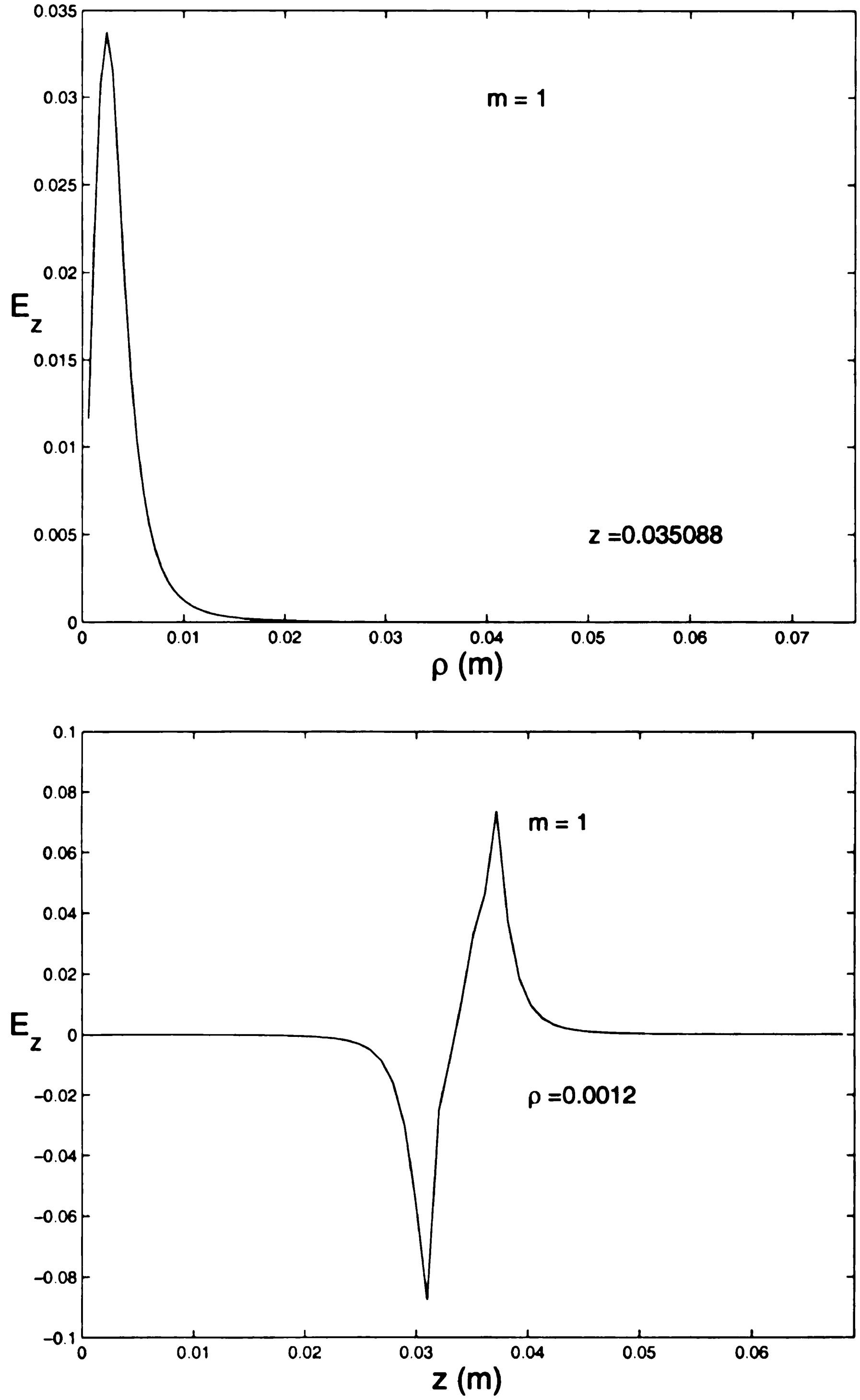

Figure 3.25 Plot of E_z of TE_{111} mode in a PEC cavity loaded with a small cylindrical material sample.

CHAPTER 4

SOLVING MAXWELL'S EQUATIONS BY FDTD IN CYLINDRICAL COORDINATES

In chapter 3, we considered the cylindrical geometries with rotational symmetries. The purpose of this chapter is to develop methods for treating problems which may not have rotational symmetries. This chapter considers the second-order and Ty(2,4) FDTD formulation and applications in cylindrical coordinates. The general 3-D FDTD formation is considered and discussed in section 4.1. There are two problems in applying cylindrical coordinate FDTD in 3-D. The first one is the singularities at $\rho = 0$. The other complication that arises in applying cylindrical coordinate FDTD in 3-D is that the cell size in the ϕ dimension decreases with decreasing ρ. This means that very small time steps may be necessary in order to satisfy the Courant stability criterion, unless the region in the vicinity of $\rho = 0$ is filled with perfect conductor or otherwise excluded. The two problems can be solved by using a set of FDTD approximation equations for $\rho = 0$ after a careful examination of the 3-D FDTD Maxwell's equations. This special FDTD approximations at $\rho = 0$ requires the loaded material to be bi-axial magnetic and without impressed or conductive current near the $\rho = 0$. For second-order method, those FDTD approximation equations are highly mode-dependent and not easy to be generalized as is discussed in section 4.2. In section 4.2, source implementation for traditional second-order FDTD approximation causes incorrect field distribution and this problem is solved by introducting the Blackman-Harris type source.

Using the higher-order spatial finite difference scheme, the approximation order can be controlled and general FDTD approximations at $\rho = 0$ can be obtained. Higher-order FDTD also requires less number of partition than that in second order scheme and hence reduces the computational time. These higher-order method is studied in section 4.3. At the end of this chapter, the FDTD formulation of constitutive equations for general Debye and Lorentz material, an extension of Debye material in section 2.3, is derived in section 4.4.

4.1 Three Dimensional FDTD Representation of Maxwell's Equations in Cylindrical Coordinates

In this section, the 3-D FDTD expressions of Maxwell's equations are derived. The differential Maxwell's equations considered here are

$$\begin{aligned} \nabla\times\vec{E} &= -\frac{\partial\vec{B}}{\partial t} \\ \nabla\times\vec{H} &= \frac{\partial\vec{D}}{\partial t}+\vec{J}_c+\vec{J}_s \end{aligned} \tag{4.1}$$

where $\vec{D} = [\varepsilon]\vec{E}$, $\vec{B} = [\mu]\vec{H}$, $\vec{J}_c = [\sigma]\vec{E}$, and $\vec{J}_c$ is the source current. The above constitutive parameters are further assumed to have the biaxial tensor form in the cylindrical coordinate system given by

$$[\alpha] = \begin{bmatrix} \alpha_\rho & 0 & 0 \\ 0 & \alpha_\phi & 0 \\ 0 & 0 & \alpha_z \end{bmatrix} \tag{4.2}$$

where α represents the electric permittivity, the magnetic permeability or the electric conductivity. For nonmagnetic dielectric material considered in this chapter, the electric conductivity of this material is assumed to be zero and the magnetic permeability is assumed to be the same as that in air.

The scalar Maxwell's equations in cylindrical coordinate are

$$\frac{\partial B_\rho}{\partial t} = \frac{\partial E_\phi}{\partial z} - \frac{1}{\rho}\frac{\partial E_z}{\partial \phi} \tag{4.3}$$

$$\frac{\partial B_\phi}{\partial t} = \frac{\partial E_z}{\partial \rho} - \frac{\partial E_\rho}{\partial z} \tag{4.4}$$

$$\frac{\partial B_z}{\partial t} = \frac{1}{\rho}\frac{\partial E_\rho}{\partial \phi} - \frac{1}{\rho}\frac{\partial}{\partial \rho}(\rho E_\phi) \tag{4.5}$$

$$\frac{\partial D_\rho}{\partial t} = \frac{1}{\rho}\frac{\partial H_z}{\partial \phi} - \frac{\partial H_\phi}{\partial z} - J_{c\rho} - J_{s\rho} \tag{4.6}$$

$$\frac{\partial D_\phi}{\partial t} = \frac{\partial H_\rho}{\partial z} - \frac{\partial H_z}{\partial \rho} - J_{c\phi} - J_{s\phi} \tag{4.7}$$

$$\frac{\partial D_z}{\partial t} = \frac{1}{\rho}\frac{\partial}{\partial \rho}(\rho H_\phi) - \frac{1}{\rho}\frac{\partial H_\rho}{\partial \phi} - J_{cz} - J_{sz} \tag{4.8}$$

where E_ρ, E_ϕ, E_z, H_r, H_ϕ, and H_z are electric and magnetic fields along ρ, ϕ, and z, respectively.

Using the FDTD notations, those finite difference equations for Maxwell's equations are obtained as:

$$\delta_t D_\rho\Big|_{i+\frac{1}{2},j,k}^{n-\frac{1}{2}} = \frac{1}{\rho_{i+\frac{1}{2},j,k}}\delta_\phi H_z\Big|_{i+\frac{1}{2},j,k}^{n-\frac{1}{2}} - \delta_z H_\phi\Big|_{i+\frac{1}{2},j,k}^{n-\frac{1}{2}} - J_{c\rho}\Big|_{i+\frac{1}{2},j,k}^{n-\frac{1}{2}} - J_{s\rho}\Big|_{i+\frac{1}{2},j,k}^{n-\frac{1}{2}} \tag{4.9}$$

$$\delta_t D_\phi\Big|_{i,j+\frac{1}{2},k}^{n-\frac{1}{2}} = \delta_z H_\rho\Big|_{i,j+\frac{1}{2},k}^{n-\frac{1}{2}} - \delta_\rho H_z\Big|_{i,j+\frac{1}{2},k}^{n-\frac{1}{2}} - J_{c\phi}\Big|_{i,j+\frac{1}{2},k}^{n-\frac{1}{2}} - J_{s\phi}\Big|_{i,j+\frac{1}{2},k}^{n-\frac{1}{2}} \tag{4.10}$$

$$\begin{aligned}\delta_t D_z\Big|_{i,j,k+\frac{1}{2}}^{n-\frac{1}{2}} &= \frac{1}{\rho_{i,j,k+\frac{1}{2}}}\left[\delta_\rho(\rho H_\phi)\Big|_{i,j,k+\frac{1}{2}}^{n-\frac{1}{2}} - \delta_\phi H_\rho\Big|_{i,j,k+\frac{1}{2}}^{n-\frac{1}{2}}\right] \\ &\quad - J_{cz}\Big|_{i,j,k+\frac{1}{2}}^{n-\frac{1}{2}} - J_{sz}\Big|_{i,j,k+\frac{1}{2}}^{n-\frac{1}{2}}\end{aligned} \tag{4.11}$$

$$\delta_t B_\rho\Big|_{i,j+\frac{1}{2},k+\frac{1}{2}}^{n} = \delta_z E_\phi\Big|_{i,j+\frac{1}{2},k+\frac{1}{2}}^{n} - \frac{1}{\rho_{i,j+\frac{1}{2},k+\frac{1}{2}}}\delta_\phi E_z\Big|_{i,j+\frac{1}{2},k+\frac{1}{2}}^{n} \tag{4.12}$$

$$\delta_t B_\phi\Big|_{i+\frac{1}{2},j,k+\frac{1}{2}}^{n} = \delta_\rho E_z\Big|_{i+\frac{1}{2},j,k+\frac{1}{2}}^{n} - \delta_z E_\rho\Big|_{i+\frac{1}{2},j,k+\frac{1}{2}}^{n} \tag{4.13}$$

$$\delta_t B_z\Big|_{i+\frac{1}{2},j+\frac{1}{2},k}^{n} = \frac{1}{\rho_{i+\frac{1}{2},j+\frac{1}{2},k}}\delta_\phi E_\rho\Big|_{i+\frac{1}{2},j+\frac{1}{2},k}^{n} - \frac{1}{\rho_{i+\frac{1}{2},j+\frac{1}{2},k}}\delta_\rho(\rho E_\phi)\Big|_{i+\frac{1}{2},j+\frac{1}{2},k}^{n} \tag{4.14}$$

where $\delta_\rho(\rho H_\phi)$ and $\delta_\rho(\rho E_\phi)$ need special treatment on ρ, and it will be discussed later.

The spatial locations of $\vec{D}$ and $\vec{H}$ are plotted in Figure 4.1, $\vec{E}$ has the same location as $\vec{D}$ does and so is $\vec{B}$ and $\vec{H}$. The sequence of FDTD calculations along time axis is shown in Figure 4.2. The $\vec{D}$, $\vec{E}$, and $\partial\vec{B}/\partial t$ are evaluated at the integer time step; but $\vec{B}$, $\vec{H}$, and $\partial\vec{D}/\partial t$ are evaluated at the half-integer time step. The order of calculation at different time steps are also described in Figure 4.2. Note that the boundary conditions are applied after the $\vec{E}$ is calculated.

Note that the terms $\frac{\partial}{\partial\rho}(\rho E_\phi)$ and $\frac{\partial}{\partial\rho}(\rho H_\phi)$ are not factorized out. The first term can be rewritten as

$$\frac{\partial}{\partial\rho}(\rho E_\phi) = E_\phi + \rho\frac{\partial E_\phi}{\partial\rho}. \tag{4.15}$$

The evaluation of E_ϕ in the right hand-side is $E_\phi\Big|^n_{i+1/2,\, j+1/2,\, k}$ which is not where E_ϕ is located and, thus, (4.15) is not used.

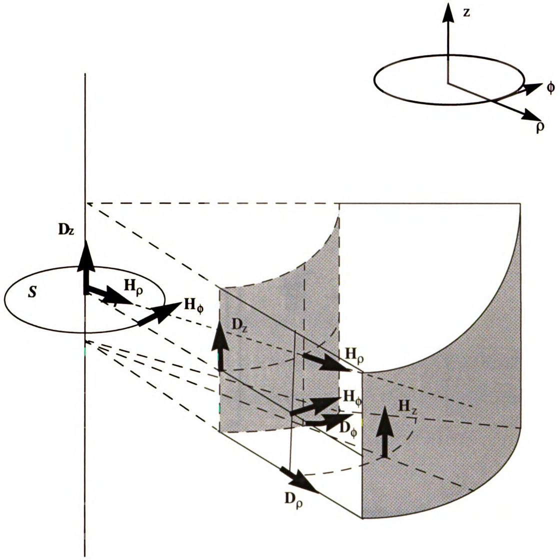

FIGURE 4.1 FDTD lattice for cylindrical coordinates.

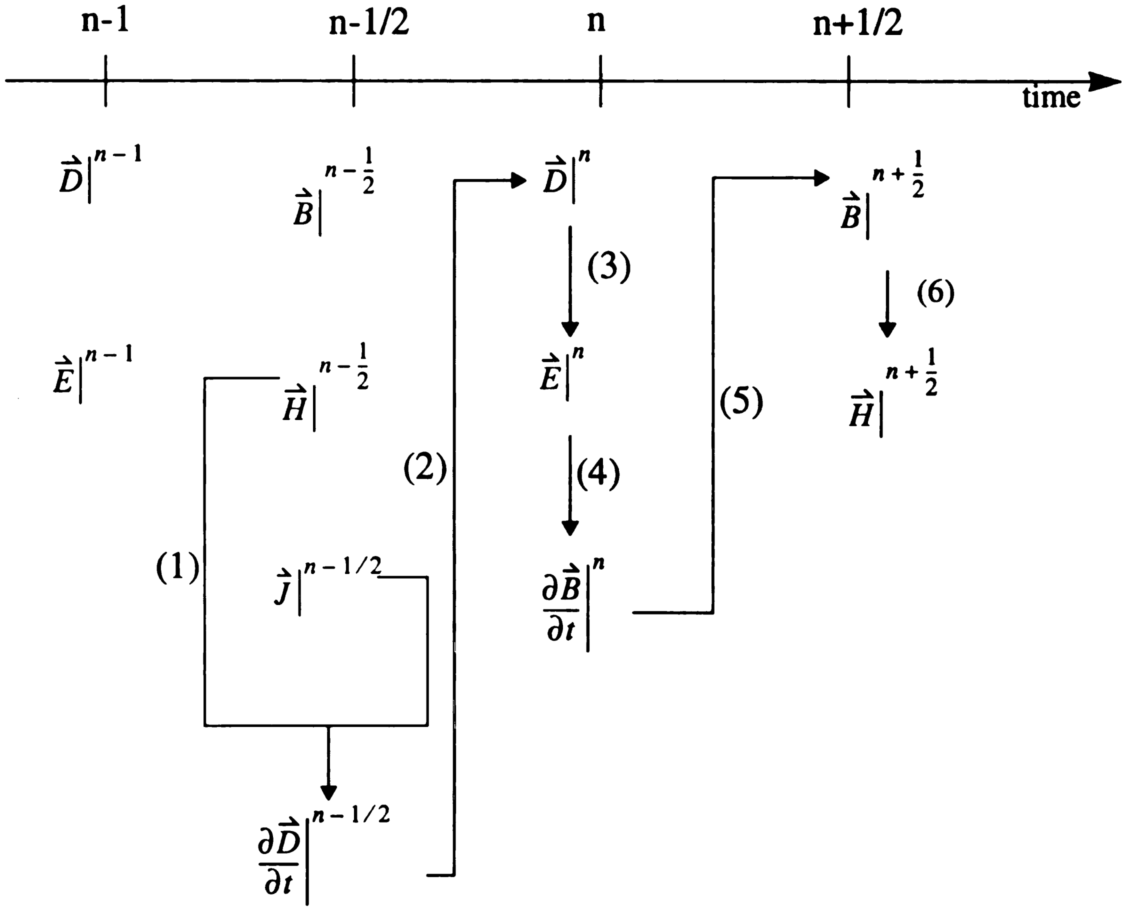

Figure 4.2 The diagram of order of FDTD calculations along time axis. The meanings of those steps are listed below.

(1) Using (4.9) to (4.11)

(2) Desired time stepping scheme for $\vec{D}$.

(3) Constitutive relation of $\vec{D}$ and $\vec{E}$ which depends on material models.

(4) Using (4.12) to (4.14). At this point, the boundary conditions are applied.

(5) Desired time stepping scheme for $\vec{B}$.

(6) Constitutive relation of $\vec{B}$ and $\vec{H}$ which depends on material models.

4.2 The Second-order Cylindrical FDTD Scheme[35]

The second-order cylindrical FDTD scheme which applies the Yee algorithm to cylindrical Maxwell equations is discussed in this section. The cylindrical FDTD formulation of Maxwell equations is presented in section 4.2.1. The singularity of cylindrical FDTD equations at $\rho = 0$ and its traditional treatments are discussed in section 4.2.2. The traditional source FDTD implementation is discussed in section 4.2.3 and an improved source implementation is also presented in this section. Finally, several numeric results are presented in section 4.2.4. The problems caused by the traditional source implementation and the improved implementation by utilizing Blackman-Harris function are also discussed in this section.

4.2.1 The Second-order Cylindrical FDTD Equations

Applying the second-order central finite difference approximation to time and spatial derivative of fields, the (4.9) to (4.14) become the finite difference Maxwell's equations in cylindrical coordinates. The finite difference equations are listed below:

$$E_\rho\Big|_{i+1/2,j,k}^{n+1} = E_\rho\Big|_{i+1/2,j,k}^{n} + \frac{\Delta t}{\varepsilon\big|_{i+1/2,j,k}} \times \left(\frac{H_z\big|_{i+1/2,j+1/2,k}^{n+1/2} - H_z\big|_{i+1/2,j-1/2,k}^{n+1/2}}{\rho_{i+1/2}\Delta\phi} - \frac{H_\phi\big|_{i+1/2,j,k+1/2}^{n+1/2} - H_\phi\big|_{i+1/2,j,k-1/2}^{n+1/2}}{\Delta z} - J_\rho\Big|_{i+1/2,j,k}^{n} \right) \tag{4.16}$$

$$E_\phi\Big|_{i,j+1/2,k}^{n+1} = E_\phi\Big|_{i,j+1/2,k}^{n} + \frac{\Delta t}{\varepsilon\big|_{i,j+1/2,k}} \times \left(\frac{H_\rho\big|_{i,j+1/2,k+1/2}^{n+1/2} - H_\rho\big|_{i,j+1/2,k-1/2}^{n+1/2}}{\Delta z} - \frac{H_z\big|_{i+1/2,j+1/2,k}^{n+1/2} - H_z\big|_{i-1/2,j+1/2,k}^{n+1/2}}{\Delta z} - J_\phi\Big|_{i,j+1/2,k}^{n} \right) \tag{4.17}$$

$$
\begin{aligned}
E_z\Big|_{i,j,k+1/2}^{n+1} = {} & E_z\Big|_{i,j,k+1/2}^{n} + \frac{2\Delta t}{\varepsilon\big|_{i,j,k+1/2}} \\
& \times\left(\frac{\rho_{i+1/2}H_\phi\big|_{i+1/2,j,k+1/2}^{n+1/2} - \rho_{i-1/2}H_\phi\big|_{i-1/2,j,k+1/2}^{n+1/2}}{\rho_{i+1/2}^2 - \rho_{i-1/2}^2}\right. \\
& - \frac{\rho_{i+1/2} - \rho_{i-1/2}}{\rho_{i+1/2}^2 - \rho_{i-1/2}^2} \times \frac{H_\rho\big|_{i,j+1/2,k+1/2}^{n+1/2} - H_\rho\big|_{i,j-1/2,k+1/2}^{n+1/2}}{\Delta\phi} \\
& \left. - J_z\Big|_{i,j,k+1/2}^{n}\right)
\end{aligned}
\tag{4.18}
$$

$$
\begin{aligned}
H_\rho\Big|_{i,j+1/2,k+1/2}^{n+1/2} = {} & H_\rho\Big|_{i,j+1/2,k+1/2}^{n-1/2} + \frac{\Delta t}{\mu\big|_{i,j+1/2,k+1/2}} \\
& \times\left(\frac{E_\phi\big|_{i,j+1/2,k+1}^{n} - E_\phi\big|_{i,j+1/2,k}^{n}}{\Delta z} -\right. \\
& \left. - \frac{E_z\big|_{i,j+1,k+1/2}^{n} - E_z\big|_{i,j,k+1/2}^{n}}{\rho_i(\Delta\phi)}\right)
\end{aligned}
\tag{4.19}
$$

$$
\begin{aligned}
H_\phi\Big|_{i+1/2,j,k+1/2}^{n+1/2} = {} & H_\phi\Big|_{i+1/2,j,k+1/2}^{n-1/2} + \frac{\Delta t}{\mu\big|_{i+1/2,j,k+1/2}} \\
& \times\left(\frac{E_z\big|_{i+1,j,k+1/2}^{n} - E_z\big|_{i,j,k+1/2}^{n}}{\Delta\rho}\right. \\
& \left. - \frac{E_\rho\big|_{i+1/2,j,k+1}^{n} - E_\rho\big|_{i+1/2,j,k}^{n}}{\Delta z}\right)
\end{aligned}
\tag{4.20}
$$

$$H_z\Big|_{i+1/2,\,j+1/2,\,k}^{n+1/2} = H_z\Big|_{i+1/2,\,j+1/2,\,k}^{n-1/2} + \frac{2\Delta t}{\mu|_{i+1/2,\,j+1/2,\,k}} \times \frac{1}{\rho_{i+1}^2-\rho_i^2}$$

$$\times\left((\rho_{i+1}-\rho_i)\times\frac{E_\rho\Big|_{i+1/2,\,j+1,\,k}^{n}-E_\rho\Big|_{i+1/2,\,j,\,k}^{n}}{\Delta\phi}\right. \quad . \tag{4.21}$$

$$\left.-\left(\rho_{i+1}E_\phi\Big|_{i+1,\,j+1/2,\,k}^{n}-\rho_i E_\phi\Big|_{i,\,j+1/2,\,k}^{n}\right)\right)$$

4.2.2 FDTD Calculations at $\rho = 0$

There are singularities in (4.18) and (4.19) in the above FDTD equations when ρ approaches to zero. Thus, those two equations can not be used in this FDTD calculation. Appropriate approximations to $E_\phi\big|_{\rho=0}$ and $H_\rho\big|_{\rho=0}$ are presented in this section.

Assume that there are no impressed current and conduction current inside the region S in Figure 4.1, we can obtain the finite difference equation for E_z at $\rho = 0$ by Ampere's law as

$$E_z\Big|_{0,\,j,\,k+\frac{1}{2}}^{n} = E_z\Big|_{0,\,j,\,k+\frac{1}{2}}^{n-1} + \frac{\Delta t}{\varepsilon}\cdot\frac{4}{r_1}H_\phi\Big|_{\frac{1}{2},\,j,\,k+\frac{1}{2}}^{n-\frac{1}{2}} \tag{4.22}$$

where r_1 is the distance along ρ for the first cell as shown in Figure 4.1.

Regarding to $H_\rho\big|_{\rho=0}$, it is used to calculate $E_\phi\big|_{\rho=0}$ in (4.17) and $E_z\big|_{\rho=0}$ in (4.18). However, $E_z\big|_{\rho=0}$ is approximated by Amper's law in (4.22). If $E_\phi\big|_{\rho=0}$ is also approximated then the calculation of H_ρ at $\rho = 0$ is not needed. Traditionally, E_ϕ at $\rho = 0$ is approximated by its analytical solution. For example, E_ϕ at $\rho = 0$ of TE_{111} mode is approximated by E_ϕ at $\rho = 1$ times *1.0015* which is the ratio of analytical solution at these two points. This approximation is highly dependent on the mode being calculated and difficult to be generalized. Other drawbacks of this approximation are the lack of order control and the number of partition along ρ cannot be too small even if the $\Delta\rho$ is much smaller than $\lambda/10$. These disadvantages can be solved theoretically by applying the Ty(2,4) FDTD to cylindrical coordinates FDTD.

4.2.3 Source Implementation

Traditionally, the way chosen to numerically incorporate an electromagnetic field excitation source inside the cavity for the empty cavity simulation is based on the specific cavity mode of resonance. Implementing a source is to select several lattice points as source points and assigning magnitudes of an electric field component at these points based on theoretical cavity field solutions[4]. These source points are driven a few cycles at a frequency close to the resonant frequency, then turned off. This technique of exciting a mode inside the cavity and then turning off the source gives the natural frequency response. Examples of excitation sources are shown in Figure 4.3.

The traditional source implementation is mode-dependent and actually gives wrong field distributions which are shown in section 4.2.4 even though the fundamental modes are calculated. However, by using the source implementation in (3.19) and Blackman-Harris function for $g(t)$, correct field distributions can be obtained. In this chapter, the second-order FDTD with traditional source implementation is denoted by T-FDTD and that FDTD with Blackman-Harris source is called BH-FDTD.

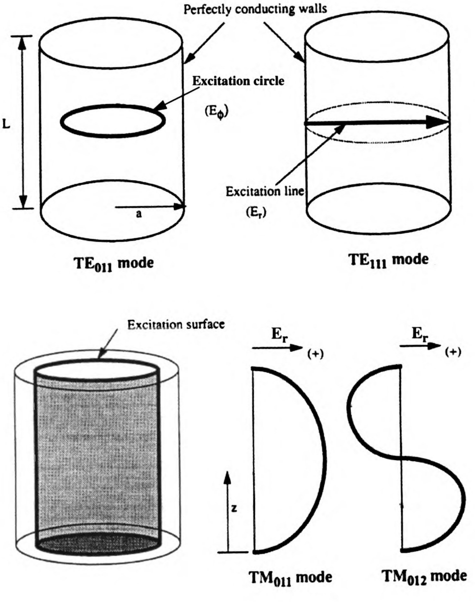

Figure 4.3 TE_{011}, TE_{111}, TM_{011}, and TM_{012} modes excitation techniques in a cylindrical cavity[35].

4.2.4 Numerical Results and Discussions

For TM_{012} mode, an empty cylindrical cavity with *0.0889* meter radius and *0.14409926* meter height are used. The number of partitions along ρ, ϕ, and z are *29*, *36*, and *29*, respectively. One time step is equal to 5×10^{-13} second and the number of total time steps is 35,000. The total stored energies of T-FDTD and BH-FDTD are plotted in Figure 4.4. The result of BH-FDTD is closer to the correct one. The field distributions of TM_{012} mode of T-FDTD and BH-FDTD are plotted in Figure 4.5 to Figure 4.8. For T-FDTD, only the field distribution of E_ρ along z in Figure 4.6 and that of E_z along z in Figure 4.8 are correct comparing to theoretic results. On the contrary, the BH-FDTD gives the correct field distributions of $\vec{E}$ field in all the figures.

Using an empty cylindrical cavity with radius equal to *0.0889* meter and height equal to *0.0669089* meter, a TE_{111} mode can be excited. The number of partitions along ρ, ϕ, and z are *59*, *36*, and *29*, respectively. One time step is equal to 1×10^{-13} second and the number of total time steps is 175,000. The total stored energies of T-FDTD and BH-FDTD of TE_{111} are plotted in Figure 4.9 and the field distributions of $\vec{E}$ field are plotted in Figure 4.10 to Figure 4.15. Observing from these figures, we found that all the field distributions calculated by T-FDTD are all incorrect. However, the field distributions of E_ρ along ϕ, E_ρ along z, E_ϕ along ϕ, and E_ϕ along z are roughly similar to correct ones. Again, the field distributions calculated by BH-FDTD are all correct comparing to theoretical results. Hence, the traditional source implementation needs to be replaced by Blackman-Harris source when calculating the fundamental modes of empty cylindrical cavity with PEC wall. Also, from our experience the Blackman-Harris source should be used for

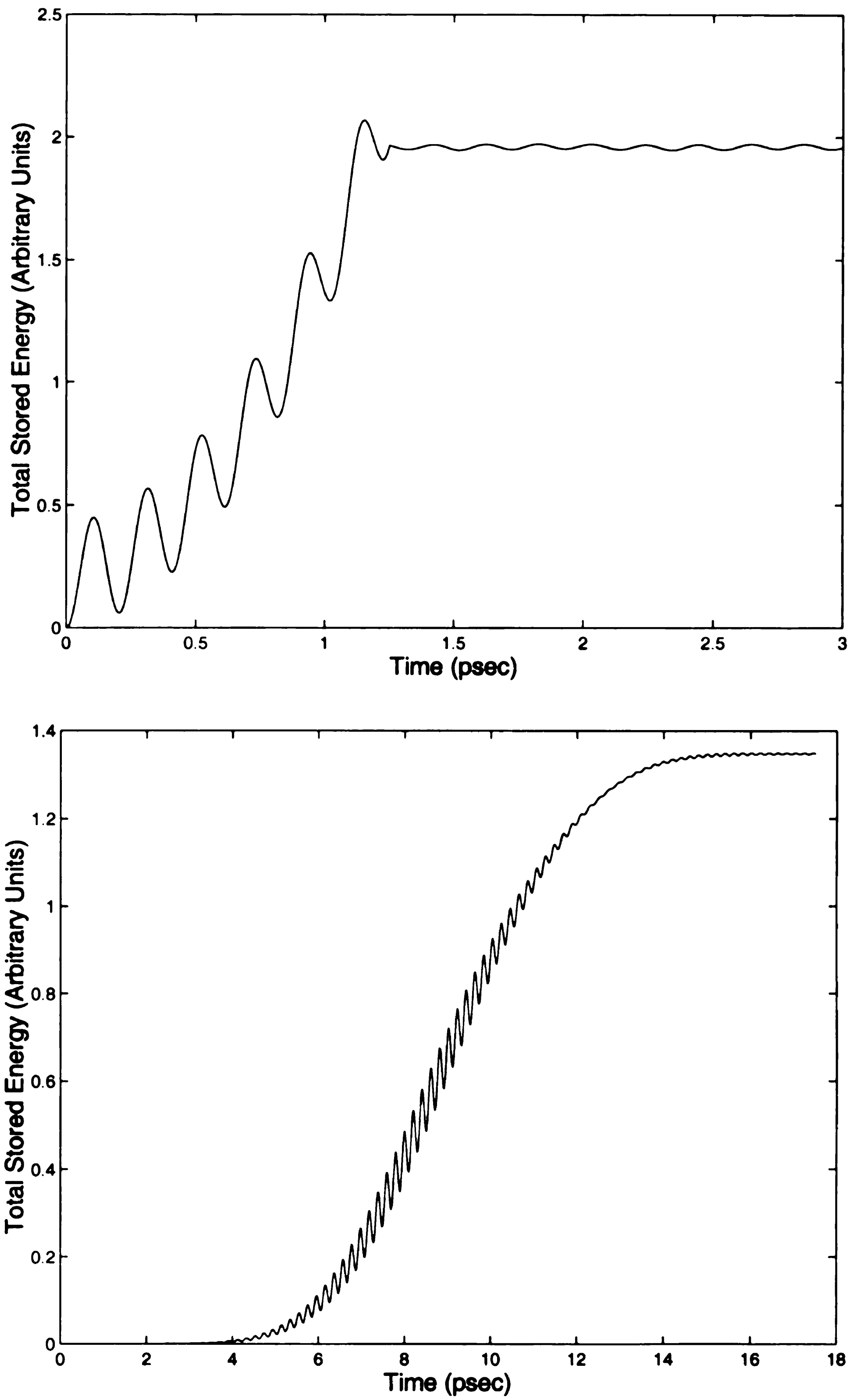

Figure 4.4 The plots of total stored energy of TM_{012} mode in a PEC empty cylindrical cavity. The upper figure is calculated by using the traditional source implementation and the lower one by using the BH source implementation.

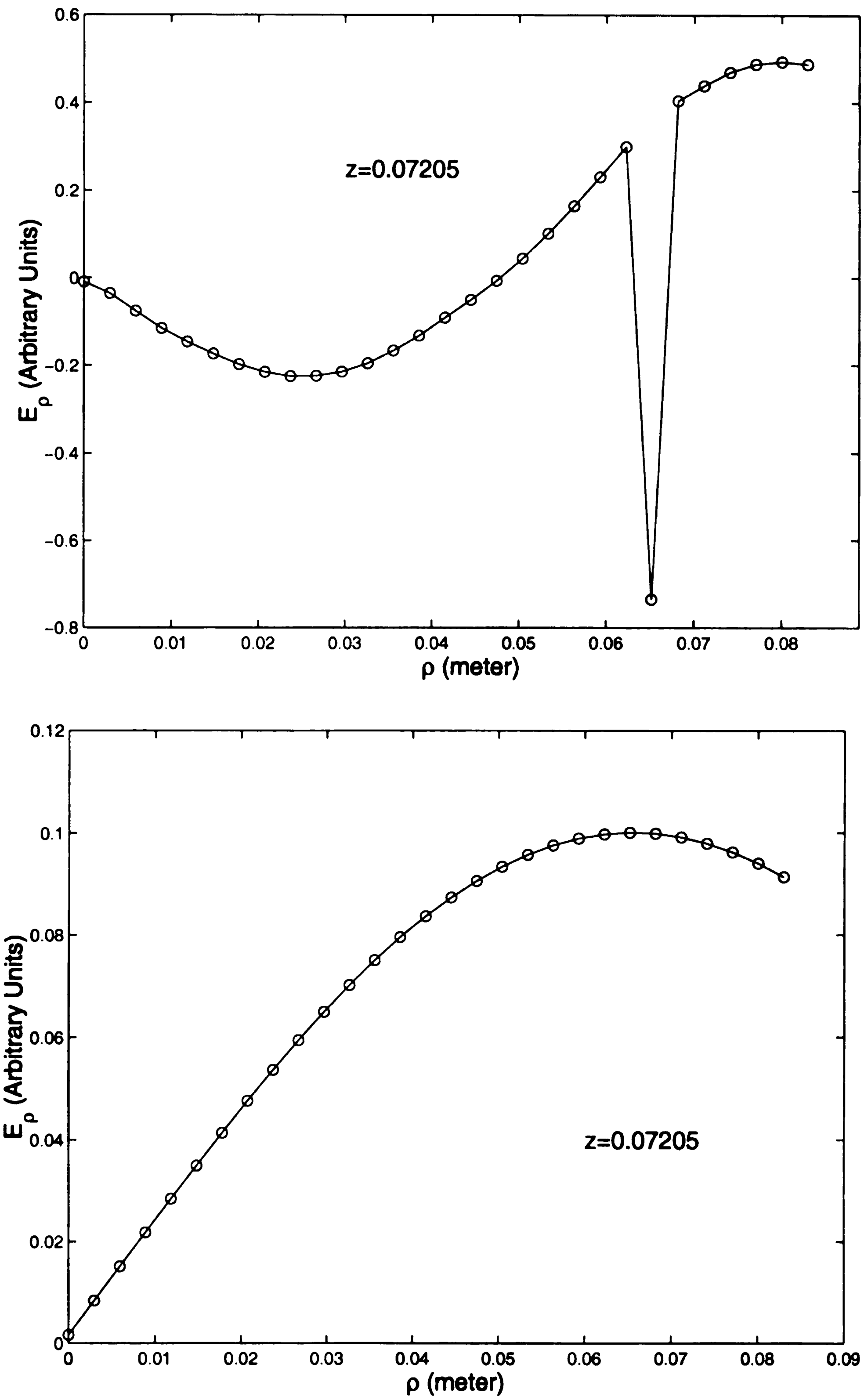

Figure 4.5 The variation of E_ρ of TM_{012} mode along the ρ direction in a PEC empty cylindrical cavity. The upper figure is calculated by using the traditional source implementation and the lower one by using the BH source implementation.

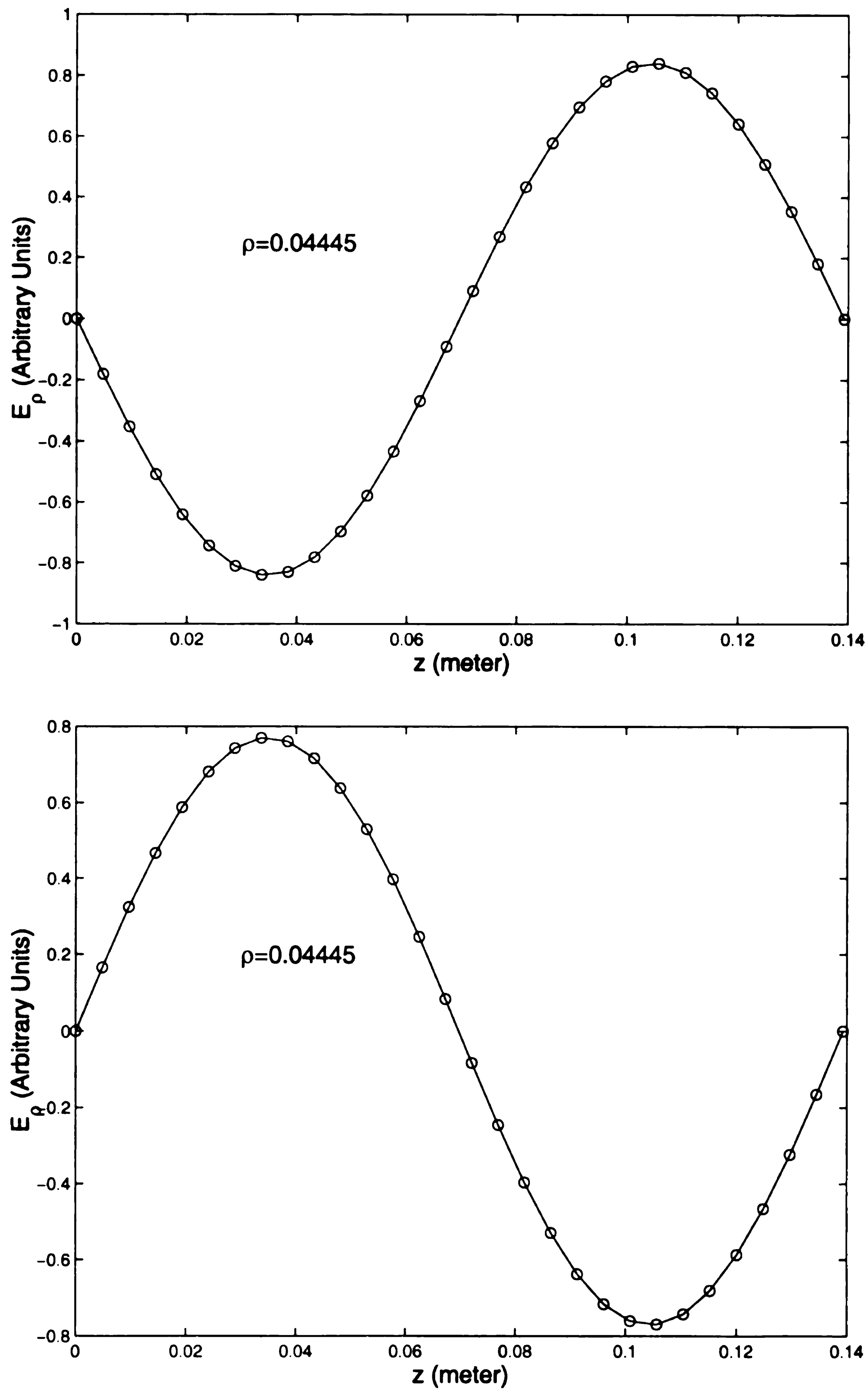

Figure 4.6 The variation of E_ρ of TM_{012} mode along the *z* direction in a PEC empty cylindrical cavity. The upper figure is calculated by using the traditional source implementation and the lower one by using the BH source implementation.

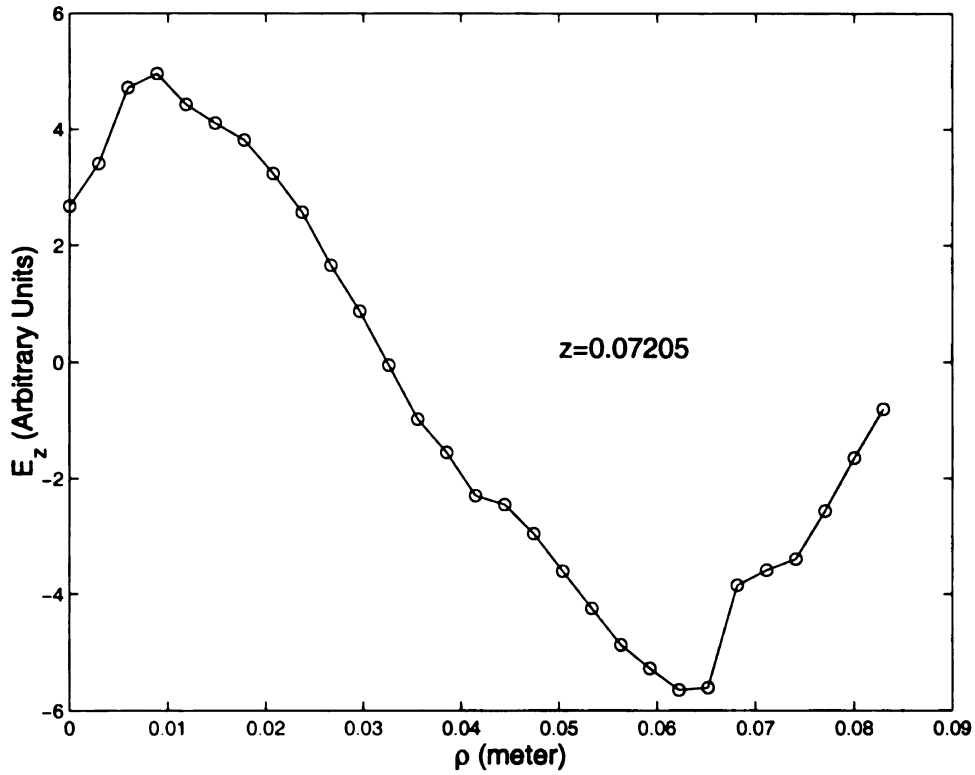

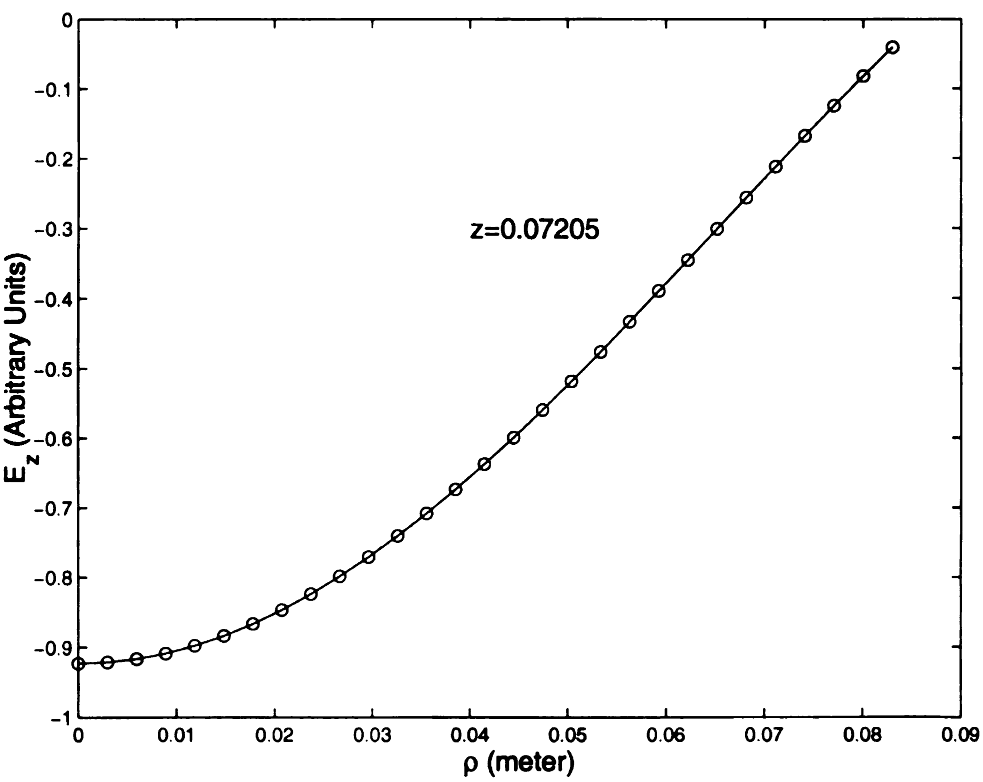

Figure 4.7 The variation of E_z of TM_{012} mode along the ρ direction in a PEC empty cylindrical cavity. The upper figure is calculated by using the traditional source implementation and the lower one by using the BH source implementation.

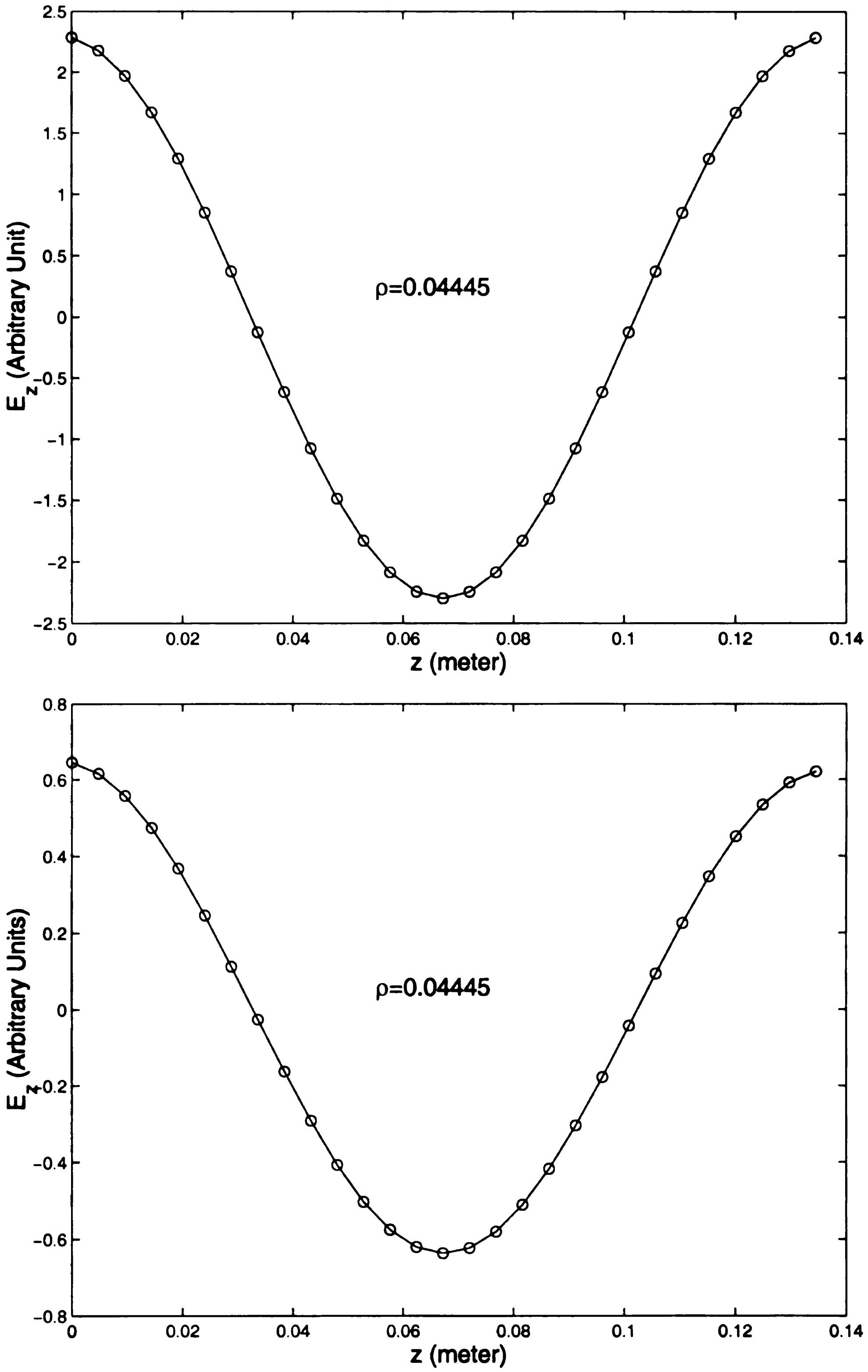

Figure 4.8 The variation of E_z of TM_{012} mode along the z direction in a PEC empty cylindrical cavity. The upper figure is calculated by using the traditional source implementation and the lower one by using the BH source implementation.

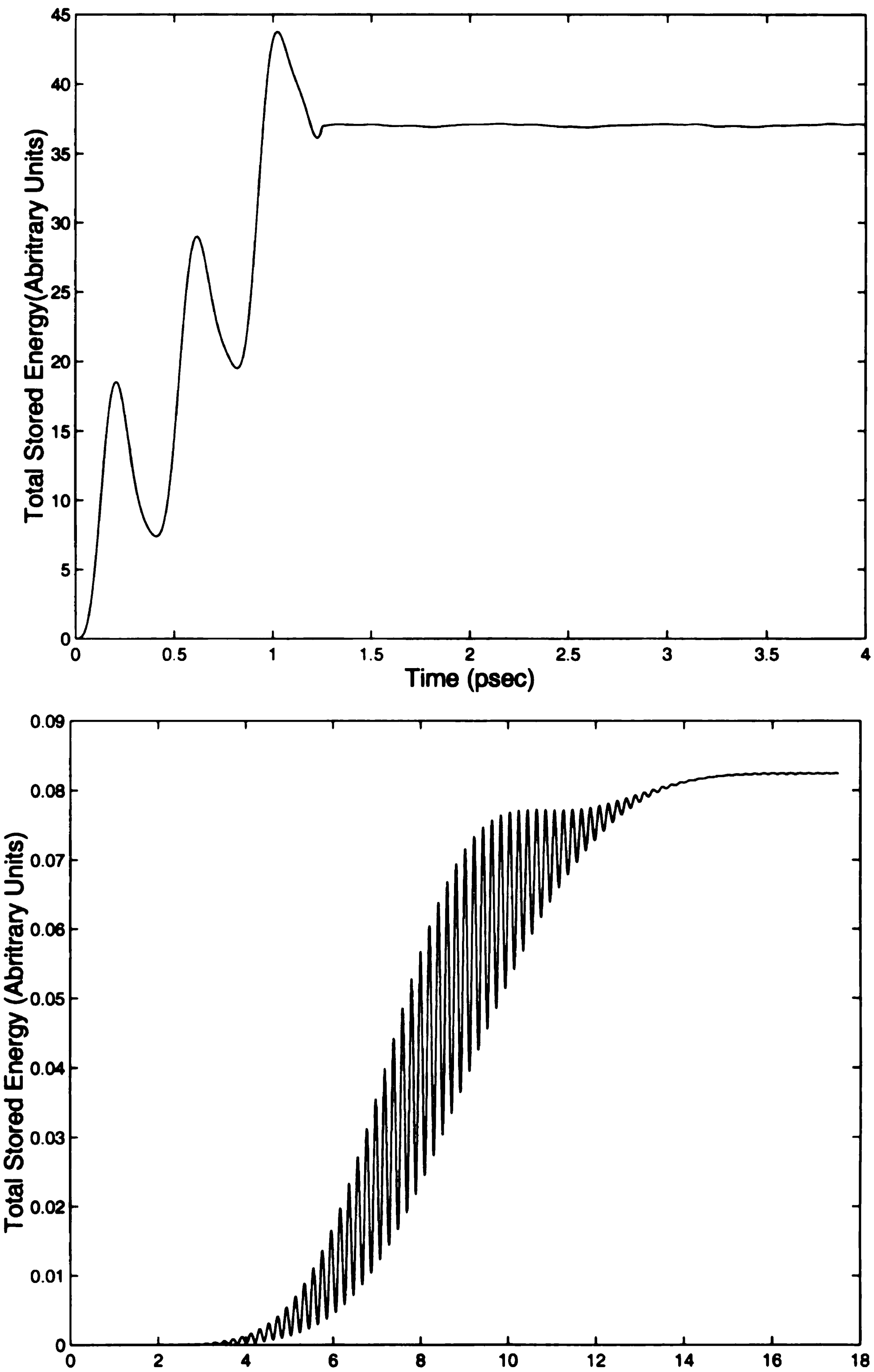

Figure 4.9 The plots of total stored energy of TE_{111} mode in a PEC empty cylindrical cavity. The upper figure is calculated by using the traditional source implementation and the lower one by using the BH source implementation.

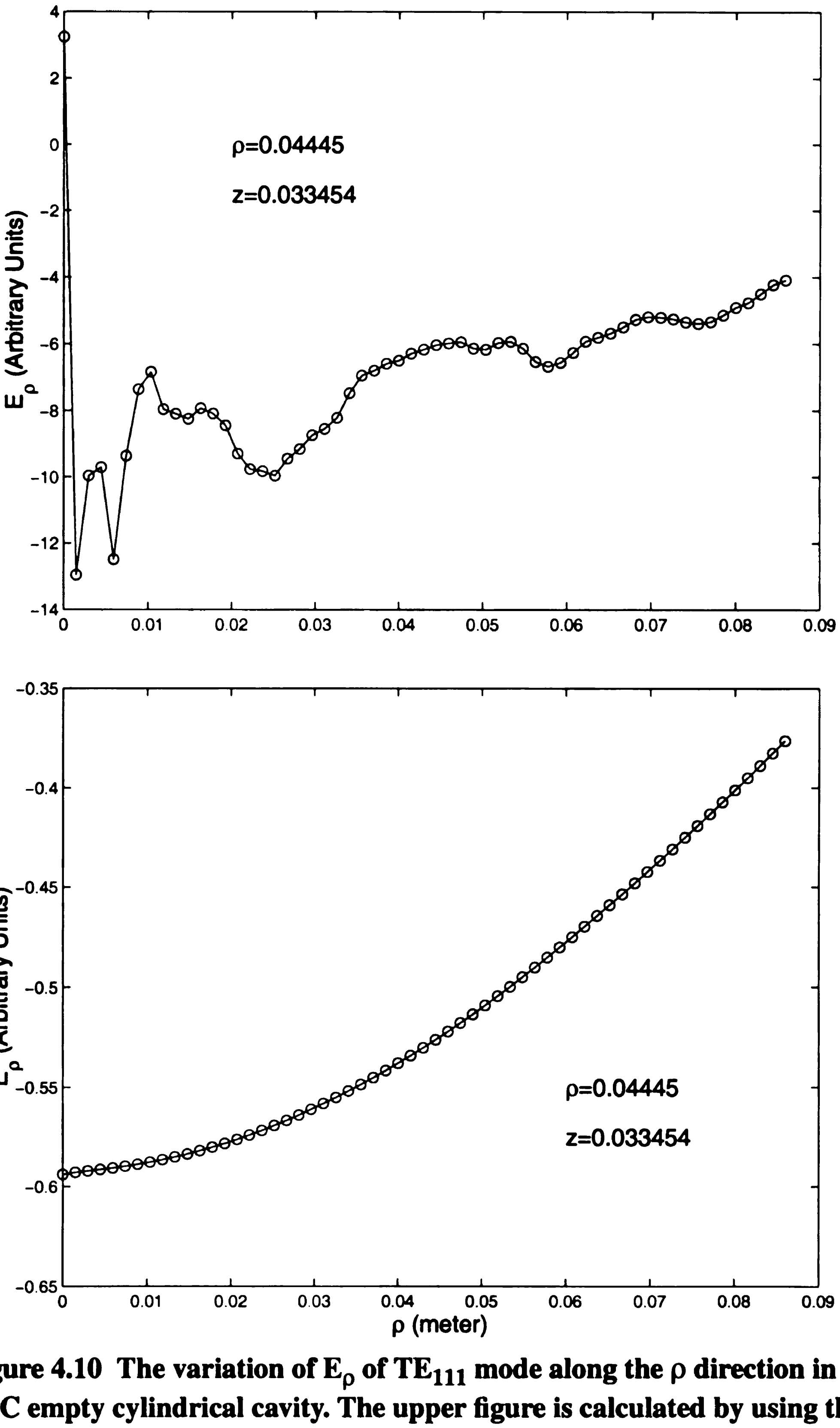

Figure 4.10 The variation of E_ρ of TE_{111} mode along the ρ direction in a PEC empty cylindrical cavity. The upper figure is calculated by using the traditional source implementation and the lower one by using the BH source implementation.

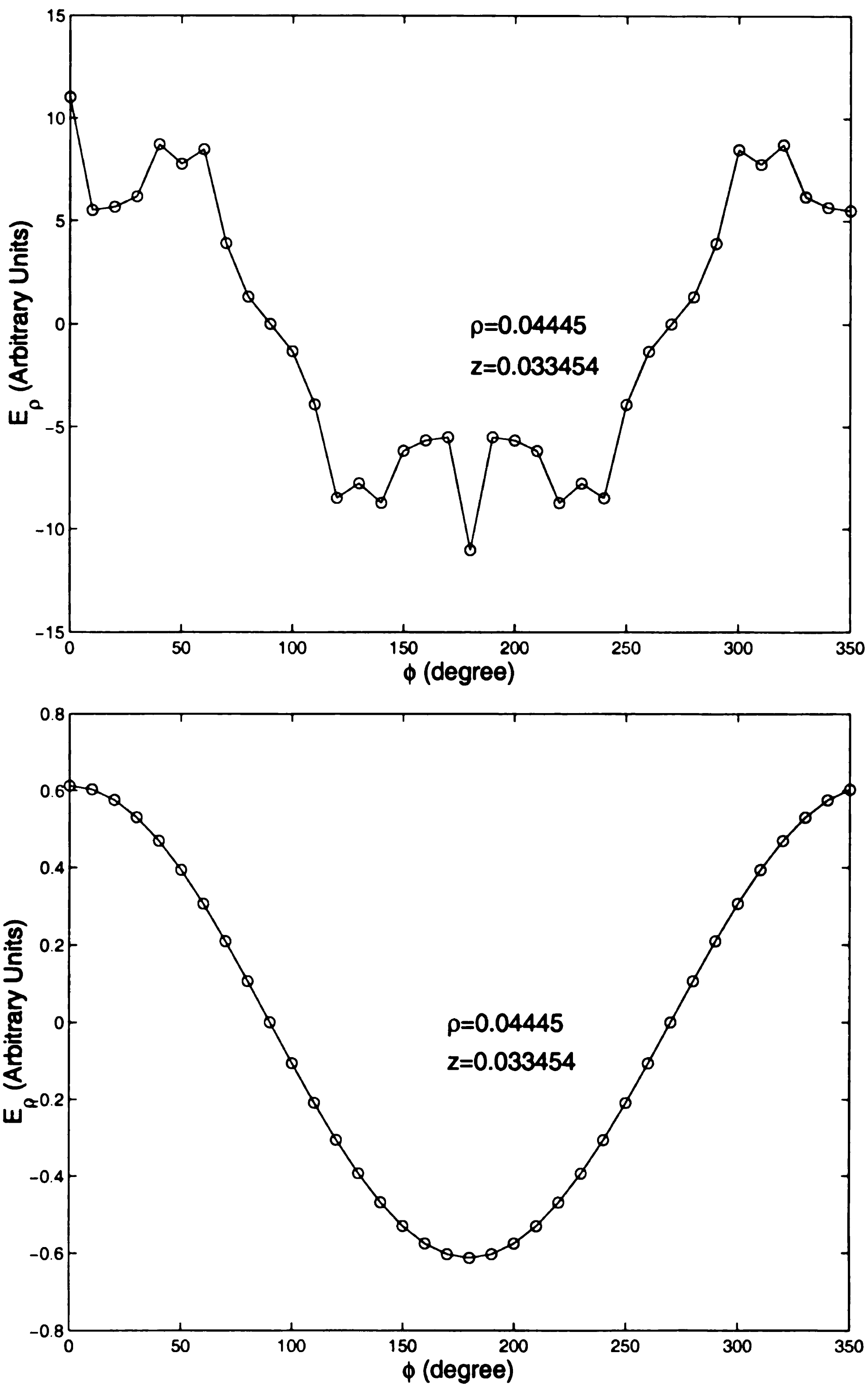

Figure 4.11 The variation of E_ρ of TE_{111} mode along the ϕ direction in a PEC empty cylindrical cavity. The upper figure is calculated by using the traditional source implementation and the lower one by using the BH source implementation.

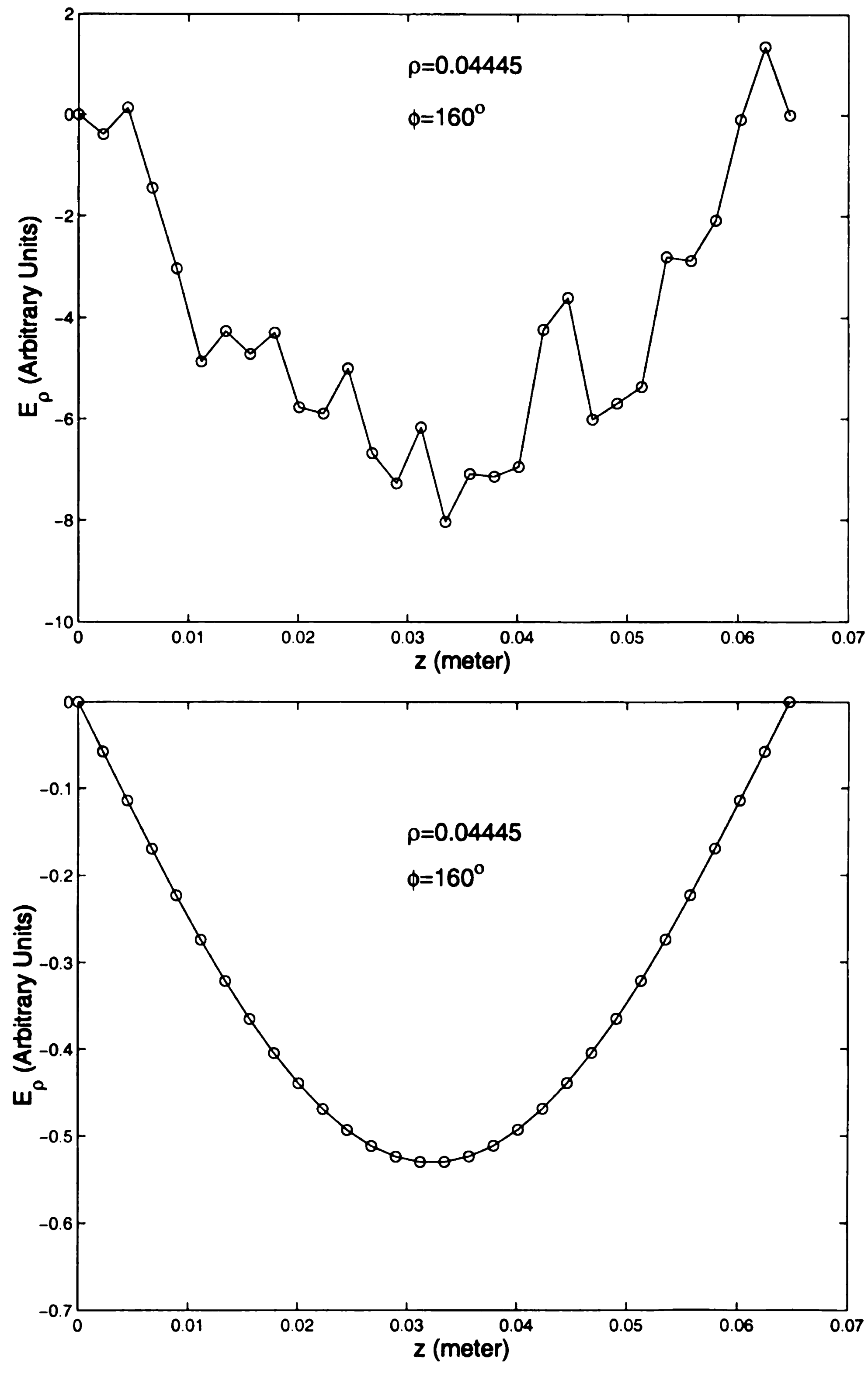

Figure 4.12 The variation of E_ρ of TE_{111} mode along the z direction in a PEC empty cylindrical cavity. The upper figure is calculated by using the traditional source implementation and the lower one by using the BH source implementation.

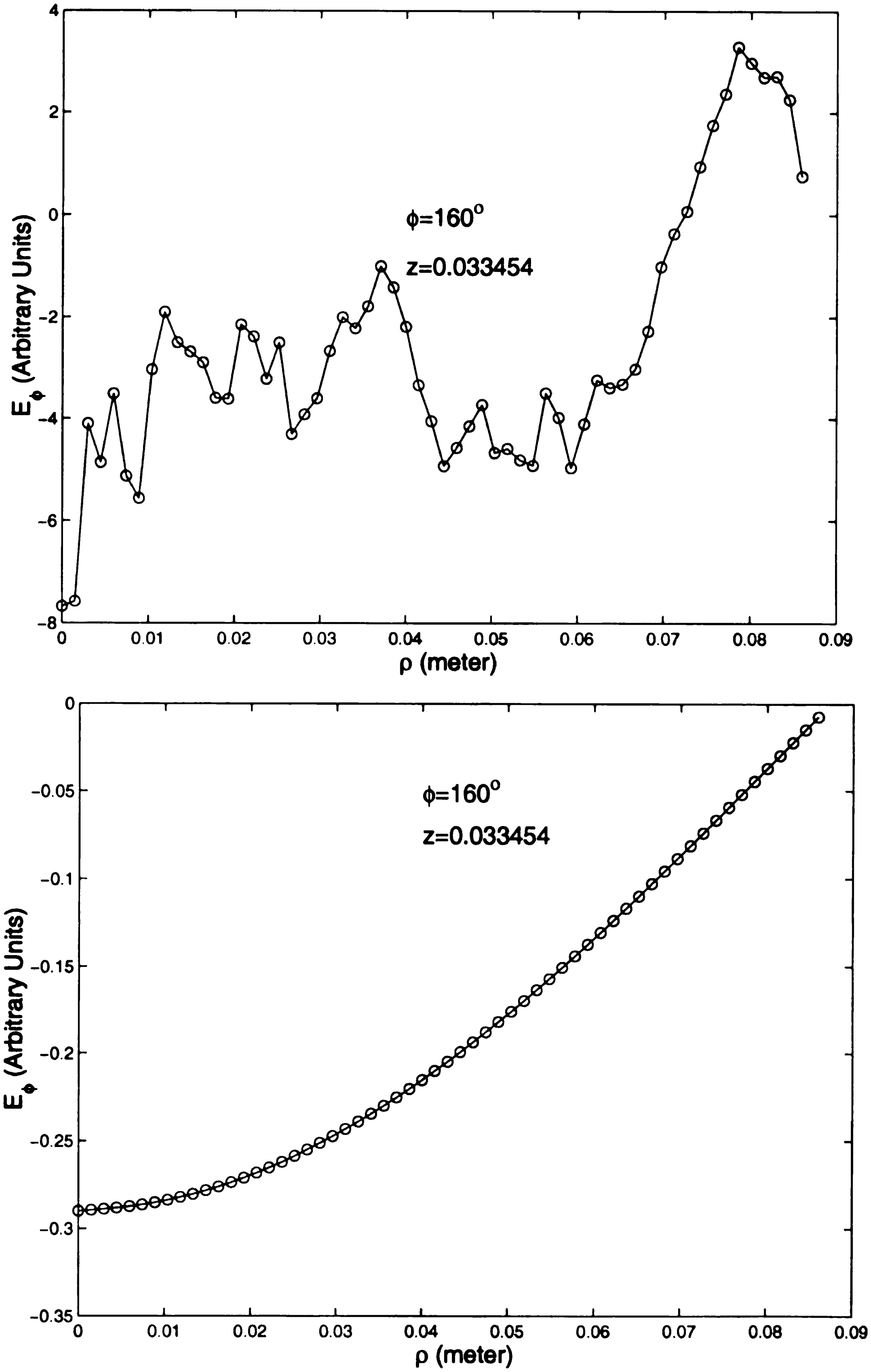

Figure 4.13 The variation of E_ϕ of TE_{111} mode along the ρ direction in a PEC empty cylindrical cavity. The upper figure is calculated by using the traditional source implementation and the lower one by using the BH source implementation.

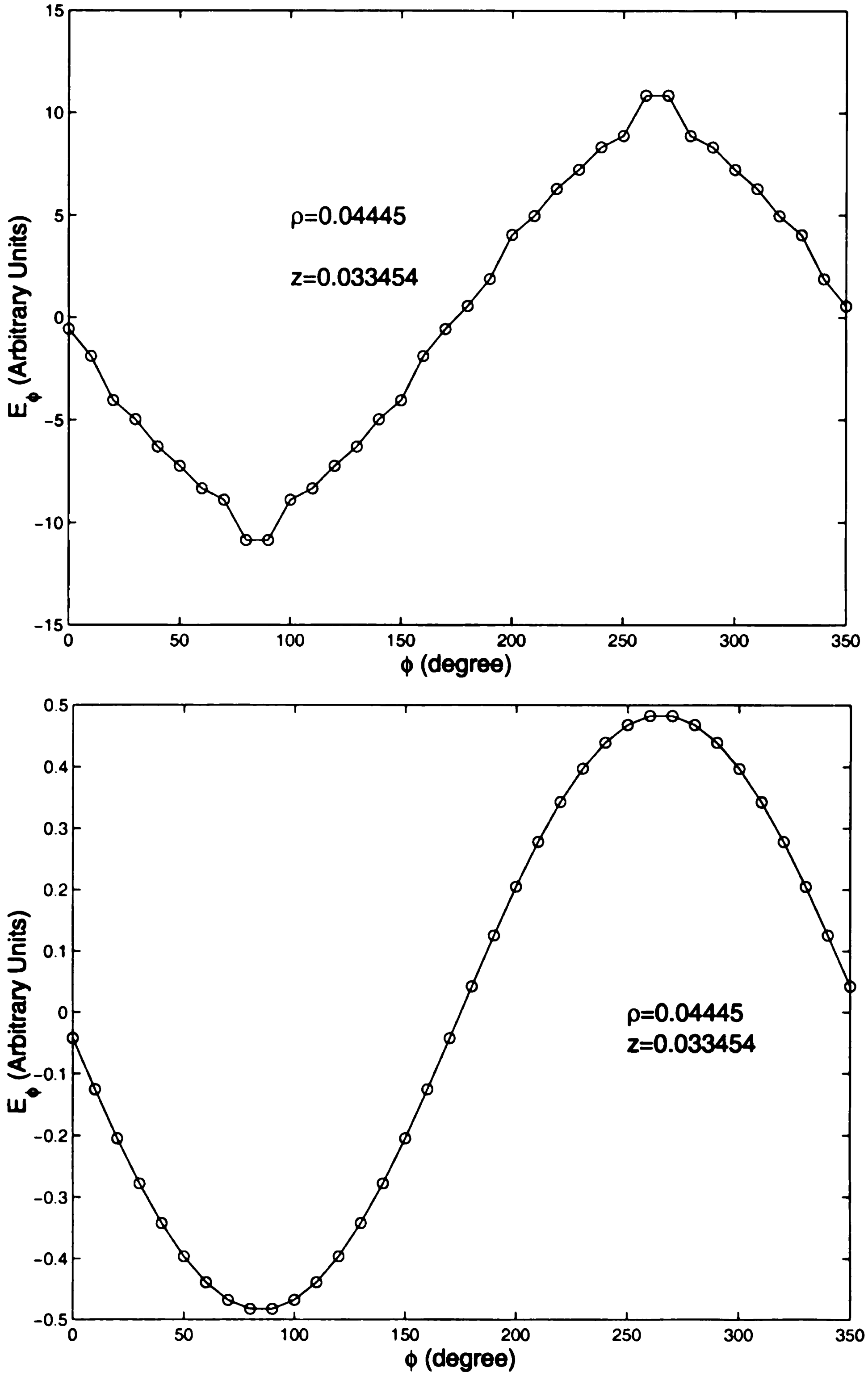

Figure 4.14 The variation of E_ϕ of TE_{111} mode along the ϕ direction in a PEC empty cylindrical cavity. The upper figure is calculated by using the traditional source implementation and the lower one by using the BH source implementation.

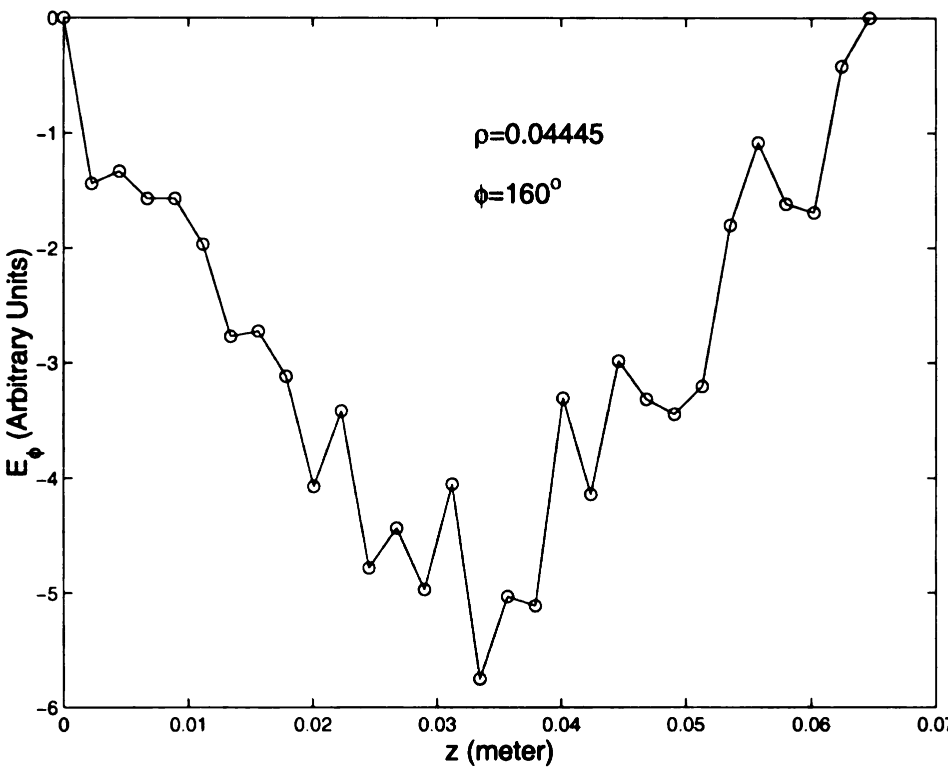

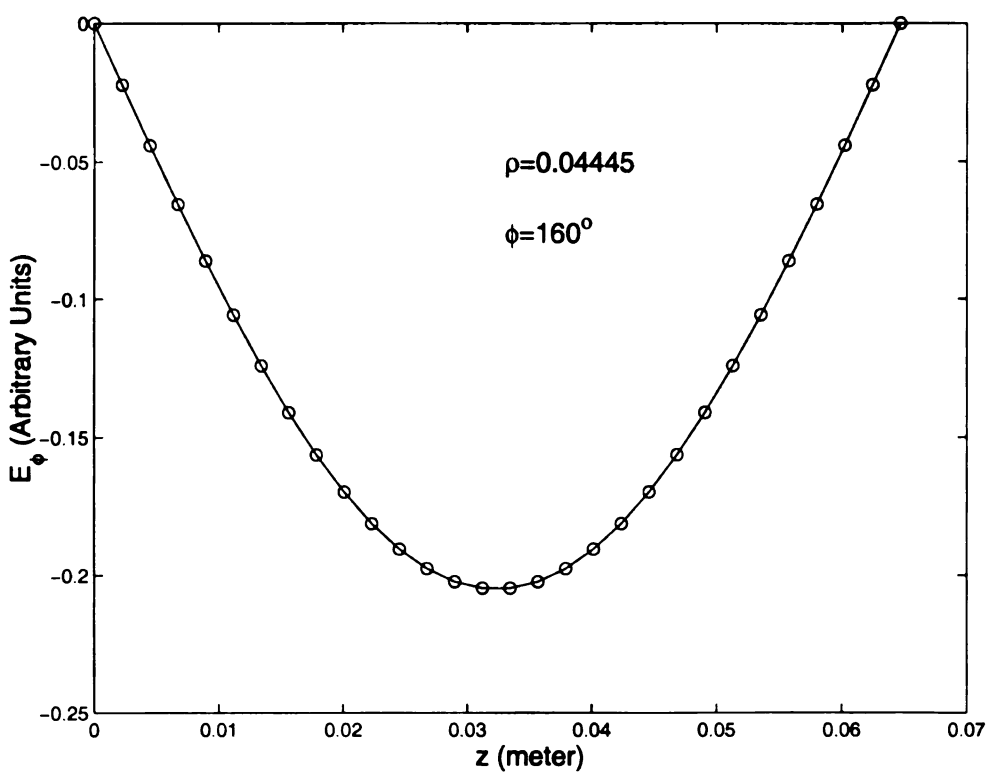

Figure 4.15 The variation of E_ϕ of TE_{111} mode along the z direction in a PEC empty cylindrical cavity. The upper figure is calculated by using the traditional source implementation and the lower one by using the BH source implementation.

lossless cavity calculation whether if the cavity is empty or not.

For a loaded lossless cylindrical cavity, the TM_{012} mode is considered. The dimensions of this empty cavity are *0.0762* meter in radius and *0.15458* meter in height. The numbers of partition along ρ, ϕ, and z are *29*, *36*, *29*, respectively, and one time step is equal to 5×10^{-13}. A small cylindrical material sample with *0.0105* meter in radius, *0.0107* meter in height, and 2.5 in relative permittivity is placed in the center of the cavity. The field distributions of E_ρ and E_z are plotted in Figure 4.16 and Figure 4.17, respectively. These field distributions are similar to those in Figure 3.14 and Figure 3.15. The ratio of E_z/E_z^i of TM_{012} mode along the z direction in the PEC cavity loaded with a small cylindrical material sample is plotted in Figure 4.18. The theoretical estimation for this case is 0.667 and the numerical results is about 0.75. This numerical result can be closer to that in Figure 3.16 if the numbers of partition along axes are increased and the dimensions of the loaded small cylinder is less than tenth of those of the cavity.

Form these numerical results, we can conclude that the BH-FDTD with traditional treatments at $\rho = 0$ gives correct field distributions of a lossless cylindrical cavity. However, the drawback of BH-FDTD is its mode-dependent due to these treatments at $\rho = 0$. By using the Ty(2,4) FDTD method, a general treatment can be obtained and a smaller number of partition along each axis is required for the same accuracy. The Ty(2,4) FDTD scheme is then expected to be the fundamental FDTD algorithm for cylindrical coordinates.

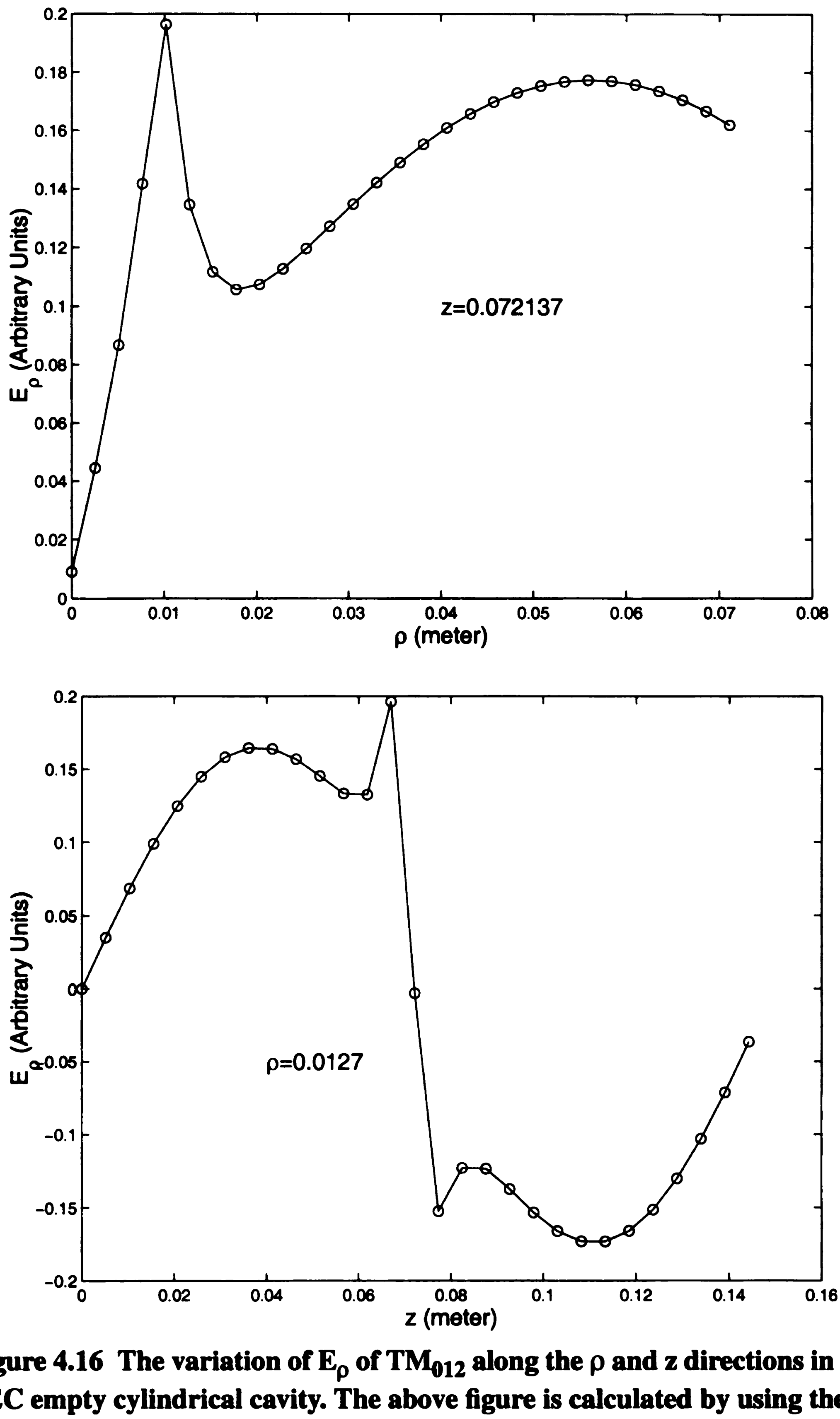

Figure 4.16 The variation of E_ρ of TM_{012} along the ρ and z directions in a PEC empty cylindrical cavity. The above figure is calculated by using the traditional source implementation and the below one by using the BH source implementation.

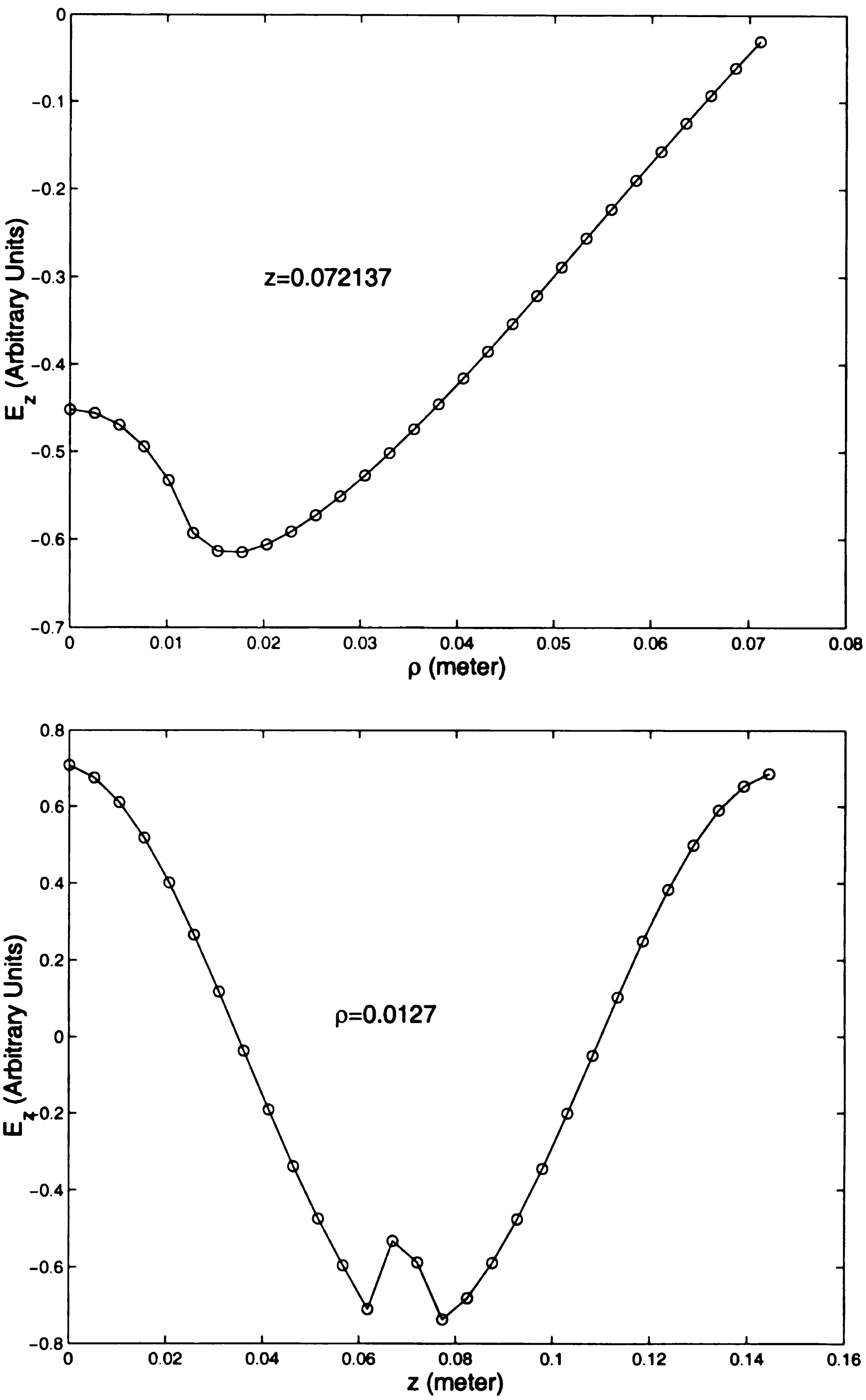

Figure 4.17 The variation of E_z of TM_{012} along the ρ and z directions in a PEC empty cylindrical cavity. The above figure is calculated by using the traditional source implementation and the below one by using the BH source implementation.

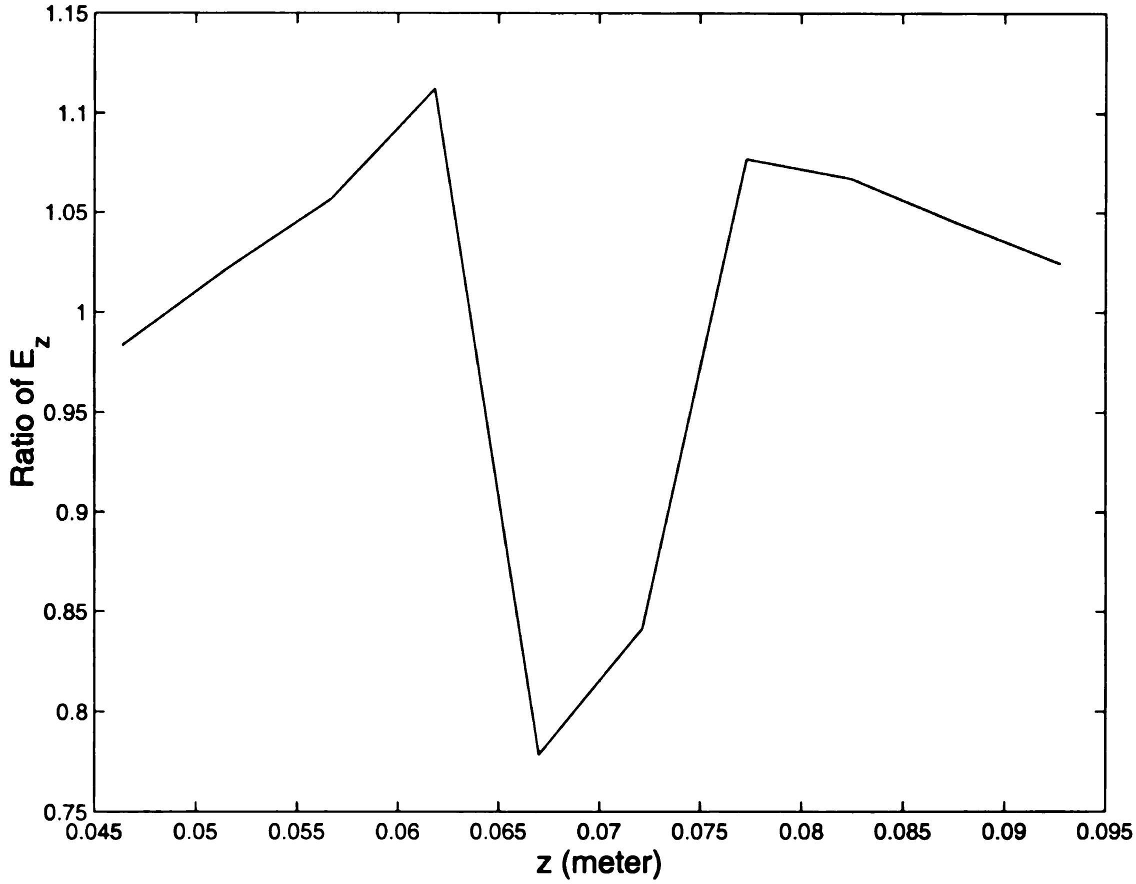

Figure 4.18 Plot of the ratio of E_z/E_z^i of TM_{012} mode along the z direction in the PEC cavity loaded with a small cylindrical material sample.

4.3 Ty(2,4) Cylindrical FDTD Scheme

Applying the implicit staggered fourth-order approximation,(2.57), to spatial derivatives of fields in (4.9) to (4.14), the Ty(2,4) cylindrical FDTD scheme is obtained. A general treatment at $\rho = 0$ for Ty(2,4) cylindrical FDTD method is discussed in section 4.3.4. The matrix equations along ρ, ϕ, and z are obtained in section 4.3.1, section 4.3.2, and section 4.3.3, respectively.

4.3.1 Derivatives of Fields in ρ direction

There are four terms in (4.9) to (4.14) which involve the derivative along ρ direction; $\delta_\rho H_z$, $\delta_\rho(\rho H_\phi)$, $\delta_\rho E_z$, and $\delta_\rho(\rho E_\phi)$.

The derivatives of H fields are considered first. Applying (2.57) to every lattice points in Figure 4.19, the following matrix equation can be obtained

$$AX = M \tag{4.23}$$

where

$$A = \begin{bmatrix} 1 & 22 & 1 & \cdot & 0 & 0 & 0 \\ 0 & 1 & 22 & 1\cdot & & 0 & 0 \\ & \cdot & \cdot & \cdot & & & \\ 0 & \cdot & 1 & 22 & 1 & 0 & 0 \\ 0 & \cdot & 0 & 1 & 22 & 1 & 0 \\ 0 & 0 & & & 1 & 22 & 1 \end{bmatrix}_{(N_\rho - 1)\times(N_\rho + 1)}, \tag{4.24}$$

$$X = \left[\left.\frac{\partial f}{\partial \rho}\right|_{\rho = 0} \left.\frac{\partial f}{\partial \rho}\right|_{\rho = 1} \left.\frac{\partial f}{\partial \rho}\right|_{\rho = 2} \cdot \quad \cdot \cdot \left.\frac{\partial f}{\partial \rho}\right|_{\rho = N_\rho - 1} \left.\frac{\partial f}{\partial \rho}\right|_{\rho = N_\rho} \right]^T, \tag{4.25}$$

and

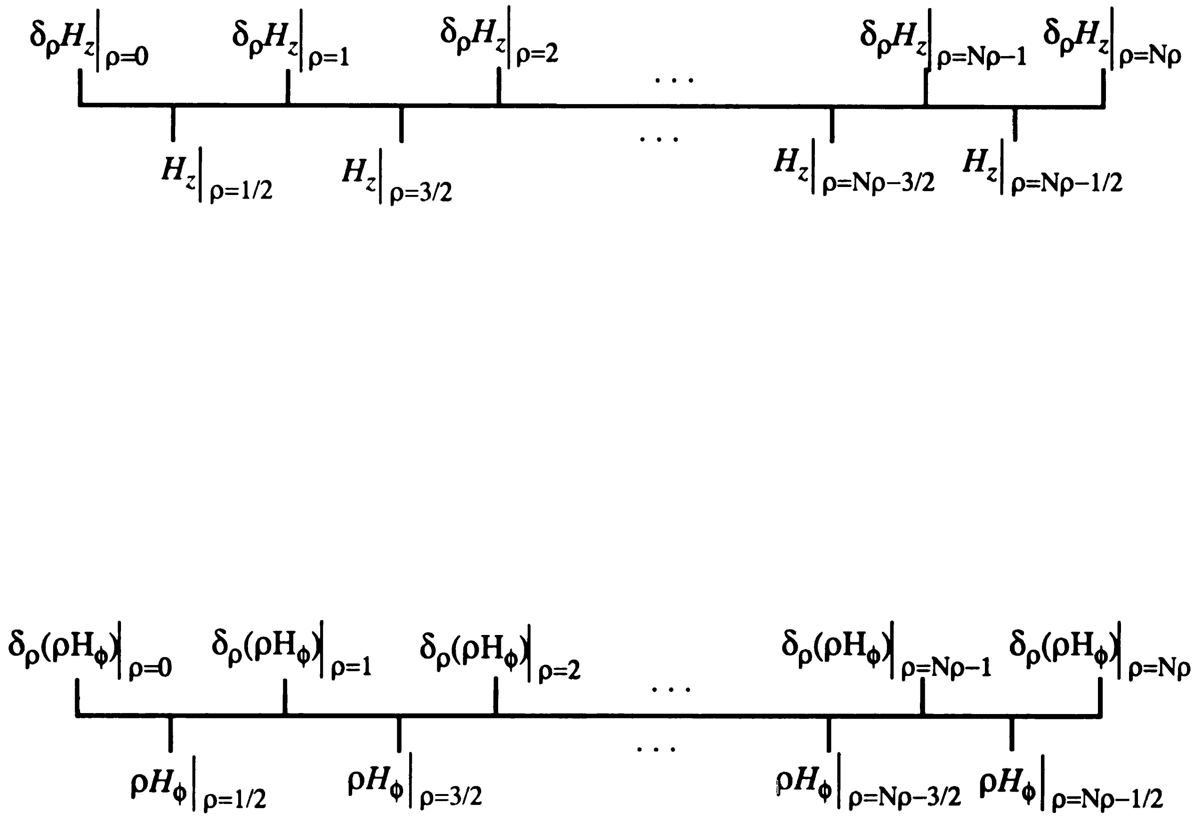

Figure 4.19 The locations of *H* field and its corresponding derivatives in ρ direction.

$$M = \frac{24}{\Delta\rho}\begin{bmatrix} f|_{\rho=3/2} - f|_{\rho=1/2} \\ f|_{\rho=5/2} - f|_{\rho=3/2} \\ \cdot \\ \cdot \\ f|_{\rho=N_\rho-3/2} - f|_{\rho=N_\rho-5/2} \\ f|_{\rho=N_\rho-1/2} - f|_{\rho=N_\rho-3/2} \end{bmatrix} \tag{4.26}$$

where N_ρ is the number of partition along the ρ direction and f is H_z or ρH_ϕ. In order to use LU decomposition, a square matrix is desired. Hence, the derivatives of H fields at $\rho = 0$ in Figure 4.19 needs to be approximated since (4.23) is a underdetermined linear equation. To maintain the fourth-order approximation for the overall FDTD scheme, this approximation at $\rho = 0$ needs to be fourth-order at least. Both fourth-order one-way difference and six-order one-way difference approximations are listed below:

Fourth-Order

$$\left.\frac{\partial f}{\partial\rho}\right|_{\rho=0} = \frac{-93f|_{\rho=\frac{1}{2}} + 229f|_{\rho=\frac{3}{2}} - 225f|_{\rho=\frac{5}{2}} + 111f|_{\rho=\frac{7}{2}} - 22f|_{\rho=\frac{9}{2}}}{24\Delta\rho} \tag{4.27}$$

Six-Order

$$\begin{aligned} \left.\frac{\partial f}{\partial\rho}\right|_{\rho=0} = {} & b_1 f|_{\rho=\frac{1}{2}} + b_2 f|_{\rho=\frac{3}{2}} - b_3 f|_{\rho=\frac{5}{2}} + b_4 f|_{\rho=\frac{7}{2}} \\ & + b_5 f|_{\rho=\frac{9}{2}} + b_6 f|_{\rho=\frac{11}{2}} + b_7 f|_{\rho=\frac{13}{2}} \end{aligned} \tag{4.28}$$

where

$$(b_1, b_2, b_3, b_4, b_5, b_6, b_7)^T = \begin{pmatrix} -5.6020833 \\ 19.024479 \\ -30.882813 \\ 30.369792 \\ -18.026042 \\ 5.9640625 \\ -0.8473983 \end{pmatrix} . \tag{4.29}$$

The results by applying these two different order approximations will be discussed later.

Hence, the new matrix equation is $AX = M$ where X is the same as (4.25),

$$A = \begin{bmatrix} 24 & 0 & 0 & & \cdot\cdot\cdot & & 0 & 0 & 0 \\ 1 & 22 & 1 & & \cdot\cdot\cdot & & 0 & 0 & 0 \\ 0 & 1 & 22 & 1 & \cdot\cdot\cdot & & 0 & 0 & 0 \\ & & & & \cdot\cdot\cdot & & & & \\ 0 & & 0 & & \cdot\cdot\cdot & 1 & 22 & 1 & 0 \\ 0 & & & & \cdot\cdot\cdot & 0 & 1 & 22 & 1 \\ 0 & & & & \cdot\cdot\cdot & 0 & 0 & 0 & 24 \end{bmatrix}_{(N_\rho + 1) \times (N_\rho + 1)} , \tag{4.30}$$

and

$$M = \frac{24}{\Delta\rho} \begin{bmatrix} \Delta\rho \left.\overline{\frac{\partial f}{\partial \rho}}\right|_{\rho = 0} \\ f|_{\rho = 3/2} - f|_{\rho = 1/2} \\ f|_{\rho = 5/2} - f|_{\rho = 3/2} \\ \cdot \\ f|_{\rho = N_\rho - 3/2} - f|_{\rho = N_\rho - 5/2} \\ f|_{\rho = N_\rho - 1/2} - f|_{\rho = N_\rho - 3/2} \\ \Delta\rho \left.\overline{\frac{\partial f}{\partial \rho}}\right|_{\rho = N_\rho} \end{bmatrix} \tag{4.31}$$

where $\left.\overline{\frac{\partial f}{\partial \rho}}\right|_{\rho = 0}$ is the approximation of $\left.\frac{\partial f}{\partial \rho}\right|_{\rho = 0}$. Another expression of (4.23) can be obtained as:

$$A = \begin{bmatrix} 22 & 1 & \cdot & \cdot & \cdot & 0 & 0 \\ 1 & 22 & 1 \cdot & \cdot & \cdot & 0 & 0 \\ & & \cdot & \cdot & \cdot & & \\ & 0 & \cdot & \cdot & \cdot & 1\ 22 & 1 \\ & & \cdot & \cdot & \cdot & 0\ 1 & 22 \end{bmatrix}_{(N_\rho - 1) \times (N_\rho - 1)}, \tag{4.32}$$

$$X = \left[\left.\frac{\partial f}{\partial \rho}\right|_{\rho = 1} \quad \left.\frac{\partial f}{\partial \rho}\right|_{\rho = 2} \quad \cdot \quad \cdot \quad \cdot \left.\frac{\partial f}{\partial \rho}\right|_{\rho = N_\rho - 1} \right]^T, \tag{4.33}$$

and

$$M = \frac{24}{\Delta\rho} \begin{bmatrix} f|_{\rho = 3/2} - f|_{\rho = 1/2} - \left.\dfrac{\Delta\rho}{24} \overline{\dfrac{\partial f}{\partial \rho}}\right|_{\rho = 0} \\ f|_{\rho = 5/2} - f|_{\rho = 3/2} \\ \cdot \\ f|_{\rho = N_\rho - 3/2} - f|_{\rho = N_\rho - 5/2} \\ f|_{\rho = N_\rho - 1/2} - f|_{\rho = N_\rho - 3/2} - \left.\dfrac{\Delta\rho}{24} \overline{\dfrac{\partial f}{\partial \rho}}\right|_{\rho = N_\rho} \end{bmatrix}. \tag{4.34}$$

The condition number of a matrix A measures how *unstable* the linear system $AX = M$ is under the perturbation of the data M. In the FDTD calculation, a small condition number which is close to 1 is desirable. The later matrix equation is used in this chapter since the condition number of matrix A in (4.32) is smaller than that in (4.30) for a same number of partition.

For derivatives of E fields along ρ direction, the $\delta_\rho E_z$ and $\delta_\rho(\rho E_\phi)$ at $\rho = 1/2$ and $\rho = N_\rho - 1/2$ has to be approximated regardless of the physical boundary condition. The locations of the field and its derivative is plotted in Figure 4.20. The matrix equation is the same as (2.73) to (2.76) and is rewritten below:

$$AX = M \tag{4.35}$$

where

$$A = \begin{bmatrix} 26 & -5 & 4 & -1 & \cdot & \cdot & 0 \\ 1 & 22 & 1 & 0 & \cdot & \cdot & 0 \\ 0 & 1 & 22 & 1 & 0 & \cdot & 0 \\ \cdot & \cdot & \cdot & \cdot & \cdot & \cdot & \cdot \\ 0 & \cdot & 0 & 1 & 22 & 1 & 0 \\ 0 & \cdot & 0 & 0 & 1 & 22 & 1 \\ 0 & \cdot & 0 & -1 & 4 & -5 & 26 \end{bmatrix}_{N_\rho \times N_\rho}, \tag{4.36}$$

$$X = \begin{bmatrix} \left.\dfrac{\partial f}{\partial \rho}\right|_{\rho = \frac{1}{2}} & \left.\dfrac{\partial f}{\partial \rho}\right|_{\rho = \frac{3}{2}} & \cdot & \cdot & \cdot & \left.\dfrac{\partial f}{\partial \rho}\right|_{\rho = N_\rho - \frac{3}{2}} & \left.\dfrac{\partial f}{\partial \rho}\right|_{\rho = N_\rho - \frac{1}{2}} \end{bmatrix}^T, \tag{4.37}$$

and

$$M = \frac{24}{\Delta\rho} \begin{bmatrix} f|_{\rho = 1} - f|_{\rho = 0} \\ f|_{\rho = 2} - f|_{\rho = 1} \\ \cdot \\ \cdot \\ f|_{\rho = N_\rho - 1} - f|_{\rho = N_\rho - 2} \\ f|_{\rho = N_\rho} - f|_{\rho = N_\rho - 1} \end{bmatrix}. \tag{4.38}$$

Note that the $\rho E_\phi|_{\rho = 0}$ in Figure 4.20 is equal to zero no matter what E_ϕ is. The approximations used for end points are

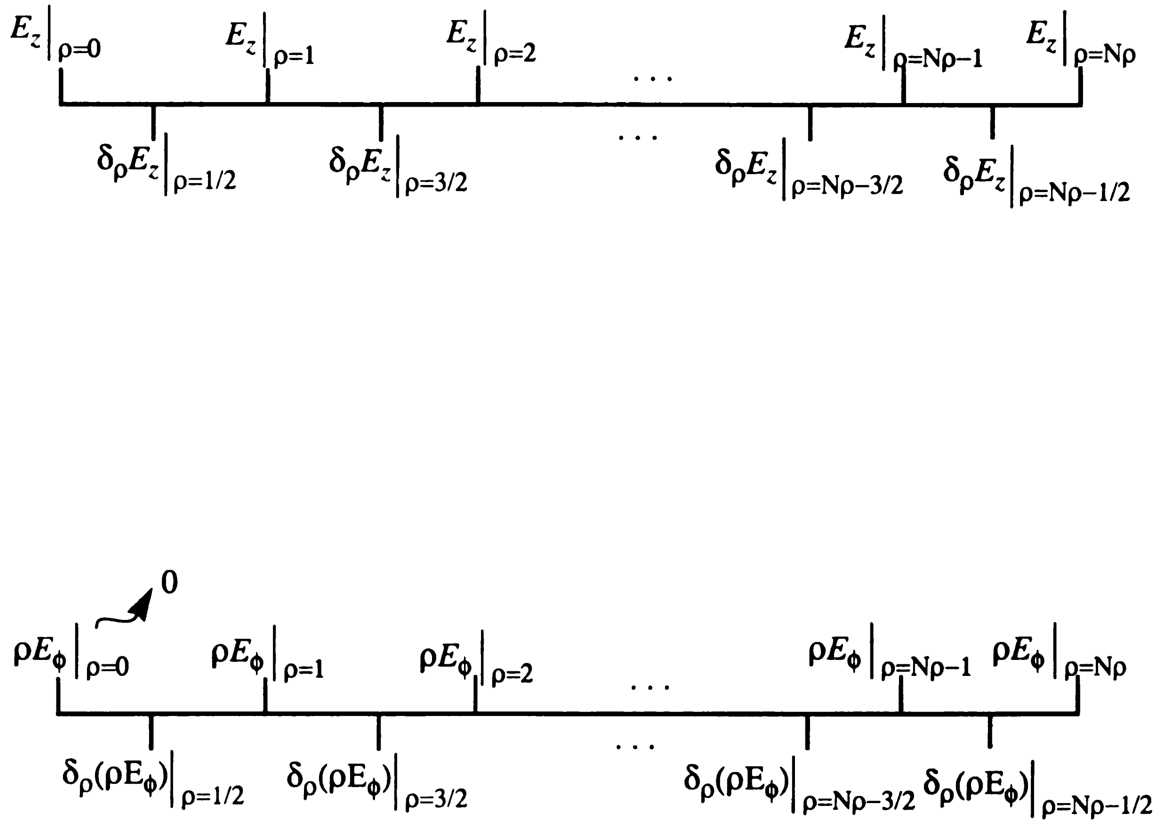

Figure 4.20 The locations of E field and its corresponding derivatives in ρ direction.

$$-\frac{1}{24}\frac{\partial f}{\partial \rho}\bigg|_{\rho=\frac{7}{2}}+\frac{1}{12}\frac{\partial f}{\partial \rho}\bigg|_{\rho=\frac{5}{2}}-\frac{5}{24}\frac{\partial f}{\partial \rho}\bigg|_{\rho=\frac{3}{2}}+\frac{13}{12}\frac{\partial f}{\partial \rho}\bigg|_{\rho=\frac{1}{2}}=\frac{f|_{\rho=1}-f|_{\rho=0}}{\Delta\rho} \tag{4.39}$$

and

$$\begin{aligned}\frac{13}{12}\frac{\partial f}{\partial \rho}\bigg|_{\rho=N_\rho-\frac{1}{2}}-\frac{5}{24}\frac{\partial f}{\partial \rho}\bigg|_{\rho=N_\rho-\frac{3}{2}}+\frac{1}{6}\frac{\partial f}{\partial \rho}\bigg|_{\rho=N_\rho-\frac{5}{2}}-\frac{1}{24}\frac{\partial f}{\partial \rho}\bigg|_{\rho=N_\rho-\frac{7}{2}}.\\ =\frac{f|_{k=N_\rho}-f|_{k=N_\rho-1}}{\Delta\rho}\end{aligned} \tag{4.40}$$

4.3.2 Derivatives of Fields in ϕ direction

For derivatives of fields in ϕ direction, there is no end points or boundary points; hence, (2.57) can be used for all the lattice points along ϕ direction. The $\delta_\phi H_z$ and $\delta_\phi H_\rho$ are considered first. Applying (2.57) to the FDTD lattices in Figure 4.21, the matrix equation for this case is

$$AX = M \tag{4.41}$$

where

$$A = \begin{bmatrix} 22 & 1 & 0 & \cdot & 1 \\ 1 & 22 & 1 & \cdot & 0 \\ \cdot & \cdot & \cdot & \cdot & 0 \\ 0 & \cdot & 1 & 22 & 1 \\ 1 & \cdot & 0 & 1 & 22 \end{bmatrix}_{N_\phi \times N_\phi}, \tag{4.42}$$

$$X = \left[\frac{\partial f}{\partial \phi}\bigg|_{\phi=0}\ \frac{\partial f}{\partial \phi}\bigg|_{\phi=1}\ \cdot\ \cdot\ \cdot\ \frac{\partial f}{\partial \phi}\bigg|_{\phi=N_\phi-2}\ \frac{\partial f}{\partial \phi}\bigg|_{\phi=N_\phi-1}\right]^T, \tag{4.43}$$

and

$$M = \frac{24}{\Delta\phi}\begin{bmatrix} f|_{\phi = 1/2} - f|_{\phi = N_\rho - 1/2} \\ f|_{\phi = 3/2} - f|_{\phi = 1/2} \\ \cdot \\ \cdot \\ f|_{\phi = N_\phi - 3/2} - f|_{\phi = N_\phi - 5/2} \\ f|_{\phi = N_\phi - 1/2} - f|_{\phi = N_\phi - 3/2} \end{bmatrix}. \tag{4.44}$$

For $\delta_\phi E_z$ and $\delta_\phi E_\rho$, the matrix equation is

$$AX = M \tag{4.45}$$

where A is the same as that in (4.42),

$$X = \left[\left.\frac{\partial f}{\partial \phi}\right|_{\phi = \frac{1}{2}} \quad \left.\frac{\partial f}{\partial \phi}\right|_{\phi = \frac{3}{2}} \quad \cdot \quad \cdot \quad \cdot \quad \left.\frac{\partial f}{\partial \phi}\right|_{\phi = N_\phi - \frac{3}{2}} \quad \left.\frac{\partial f}{\partial \phi}\right|_{\phi = N_\phi - \frac{1}{2}}\right]^T \tag{4.46}$$

and

$$M = \frac{24}{\Delta\phi}\begin{bmatrix} f|_{\phi = 1} - f|_{\phi = 0} \\ f|_{\phi = 2} - f|_{\phi = 1} \\ \cdot \\ \cdot \\ f|_{\phi = N_\phi - 1} - f|_{\phi = N_\phi - 2} \\ f|_{\phi = 0} - f|_{\phi = N_\phi - 1} \end{bmatrix}. \tag{4.47}$$

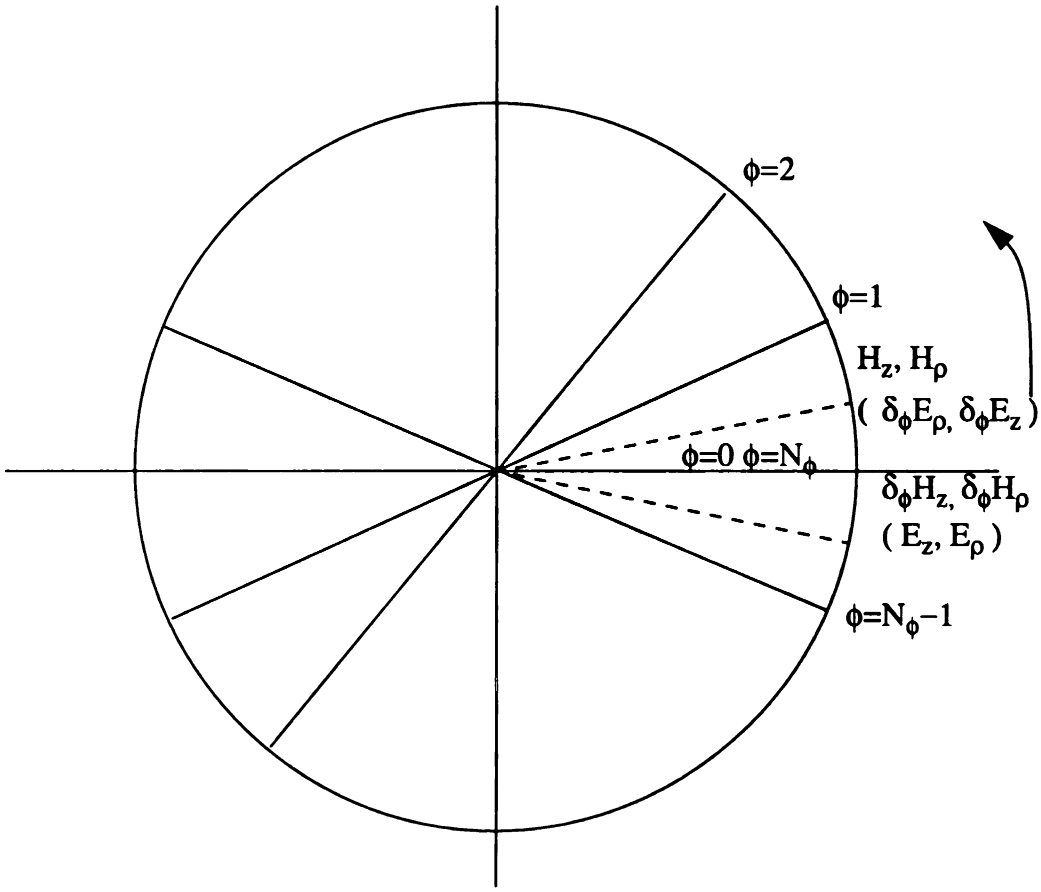

Figure 4.21 The FDTD lattice along the ϕ direction.

4.3.3 Derivatives of Fields in z direction

The calculation of derivatives of fields in the z direction is similar to that in 2.3.4 and 2.3.5. The matrix equation for derivatives of magnetic fields, $\delta_z H_\phi$ and $\delta_z H_\rho$, is

$$AX = M \tag{4.48}$$

where

$$A = \begin{bmatrix} 22 & 1 & 0 & \cdot & 0 \\ 1 & 22 & 1 & \cdot & 0 \\ \cdot & \cdot & \cdot & \cdot & 0 \\ 0 & \cdot & 1 & 22 & 1 \\ 0 & \cdot & 0 & 1 & 22 \end{bmatrix}_{(N_z-1)\times(N_z-1)}, \tag{4.49}$$

$$X = \begin{bmatrix} \left.\frac{\partial f}{\partial z}\right|_{z=1} & \left.\frac{\partial f}{\partial z}\right|_{z=2} & \cdot & \cdot & \cdot \left.\frac{\partial f}{\partial z}\right|_{z=N_z-2} & \left.\frac{\partial f}{\partial z}\right|_{z=N_z-1} \end{bmatrix}^T. \tag{4.50}$$

and

$$M = \frac{24}{\Delta z}\begin{bmatrix} f|_{z=3/2} - f|_{z=1/2} - \left.\frac{\Delta z}{24}\frac{\overline{\partial f}}{\partial z}\right|_{z=0} \\ f|_{z=5/2} - f|_{z=3/2} \\ \cdot \\ \cdot \\ f|_{z=N_z-3/2} - f|_{z=N_z-5/2} \\ f|_{z=N_z-1/2} - f|_{z=N_z-3/2} - \left.\frac{\Delta z}{24}\frac{\overline{\partial f}}{\partial z}\right|_{z=N_z} \end{bmatrix}. \tag{4.51}$$

For PEC boundary, the $\left.\frac{\overline{\partial f}}{\partial z}\right|_{z=0}$ and $\left.\frac{\overline{\partial f}}{\partial z}\right|_{z=N_z}$ are all equal to zero, but these quantities need to be approximated by (4.27) or (4.28), respectively for FEC boundary.

For derivatives of electric fields, $\delta_z E_\phi$ and $\delta_z E_\rho$, the matrix equation is (4.48) with

$$A = \begin{bmatrix} 26 & -5 & 4 & -1 & \cdot & \cdot & 0 \\ 1 & 22 & 1 & 0 & \cdot & \cdot & 0 \\ 0 & 1 & 22 & 1 & 0 & \cdot & 0 \\ \cdot & \cdot & \cdot & \cdot & \cdot & \cdot & \cdot \\ 0 & \cdot & 0 & 1 & 22 & 1 & 0 \\ 0 & \cdot & 0 & 0 & 1 & 22 & 1 \\ 0 & \cdot & 0 & -1 & 4 & -5 & 26 \end{bmatrix}_{N_z \times N_z}, \tag{4.52}$$

$$X = \left[\left.\frac{\partial f}{\partial z}\right|_{z=\frac{1}{2}} \quad \left.\frac{\partial f}{\partial z}\right|_{z=\frac{3}{2}} \quad \cdot \quad \cdot \quad \cdot \quad \left.\frac{\partial f}{\partial z}\right|_{z=N_z-\frac{3}{2}} \quad \left.\frac{\partial f}{\partial z}\right|_{z=N_z-\frac{1}{2}} \right]^T \tag{4.53}$$

and

$$M = \frac{24}{\Delta z} \begin{bmatrix} f|_{z=1} - f|_{z=0} \\ f|_{z=2} - f|_{z=1} \\ \cdot \\ \cdot \\ f|_{z=N_z-1} - f|_{f=N_z-2} \\ f|_{z=N_z} - f|_{z=N_z-1} \end{bmatrix}. \tag{4.54}$$

4.3.4 FDTD Calculations at $\rho = 0$

Due to the singularity at $\rho = 0$, special treatments need to be applied to those finite difference equations which contain divergent terms. At the first glance, the first two terms on the right hand side of (4.11) and the second term on the right hand side of (4.12) become infinite or undefined when ρ approaches to zero. Hence, this two equations can not be used for field calculations at $\rho = 0$. Thus, the FDTD equations from (4.9) to (4.14) at $\rho = 0$ are examined one by one in this section.

Equation (4.9) is still valid for $\rho = 0$ and is used to calculate D_ρ which is located at half-integer space step along the ρ axis. For $\rho = 0$, this equation becomes

$$\delta_t D_\rho\Big|_{\frac{1}{2}, j, k}^{n-\frac{1}{2}} = \frac{1}{\rho_{\frac{1}{2}, j, k}} \delta_\phi H_z\Big|_{\frac{1}{2}, j, k}^{n-\frac{1}{2}} - \delta_z H_\phi\Big|_{\frac{1}{2}, j, k}^{n-\frac{1}{2}} - J_{c\rho}\Big|_{\frac{1}{2}, j, k}^{n-\frac{1}{2}} - J_{s\rho}\Big|_{\frac{1}{2}, j, k}^{n-\frac{1}{2}} . \tag{4.55}$$

Equation (4.10) is valid for $\rho = 0$ if $\delta_z H_\rho$ at $\rho = 0$ is known. Here we cannot only approximate $\delta_t D_\phi$ at $\rho = 0$ and ignore $\delta_z H_\rho$ at $\rho = 0$ since it is required in (4.51). Moreover, H_ρ at $\rho = 0$ is also required in (4.51); hence, H_ρ at $\rho = 0$ needs to be approximated which is discussed later in this section.

Equation (4.12) also has divergent terms so this equation can not be used for $\rho = 0$. B_ρ at $\rho = 0$ is approximated by the following equation

$$-\frac{1}{24}\frac{\partial B_\rho}{\partial \rho}\bigg|_{\rho = \frac{7}{2}} + \frac{1}{12}\frac{\partial B_\rho}{\partial \rho}\bigg|_{\rho = \frac{5}{2}} - \frac{5}{24}\frac{\partial B_\rho}{\partial \rho}\bigg|_{\rho = \frac{3}{2}} + \frac{13}{12}\frac{\partial B_\rho}{\partial \rho}\bigg|_{\rho = \frac{1}{2}} = \frac{B_\rho|_{\rho = 1} - B_\rho|_{\rho = 0}}{\Delta \rho} \tag{4.56}$$

which is a fourth-order approximation. In order to obtain the derivatives of B_ρ with respect to ρ, both $\partial B_\rho / \partial \rho$ at $\rho = 1/2$ and $\rho = N_\rho - 1/2$ need to be approximated by

$$\frac{\partial B_\rho}{\partial \rho}\bigg|_{\rho = \frac{1}{2}} = \frac{-93 B_\rho|_{\rho = 1} + 229 B_\rho|_{\rho = 2} - 225 B_\rho|_{\rho = 3} + 111 B_\rho|_{\rho = 4} - 22 B_\rho|_{\rho = 5}}{24 \Delta \rho} \tag{4.57}$$

and

$$\begin{aligned}\frac{\partial B_\rho}{\partial \rho}\bigg|_{\rho = N_\rho - \frac{1}{2}} = {} & (-93 B_\rho|_{\rho = N_\rho - 1} + 229 B_\rho|_{\rho = N_\rho - 2} - 225 B_\rho|_{\rho = N_\rho - 3} \\ & + 111 B_\rho|_{\rho = N_\rho - 4} - 22 B_\rho|_{\rho = N_\rho - 5}) / (24 \Delta \rho)\end{aligned} , \tag{4.58}$$

respectively. The matrix equation is $AX=M$ where

$$A = \begin{bmatrix} 22 & 1 & 0 & \cdot & 0 \\ 1 & 22 & 1 & \cdot & 0 \\ \cdot & \cdot & \cdot & \cdot & 0 \\ 0 & \cdot & 1 & 22 & 1 \\ 0 & \cdot & 0 & 1 & 22 \end{bmatrix}_{(N_\rho - 2)\times(N_\rho - 2)}, \tag{4.59}$$

$$X = \left[\left.\frac{\partial B_\rho}{\partial \rho}\right|_{\rho = \frac{3}{2}} \quad \left.\frac{\partial B_\rho}{\partial \rho}\right|_{\rho = \frac{5}{2}} \quad \cdot \quad \cdot \quad \cdot \left.\frac{\partial B_\rho}{\partial \rho}\right|_{\rho = N_z - \frac{5}{2}} \quad \left.\frac{\partial B_\rho}{\partial \rho}\right|_{\rho = N_z - \frac{3}{2}} \right]^T, \tag{4.60}$$

and

$$M = \frac{24}{\Delta\rho} \begin{bmatrix} B_\rho|_{\rho=2} - B_\rho|_{\rho=1} - \left.\dfrac{\Delta\rho}{24}\overline{\dfrac{\partial B_\rho}{\partial \rho}}\right|_{\rho = 1/2} \\ B_\rho|_{\rho=3} - B_\rho|_{\rho=2} \\ \cdot \\ B_\rho|_{\rho=N_\rho - 2} - B_\rho|_{\rho=N_\rho - 3} \\ B_\rho|_{\rho=N_\rho - 1} - B_\rho|_{\rho=N_\rho - 2} - \left.\dfrac{\Delta\rho}{24}\overline{\dfrac{\partial B_\rho}{\partial \rho}}\right|_{\rho = N_\rho - 1/2} \end{bmatrix} \tag{4.61}$$

where $\left.\overline{\frac{\partial B_\rho}{\partial \rho}}\right|_{\rho = 1/2}$ and $\left.\overline{\frac{\partial B_\rho}{\partial \rho}}\right|_{\rho = N_\rho - 1/2}$ are the approximations of $\frac{\partial B_\rho}{\partial \rho}$ at $\rho = 1/2$ and $\rho = N_\rho - 1/2$, respectively. The values of B_ρ at $\rho = 1$ to $\rho = N_\rho - 1$ can be calculated by (4.12) first, vector X is solved, and then B_ρ at $\rho = 0$ can be obtained. The value of H_ρ at $\rho = 0$ can be obtained by applying the constitutive relation.

Equation (4.11) definitely cannot be used at $\rho = 0$ due to the divergent and undefined terms on the right hand side. Assume that there is no impressed current but with a conduction current inside region S in Figure 4.1, we can obtain the finite difference equation for D_z at $\rho = 0$ by Ampere's law as

$$\delta_t D_z\Big|_{0,\,j,\,k+\frac{1}{2}}^{n-\frac{1}{2}} + \sigma_z \varepsilon_z \frac{D_z\big|^n + D_z\big|^{n-1}}{2} = \frac{4}{r_1} H_\phi\Big|_{\frac{1}{2},\,j,\,k+\frac{1}{2}}^{n-\frac{1}{2}} \tag{4.62}$$

where r_1 is the distance along ρ for the first cell. A more general approximation can be obtained by similar approximation which is presented in the approximation of H_ρ at $\rho = 0$. Replacing H_ρ by E_z from (4.56) to (4.61), the fourth-order approximation of E_z at $\rho = 0$ can be obtained.

Equation (4.13) is valid for $\rho = 0$ and it becomes

$$\delta_t B_\phi\Big|_{\frac{1}{2},\,j,\,k+\frac{1}{2}}^{n} = \delta_\rho E_z\Big|_{\frac{1}{2},\,j,\,k+\frac{1}{2}}^{n} - \delta_z E_\rho\Big|_{\frac{1}{2},\,j,\,k+\frac{1}{2}}^{n}. \tag{4.63}$$

Equation (4.14) is valid for $\rho = 0$, and it becomes

$$\delta_t B_z\Big|_{\frac{1}{2},\,j+\frac{1}{2},\,k}^{n} = \frac{1}{\rho_{\frac{1}{2},\,j+\frac{1}{2},\,k}} \delta_\phi E_\rho\Big|_{\frac{1}{2},\,j+\frac{1}{2},\,k}^{n} - \frac{1}{\rho_{\frac{1}{2},\,j+\frac{1}{2},\,k}} \delta_\rho(\rho E_\phi)\Big|_{\frac{1}{2},\,j+\frac{1}{2},\,k}^{n} \tag{4.64}$$

where the location of ρ in $\delta_\rho(\rho E_\phi)$ depends on that of E_ϕ.

4.4 Time Domain Finite Difference Equations of Constitutive Relations

The electric permittivity used in this chapter is modeled with the general Debye or Lorentz equations.

The Debye equation is

$$\varepsilon(\omega) = \varepsilon'(\omega) - j\varepsilon''(\omega) = \varepsilon'_{\infty} + \sum_{k=1}^{M} \frac{\varepsilon'_{sk} - \varepsilon'_{\infty}}{1 + j\omega\tau_{ek}}, \tag{4.65}$$

and the general Lorentz equation is

$$\varepsilon(\omega) = \varepsilon'(\omega) - j\varepsilon''(\omega) = \varepsilon'_{\infty} + (\varepsilon'_{s} - \varepsilon'_{\infty}) \sum_{k=1}^{M} \frac{G_k \omega_k^2}{(\omega_k^2 - \omega^2) + j\omega\upsilon_k} \tag{4.66}$$

where ω_k is the k-th resonant frequency, υ_k is the k-th damping frequency, $\varepsilon'_{\infty} = \varepsilon(\infty)$,

$\varepsilon'_0 = \varepsilon(0)$ and $\sum_{k=1}^{M} G_k = 1$.

The scalar constitutive relations modeled with Debye relation between $\vec{E}$ and $\vec{D}$ in time domain can be obtained as:

$$D_\alpha(t) = \varepsilon'_{\alpha\infty} E_\alpha(t) + \sum_{k=1}^{M} P_{\alpha k}(t) \tag{4.67}$$

where

$$P_{\alpha k}(t) + \tau_{\alpha e k} \frac{\partial P_{\alpha k}(t)}{\partial t} = (\varepsilon'_{\alpha s k} - \varepsilon'_{\alpha\infty}) E_\alpha(t) \tag{4.68}$$

and α is one of ρ, ϕ, or z. By the same way, the scalar constitutive relations modeled with Lorent equation in time domain is

$$D_\alpha(t) = \varepsilon'_{\alpha\infty} E_\alpha(t) + (\varepsilon'_{\alpha s} - \varepsilon'_{\alpha\infty}) \sum_{k=1}^{M} P_{\alpha k}(t) \tag{4.69}$$

where

$$\frac{\partial^2 P_{\alpha k}(t)}{\partial t^2} + \upsilon_{\alpha k} \frac{\partial P_{\alpha k}(t)}{\partial t} + \omega_{\alpha k}^2 P_{\alpha k}(t) = G_{\alpha k} \omega_{\alpha k}^2 E_\alpha(t) \tag{4.70}$$

and only the damping case with $\upsilon_{\alpha k}^2 - 4\omega_{\alpha k}^2 < 0$ is considered.

The constitutive relations for Debye material in finite difference form are

$$D_\alpha\Big|^n = \varepsilon'_{\alpha\infty} E_\alpha\Big|^n + \sum_{k=1}^{M} P_{\alpha k}\Big|^n \tag{4.71}$$

and

$$P_{\alpha k}\Big|^n + \tau_{\alpha e k}\delta_t P_{\alpha k}\Big|^n = (\varepsilon'_{\alpha s k} - \varepsilon'_{\alpha\infty}) E_\alpha\Big|^n \tag{4.72}$$

and that for Lorentz material are

$$D_\alpha\Big|^n = \varepsilon'_{\alpha\infty} E_\alpha\Big|^n + (\varepsilon'_{\alpha s} - \varepsilon'_{\alpha\infty}) \sum_{k=1}^{M} P_{\alpha k}\Big|^n \tag{4.73}$$

and

$$\delta_t^2 P_{\alpha k}\Big|^n + \upsilon_{\alpha k}\delta_t P_{\alpha k}\Big|^n + \omega_{\alpha k}^2 P_{\alpha k}\Big|^n = G_{\alpha k}\omega_{\alpha k}^2 E_\alpha\Big|^n . \tag{4.74}$$

If the second-order time stepping is used, then (4.72) and (4.74) can be rewritten as

$$P_{\alpha k}\Big|^n = -\frac{2\Delta t}{\tau_{\alpha e k}} P_{\alpha k}\Big|^{n-1} + P_{\alpha k}\Big|^{n-2} + \frac{2\Delta t}{\tau_{\alpha e k}}(\varepsilon'_{\alpha s k} - \varepsilon'_{\alpha\infty}) E_\alpha\Big|^n \tag{4.75}$$

and

$$\begin{aligned} P_{\alpha k}\Big|^n = {} & (-2\gamma - \gamma\omega_{\alpha k}^2) P_{\alpha k}\Big|^{n-1} + (1 + 5\gamma) P_{\alpha k}\Big|^{n-2} - 4\gamma P_{\alpha k}\Big|^{n-3} + \gamma P_{\alpha k}\Big|^{n-4} \\ & + \gamma G_{\alpha k}\omega_{\alpha k}^2 E_\alpha\Big|^{n-1} \end{aligned} \tag{4.76}$$

where $\gamma = 2/(\upsilon_{\alpha k}\Delta t)$.

CHAPTER 5

CONCLUSIONS

In this dissertation, the finite-difference time-domain(FDTD) method is employed to quantify the induced electromagnetic field in a material sample placed in an energized microwave cavity. Due to the discrete nature of FDTD methods, the stability condition and the numerical dispersion becomes major problems when it is applied to EM problems. Generally, smaller Courant-Friedrichs-Lewy(CFL) values lead to the more stable FDTD scheme. However, smaller CFL values will cause a larger phase error which is not desirable in the FDTD calculation. Hence, the maximum CFL value for a stable FDTD scheme which leads to a minimum phase error and also demands a smallest number of grid cells in one wavelength is desired for FDTD calculation. This optimization can be achieved by the analysis of the numerical dispersion equation for the FDTD scheme which is demonstrated in section 2.2.2.

The traditional second-order FDTD method by Yee in rectangular coordinates is shown to be an efficient solver for closed boundary rectangular cavities if the object within several wavelengths is considered. For electrically large objects or cavities, the larger number of grids and phase error will dramatically slow down the calculation and destroy the numerical accuracy. Either higher-order scheme or other methods need to be introduced to deal with the electrically larger objects. Higher-order FDTD schemes reduce the number of grid if the same phase error for the second-order is required. However, the explicit higher-order FDTD scheme not only increases the stencil with more field points but also complicates the treatment of lattice points near the physical boundary. The implicit higher-order FDTD schemes uses the same number of field points as that in Yee's algorithm. The increased calculation time by the matrix multiplication in implicit higher-order FDTD scheme is compensated by the decrease of the number of grids in one wavelength. The Ty(2,4) method, which employed the second-order approximation in time stepping and the implicit fourth-order in the spatial stepping, is shown to lead to an easy implementation in section 2.3.4 and section 2.3.5. Although the dimensions of rectangular cavities under consideration are close to the wavelength of microwave, the Ty(2,4) is highly applicable to higher frequency EM problems or microwave problems with small size devices.

The quality factor, Q, and the resonant frequency are two important measurement factors of cavities. By using the time-domain Poynting's theorem derived in section 2.4.2, Q value can be obtained from the FDTD calculation and (2.116). The resonant frequency can be obtained by applying the fast Fourier transform (FFT) to field data verse time. For lossless cavities case, the FFT approach may be practical since we can control the time step to turn off the source. For lossy cavities case, the FFT approach may become impractical since the number of time steps to reach the steady state can be very large. On the other hand, both the quality factor and the resonant frequency of a cavity can be obtained by using the Prony method in section 2.5. The numerical results in section 2.8 shows that the prediction of Q and the resonant frequency by Prony method is close to those by time domain Poynting theorem and the FFT.

The singularities introduced by the FDTD method at the center of a cylindrical cavity is a major problem in the application of the FDTD method. For cylindrical cavities loaded with a symmetric material sample, the BOR FDTD method is the most efficient method to perform the FDTD calculation as shown in chapter 3. The treatment of singularities in the BOR FDTD method is also discussed in section 3.1.3. Since the BOR FDTD method is a 2.5D FDTD scheme, the calculation is much faster than that in a 3D case. Hence, the number of partition can be set to a much larger number and more detail around discontinuity can be obtained. A conclusion can be drawn from section 3.2.1 is that the PEC boundary can be assumed in most cavity calculations with the metal wall having a conductivity larger than 10^4.

For general cylindrical cavities loaded with samples of arbitrary shape, the 3D cylindrical FDTD method needs to be employed. The traditional second-order cylindrical 3D FDTD method suffers the problem of the mode-dependent source implementation and the treatment of sigularities. By using the Blackman-Harris(BH) source, it solves the source problem in the traditional second-order 3D FDTD method. In order to obtain a general 3D FDTD method, a fourth-order treatment for sigularities is proposed in section 4.3.4 to replace the mode-dependent treatment in second-order FDTD method. Combining with the implicit staggered fourth-oder FDTD method, this proposed Ty(2,4) FDTD method in cylindrical coordinates solves those problems in the traditional second-order FDTD method. However, the implementation of this Ty(2.4) FDTD method in cylindrical coordinates suffers a numerical instability at this point.

The techniques developed in this study including the Ty(2,4) scheme in rectangular and cylindrical coordinates and the time-domain power analysis may be useful for a wide range of EM problems. Some topics which are relevant for further study in the future are:

(1) Optimization of the numerical dispersion equation.

(2) Power analysis of other material models; e.g., Lorentz material.

(3) Extend the Ty(2,4) FDTD method for magnetic material.

(4) Investigating the implementation of proposed Ty(2,4) FDTD method in cylindrical coordinates and the analysis of the corresponding numerical dispersion equations

(5) Incorporate with thermal equations in the Ty(2,4) forms with a Ty(2,4) FDTD method, and perfect matched layer (PML) for the Ty(2,4) FDTD method.

APPENDIX A

DERIVATION OF FOURTH-ORDER FINITE DIFFERENCE APPROXIMATION

In section 2.3.1, several fourth-order finite difference approximations to spatial derivatives are presented. This appendix details the derivation of those finite difference approximations based on the Taylor's expansion. The explicit scheme have only one unknown in the approximation; on the contrary, the implicit scheme have more than one unknown in the approximation. The locations of the field point and its derivative also play a role in the approximations. The collocated scheme has the field point and its derivative at the same location; on the contrary, the staggered scheme has the field point and its derivative at different locations with a half step spatial difference. Generally, three field points are involved in the second-order approximation and five points, including field points or their derivatives, for the fourth-order approximation.

For explicit collocated scheme, the following Taylor' expansions are used:

$$u_{i+1} = u_i + \Delta x \cdot u_i^{(1)} + \frac{(\Delta x)^2}{2!} \cdot u_i^{(2)} + \frac{(\Delta x)^3}{3!} \cdot u_i^{(3)} + \frac{(\Delta x)^4}{4!} \cdot u_i^{(4)} + \dots \qquad \text{(A.1)}$$

$$u_{i-1} = u_i - \Delta x \cdot u_i^{(1)} + \frac{(\Delta x)^2}{2!} \cdot u_i^{(2)} - \frac{(\Delta x)^3}{3!} \cdot u_i^{(3)} + \frac{(\Delta x)^4}{4!} \cdot u_i^{(4)} + \dots \qquad \text{(A.2)}$$

$$u_{i+2} = u_i + (2\Delta x)\cdot u_i^{(1)} + \frac{(2\Delta x)^2}{2!}\cdot u_i^{(2)} + \frac{(2\Delta x)^3}{3!}\cdot u_i^{(3)} + \frac{(2\Delta x)^4}{4!}\cdot u_i^{(4)} + \dots \tag{A.3}$$

$$u_{i-2} = u_i - (2\Delta x)\cdot u_i^{(1)} + \frac{(2\Delta x)^2}{2!}\cdot u_i^{(2)} - \frac{(2\Delta x)^3}{3!}\cdot u_i^{(3)} + \frac{(2\Delta x)^4}{4!}\cdot u_i^{(4)} + \dots. \tag{A.4}$$

Multiply (A.1) by α, (A.2) by β, (A.3) by γ, (A.4) by δ and sum all these new equations together; then setting the sum of the coefficients for u_i, $u_i^{(2)}$, $u_i^{(3)}$ to be zero and that of $u_i^{(1)}$ to be one. The following equation is obtained,

$$\left\{\begin{array}{c} \alpha+\beta+\gamma+\delta = 0 \\ \alpha-\beta+2\gamma-2\delta = 1 \\ \alpha+\beta+4\gamma+4\delta = 0 \\ \alpha-\beta+8\gamma-8\delta = 0 \end{array}\right. . \tag{A.5}$$

The solution for (A.5) is $\alpha = 8/12$, $\beta = -8/12$, $\gamma = -1/12$, and $\delta = 1/12$. Hence, the explicit collocated approximation is

$$\left(\frac{\partial u}{\partial x}\right)_i \cong \frac{8(u_{i+1}-u_{i-1})-(u_{i+2}-u_{i-2})}{12\Delta x}. \tag{A.6}$$

For the explicit staggered scheme, the following Taylor's expansions are used:

$$u_{i+1/2} = u_i + \frac{\Delta x}{2}\cdot u_i^{(1)} + \frac{(\Delta x/2)^2}{2!}\cdot u_i^{(2)} + \frac{(\Delta x/2)^3}{3!}\cdot u_i^{(3)} + \frac{(\Delta x/2)^4}{4!}\cdot u_i^{(4)} + \dots \tag{A.7}$$

$$u_{i-1/2} = u_i - \frac{\Delta x}{2}\cdot u_i^{(1)} + \frac{(\Delta x/2)^2}{2!}\cdot u_i^{(2)} - \frac{(\Delta x/2)^3}{3!}\cdot u_i^{(3)} + \frac{(\Delta x/2)^4}{4!}\cdot u_i^{(4)} + \dots \tag{A.8}$$

$$u_{i+3/2} = u_i + \frac{3\Delta x}{2}\cdot u_i^{(1)} + \frac{(3\Delta x/2)^2}{2!}\cdot u_i^{(2)} + \frac{(3\Delta x/2)^3}{3!}\cdot u_i^{(3)} + \frac{(3\Delta x/2)^4}{4!}\cdot u_i^{(4)} + . \tag{A.9}$$

$$u_{i-3/2} = u_i - \frac{3\Delta x}{2}\cdot u_i^{(1)} + \frac{(3\Delta x/2)^2}{2!}\cdot u_i^{(2)} - \frac{(3\Delta x/2)^3}{3!}\cdot u_i^{(3)} + \frac{(3\Delta x/2)^4}{4!}\cdot u_i^{(4)} + . \tag{A.10}$$

Use the similar procedures in the derivation of the explicit collocated scheme, the following set of equations is obtained

$$\begin{cases} \alpha + \beta + \gamma + \delta = 0 \\ \frac{1}{2}\alpha - \frac{1}{2}\beta + \frac{3}{2}\gamma - \frac{3}{2}\delta = 1 \\ \frac{1}{4}\alpha + \frac{1}{4}\beta + \frac{9}{4}\gamma + \frac{9}{4}\delta = 0 \\ \frac{1}{8}\alpha - \frac{1}{8}\beta + \frac{27}{8}\gamma - \frac{27}{8}\delta = 0 \end{cases} \qquad \text{(A.11)}$$

The solution for (A.11) is $\alpha = 27/24$, $\beta = -27/24$, $\gamma = -1/24$, and $\delta = 1/24$ and the explicit staggered scheme is

$$\left(\frac{\partial u}{\partial x}\right)_i \cong \frac{27(u_{i+1/2} - u_{i-1/2}) - (u_{i+3/2} - u_{i-3/2})}{24\Delta x} \qquad \text{(A.12)}$$

For the implicit collocated scheme, the following Taylor's expansions are used:

$$u_{i+1} = u_i + \Delta x \cdot u_i^{(1)} + \frac{(\Delta x)^2}{2!} \cdot u_i^{(2)} + \frac{(\Delta x)^3}{3!} \cdot u_i^{(3)} + \frac{(\Delta x)^4}{4!} \cdot u_i^{(4)} + \dots \qquad \text{(A.13)}$$

$$u_{i-1} = u_i - \Delta x \cdot u_i^{(1)} + \frac{(\Delta x)^2}{2!} \cdot u_i^{(2)} - \frac{(\Delta x)^3}{3!} \cdot u_i^{(3)} + \frac{(\Delta x)^4}{4!} \cdot u_i^{(4)} + \dots \qquad \text{(A.14)}$$

$$u_{i+1}^{(1)} = u_i^{(1)} + \Delta x \cdot u_i^{(2)} + \frac{(\Delta x)^2}{2!} \cdot u_i^{(3)} + \frac{(\Delta x)^3}{3!} \cdot u_i^{(4)} + \frac{(\Delta x)^4}{4!} \cdot u_i^{(5)} + \dots \qquad \text{(A.15)}$$

$$u_{i-1}^{(1)} = u_i^{(1)} - \Delta x \cdot u_i^{(2)} + \frac{(\Delta x)^2}{2!} \cdot u_i^{(3)} - \frac{(\Delta x)^3}{3!} \cdot u_i^{(4)} + \frac{(\Delta x)^4}{4!} \cdot u_i^{(5)} + \dots. \qquad \text{(A.16)}$$

The corresponding equations for α, β, γ, and δ are

$$
\begin{cases}
\alpha+\beta = 0 \\
(\alpha-\beta)\Delta x+\gamma+\delta = 1 \\
\left(\frac{1}{4}\alpha+\frac{1}{4}\beta\right)\Delta x+(\gamma-\delta) = 0 \\
\left(\frac{1}{6}\alpha-\frac{1}{6}\beta\right)\Delta x+\left(\frac{1}{2}\gamma+\frac{1}{2}\delta\right) = 0
\end{cases}
\tag{A.17}
$$

and the solution is $\alpha = 3/(4\Delta x)$, $\beta = -3/(4\Delta x)$, $\gamma = -1/4$, and $\delta = -1/4$. Hence, the implicit collocated scheme is

$$
\frac{\left(\frac{\partial u}{\partial x}\right)_{i+1}+\left(\frac{\partial u}{\partial x}\right)_{i-1}}{6}+\frac{2}{3}\left(\frac{\partial u}{\partial x}\right)_i \cong \frac{u_{i+1}-u_{i-1}}{2\Delta x}.
\tag{A.18}
$$

For the implicit staggered scheme, the following Taylor's expansions are used:

$$
u_{i+1/2} = u_i+\frac{\Delta x}{2}\cdot u_i^{(1)}+\frac{(\Delta x/2)^2}{2!}\cdot u_i^{(2)}+\frac{(\Delta x/2)^3}{3!}\cdot u_i^{(3)}+\frac{(\Delta x/2)^4}{4!}\cdot u_i^{(4)}+\ldots
\tag{A.19}
$$

$$
u_{i-1/2} = u_i-\frac{\Delta x}{2}\cdot u_i^{(1)}+\frac{(\Delta x/2)^2}{2!}\cdot u_i^{(2)}-\frac{(\Delta x/2)^3}{3!}\cdot u_i^{(3)}+\frac{(\Delta x/2)^4}{4!}\cdot u_i^{(4)}+\ldots
\tag{A.20}
$$

$$
u_{i+1}^{(1)} = u_i^{(1)}+\Delta x\cdot u_i^{(2)}+\frac{(\Delta x)^2}{2!}\cdot u_i^{(3)}+\frac{(\Delta x)^3}{3!}\cdot u_i^{(4)}+\frac{(\Delta x)^4}{4!}\cdot u_i^{(5)}+\ldots
\tag{A.21}
$$

$$
u_{i-1}^{(1)} = u_i^{(1)}-\Delta x\cdot u_i^{(2)}+\frac{(\Delta x)^2}{2!}\cdot u_i^{(3)}-\frac{(\Delta x)^3}{3!}\cdot u_i^{(4)}+\frac{(\Delta x)^4}{4!}\cdot u_i^{(5)}+\ldots.
\tag{A.22}
$$

The corresponding equations for α, β, γ, and δ are

$$\begin{cases} \alpha+\beta = 0 \\ \left(\frac{1}{2}\alpha-\frac{1}{2}\beta\right)\Delta x+\gamma+\delta = 1 \\ \left(\frac{1}{8}\alpha+\frac{1}{8}\beta\right)\Delta x+(\gamma-\delta) = 0 \\ \left(\frac{1}{48}\alpha-\frac{1}{48}\beta\right)\Delta x+\left(\frac{1}{2}\gamma+\frac{1}{2}\delta\right) = 0 \end{cases} \tag{A.23}$$

and the solution is $\alpha = 12/(11\Delta x)$, $\beta = -12/(11\Delta x)$, $\gamma = -1/22$, and $\delta = -1/22$. Hence, the implicit staggered scheme is

$$\frac{\left(\frac{\partial u}{\partial x}\right)_{i+1}+\left(\frac{\partial u}{\partial x}\right)_{i-1}}{24}+\frac{11}{12}\left(\frac{\partial u}{\partial x}\right)_i \cong \frac{u_{i+1/2}-u_{i-1/2}}{\Delta x}. \tag{A.24}$$

The fourth-order approximation at the points half-integer grid away from the boundary in (2.71) and (2.72) can be obtained by assuming

$$\delta\left(\frac{\partial u}{\partial x}\right)_{7/2}+\gamma\left(\frac{\partial u}{\partial x}\right)_{5/2}+\beta\left(\frac{\partial u}{\partial x}\right)_{3/2}+\alpha\left(\frac{\partial u}{\partial x}\right)_{1/2} \cong \frac{u_1-u_0}{\Delta x}. \tag{A.25}$$

Using the following Tayor's expansions:

$$u_{1/2} = u_0+\frac{\Delta x}{2}\cdot u_0^{(1)}+\frac{(\Delta x/2)^2}{2!}\cdot u_0^{(2)}+\frac{(\Delta x/2)^3}{3!}\cdot u_0^{(3)}+\frac{(\Delta x/2)^4}{4!}\cdot u_0^{(4)}+\dots \tag{A.26}$$

$$u_1^{(1)} = u_0^{(1)}+\Delta x\cdot u_1^{(2)}+\frac{(\Delta x)^2}{2!}\cdot u_1^{(3)}+\frac{(\Delta x)^3}{3!}\cdot u_1^{(4)}+\frac{(\Delta x)^4}{4!}\cdot u_1^{(5)}+\dots \tag{A.27}$$

$$u_{3/2} = u_0+\frac{3\Delta x}{2}\cdot u_0^{(1)}+\frac{(3\Delta x/2)^2}{2!}\cdot u_0^{(2)}+\frac{(3\Delta x/2)^3}{3!}\cdot u_0^{(3)}+\frac{(3\Delta x/2)^4}{4!}\cdot u_0^{(4)}+\dots \tag{A.28}$$

$$u_{5/2} = u_0+\frac{5\Delta x}{2}\cdot u_0^{(1)}+\frac{(5\Delta x/2)^2}{2!}\cdot u_0^{(2)}+\frac{(5\Delta x/2)^3}{3!}\cdot u_0^{(3)}+\frac{(5\Delta x/2)^4}{4!}\cdot u_0^{(4)}+\dots \tag{A.29}$$

and

$$u_{7/2} = u_0 + \frac{7\Delta x}{2} \cdot u_0^{(1)} + \frac{(7\Delta x/2)^2}{2!} \cdot u_0^{(2)} + \frac{(7\Delta x/2)^3}{3!} \cdot u_0^{(3)} + \frac{(7\Delta x/2)^4}{4!} \cdot u_0^{(4)} + \dots \quad \text{(A.30)}$$

the solution is $\alpha = 13/12$, $\beta = -5/24$, $\gamma = 1/12$, and $\delta = -1/24$.

The one-way fourth-order finite difference approximations in (2.81) and (2.82) can be obtained by assuming

$$\left(\frac{\partial u}{\partial x}\right)_0 = \frac{\alpha u_{1/2} + \beta u_{3/2} + \gamma u_{5/2} + \delta u_{7/2} + \eta u_{9/2}}{\Delta x} \quad \text{(A.31)}$$

with (A.26), (A.28), (A.29), (A.30) and

$$u_{9/2} = u_0 + \frac{9\Delta x}{2} \cdot u_0^{(1)} + \frac{(9\Delta x/2)^2}{2!} \cdot u_0^{(2)} + \frac{(9\Delta x/2)^3}{3!} \cdot u_0^{(3)} + \frac{(9\Delta x/2)^4}{4!} \cdot u_0^{(4)} + \dots \quad \text{(A.32)}$$

The solution is $\alpha = -31/8$, $\beta = 229/24$, $\gamma = -75/8$, $\delta = 37/8$, and $\eta = -11/12$.

APPENDIX B

DERIVATION OF NUMERICAL DISPERSION RELATION FOR IMPLICIT STAGGERED SCHEME

In (2.70), the numerical dispersion relation of the implicit staggered FDTD scheme is presented. The derivation of this equation provides fundamental derivation of those matrix equations in Ty(2,4) FDTD scheme. In this appendix, the derivation of (2.70) is detailed.

Consider Maxwell's equations in a normalized region of free space with $\mu = 1$, $\varepsilon = 1$, $\sigma = 1$, and $c = 1$ and obtain

$$j\nabla\times\vec{V} = \frac{\partial\vec{V}}{\partial t} \tag{B.1}$$

where $\vec{V} = \vec{H} + j\vec{E}$ and

$$\nabla\times\vec{V} = \hat{x}\left(\frac{\partial V_z}{\partial y} - \frac{\partial V_y}{\partial z}\right) + \hat{y}\left(\frac{\partial V_x}{\partial z} - \frac{\partial V_z}{\partial x}\right) + \hat{z}\left(\frac{\partial V_y}{\partial x} - \frac{\partial V_x}{\partial y}\right). \tag{B.2}$$

Let

$$\vec{V}\Big|_{I,J,K}^{n} = \vec{V}_0 e^{j(\kappa_x I\Delta x + \kappa_y J\Delta y + \kappa_z K\Delta z + \omega n\Delta t)} \tag{B.3}$$

where κ_x, κ_y, and κ_z are the wave numbers along x, y, and z axes, respectively in the computational space.

Consider the x component of (B.1) at point (I, J, K) which is

$$j\left(\frac{\partial V_z}{\partial y} - \frac{\partial V_y}{\partial z}\right)\bigg|_{I,J,K} = \frac{\partial V_x}{\partial t}\bigg|_{I,J,K}. \tag{B.4}$$

The second-order finite difference approximation of the time derivative of V_x is

$$\frac{\partial V_x}{\partial t}\bigg|_{I,J,K} = \frac{V|_{I,J,K}^{n+1/2} - V|_{I,J,K}^{n-1/2}}{\Delta t} = -2j\frac{\sin(\omega\Delta t/2)}{\Delta t}V_x|_{I,J,K}. \tag{B.5}$$

The time derivatives of V_y and V_z can be obtained by replacing index x with y and z. For $\partial V_z/\partial y$ component, V_z is assumed to be located at the half integer position in space and $\partial V_z/\partial y$ is located at the integer position in space. The one-way fourth-order approximation for numerical boundary used is assumed to be

$$\frac{\partial V_z}{\partial y}\bigg|_{j=0} = \bar{a}V_z\Big|_{j=\frac{1}{2}} + bV_z\Big|_{j=\frac{3}{2}} + cV_z\Big|_{j=\frac{5}{2}} + dV_z\Big|_{j=\frac{7}{2}} + eV_z\Big|_{j=\frac{9}{2}}. \tag{B.6}$$

for $j = 0$. The numerical approximation for $j = N_y$ can be obtained by similarity and is listed below:

$$\begin{aligned}\frac{\partial V_z}{\partial y}\bigg|_{j=N_y} &= \bar{a}V_z\Big|_{j=N_y-\frac{1}{2}} + bV_z\Big|_{j=N_y-\frac{3}{2}} + cV_z\Big|_{j=N_y-\frac{5}{2}} + dV_z\Big|_{j=N_y-\frac{7}{2}}\\ &\quad + eV_z\Big|_{j=N_y-\frac{9}{2}}\end{aligned}. \tag{B.7}$$

Apply the implicit staggered four-order finite difference approximation, (2.57), to every lattice point along y axis, a set of equations is obtained as follow:

$$\frac{1}{24}\frac{\partial V_z}{\partial y}\bigg|_{j=0} + \frac{11}{12}\frac{\partial V_z}{\partial y}\bigg|_{j=1} + \frac{1}{24}\frac{\partial V_z}{\partial y}\bigg|_{j=2} \cong \frac{V_z|_{j=3/2} - V_z|_{j=1/2}}{\Delta y}$$

$$\frac{1}{24}\frac{\partial V_z}{\partial y}\bigg|_{j=1} + \frac{11}{12}\frac{\partial V_z}{\partial y}\bigg|_{j=2} + \frac{1}{24}\frac{\partial V_z}{\partial y}\bigg|_{j=3} \cong \frac{V_z|_{j=5/2} - V_z|_{j=3/2}}{\Delta y}$$

$$\vdots \qquad .(B.8)$$

$$\frac{1}{24}\frac{\partial V_z}{\partial y}\bigg|_{j=N_y-3} + \frac{11}{12}\frac{\partial V_z}{\partial y}\bigg|_{j=N_y-2} + \frac{1}{24}\frac{\partial V_z}{\partial y}\bigg|_{j=N_y-1} \cong \frac{V_z|_{j=N_y-3/2} - V_z|_{j=N_y-5/2}}{\Delta y}$$

$$\frac{1}{24}\frac{\partial V_z}{\partial y}\bigg|_{j=N_y-2} + \frac{11}{12}\frac{\partial V_z}{\partial y}\bigg|_{j=N_y-1} + \frac{1}{24}\frac{\partial V_z}{\partial y}\bigg|_{j=N_y} \cong \frac{V_z|_{j=N_y-1/2} - V_z|_{j=N_y-3/2}}{\Delta y}$$

Combining with the numeric boundary condition in (B.6), the above equation can be rewritten in a matrix form of

$$AX = B \qquad (B.9)$$

where

$$A = \begin{bmatrix} 1 & 0 & 0 & \cdot & 0 \\ \frac{1}{24} & \frac{22}{24} & \frac{1}{24} & \cdot & 0 \\ \cdot & \cdot & \cdot & \cdot & 0 \\ 0 & \cdot & \frac{1}{24} & \frac{22}{24} & \frac{1}{24} \\ 0 & \cdot & 0 & 0 & 1 \end{bmatrix}_{(N_y+1)\times(N_y+1)}, \qquad (B.10)$$

$$X = \left[\frac{\partial V_z}{\partial y}\bigg|_{j=0} \quad \frac{\partial V_z}{\partial y}\bigg|_{j=1} \quad \cdot \quad \cdot \quad \cdot \frac{\partial V_z}{\partial y}\bigg|_{j=N_y-2} \quad \frac{\partial V_z}{\partial y}\bigg|_{j=N_y-1} \quad \frac{\partial V_z}{\partial y}\bigg|_{j=N_y}\right]^T, \qquad (B.11)$$

$$B = \begin{bmatrix} \bar{a}V_z\big|_{j=\frac{1}{2}} + bV_z\big|_{j=\frac{3}{2}} + cV_z\big|_{j=\frac{5}{2}} + dV_z\big|_{j=\frac{7}{2}} + eV_z\big|_{j=\frac{9}{2}} \\ \dfrac{V_z\big|_{j=3/2} - V_z\big|_{j=1/2}}{\Delta y} \\ \dfrac{V_z\big|_{j=5/2} - V_z\big|_{j=3/2}}{\Delta y} \\ \cdot \\ \cdot \\ \cdot \\ \dfrac{V_z\big|_{j=N_y-3/2} - V_z\big|_{j=N_y-5/2}}{\Delta y} \\ \dfrac{V_z\big|_{j=N_y-1/2} - V_z\big|_{j=N_y-3/2}}{\Delta y} \\ \bar{a}V_z\big|_{j=N_y-\frac{1}{2}} + bV_z\big|_{j=N_y-\frac{3}{2}} + cV_z\big|_{j=N_y-\frac{5}{2}} + dV_z\big|_{j=N_y-\frac{7}{2}} + eV_z\big|_{j=N_y-\frac{9}{2}} \end{bmatrix} . \quad \text{(B.12)}$$

The matrix B is rewritten as follow

$$B = \frac{1}{\Delta y}\begin{bmatrix} \bar{a} & b & c & d & e & & & & & \\ -1 & 1 & 0 & 0 & 0 & & & & & \\ 0 & -1 & 1 & 0 & 0 & & & & & \\ & & & \cdot & \cdot & \cdot & & & & \\ & & & \cdot & \cdot & \cdot & & & & \\ & & & & & 0 & 0 & -1 & 1 & 0 \\ & & & & & 0 & 0 & 0 & -1 & 1 \\ & & & & & e & d & c & b & \bar{a} \end{bmatrix}\begin{bmatrix} V_z\big|_{j=1/2} \\ V_z\big|_{j=3/2} \\ \cdot \\ \cdot \\ \cdot \\ V_z\big|_{j=N_y-3/2} \\ V_z\big|_{j=N_y-1/2} \end{bmatrix} = \frac{1}{\Delta y}M\bar{V} \quad \text{(B.13)}$$

where M is a $(N_y+1)\text{x}N_y$ matrix and $\bar{V}$ is a vector with N_y dimension. Hence, the vector X can be obtained as

$$X = \frac{1}{\Delta y}(A^{-1}M)\bar{V} = \frac{1}{\Delta y}\bar{M}\bar{V}. \quad \text{(B.14)}$$

For a point with $j = l$, the derivative of V_z is listed below:

$$\left.\frac{\partial V_z}{\partial y}\right|_{I,\, j\, =\, l,\, K} = \frac{1}{\Delta y}\sum_{\beta=0}^{N_y-1} \bar{m}_{l\beta} V_z\Big|_{I,\, j\, =\, \frac{2\beta+1}{2},\, K} \tag{B.15}$$

where $\bar{m}_{l\beta}$ is the element of $\overline{M}$ at lth row and βth column. According to (B.3), $V_z\big|_{j\, =\, (2\beta+1)/2}$ can be rewritten as follow:

$$V_z\Big|_{I,\, j\, =\, \frac{2\beta+1}{2},\, K} = V_z\big|_{I,\, j\, =\, l,\, K} \cdot e^{-j\left[\kappa_y\left(l - \frac{2\beta+1}{2}\right)\Delta y\right]}. \tag{B.16}$$

Hence, (B.15) becomes

$$\left.\frac{\partial V_z}{\partial y}\right|_{I,\, j\, =\, l,\, K} = \frac{V_z\big|_{I,\, j\, =\, l,\, K}}{\Delta y} \cdot \sum_{\beta=0}^{N_y-1} \bar{m}_{l\beta} e^{-j\left[\kappa_y\left(l - \frac{2\beta+1}{2}\right)\Delta y\right]}. \tag{B.17}$$

Similarly, we obtain

$$\left.\frac{\partial V_y}{\partial z}\right|_{I,\, J,\, k\, =\, q} = \frac{V_y\big|_{I,\, J,\, k\, =\, q}}{\Delta z} \cdot \sum_{\gamma=0}^{N_z-1} \bar{m}_{q\gamma} e^{-j\left[\kappa_z\left(q - \frac{2\gamma+1}{2}\right)\Delta z\right]}. \tag{B.18}$$

Hence, (B.4) leads to

$$\begin{aligned} &\frac{V_x\big|_{I,J,K}}{\Delta t} \cdot 2\sin(\omega\Delta t/2) + \frac{V_z\big|_{I,J,K}}{\Delta y} \cdot \sum_{\beta=0}^{N_y-1} \bar{m}_{J\beta} e^{-j\left[\kappa_y\left(J - \frac{2\beta+1}{2}\right)\Delta y\right]} \\ &\qquad - \frac{V_y\big|_{I,J,K}}{\Delta z} \cdot \sum_{\gamma=0}^{N_z-1} \bar{m}_{K\gamma} e^{-j\left[\kappa_z\left(K - \frac{2\gamma+1}{2}\right)\Delta z\right]} = 0 \end{aligned} \tag{B.19}$$

Similarly, the y component and z component of (B.1) at point (I, J, K) are

$$\frac{V_y|_{I,J,K}}{\Delta t}\cdot 2\sin(\omega\Delta t/2)+\frac{V_x|_{I,J,K}}{\Delta z}\cdot\sum_{\gamma=0}^{N_z-1}\overline{m}_{K\gamma}e^{-j\left[\kappa_z\left(K-\frac{2\gamma+1}{2}\right)\Delta z\right]}$$
$$-\frac{V_z|_{I,J,K}}{\Delta x}\cdot\sum_{\alpha=0}^{N_x-1}\overline{m}_{I\alpha}e^{-j\left[\kappa_x\left(I-\frac{2\alpha+1}{2}\right)\Delta x\right]}=0 \qquad (B.20)$$

and

$$\frac{V_z|_{I,J,K}}{\Delta t}\cdot 2\sin(\omega\Delta t/2)+\frac{V_y|_{I,J,K}}{\Delta x}\cdot\sum_{\alpha=0}^{N_x-1}\overline{m}_{I\alpha}e^{-j\left[\kappa_x\left(I-\frac{2\alpha+1}{2}\right)\Delta x\right]}$$
$$-\frac{V_x|_{I,J,K}}{\Delta y}\cdot\sum_{\beta=0}^{N_y-1}\overline{m}_{J\beta}e^{-j\left[\kappa_y\left(J-\frac{2\beta+1}{2}\right)\Delta y\right]}=0 \qquad (B.21)$$

Equations (B.19), (B.20), and (B.21) can be rewritten in a matrix form,

$$AV = 0 \qquad (B.22)$$

where A is 3x3 matrix as shown in (B.27) and

$$V = \begin{bmatrix} V_x|_{I,J,K} \\ V_y|_{I,J,K} \\ V_z|_{I,J,K} \end{bmatrix}. \qquad (B.23)$$

By taking the determinant of A to be zero and restoring the light speed into the time related terms, the dispersion relation is obtained as

$$\left[\frac{2\sin(\omega\Delta t/2)}{c\Delta t}\right]^2 = \left[\frac{\sum_{\alpha=0}^{N_x-1} \bar{m}_{I\alpha} e^{-j\left[\kappa_x\left(I-\frac{2\alpha+1}{2}\right)\Delta x\right]}}{\Delta x}\right]^2 + \left[\frac{\sum_{\beta=0}^{N_y-1} \bar{m}_{J\beta} e^{-j\left[\kappa_y\left(J-\frac{2\beta+1}{2}\right)\Delta y\right]}}{\Delta y}\right]^2 + \left[\frac{\sum_{\gamma=0}^{N_z-1} \bar{m}_{K\gamma} e^{-j\left[\kappa_z\left(K-\frac{2\gamma+1}{2}\right)\Delta z\right]}}{\Delta z}\right]^2 \tag{B.24}$$

Assuming uniform partition along x, y, and z axes, $\Delta = \Delta x = \Delta y = \Delta z$, the dispersion relation becomes

$$\frac{12}{a^2}\left[\sin\left(\frac{a\pi}{\sqrt{3}R}\right)\right]^2 = \left[\sum_{\alpha=0}^{N_x-1} \bar{m}_{I\alpha} e^{-j\left[\kappa_x\left(I-\frac{2\alpha+1}{2}\right)\Delta\right]}\right]^2 + \left[\sum_{\beta=0}^{N_y-1} \bar{m}_{J\beta} e^{-j\left[\kappa_y\left(J-\frac{2\beta+1}{2}\right)\Delta\right]}\right]^2 + \left[\sum_{\gamma=0}^{N_z-1} \bar{m}_{K\gamma} e^{-j\left[\kappa_z\left(K-\frac{2\gamma+1}{2}\right)\Delta\right]}\right]^2 \tag{B.25}$$

where $a = \sqrt{3}c\Delta t/\Delta$ which is the CFL number and $R = \lambda/\Delta$ which is the number of cells in one wavelength. Let $\vec{\kappa} = \kappa_x\hat{x} + \kappa_y\hat{y} + \kappa_z\hat{z}$, then (B.25) can be further simplified as follows,

$$\begin{aligned}\frac{12}{a^2}\left[\sin\left(\frac{a\pi}{\sqrt{3}R}\right)\right]^2 = {} & \left[\sum_{\alpha=0}^{N_x-1} \bar{m}_{I\alpha} e^{-j\frac{\bar{\kappa}\sin\theta\cos\phi(2I-2\alpha-1)}{R}}\right]^2 \\ & + \left[\sum_{\beta=0}^{N_y-1} \bar{m}_{J\beta} e^{-j\frac{\bar{\kappa}\sin\theta\sin\phi(2J-2\beta-1)}{R}}\right]^2 \\ & + \left[\sum_{\gamma=0}^{N_z-1} \bar{m}_{K\gamma} e^{-j\frac{\bar{\kappa}\cos\theta(2K-2\gamma-1)}{R}}\right]^2\end{aligned} \tag{B.26}$$

$$A = \begin{bmatrix} \dfrac{2\sin(\omega\Delta t/2)}{\Delta t} & -\dfrac{\sum\limits_{\beta=0}^{N_z-1} \bar{m}_{K\beta} e^{-j\left[\kappa_z\left(K-\frac{2\beta+1}{2}\right)\Delta z\right]}}{\Delta z} & \dfrac{\sum\limits_{\alpha=0}^{N_y-1} \bar{m}_{J\alpha} e^{-j\left[\kappa_y\left(J-\frac{2\alpha+1}{2}\right)\Delta y\right]}}{\Delta y} \\ \dfrac{\sum\limits_{\alpha=0}^{N_z-1} \bar{m}_{K\alpha} e^{-j\left[\kappa_z\left(K-\frac{2\alpha+1}{2}\right)\Delta z\right]}}{\Delta z} & \dfrac{2\sin(\omega\Delta t/2)}{\Delta t} & -\dfrac{\sum\limits_{\beta=0}^{N_x-1} \bar{m}_{I\beta} e^{-j\left[\kappa_x\left(I-\frac{2\beta+1}{2}\right)\Delta x\right]}}{\Delta x} \\ -\dfrac{\sum\limits_{\beta=0}^{N_y-1} \bar{m}_{J\beta} e^{-j\left[\kappa_y\left(J-\frac{2\beta+1}{2}\right)\Delta y\right]}}{\Delta y} & \dfrac{\sum\limits_{\alpha=0}^{N_x-1} \bar{m}_{I\alpha} e^{-j\left[\kappa_x\left(I-\frac{2\alpha+1}{2}\right)\Delta x\right]}}{\Delta x} & \dfrac{2\sin(\omega\Delta t/2)}{\Delta t} \end{bmatrix} \quad \text{(B.27)}$$

where

$$\bar{\kappa} = \frac{\lambda\tilde{\kappa}}{2} = \frac{\pi}{v_p/c}. \tag{B.28}$$

Hence, the ratio of wave propagation speed in the computational space to that in the physical space is equal to the ratio of π to $\bar{\kappa}$.

APPENDIX C

DERIVATION OF EQUATION (2.107)

In section 2.4.2, the time domain version of Poynting theorem is derived and $g_x(t)$ is a key factor in calculating stored and dissipated power in time domain. In this appendix, the derivation of time domain expression of $g_x(t)$ is detailed.

The function, $g_x(t)$, is the inverse Fourier transform of $E_x(\omega)/[1 + (\omega\tau_{ex})^2]$ and can be rewritten as follow:

$$\begin{aligned} g(x) &= \Im^{-1}\left\{\frac{E_x(\omega)}{1+(\omega\tau_{ex})^2}\right\} \\ &= \Im^{-1}\{E_x(\omega)\} \otimes \Im^{-1}\left(\left\{\frac{1}{1+(\omega\tau_{ex})^2}\right\}\right) \\ &= E_x(t) \otimes \left\{\frac{1}{2\tau_{ex}} e^{\frac{-|t|}{\tau_{ex}}}\right\} \\ &= \frac{1}{2\tau_{ex}} \int_0^t e^{\frac{-|\tau|}{\tau_{ex}}} E_x(t-\tau)d\tau \end{aligned} \tag{C.1}$$

where $E_x(t-\tau)$ is a causal signal; that is, $E_x(t-\tau)$ is equal to zero when $t < \tau$ and the system is a causal system; that is, $e^{-|\tau|/\tau_{ex}}$ is equal to zero when $\tau < 0$. Discreting (C.1) by using the approximation in Figure C.1, the discrete version of $g_x(t)$ is

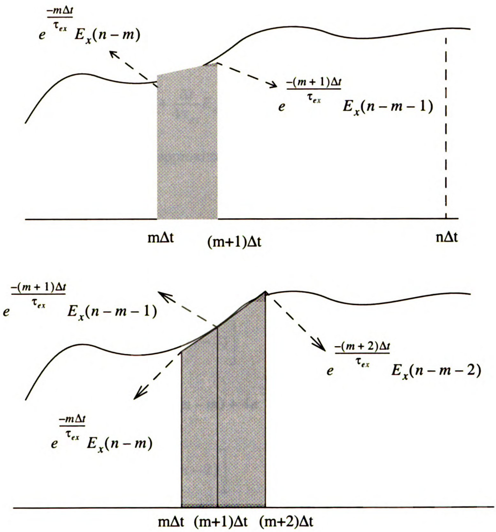

FIGURE C.1 Approximation of integrant in (C.1)

$$
\begin{aligned}
g(n) &= \frac{1}{2\tau_{ex}}\sum_{m=0}^{n-1}\frac{\Delta t}{2}\left[e^{-\frac{m\Delta t}{\tau_{ex}}}E_x(n-m)+e^{-\frac{(m+1)\Delta t}{\tau_{ex}}}E_x(n-m-1)\right] \\
&= \frac{1}{2\tau_{ex}}\sum_{m=1}^{n-1}\frac{\Delta t}{2}\left[e^{-\frac{m\Delta t}{\tau_{ex}}}E_x(n-m)+e^{-\frac{(m+1)\Delta t}{\tau_{ex}}}E_x(n-m-1)\right] \\
&\quad + \frac{1}{2\tau_{ex}}\frac{\Delta t}{2}\left[E_x(n)+e^{-\frac{\Delta t}{\tau_{ex}}}E_x(n-1)\right] \\
&= e^{-\frac{\Delta t}{\tau_{ex}}}g(n-1)+\frac{\Delta t}{4\tau_{ex}}E_x(n)+\frac{\Delta t}{4\tau_{ex}}e^{-\frac{\Delta t}{\tau_{ex}}}E_x(n-1)
\end{aligned}
\qquad \text{(C.1)}
$$

A more accurate recursive approximation can be obtained as follows by using three field points in Figure C.1:

$$
\begin{aligned}
g(n) &= \frac{1}{2\tau_{ex}}\sum_{m=0}^{n-2}\Delta t\left[\frac{1}{3}e^{-\frac{m\Delta t}{\tau_{ex}}}E_x(n-m)+\frac{4}{3}e^{-\frac{(m+1)\Delta t}{\tau_{ex}}}E_x(n-m-1)\right. \\
&\quad \left. +\frac{1}{3}e^{-\frac{(m+2)\Delta t}{\tau_{ex}}}E_x(n-m-2)\right] \\
&= \frac{1}{2\tau_{ex}}\sum_{m=1}^{n-2}\frac{\Delta t}{3}\left[e^{-\frac{m\Delta t}{\tau_{ex}}}E_x(n-m)+4e^{-\frac{(m+1)\Delta t}{\tau_{ex}}}E_x(n-m-1)\right. \\
&\quad \left. +e^{-\frac{(m+2)\Delta t}{\tau_{ex}}}E_x(n-m-2)\right] \\
&\quad + \frac{1}{2\tau_{ex}}\frac{\Delta t}{3}\left[E_x(n)+4e^{-\frac{\Delta t}{\tau_{ex}}}E_x(n-1)+e^{-\frac{2\Delta t}{\tau_{ex}}}E_x(n-2)\right] \\
&= e^{-\frac{\Delta t}{\tau_{ex}}}g(n-1)+\frac{\Delta t}{6\tau_{ex}}E_x(n)+\frac{2\Delta t}{3\tau_{ex}}e^{-\frac{\Delta t}{\tau_{ex}}}E_x(n-1)+\frac{\Delta t}{6\tau_{ex}}e^{-\frac{2\Delta t}{\tau_{ex}}}E_x(n-2)
\end{aligned}
\qquad \text{(C.2)}
$$

where (C.2) needs to store one more history of E_x than (C.1) does.

APPENDIX D

DERIVATION OF EQUATIONS (3.7) AND (3.8)

The term $\nabla \times \vec{E}$ in (3.2) is

$$
\begin{aligned}
\nabla \times & \sum_{m=0}^{\infty} (\vec{e}_u \cos m\phi + \vec{e}_v \sin m\phi) \\
&= \sum_{m=0}^{\infty} [\nabla \times (\vec{e}_v \sin m\phi) + \nabla \times (\vec{e}_u \cos m\phi)] \\
&= \sum_{m=0}^{\infty} [(\sin m\phi \nabla \times \vec{e}_v + \nabla \sin m\phi \times \vec{e}_v) + (\cos m\phi \nabla \times \vec{e}_u + \nabla \cos m\phi \times \vec{e}_u)] \\
&= \sum_{m=0}^{\infty} \left[\sin m\phi \left(\nabla \times \vec{e}_v - \frac{m}{\rho} \hat{\phi} \times \vec{e}_u \right) + \cos m\phi \left(\frac{m}{\rho} \hat{\phi} \times \vec{e}_v + \nabla \times \vec{e}_u \right) \right]
\end{aligned}
\tag{D.1}
$$

and those terms in the right hand side of (3.2) lead to

$$
\begin{aligned}
-[\mu]\frac{\partial \vec{H}}{\partial t} + [\sigma^*]\vec{H} &= -[\mu]\frac{\partial}{\partial t} \sum_{m=0}^{\infty} (\vec{h}_u \cos m\phi + \vec{h}_v \sin m\phi) \\
&\quad + [\sigma^*] \sum_{m=0}^{\infty} (\vec{h}_u \cos m\phi + \vec{h}_v \sin m\phi) \\
&= \sum_{m=0}^{\infty} \cos m\phi \left(-[\mu]\frac{\partial \vec{h}_u}{\partial t} + [\sigma^*]\vec{h}_u \right) \\
&\quad + \sum_{m=0}^{\infty} \sin m\phi \left(-[\mu]\frac{\partial \vec{h}_v}{\partial t} + [\sigma^*]\vec{h}_v \right) \cdot
\end{aligned}
\tag{D.2}
$$

From (D.1) and (D.2), we obtain (3.8),

$$\pm\frac{m}{\rho}\hat{\phi}\times\vec{e}_{v,u}+\nabla\times\vec{e}_{u,v} = -[\mu]\frac{\partial\vec{h}_{u,v}}{\partial t}+[\sigma^*]\vec{h}_{u,v}. \tag{D.3}$$

For $\nabla\times\vec{H}$ in (3.1), the following equation is obtained,

$$\begin{aligned}
&\nabla\times\sum_{m=0}^{\infty}(\vec{h}_u\cos m\phi+\vec{h}_v\sin m\phi)\\
&=\sum_{m=0}^{\infty}[\nabla\times(\vec{h}_u\cos m\phi)+\nabla\times(\vec{h}_v\sin m\phi)]\\
&=\sum_{m=0}^{\infty}[(\sin m\phi\nabla\times\vec{h}_v+\nabla\sin m\phi\times\vec{h}_v)+(\cos m\phi\nabla\times\vec{h}_u+\nabla\cos m\phi\times\vec{h}_u)]\\
&=\sum_{m=0}^{\infty}\left[\sin m\phi\left(\nabla\times\vec{h}_v-\frac{m}{\rho}\hat{\phi}\times\vec{h}_u\right)+\cos m\phi\left(\frac{m}{\rho}\hat{\phi}\times\vec{h}_v+\nabla\times\vec{h}_u\right)\right]
\end{aligned} \tag{D.4}$$

and those terms in the right hand side of (3.1) lead to

$$\begin{aligned}
[\varepsilon]\frac{\partial\vec{E}}{\partial t}+[\sigma]\vec{E}+\vec{J}_s &= [\varepsilon]\sum_{m=0}^{\infty}\left(\frac{\partial\vec{e}_u}{\partial t}\cos m\phi+\frac{\partial\vec{e}_v}{\partial t}\sin m\phi\right)\\
&\quad+[\sigma]\sum_{m=0}^{\infty}(\vec{e}_u\cos m\phi+\vec{e}_v\sin m\phi)\\
&\quad+\sum_{m=0}^{\infty}(\vec{j}_u\cos m\phi+\vec{j}_v\sin m\phi)\\
&=\sum_{m=0}^{\infty}\left[\cos m\phi\left([\varepsilon]\frac{\partial\vec{e}_u}{\partial t}+[\sigma]\vec{e}_u+\vec{j}_u\right)+\sin m\phi\left([\varepsilon]\frac{\partial\vec{e}_v}{\partial t}+[\sigma]\vec{e}_v+\vec{j}_v\right)\right].
\end{aligned} \tag{D.5}$$

Comparing (D.4) and (D.5), we obtain (3.7),

$$\pm\frac{m}{\rho}\hat{\phi}\times\vec{h}_{v,u}+\nabla\times\vec{h}_{u,v} = [\varepsilon]\frac{\partial\vec{e}_{u,v}}{\partial t}+[\sigma]\vec{e}_{u,v}+j_{u,v}. \tag{D.6}$$

BIBLIOGRAPHY

[1] John, D., Jr. Anderson, *Computational Fluid Dynamics: The Basics With Applications,* McGraw-Hill, New York, NY, 1995.

[2] K. S. Yee, "Numerical solution of inital boundary value problems involving Maxwell's equations in isotropic media," *IEEE Trans. Antennas and Propagation*, vol. 14, no. 3, pp. 302-307, 1966.

[3] A. Taflove and M. E. Brodwin, "Numerical solution of steady-state electromagnetic scattering problems using the time-dependent Maxwell's equations," *IEEE Trans. Microwave Theory and Techniques*, vol. 23, no. 8, pp. 623-630, 1975.

[4] D. H. Choi and W. J. R. Hoefer, "The finite-difference time-domain and its application to eigenvalue problems," *IEEE Trans. Microwave Theory and Techniques*, vol. 34, no. 12, pp. 1464-1469, 1986.

[5] A. Navarro, M. J. Nunez, and E. Martin, "Finite difference time domain FFT method applied to axially symmetrical electromagnetic resonant devices," *IEE Proc.*, vol. 137, no. 3, pp. 193-196, June, 1990.

[6] A. Navarro, M. J. Nunez, and E. Martin, "Study of TE_0 and TM_0 modes in dielectric resonators by a finite difference time-domain method coupled with the discrete Fourier transform," *IEEE Trans. Microwave Theory and Techniques,* vol. 39, no.1, pp. 14-17, 1991.

[7] F. Liu, I. Turner, and M. Bialkowski, "A finite-difference time-domain simulation of power density distribution in a dielectric loaded microwave cavity," *Journal of Microwave Power and Electromagnetic Energy,* Vol. 29, pp138-148, 1994.

[8] C. Su and J. Guan, "Finite-Difference Analysis of Dielectric-Loaded Cavities Using the Simultaneous Iteration of the Power Method with the Chebyshev Acceleration Technique," *IEEE Trans. Microwave Theory and Techniques*, vol. 42, no. 10, pp. 1998-2006, 1994.

[9] F. Torres and B. Jecko, "Complete FDTD analysis of microwave heating processing in frequency-dependent and temperature-dependent media," *IEEE Trans. Microwave Theory Tech.*, Vol. MTT-45, pp108-117, 1997.

[10] J. Guan and C. Su, "Resonant Frequencies and Field Distributions for the Shielded

Uniaxially Anisotropic Dielectric Resonantor by the FD-SIC Method," *IEEE Trans. Microwave Theory Tech.*, Vol. MTT-45, no. 10, pp1767-1777, 1997.

[11] J. Fang, "*Time Domain Finite Difference Computation for Maxwell's Equations*," Ph.D. thesis, University of California at Berkeley, Berkeley, CA, 1989.

[12] T. Deveze, L. Beaulie, and W. Tabbara, "An absorbing boundary condition for the fourth order FDTD Scheme," *IEEE Antennas and Propagation Society International Symposium*, pp. 342-345, July, 1992.

[13] S. K. Lele, "Compact finite difference schemes with spectral-like resolution," *J. of Computat. Phys.*, vol. 103, pp. 16-42, 1992.

[14] J. L. Young, D. Gaitonde and J. S. Shang, "Towards the contruction of a fourth order difference scheme for transient EM wave simulation: Staggered grid approach," *IEEE Trans. Antennas and Propagation*, vol. 45, no. 11, pp. 1573-1580, 1997.

[15] M. H. Carprnter, D. Gottlieb, and S. Abarbanel, "The Stability of Numerical Boundary Treatments for Compact High-Order Finite-Difference Schemes," *J. of Computat. Phys.*, vol. 108, pp. 272-295, 1993.

[16] A. Taflove, *Computational Electrodynamics: The Finite-Difference Time-Domain Method*, Artech House, Boston, MA, 1995.

[17] A. Taflove, *Advances in Computational Electrodynamics: The Finite-Difference Time-Domain Method*, Artech House, Boston, MA, 1998.

[18] F. B. Hildebrand, *Introduction to Numerical Analysis*, McGraw-Hill, NewYork, NY, 1974.

[19] C. A. Balanis, *Advanced Engineering Electromagnetics*, John Wiley & Sons, New York, NY, 1989.

[20] F. J. Harris, "On the use of windows for harmonic analysis with discrete Fourier transform," *Proc. IEEE*, vol. 66, pp.51-83, Jan. 1978.

[21] J. A. Pereda, L. A. Vielva, and A. Prieto, "Computation of resonant frequencies and quality factors of open dielectric resonantors by a combination of the finite-difference time-domain (FDTD) and Prony's methods," *IEEE Microwave and Guided Wave Letters*, vol. 2, 1992, pp. 431-433.

[22] R. Kumaresan, and D. W. Tufts, "Estimating the parameters of exponentially damped sinusoids and pole-zero modeling in noise," *IEEE Trans. Acoustics, Speech, and Signal Processing*, vol. 30, 1982, pp. 1380-1419.

[23] K. M. Chen, EE836 Class Notes, Michigan State University.

[24] J. D. Jackson, *Classical Electrodynamics*, John-Wiley, New York, NY, 1975.

[25] D. B. Davidson, and R. W. Ziolkowski, "Body of revolution finite-difference time-domain modeling of space time focusing by a three dimensional lens," *J. Optical Society of America*, June 1993.

[26] K. M. Chen, *Notes for EE 836*, Michigan State University.

[27] D. B. Davidson, "Body-of-revolution finite-difference time-domain modeling of space-time focusing by a three-dimensional lens," *J. Optical Society of America*, vol. 11, no.4, pp. 1471-1490, 1994.

[28] Y. Chen, R. Mittra, and P. Harms, "Finite-Difference Time-Domain Algorithm for Solving Maxwell's Equations in Rotationally Symmetric Geometies," *IEEE Trans. Microwave Theory and Techniques*, vol. 44, 1996, pp. 832-839.

[29] J. G. Maloney and G. S. Smith, "The use of surface impedance concepts in the finite-difference time-domain method," *IEEE Trans. Antennas Propagat.*, vol. 40, no. 1, pp. 38--48, 1992.

[30] S. Kellali, B. Jecko, and A. Reineix, "Implementation of a surface impedance formalism at oblique incident in FDTD method," *IEEE Trans. Electromagnetic Compatibility*, vol. 35, no. 3, pp. 347-356, 1993.

[31] K. S. Oh and J. E. Schutt-Aine, "An efficient implementation of surface impedance boundary conditions for the finite-difference time-domain method," *IEEE Trans. Antennas and Propagation,* vol. 43, no. 7, pp. 660-666, 1995.

[32] D. M. Sullivan, " Z transforms theory and FDTD method," *IEEE Trans. Antennas and Propagation,* vol. 44, no.1, pp. 28-34, 1996.

[33] J. H. Beggs, "A FDTD Surface Impedance Boundary Condition Using Z-Transforms," *Applied Computational Electromagnetics Society Journal*, vol. 13, no. 1, pp.14-24, 1998.

[34] J. G. Proakis and D. G. Manolakis, *Digital Signal Processing*, Macmillan, New York, New York, 1992.

[35] W. Y. Tan, "Modeling The Electromagnetic Field and The Plasma Excitation in A Moderate Pressure Microwave Cavity Plasma Source," *Ph.D. Dissertation*, Michigan State University, 1994.

[36] D. M. Sullivan, "A Frequency-Dependent FDTD Method for Biological Applications," *IEEE Trans. Antennas and Propagation*, vol. 40, no. 3, pp. 532-539, 1992.

[37] Om P. Gandhi, Ben-Qing Gao, and Jin-Yuan Chen, "A Frequency-Dependent Finite-Difference Time-Domain Formulation for General Dispersive Media," *IEEE*

Trans. Microwave Theory and Techniques, vol. 41, no. 4, pp. 658-665,1993.

[38] J. L. Young, A. Kittichartphayak, Y. M. Kwok, and D. Sullivan, "On the Dispersion Errors Related to $(FD)^2TD$ Type Schemes", *IEEE Trans. Microwave Theory and Techniques,* vol. 43, no. 8, pp. 1902-1910, 1995.